POLYTECHNIQUE MONTRÉAL

affiliée à l'Université de Montréal

Subject-Specific Computational Musculoskeletal Modeling of Human Trunk in Lifting: Role of Age, Sex, Body Weight and Body Height

FARSHID GHEZELBASH

Département de Génie Mécanique

Thèse présentée en vue de l'obtention du diplôme de *Philosophiæ Doctor*

Génie Mécanique

Décembre 2019

POLYTECHNIQUE MONTRÉAL

affiliée à l'Université de Montréal

Cette thèse intitulée :

Subject-Specific Computational Musculoskeletal Modeling of Human Trunk in Lifting: Role of Age, Sex, Body Weight and Body Height

présentée par **Farshid GHEZELBASH**

en vue de l'obtention du diplôme de *Philosophiæ Doctor*

a été dûment acceptée par le jury d'examen constitué de :

Aouni A. LAKIS, président
Aboulfazl SHIRAZI-ADL, membre et directeur de recherche
André PLAMONDON, membre et codirecteur de recherche
L'Hocine YAHIA, membre
Richard PREUSS, membre externe

ACKNOWLEDGEMENTS

Firstly and mostly, I sincerely and gratefully thank Professor Shirazi-Adl for his supports and guidance during my PhD, and I thank Dr. Plamondon for his contributions and visions particularly on practical aspects of this work. I should also thank Dr. Navid Arjmand, Professor Mohamad Parnianpour, Ms. Sophie Bellefeuille (for data collection), Mr. Hakim Mecheri (for data processing) and Dr. Zakaria El-Ouaaid (for performing experiments and data preparation). I would like to thank funding agencies (IRSST and FRQNT) for the roof over my head and the food on my table.

I would like to thank my family (Maman, Baba and Shadi) for their unconditional supports, and I thank my Mom for being the only person in the whole universe who believes that her son is the "BEST" (though I strongly disagree). I would like to thank two influential figures in my life Dr. Mohammadi and Solaleh – my wife – for changing my life for the better. Thank you Solaleh for supporting and accepting me; you are the best (then pizza is the best): ♡ + xoxox.

RÉSUMÉ

Les troubles musculosquelettiques sont parmi les problèmes de santé les plus fréquents et les plus coûteux au monde. Les maux de dos figurent en deuxième position sur la liste des états chroniques les plus répandus au Canada et quatre adultes sur cinq souffriront de lombalgie un jour ou l'autre de leur vie. Les efforts excessifs sur la colonne vertébrale constituent l'un des facteurs de risque potentiels de lombalgie et peuvent initier ou générer de la douleur et de la dégénérescence des disques. À cet effet, plusieurs études s'accordent pour affirmer qu'une estimation juste des charges vertébrales est utile pour une prévention efficace des blessures et pour des programmes de réadaptation appropriés. Toutefois, il n'existe pas de méthodes directes pour mesurer les charges vertébrales et de plus, toutes les méthodes indirectes (comme la mesure de la pression intradiscale – PID – et l'estimation au moyen de prothèse discale instrumentée) sont invasives et limitées. Les modèles musculosquelettiques (MS) offrent toutefois une alternative intéressante en estimant de manière non invasive, économique et précise les forces musculaires, les charges vertébrales ainsi que la stabilité de la colonne vertébrale en tenant compte des différences individuelles.

Dans cette thèse, un modèle MS du tronc par éléments finis (EF) guidé par la cinématique a été mis à niveau. L'architecture des origines et insertions musculaires a été améliorée, une unité vertébrale comprenant un disque déformable a été ajoutée (T11-T12) et un nouvel algorithme de mise à l'échelle a été introduit afin d'explorer les effets du sexe, de l'âge, du poids et de la taille sur la biomécanique et les charges appliquées sur la colonne vertébrale. Au moyen de données issues d'imageries médicales et à partir de principes biomécaniques, l'algorithme de mise à l'échelle a permis d'ajuster l'architecture musculaire (les bras de levier des muscles et les aires transverses), la géométrie et les propriétés passives ligamentaires de la colonne vertébrale ainsi que la charge gravitationnelle, le tout en fonction du sexe, de l'âge, du poids et de la taille. Une analyse de sensibilité a été effectuée au moyen d'une analyse factorielle multiple. Les données d'entrées du modèle (sexe, âge, poids et taille) ont été modifiées à l'intérieur de plages physiologiques (sexe : femme et homme ; âge : 35 à 60 ans ; poids : 50 à 120 kg ; taille : 150 à 190 cm) tandis que le modèle personnalisé par EF était guidé par une cinématique spécifique à l'âge et au sexe lors de différentes tâches de flexion avant avec ou sans charges manuelles. Des graphiques illustrant les effets principaux et des analyses de variance ont été utilisés pour évaluer les effets des données d'entrées sur le chargement au dos. Le poids du corps a été le facteur le plus influent, en expliquant

99 % du chargement lombaire en compression et 96 % de celui en cisaillement, alors que les effets de la taille, du sexe et de l'âge (<5 %) étaient minimes. Aussi, pour des poids et des tailles similaires aux hommes, les femmes supportaient généralement des charges plus importantes au dos (5 % en compression, 9 % en cisaillement)

La prévalence de l'obésité, dont l'indice de masse corporelle (IMC) dépasse les 30 kg/m^2, est en croissance constante dans les pays développés comme dans les pays en voie de développement et a atteint un seuil critique « d'épidémie mondiale ». Bien que l'obésité soit associée à plusieurs problèmes au dos (ex. : dégénération discale, fractures vertébrales, maux de dos), le rôle de la biomécanique dans les problèmes liés à l'obésité demeure inconnu. La distribution du tissu adipeux varie considérablement d'un individu obèse à un autre, et ce, même dans les cas d'IMC et de poids identiques. On retrouve différentes formes d'obésité, dont celle « en pomme » et celle « en poire » (androïde et gynoïde respectivement). Le rôle de l'obésité et des formes d'obésité sur les charges supportées par la colonne vertébrale et sur les fractures de compression vertébrale a été étudié à l'aide du modèle personnalisé mis à jour. Trois formes distinctes d'obésité (correspondant à une taille de circonférence minimale, moyenne et maximale) pour un poids et un IMC identiques ont été simulées au moyen de mensurations anthropométriques obtenues à partir de 5852 individus obèses et d'une analyse par composantes principales. L'obésité a des conséquences significatives sur le chargement lombaire : la compression sur L4-L5 a bondi de 16 % (2820 N vs 3350 N) pour une flexion avant sans charges lorsque l'IMC a augmenté de 31 kg/m^2 à 39 kg/m^2. Dans une comparaison entre une taille de circonférence minimale (obésité en forme de poire) et celle d'une circonférence maximale (obésité en forme de pomme), le chargement lombaire a subi une augmentation similaire à celle d'ajouter 20 kg de poids supplémentaire, ainsi qu'un risque de fracture de fatigue vertébrale sept fois plus élevé. En somme, l'obésité et les formes d'obésité ont une influence considérable sur la biomécanique de la colonne vertébrale, et donc, devraient être prises en compte lors d'une modélisation spécifique aux sujets.

En plus de servir à l'évaluation de la force maximale du tronc et à la normalisation de l'électromyographie (EMG), les contractions musculaires volontaires maximales (CVM) peuvent être utilisées pour calibrer et valider les modèles MS. La performance du modèle MS personnalisé a été étudiée en comparant les activités musculaires estimées avec les EMG durant diverses tâches de CVM. Le stress musculaire maximal des muscles du tronc a également été calculé pour chaque

sujet. Ce dernier a varié considérablement entre différents sujets et groupes musculaires. Le muscle grand droit et le muscle oblique externe de l'abdomen ont eu, respectivement, le plus petite (0,40 ±0,22 MPa) et la plus grande valeur (0,99 ±0,29 MPa) de stress musculaire maximal parmi les groupes de muscles. Pour les CVM en flexion et en extension, les activités musculaires estimées correspondaient adéquatement avec les EMG. Cependant, cette correspondance était faible pour les CVM en flexion latérale et rotations axiales. Le chargement lombaire des femmes était en général plus faible que celui des hommes. Les charges vertébrales maximales lors des CVM ont été obtenues lors des efforts en extension (compression d'environ 6000 N à L5-S1) tandis que les plus faibles ont été enregistrées en flexion avant (compression d'environ 3000 N à L5-S1) ; les participants ont subi des chargements lombaires assez importants durant des CVM en flexion latérale et rotation axiale. (5500 N en compression et 1700 N en cisaillement). La prédiction exacte du stress musculaire maximal et l'évaluation complète de la performance d'un modèle MS nécessitent la prise en compte des tâches de CVM dans toutes les directions et l'application des moments dans les plans principaux et couplés du modèle.

Une simulation adéquate des ligaments passifs de la colonne vertébrale, l'une des composantes majeures d'un modèle MS du tronc, est d'une importance capitale. Les modèles détaillés d'EF peuvent capturer avec précision les réactions non linéaires et temporelles de la colonne vertébrale. Toutefois, en raison des coûts de calcul importants des modèles détaillés d'éléments finis, des modèles simplifiés (c.-à-d. à partir de joints sphériques et de poutres ayant des propriétés passives linéaires ou non linéaires) sont couramment utilisés dans les principaux modèles MS. Par conséquent, la précision et la validité de l'utilisation de modèles simplifiés et de leur positionnement antéro-postérieur dans l'estimation de la cinématique de la colonne vertébrale ligamentaire, des forces musculaires et des charges spinales ont été étudiées. Contrairement aux poutres, les articulations de type sphérique négligeaient les degrés de liberté en translation et n'ont pas réussi à prédire la cinématique de la colonne lombaire avec précision, surtout dans la direction craniocaudale. Les poutres et les joints sphériques non linéaires ont prédit de manière satisfaisante la PID en comparaison avec les mesures *in vivo* d'activités physiques variées. En revanche, l'utilisation des poutres ou des joints sphériques aux propriétés linéaires passives n'a donné que des résultats valides que pour des angles de flexion d'amplitude faible ou modérée (<40 º). En négligeant les propriétés passives des articulations (joints sphériques sans frottement), on a

considérablement augmenté le chargement lombaire en compression et en cisaillement, de 32 % et 63 % respectivement. Le déplacement postérieur (de 8 mm) d'une articulation simplifiée a augmenté les charges lombaires (en compression et en cisaillement) d'environ 20 %, tandis qu'un déplacement vers l'avant (2 mm) a diminué de 10 % la compression et de 18 % la force de cisaillement. De plus, un déplacement postérieur du modèle simplifié a réduit la force passive des muscles agonistes, et ce, tout en augmentant leurs composantes actives. Les modèles d'articulation simplifiés avec des propriétés passives non linéaires devraient se situer entre -2 à +4 mm (+ : postérieur) du centre du disque pour des prédictions justes des forces sur la colonne vertébrale et des forces musculaires actives/passives.

L'obtention de résultats valides à l'aide des modèles MS exige des moyens considérables comme une collecte complète de données (ex. : cinématiques, EMG), un laboratoire bien équipé et une formation suffisante. Par ailleurs, des équations de régression faciles à utiliser ont précédemment été mises au point pour estimer le chargement lombaire. Cependant, ces équations ne tiennent pas compte de l'anthropométrie des participants (ex. : poids et taille) fondée sur une approche physiologique, et elles négligent souvent l'asymétrie de la tâche. Dans cette partie de l'étude, des équations de régression spécifiques aux sujets ont été développées pour prédire le chargement lombaire (à L4-L5 et L5-S1) en utilisant un modèle d'EF guidé par la cinématique. L'exactitude de ce modèle et des équations de régression ont été évaluées en comparant les activités musculaires estimées par le modèle avec ceux obtenus au moyen de l'EMG et des PDI calculées avec ceux de la littérature existante. Les valeurs estimées de la PDI spécifiques aux sujets présentaient des corrélations élevées avec les résultats d'études *in vivo* lors de tâches symétriques et asymétriques (R^2=0.82). Dans le cas des tâches symétriques, les estimations d'activité musculaire étaient raisonnablement comparables avec les résultats d'EMG. Toutefois, dans les tâches asymétriques, les estimations étaient moyennement (muscles du dos) ou faiblement (muscles de l'abdomen) en accord avec les EMG. En somme, les équations de régression développées peuvent être utilisées dans le but d'estimer le chargement lombaire dans des tâches de levage symétriques et asymétriques. Ces équations personnalisées pourraient servir à l'évaluation des risques de blessure au dos lors d'activités de manutention.

En résumé, un modèle MS d'EF guidé par la cinématique, mis à jour par une architecture musculaire améliorée, un disque déformable additionnel (T11-T12) et un nouvel algorithme de

mise à l'échelle a été utilisé pour examiner la biomécanique personnalisée de la colonne vertébrale. En personnalisant tous les paramètres du modèle MS (les bras de levier des muscles, les aires transverses musculaires, le chargement gravitationnel, la géométrie de la colonne, les propriétés passives et la cinématique de la colonne vertébrale), et en effectuant une analyse de sensibilité sur les données d'entrées du modèle (sexe, âge, taille et poids), il a été démontré que le poids d'une personne influence nettement les forces de chargement subies par la colonne vertébrale, alors que l'influence des autres facteurs était plutôt faible. Deux formes distinctes d'obésité ont été reconstituées à partir d'un ensemble de données anthropométriques disponibles dans la littérature. Les résultats ont établi que l'obésité et les formes d'obésité (formes en pomme ou en poire) affectent, toutes les deux, les forces sur la colonne vertébrale ainsi que le risque de fracture de fatigue vertébrale. Lors de tâches de CVM (en extension, en flexion, en flexion latérale et en rotation axiale), les grandeurs du stress musculaire variaient substantiellement parmi les sujets et différents groupes musculaires. Dans le cas des CVM en flexion et en extension, les valeurs prédites d'activité musculaire par le modèle personnalisé étaient près des EMG enregistrés, alors que les prédictions concernant les CVM en rotation axiale et en flexion latérale n'avaient pas la même exactitude. Des poutres et des joints sphériques ayant des propriétés non linéaires (d'une position variant de -2 à +4 mm [+ : postérieur] du centre des disques) prédisait avec exactitudes les cinématiques de la colonne vertébrale, le chargement lombaire et les activités musculaires. Par contre, les modèles articulaires qui avaient des propriétés linéaires ou qui n'avaient pas de degrés de liberté en translation détérioraient l'exactitude des prédictions. Enfin, des équations de régression faciles à utiliser ont été mises au point dans le but de prédire les forces de compression et de cisaillement subies par la colonne vertébrale (aux niveaux L4-L5 et L5-S1) lors de tâches symétriques et asymétriques. Les équations personnalisées ont correctement estimé les valeurs de PID en comparant les valeurs calculées avec les résultats mesurés *in vivo* retrouvés dans la littérature. Lors de plusieurs tâches symétriques et asymétriques, les valeurs estimées des activités musculaires étaient moyennement (pour les muscles du dos) à faiblement (pour les muscles abdominaux) comparables avec les EMG enregistrés des participants. Par conséquent, les équations de régression proposées peuvent être utilisées pour évaluer les risques de blessures lors d'activités de manutention.

ABSTRACT

Musculoskeletal disorders are one the most frequent and costly disabilities in the world. Back problems are the second most common chronic condition in Canada. Four out of five adults experience low back pain in their lifetime. As one of the potential risk factors of back pain, excessive loads on the spine can initiate and promote disc degeneration and pain, so accurate estimation of spinal loads are helpful in designing effective prevention, evaluation, and treatment programs. There is no direct method to measure spinal loads, and all indirect methods (intradiscal pressure – IDP – and instrumented vertebral replacement) are invasive and scarce. Alternatively, musculoskeletal (MS) models with physiological scaling algorithms economically and accurately estimate muscle forces, spinal loads and spinal stability margin by taking into account individual differences.

An existing kinematics driven (KD) finite element (FE) MS musculoskeletal model of the trunk has been upgraded in this work by refining the muscle architecture, by adding a new deformable disc level (T11-T12), and by introducing a novel scaling algorithm to explore likely effects of sex, age, body weight (BW) and body height (BH) on spine biomechanics and spinal loads. By using imaging datasets and biomechanical principles, the scaling algorithm adjusted the muscle architecture (muscle moment arms and cross-sectional areas), spine geometry, passive properties of the ligamentous spine and gravity loads based on subject's sex, age, BH and BW. To perform a sensitivity analysis in a full-factorial design, model inputs (i.e., sex, age, BH and BW) were altered within physiological ranges (sex: female and male; age: 35-60 years; BH: 150-190 cm; BW:50-120 kg) while the personalized KD-FE model of the trunk was driven with sex- and age-specific kinematics during different forward flexion tasks with and without a hand-load. Main effect plots and the analysis of variance were employed to investigate effects of inputs on spinal loads. As the most influential factor, BW contributed 99% to compression and 96% to shear spinal loads while effects of BH, sex and age (<5%) remained much smaller. At identical BH, BW and waist circumference, females had slightly greater spinal loads (5% in compression; 9% in shear).

The prevalence of obesity (body mass index; BMI>30 kg/m^2) is rising in both developed and developing countries, and has reached "global epidemic" proportions. Although obesity has been associated with various back problems (e.g., disc degeneration, vertebral fracture and back pain),

the likely role of biomechanics in obesity-related back problems is still unknown. At identical BMI and BW, fat distribution varies substantially from one obese individual to another. Different obesity types have qualitatively been described as apple- and pear-shaped (or android and gynoid). Therefore, effects of obesity and obesity shapes on spinal loads and vertebral compression fracture were investigated by using the upgraded subject-specific model. At identical BW and BH, three distinct obesity shapes (corresponding to minimum, average and maximum waist circumferences) were reconstructed by using available anthropometric measurements of 5852 obese individuals and principal component analysis. Obesity markedly affected spinal loads; L4-L5 compression increased by 16% (2820 N vs 3350 N) in forward flexion without a hand-load when BMI increased from 31 kg/m^2 to 39 kg/m^2. Greater waist circumferences (apple-shaped obesity) in comparison with smaller waist circumferences (pear-shaped obesity) increased spinal loads to the extent of gaining 20 kg additional BW and the risk of vertebral fatigue fracture by up to ~7 times. Therefore, both obesity and obesity shapes substantially affected spine biomechanics and should be taken into account in subject-specific modeling of the spine.

Apart from serving in the trunk strength quantification and electromyography (EMG) normalization, maximum voluntary exertions (MVEs) can be used to calibrate and validate MS models. The performance of the current upgraded subject-specific MS model was investigated by comparing estimated muscle activities with reported EMGs during various MVE tasks. Maximum muscle stresses of trunk muscles were also calculated for each subject individually. Estimated maximum muscle stresses varied substantially among subjects and different muscle groups; rectus abdominis and external oblique had the smallest (0.40±0.22 MPa) and largest (0.99±0.29 MPa) maximum muscle stresses, respectively. In sagittal symmetric MVEs (extension and flexion), estimated muscle activities were found in satisfactory agreement with measured reported EMGs while in lateral and axial MVEs, the agreement was rather weak. Females in general had smaller spinal loads. Peak spinal loads were obtained in extension MVE (~6000 N compression at L5-S1) while flexion MVE yielded the smallest spinal loads (~3000 N compression at L5-S1); subjects experienced rather large spinal loads (5500 N in compression and 1700 N in shear) under lateral and axial MVEs. Accurate prediction of maximum muscle stresses and comprehensive evaluation of the performance of a MS model require the consideration of MVE tasks in all directions with the application of both primary and coupled moments to the model.

Accurate simulation of the passive ligamentous spine, as one of the integral components of a trunk MS model, is of great importance. Detailed FE models can accurately capture nonlinear and time-dependent responses of the spine; however, due to the significant computational costs of detailed FE models, simplified models (i.e., spherical joints/beams with linear/nonlinear passive properties) are commonly used in the trunk MS models. Therefore, the accuracy and validity of using simplified models and their anterior-posterior positioning in estimating kinematics of the ligamentous spine, muscle forces and spinal loads were investigated. Unlike beam elements, spherical joints overlooked translational degrees of freedom and failed to accurately predict kinematics of the lumbar spine particularly in the cranial-caudal direction. Nonlinear shear deformable beams and spherical joints were found to satisfactorily predict IDPs in comparison with *in vivo* measurements during various activities. In contrast, using beams or spherical joints with linear passive properties yielded valid results only in small to moderate flexion angles ($<40^{o}$). Neglecting passive properties of joints (frictionless spherical joints) substantially increased compression and shear spinal loads by 32% and 63%. Shifting a simplified joint posteriorly (by 8 mm) increased spinal loads (compression and shear) by ~20% while an anterior shift (by 2 mm) decreased spinal loads by 10% and 18% in compression and shear directions. Moving simplified joint models posteriorly reduced also passive muscle forces of agonist muscles while increasing their active components. Simplified joint models with nonlinear passive properties should be located in -2 to +4 mm (+: posterior) range from the disc center for accurate predictions of spinal loads and active/passive muscle forces.

Obtaining reasonably accurate results by MS models requires comprehensive data collection (e.g., kinematics, EMG), equipped laboratory, and sufficient training. Alternatively, easy to use regression equations have previously been developed to estimate spinal loads, but they do not take account of personalized anthropometric factors (e.g., BW and BH) based on a physiological approach and often overlook task asymmetry. Thus, in this work, subjects-specific regression equations were developed to predict spinal loads at lower spinal levels (L4-L5 and L5-S1) by using the upgraded KD-FE model, and the Accuracy of the model and regression equations were subsequently evaluated by comparing estimated muscle activities and IDPs with reported measurements. Estimated subject-specific IDPs from regression equations had strong correlation with *in vivo* measurements during various symmetric and asymmetric tasks (R^2=0.82). In

symmetric tasks, estimated muscle activities were found in satisfactory agreement with measured EMGs, but in asymmetric tasks, the estimations had moderate (back muscles) to weak (abdominal muscles) agreement with measurements. For workplace evaluation and biomechanical risk assessment of manual material handling tasks, such developed individualized regression equations can be employed to estimate spinal loads during various symmetric and asymmetric lifting activities.

In summary, a KD-FE MS model of the trunk with an upgraded muscle architecture, an additional deformable level (T11-T12) and a novel scaling algorithm was employed to investigate subject-specific spine biomechanics. By using personalized muscle moment arms, muscle cross-sectional areas, distributed gravity loads, spine geometry, nonlinear passive properties of the spine and spine kinematics (sex- and age-specific), the full factorial sensitivity analysis on model inputs (sex, age, BH and BW) showed that BW markedly affected spinal loads while remaining factors played a minor role. Distinct obesity shapes were reconstructed from anthropometric datasets available in the literature, and both obesity and obesity shapes (apple- and pear-shaped) were found to substantially affected spinal loads and the risk of vertebral fatigue fracture. Calculated muscle stresses, calibrated in MVE tasks (extension, flexion, lateral and axial), varied noticeably among subjects and different muscle groups. In flexion and extension MVEs, the subject-specific model predicted muscle activities in close agreement with reported EMGs while in axial and lateral MVEs, the agreement was weak. Simulating passive spinal motion segments, beams and spherical joints with nonlinear properties (located in -2 to +4 mm (+: posterior) range from disc centers), accurately predicted kinematics of the spine, spinal loads and muscle activities. In contrast, joint models with linear properties and/or no translational degrees-of-freedom were noted to deteriorate the accuracy of predictions. Easy to use subject-specific regression equations were developed to predict compression and shear spinal loads (at L4-L5 and L5-S1) in symmetric and asymmetric tasks. The proposed equations satisfactorily estimated IDPs in comparison with *in vivo* measurements. Proposed regression equations can be used for personalized biomechanical risk assessment of lifting tasks. Estimated muscle activities had moderate (back muscles) to weak (abdominal muscles) agreement with reported EMGs in various symmetric and asymmetric tasks.

TABLE OF CONTENT

LIST OF TABLES

LIST OF FIGURES

LIST OF SYMBOLS AND ABBREVIATIONS

ANOVA	Analysis of variance
BH	Body height
BMI	Body mass index
BW	Body weight
EMG	Electromyography
EO	External oblique
FE	Finite element
IAP	Intra-abdominal pressure
ICoR	instantaneous center of rotation
ICPL	Iliocostalis pars lumborum
ICPT	Iliocostalis Pars Thoracic
IDP	Intra-discal pressure
IO	Internal oblique
IP	Iliopsoas
KD	Kinematics-driven
LGPL	Longissimus pars lumborum
LGPT	Longissimus pars thoracic
MF	Multifidus
MVE	Maximum voluntary exertion
NIOSH	National institute of occupational safety and health
NLE	NIOSH lifting equation
PC	Principal component
PCSA	Physiological cross-sectional area
QL	Quadratus lumborum
RA	Rectus abdominis
RMSE	Root mean squared error
SD	Standard deviation
WHO	World health organization

LIST OF APPENDICES

CHAPTER 1 INTRODUCTION

1.1 Human Spine

As a complex and intrinsically unstable structure (Crisco, Panjabi, Yamamoto, & Oxland, 1992; Shirazi-Adl & Pamianpour, 1993), human spine transmits rather large loads to lower extremities and deforms significantly in all physiological planes while performing daily, occupational and recreational tasks. Human spine, without sacrum, is categorized into three distinct regions (cervical, thoracic and lumbar) with 24 bony vertebrae (cervical spine: C1 to C7; thoracic spine: T1 to T12; lumbar spine: L1 to L5). Two adjacent vertebrae with the intervertebral disc, ligaments, and facet joints in between are referred to as a motion segment. Each vertebra consists of an anterior vertebral body (made of cancellous bone covered by a thin layer of cortical bone) as well as a posterior arch (a base for facet articulations as well as ligament and muscle attachments), Figure 1.2. The posterior arch has two pedicles (stemming from the anterior vertebral body), a lamina and 5 processes (transverse, spinous and articular processes), Figure 1.2. Articular processes of two adjacent vertebrae in combination with their thin cartilage layers, synovial membrane (to facilitate articulation) and capsular ligaments (to stabilize the joint) form the facet joints, which transmit forces and limit inter vertebral motions. Between two adjacent vertebrae, a compliant intervertebral disc is located with a composite non-homogenous and multi-phasic structure. An intervertebral disc is divided into three main regions: 1- annulus fibrosus, 2- nucleus pulposus and 3- cartilaginous endplates. Mainly made from collagen types I and II, the annulus fibrosus forms the outer portion of the disc (Figure 1.2) and consists of 15 to 25 concentric layers (called lamellae), encircling the nucleus pulposus, Figure 1.2 (Marchand & Ahmed, 1990). Nucleus pulposus, located in the center (Figure 1.2), encompasses 30-50% of the total cross sectional area of a disc (Alkalay, 2002). It is mostly made of water (80-90% wet weight (Antoniou et al., 1996; Lipson & Muir, 1981)), proteoglycans (14% wet weight (Berthet-Colominas, Miller, Herbage, Ronziere, & Tocchetti, 1982; Inerot & Axelsson, 1991)), collagen fibers, elastin and chondrocytes. While developing an internal pressure under applied compression, it supports applied force and stiffens the annulus fibrosus by preventing inward bulge of inner annulus layers. On the top and the bottom, two rather thin endplates bound the intervertebral disc and attach it to adjacent vetebrae (Figure 1.2). With the average thickness of 0.5 mm (Adams, 2015), the hyaline cartilaginous endplate has a highly dense and organized collagen fibers (type-II) (Cassinelli, Hall, & Kang, 2001).

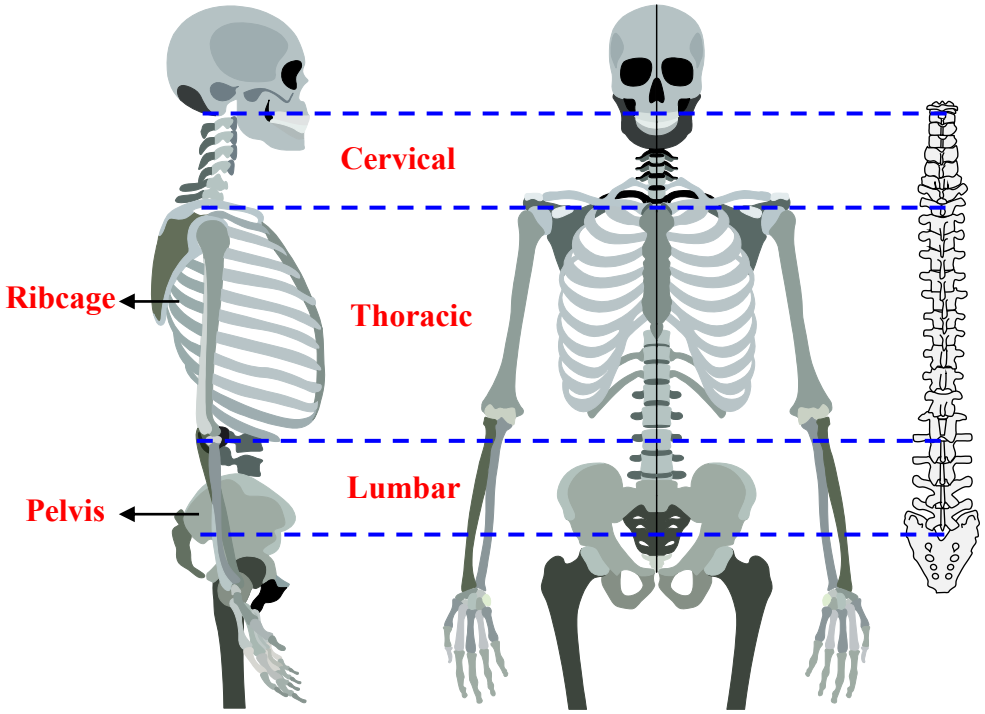

Figure 1.1 Different regions of spine (cervical, thoracic and lumbar)

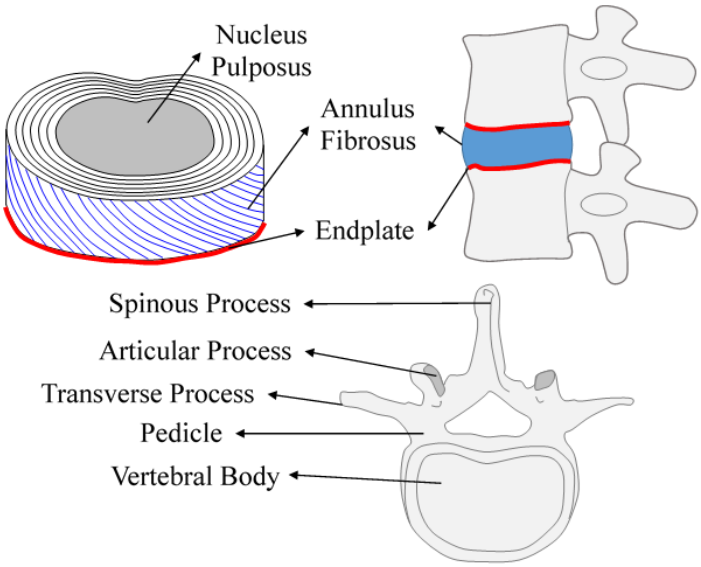

Figure 1.2 Schematic illustration of a vertebra and an intervertebral disc as well as their components

Spinal ligaments connect two adjacent vertebrae, increase the stability of a motion segment and limit the deformation of the intervertebral disc (Heuer, Schmidt, & Wilke, 2008; Pintar, Cusick, Yoganandan, Reinartz, & Mahesh, 1992; Sharma, Langrana, & Rodriguez, 1995). Posterior ligaments (longitudinal, capsular, interspinous, flavum, intertransverse and supraspinous) in general carry loads during flexion while anterior longitudinal ligament load-bearing contribution is more pronounced in torsion and extension (Panjabi, Goel, & Takata, 1982; Tencer, Ahmed, & Burke, 1982). The only load-bearing ligament under all moments is the capsular ligament (Zander, Dreischarf, Timm, Baumann, & Schmidt, 2017).

Located at the lower part of the trunk and sitting on the femurs at hip joints, the pelvis provides insertion for the back and abdominal muscles particularly at the sacrum and ilium while transferring the load to the lower extremity, Figure 1.1. With bony and cartilaginous structures, ribcage is composed of multiple ribs (bone), which in general, are attached via joints to vertebrae posteriorly and to the sternum anteriorly. Apart from protecting critical internal organs (such as lungs and heart), the ribcage provides the support for many small (intercostal muscles) and large (iliocostalis and longissimus) muscles. Pelvic floor (at the bottom) and diaphragm (a thin muscle attached to lower ribs) bound the abdominal cavity and play passive roles in generating intra-abdominal pressure (IAP).

1.2 Low Back Pain

Work-related musculoskeletal disorders have been identified as the most frequent and costly disability in the western countries. Back pain as the leading cause of disability tops this list (Hoy et al., 2012; Hoy et al., 2014). Four out of five adults experience back pain in their lifetime (Swink Hicks et al., 2002; van Tulder & Koes, 2002). Back problems are the second most common chronic condition (after food allergies) in Canada (Schultz & Kopec, 2003). In 1994 and in Canada alone, total cost of back related disorders was estimated at 6-10 billion dollars (=9.6-16 billion dollars; adjusted for inflation in 2019) (Coyte, Asche, Croxford, & Chan, 1998). Apart from the substantial economic burden on the society (i.e., loss of productivity, health care expenses, compensation costs), affected population suffers physically and mentally of debilitating pain and experiences substantial loss in the quality of life (Montazeri & Mousavi, 2010).

Multiple risk factors have been indicated to play causative roles in back pain such as genetics, psychosocial and biomechanical factors (Wang & Battié, 2014). Excessive loads on the lumbar spine are recognized as one the causes of back injuries, disc degeneration and back pain (Adams, Freeman, Morrison, Nelson, & Dolan, 2000; Adams & Roughley, 2006). Therefore, accurate estimation of muscle forces and loads on spine in various daily and occupational activities is crucial in effective prevention, workplace design, treatment and management of back disorders. There is no direct way of measuring spinal loads, and because of the invasive nature of indirect methods (i.e., intradiscal pressure measurements (Sato, Kikuchi, & Yonezawa, 1999; Wilke, Neef, Hinz, Seidel, & Claes, 2001; Wilke, Neef, Caimi, Hoogland, & Claes, 1999), instrumented vertebral replacements (Rohlmann, Gabel, Graichen, Bender, & Bergmann, 2007)), thus, musculoskeletal biomechanical models have long been recognized as viable alternatives.

CHAPTER 2 LITERATURE REVIEW

2.1 Musculoskeletal Biomechanical Models

Musculoskeletal models aim to determine muscle forces and joint loads, yet the redundancy problem poses as the main obstacle. Redundancy means that unknowns (muscle forces) outnumber available equations (equilibrium equations), so standard solution procedures cannot compute muscle forces. Instead, different algorithms have been developed to address the redundancy problem and to estimate muscle forces. There are two main algorithms to solve the dynamics of redundant systems (Otten, 2003); in the inverse dynamics method, motions are known and taken as inputs, and joint net internal loads (due to passive tissues and muscle forces) are calculated while in the forward dynamics, motions are calculated from some a-priori estimated muscle forces (Otten, 2003). To drive a musculoskeletal model in the forward dynamics approach, muscle forces can be estimated from recorded electromyography (EMG) in conjunction with a muscle model (e.g., Hill or Huxley muscle model (Hayashibe & Guiraud, 2013)) or from a control law (Happee, de Bruijn, Forbes, & van der Helm, 2017; Nikooyan, Veeger, Chadwick, Praagman, & van der Helm, 2011). In this section, I focus on the existing inverse dynamics musculoskeletal models based on their method of estimating muscle forces while neglecting irrelevant and less popular algorithms such as the stochastic methods (Lin et al., 2012; Mirka & Marras, 1993).

2.1.1 Reduction Method

This is the simplest method in which some muscles are neglected while others are combined into synergistic muscle groups. Due to the decrease in the number of unknowns (muscle forces), the redundant system is resolved into a deterministic problem and muscle forces can be calculated (Chaffin, 1969; Freivalds, Chaffin, Garg, & Lee, 1984; McGill & Norman, 1985; Schultz, Andersson, Örtengren, Björk, & Nordin, 1982). Spinal forces (compression and shear) are subsequently obtained in the post-processing stage by utilizing force equilibrium equations. Conceding numerous simplifying assumptions (e.g., using single joint models, neglecting or grouping muscles, etc.) takes its toll, and therefore, this method does not offer acceptable accuracy and robustness.

2.1.2 EMG-Driven Method

EMG-driven models use recorded EMG signals to drive the model while assuming that EMG signals are related to forces in muscles (Granata & Marras, 1995; Jia, Kim, & Nussbaum, 2011; van Dieën, Cholewicki, & Radebold, 2003). EMG-driven models are calibrated during maximal (Cholewicki, McGill, & Norman, 1995; Granata & Marras, 1993; McGill, 1992) or sub-maximal (Cholewicki, van Dieën, Lee, & Reeves, 2011; Dufour, Marras, & Knapik, 2013) exertions. This approach, however, has several shortcomings: 1- EMG-force equation is an empirical relation, 2- Calculated muscle forces do not necessarily satisfy equilibrium equations at various joints, 3- EMG-driven models utilize single-joint models causing erroneous results (Arjmand, Shirazi-Adl, & Parnianpour, 2007), 4- Recording EMG is limited to superficial muscles, time-consuming and costly (requires equipment), and 5- EMG signals are susceptible to contamination (e.g., cross-talk, power line noise). Nevertheless, EMG-driven models are considered biologic in accounting for antagonistic coactivation as well as intra- and inter-subject variabilities.

2.1.3 Optimization Method

To determine muscle forces, optimization-driven models assume that the central nervous system optimizes a cost function (or a combination of cost functions) (Arjmand & Shirazi-Adl, 2006c; Crowninshield & Brand, 1981; Dul, Johnson, Shiavi, & Townsend, 1984). Muscle forces cannot be determined arbitrarily, hence, the optimization problem is subjected to physiological and physical constraints (Christophy, Senan, Lotz, & O'Reilly, 2012; De Zee, Hansen, Wong, Rasmussen, & Simonsen, 2007; Ignasiak, Dendorfer, & Ferguson, 2016a; Khurelbaatar, Kim, & Kim, 2015). Various cost functions such as linear (Kaufman, Au, Litchy, & Chao, 1991), double-linear (Bean, Chaffin, & Schultz, 1988) and quadratic or cubic sum of muscle stresses (Bruno, Bouxsein, & Anderson, 2015) have been proposed, but in general, nonlinear cost functions provide more realistic results (Arjmand & Shirazi-Adl, 2006c; Bottasso, Prilutsky, Croce, Imberti, & Sartirana, 2006; Tsirakos, Baltzopoulos, & Bartlett, 1997). Unlike the EMG-driven method, the optimization method fully satisfies equilibrium equations and does not require EMG recording setup. Nevertheless, the approach does not automatically account for inter- and intra-subject variabilities and cannot predict antagonist muscle co-activities reported during various activities (El Ouaaid, Shirazi-Adl, Arjmand, & Plamondon, 2013a; Hughes & Chaffin, 1988; Raikova, 1999;

Stokes & Gardner-Morse, 2001). As a further shortcoming, the optimization method does not ensure spinal stability (Brown & Potvin, 2005; Stokes & Gardner-Morse, 2001) unless the stability criterion is considered as an additional constraint (Granata & Wilson, 2001; Hajihosseinali, Arjmand, Shirazi-Adl, Farahmand, & Ghiasi, 2014). This shortcoming, however, is shared by other methods as well. To circumvent the absence of antagonistic coactivity, some optimisation methods have set minimum non-zero positive thresholds for muscle activity or coactivity moments estimated based on recorded EMG data (El Ouaaid, Arjmand, Shirazi-Adl, & Parnianpour, 2009).

Among existing optimization-driven trunk models, kinematics-driven (KD) nonlinear finite element (FE) musculoskeletal model of the trunk has demonstrated its validity and predictive power in a broad range of applications from static (Arjmand & Shirazi-Adl, 2006a; El-Rich, Shirazi-Adl, & Arjmand, 2004) to dynamic (Bazrgari, Shirazi-Adl, & Kasra, 2008; Shahvarpour, Shirazi-Adl, Larivière, & Bazrgari, 2015b) and stability analyses (Bazrgari & Shirazi-Adl, 2007; El Ouaaid et al., 2009; Shahvarpour, Shirazi-Adl, Larivière, & Bazrgari, 2015a). It takes account of nonlinear passive properties of both ligamentous spine and muscles, muscle wrapping (Arjmand, Shirazi-Adl, & Bazrgari, 2006), all translational degrees of freedom (Ghezelbash, Arjmand, & Shirazi-Adl, 2015; Meng et al., 2015), physiological partitioning of gravity, inertia and damping at different segments and satisfaction of equilibrium conditions at all lumbar/thoracolumbar joints and directions (Arjmand et al., 2007). Moreover, it considers the stiffening role of compressive forces on passive responses of motion segments (Gardner-Morse & Stokes, 2004b; Shirazi-Adl, 2006). Above all, this approach is biologic in accounting as input data for measured trunk kinematics in various tasks.

2.1.4 Hybrid Method

The combination of EMG and optimization approaches constitutes a hybrid method which is alternatively called EMGAO (EMG Assisted by Optimization). Similar to EMG-driven models, this method initially uses EMG signals to estimate reference muscle forces; then, optimization is used to alter reference muscle forces so that altered values satisfy equilibrium equations. Though various cost functions have been proposed (Cholewicki & McGill, 1996; Mohammadi, Arjmand, & Shirazi-Adl, 2015; Vigouroux, Quaine, Labarre-Vila, & Moutet, 2006), all cost functions aim to make the least deviation from the reference values. Unlike the EMG-driven method, this approach

guarantees mechanical equilibrium, and unlike optimization-driven models, hybrid models predict antagonist co-activities. Many shortcomings of EMG-driven methods, listed earlier, exist here as well.

2.2 Model Scaling

Due to anthropometric differences between individuals, personalization or scaling schemes have been introduced in some model studies. For instance, imaging techniques have been used to reconstruct individual muscle geometries and bony structures (Gerus et al., 2013; Martelli, Kersh, & Pandy, 2015; Valente, Pitto, Stagni, & Taddei, 2015). This approach, though accurate, is however time-consuming, expensive and semi-automated. Alternatively, scaling factors (isotropic or anisotropic) have been employed for adaptation of generic models (Damsgaard, Rasmussen, Christensen, Surma, & de Zee, 2006; Delp et al., 2007; Rasmussen et al., 2005). Though being fast and automated, the method is heuristic with simplifications that can cause errors (Scheys, Spaepen, Suetens, & Jonkers, 2008). Using AnyBody Modelling System and the scaling technique, effect of changes in body weight, BW, (50-120 kg) and body height, BH, (150-200 cm) on spinal loads was investigated (Han, Rohlmann, Zander, & Taylor, 2013b). Although spinal loads altered nearly linearly with changes in both BW and BH but the effect of the former on response was found to be much greater than that of the latter. In this model study, linear scaling was used in the model geometry and muscle cross-sectional areas. The corresponding effects of personalized factors on spinal passive properties were not considered. Recently, an optimization-based scaling method for dynamic tasks that require motion capture measurements have been proposed (Lund, Andersen, de Zee, & Rasmussen, 2015). Hajihosseinali, Arjmand, and Shirazi-Adl (2015) developed an automated anisotropic scaling method where the geometry (area and lever arm) of each muscle was altered in accordance with available imaging data sets (Anderson, D'Agostino, Bruno, Manoharan, & Bouxsein, 2012) while accounting for variations only in the subject's BW. It is evident, hence, that a comprehensive, automated and accurate image-based method has not yet been introduced to personalize models. Moreover, existing scaling methods overlook expected crucial alterations in spinal passive properties as well as moment arms of muscles and gravity load at different levels as age, sex, BW and BH change.

Table 2.1. Comparing qualitative lifting tools

Parameter	*3DSSPP*	*HCBCF*	*McGill, Norman, and Cholewicki (1996)*	*Arjmand et al. (2012 and 2013)*	*AnyBody*
Equilibrium at all spinal levels	✗	✗	✓	✓	✓
Wrapping of muscles	✗	✗	✗	✓	✓*
Lumbar posture	✗	✗	✗	✓	✓
Trunk rotation	✓	✓	✗	✓	✓
Asymmetry in tasks	✓*	✗	✓	✓*	✓
Segmental degrees of freedom	✗	✗	✓*	✓	✓*
Comprehensive muscle architecture	✗	✗	✓	✓	✓
Passive ligamentous contribution	✗	✗	✓	✓	✓*
Compression force calculation	✓	✓*	✓*	✓	✓
Shear force calculation	✓	✗	✗	✓	✓
Subject body weight	✓*	✓	✗	✗	✓
Subject body height	✓*	✓	✗	✗	✓
Subject age	✗	✗	✗	✗	✗
Subject sex	✓	✓	✗	✗	✗
Physiological-based personalization	✗	✗	✗	✗	✗
Ease of use	✓*	✓	✓	✓	✗

✓: Accounted; ✗: Neglected; *: Limited

2.3 Lifting Analysis Tools

Due to complexities in trunk musculoskeletal models, ergonomists do not directly use musculoskeletal models to estimate spinal loads and evaluate associated risks in various activities. Ergonomists prefer instead other simple and available tools (e.g., interactive software, regression equations). Though being popular among ergonomists, 3DSSPP (University of Michigan, Center for Ergonomics) does not take account of muscle wrapping (Arjmand et al., 2006), translational degrees of freedom at spinal joints and a comprehensive muscle architecture. Furthermore, 3DSSPP does not satisfy equilibrium equations at all spinal levels.

In comparison with 3DSSPP, AnyBody Modelling System (Damsgaard et al., 2006) and OpenSim (Delp et al., 2007) are more advanced computer software. They benefit from a comprehensive muscle architecture, a muscle wrapping algorithm and multi-joint passive spine. Nonetheless, these programs neglect translational degrees of freedom at discs, fix center of rotation at each disc level, and the nonlinear behavior of the ligamentous spine. For model scaling, they utilize heuristic methods rather than physiological-based approaches (Rasmussen et al., 2005). Moreover, obtaining reasonably accurate results with these programs needs a high level of expertise.

Regression equations are simple and practical alternatives for those models and programs. McGill et al. (1996) proposed a third-order polynomial that calculates the L4-L5 compression in 3D tasks based on net moments in 3 anatomical planes. The third-order polynomial was fitted into the results of an EMGAO model including 90 muscle fascicles. As major shortcomings, the third-order polynomial is limited to the L4-L5 compression, overlooks shear forces and other spinal loads (Rajaee, Arjmand, Shirazi-Adl, Plamondon, & Schmidt, 2015), and dependent only on moments as input and not the position and orientation of external loads (El Ouaaid, Shirazi-Adl, & Plamondon, 2015). By using 3DSSPP (with all stated shortcomings) in 6000 lifting tasks, Merryweather, Loertscher, and Bloswick (2008) proposed a gender-specific hand-calculation back compressive force (HCBCF) model. The HCBCF model can predict the L5-S1 compression while overlooking shear forces and spinal levels elsewhere. Using the results of the KD-FE model along with the response surface method, Arjmand et al. (Arjmand, Plamondon, Shirazi-Adl, Lariviere, & Parnianpour, 2011; Arjmand, Plamondon, Shirazi-Adl, Parnianpour, & Larivière, 2012) proposed predictive equations for the calculation of spinal loads (shear and compression) at the L4-L5 and L5-S1 levels. The proposed equations, however, did not account for asymmetric postures although

considering asymmetric loads. As a common and major shortcoming among existing regression equations, effects of personal factor (i.e., BW, BH, age and sex) on spinal loads are neglected.

Results of web-based surveys showed that the National Institute of Occupational Safety and Health (NIOSH) equation is one the most popular tools among Canadian certified ergonomists (Pascual & Naqvi, 2008). The NIOSH lifting equation (NLE) provides ergonomists with a weight limit for a lifting activity (Waters, Putz-Anderson, Garg, & Fine, 1993). To estimate the weight limit, the NLE adjusts a 23 kg load by six factors (e.g., vertical travel distance of the lift, frequency of the lift). Although Waters et al. (1993) claimed that the recommended weight limit does not increase the risk of incurring back pain, Arjmand, Amini, Shirazi-Adl, Plamondon, and Parnianpour (2015) showed that the recommended weight limit can generate spinal loads beyond the safe limit (i.e., 3400 N in compression, recommended by NIOSH). Another available tool is Snook's lifting table (Snook & Ciriello, 1991). In contrast to existing biomechanical approaches and tools, Snook and Ciriello (1991) used psychophysical methodology to propose the lifting table. Snook's lifting table recommends a weight limit and does not estimate spinal loads. Both NLE and Snook's lifting table conceded many simplifying assumptions and did not use solid biomechanical methodologies.

2.4 Obesity

Obesity rates have been tripled in the past four decades, and by affecting more than 1.9 billion adults word-wide, it has reached a "global epidemic" proportion (WHO, 2016a). With the prevalence of 27% in Quebec and 40% in US, these high rates continue to rise in US, UK and Canada (Statistics Canada, 2019; Wang, McPherson, Marsh, Gortmaker, & Brown, 2011). Obesity has been recognized as one of the risk factors for the disc degeneration (Liuke et al., 2005; Takatalo et al., 2013), vertebral fracture (Paik et al., 2019) and back pain (Leboeuf–Yde, Kyvik, & Bruun, 1999; Shiri, Karppinen, Leino-Arjas, Solovieva, & Viikari-Juntura, 2009); nevertheless, underlying pathomechanics of foregoing problems are still unknown. Existing measures of obesity and adiposity (BMI and waist-to-hip ratio) overlook important individual differences among obese people such as variations in the distribution of adipose tissue along the body; therefore, individualized models should take into account such differences when investigating obesity.

2.5 Motion Segment Simulation Techniques

As one of the integral and influential components of a trunk musculoskeletal model, passive ligamentous spine should be simulated as accurately as possible especially under heavier tasks and at larger motions. Detailed FE models can capture nonlinear and time-dependent responses of the spine by using elastic, viscoelastic and poroelastic theories (Argoubi & Shirazi-Adl, 1996; Shirazi-Adl, Ahmed, & Shrivastava, 1986; Walter et al., 2014), but using detailed FE models in musculoskeletal models substantially increases the computational costs. Therefore, spherical joints with linear (Bassani, Stucovitz, Qian, Briguglio, & Galbusera, 2017; Ignasiak et al., 2016a) and nonlinear (Cholewicki & McGill, 1994, 1996) rotational springs or beams with linear (Stokes & Gardner-Morse, 2001) and nonlinear (Arjmand & Shirazi-Adl, 2005; Arjmand et al., 2006) passive properties are commonly used in musculoskeletal models. Although some studies have highlighted the importance of considering translational degrees of freedom in joints (Ghezelbash et al., 2015; Meng et al., 2015), and although many musculoskeletal models have employed either beams or spherical joints to simulate the passive ligamentous spine, the accuracy and validity of such simplified models in predicting spine kinematics, muscle forces and spinal loads have remained unknown.

2.6 Objectives

The foregoing literature review demonstrates that among available lifting analysis tools, some are very complicated to use while others have conceded multiple simplifications (Table 2.1) (Rajaee et al., 2015). Despite the fact that anthropometric factors affect spinal loads, no existing tool considers those factors by using a physiological-based method (Table 2.1). Consequently, no qualitative, subject-specific and accurate tool yet exists to assist the ergonomists in the accurate evaluation of injury risks during a lifting activity. Furthermore, although the prevalence of obesity as well as obesity related back pain are on the rise, no study has yet explored the likely effects of obesity and obesity shape on spine biomechanics. Additionally, musculoskeletal models commonly use simplified models (linear/nonlinear spherical-joints/beams) to represent passive ligamentous spine, but the performance of such elements to realistically replicate the kinematics and kinetics of spine remains unknown. Detailed objectives of this dissertation are hence set as follows:

- Upgrade the existing KD-FE model of the trunk (Arjmand & Shirazi-Adl, 2006a; Shahvarpour, Shirazi-Adl, & Larivière, 2016) by refining the muscle architecture and adding a new deformable thoracic level (T11-T12 disc).
- Scale (or personalize or individualize) the muscle anatomy (geometry and cross sectional area) and passive joint properties of the upgraded KD-FE model in accordance with the subject's BW, BH, sex and age.
- Validate this novel personalized KD-FE model by comparing its estimated muscle activities and intradiscal pressures (IDPs) with measured EMG signals and IDPs at various symmetric and asymmetric activities as well as maximum voluntary exertions.
- Carry out a comprehensive sensitivity analysis on independent input variables (BW, BH, sex and age) when estimating trunk muscle forces and spinal forces (as output variables) to identify the crucial independent variables.
- Explore likely effects of obesity and obesity shapes (i.e., different distribution of adipose tissue) on spinal loads, the risk of vertebral fracture and spinal stability.
- Investigate the relative performance of simplified models (i.e., spherical joints and shear deformable beams), the effects of using linearized passive properties (instead of the more accurate nonlinear properties), and the role of positioning of simplified models when predicting trunk kinematics and kinetics as well spinal loads and muscles forces.
- Analyse various symmetric/asymmetric lifts toward the development of appropriate user-friendly regression equations that estimate spinal loads for various anthropometry parameters, posture and weight magnitude/position.

2.7 Structure of the Dissertation

The structure of the dissertation is illustrated in Figure 2.1.

Figure 2.1 Structure of the dissertation

CHAPTER 3 ARTICLE 1: SUBJECT-SPECIFIC BIOMECHANICS OF TRUNK: MUSCULOSKELETAL SCALING, INTERNAL LOADS AND INTRADISCAL PRESSURE ESTIMATION

Authors: F. Ghezelbash, A. Shirazi-Adl, N. Arjmand, Z. El-Ouaaid, and A. Plamondon

Published in *Biomechanics and Modeling in Mechanobiology* 15.6 (2016): 1699-1712

3.1 Introduction

The role of biomechanical factors in low back pain (da Costa & Vieira, 2010; Ferguson & Marras, 1997; Heneweer, Staes, Aufdemkampe, van Rijn, & Vanhees, 2011) and disc degeneration (Adams & Roughley, 2006) has long been realized. Due to the invasive nature of *in vivo* attempts to estimate spinal loads via intradiscal pressure sensors (Nachemson, 1960; Sato et al., 1999; Schultz, Andersson, Ortengren, Haderspeck, & Nachemson, 1982; Wilke et al., 1999) and instrumented vertebral implants (Dreischarf et al., 2015a; Rohlmann et al., 2013b), musculoskeletal biomechanical models have emerged as essential, robust and accurate alternative and complementary tools (Reeves & Cholewicki, 2003).

In comparison to the existing optimization-driven (Christophy et al., 2012; De Zee et al., 2007; Khurelbaatar et al., 2015), EMG-driven (Granata & Marras, 1995; Jia et al., 2011; van Dieën et al., 2003) and hybrid (Cholewicki & McGill, 1996; Gagnon, Arjmand, Plamondon, Shirazi-Adl, & Larivière, 2011; Mohammadi et al., 2015) trunk models, our kinematics-driven (KD) nonlinear finite element (FE) musculoskeletal model of the trunk has demonstrated its validity and predictive power in a broad range of applications from static (Arjmand & Shirazi-Adl, 2006a; El-Rich et al., 2004) to dynamic (Bazrgari et al., 2008; Shahvarpour et al., 2015b) and stability analyses (Bazrgari & Shirazi-Adl, 2007; El Ouaaid et al., 2009; Shahvarpour et al., 2015a). It takes account of nonlinear passive properties of both ligamentous spine and muscles, muscle wrapping (Arjmand et al., 2006), all translational degrees of freedom (Ghezelbash et al., 2015; Meng et al., 2015), physiological partitioning of gravity, inertia and damping at different segments and satisfaction of equilibrium conditions at all lumbar/thoracolumbar joints and directions (Arjmand et al., 2007). Moreover, it considers the stiffening role of compressive forces on passive responses of motion segments (Gardner-Morse & Stokes, 2004b; Shirazi-Adl, 2006).

Due to anthropometric differences between individuals, personalization or scaling schemes have been introduced in some model studies. For instance, imaging techniques have been used to reconstruct individual muscles geometry and bony structures (Gerus et al., 2013; Martelli et al., 2015; Valente et al., 2015). This approach, though accurate, is however time-consuming, expensive and semi-automated. Alternatively, scaling factors (isotropic or anisotropic) have been employed for model adaptation (Damsgaard et al., 2006; Delp et al., 2007; Rasmussen et al., 2005). Though being fast and automated, the method is heuristic with simplifications that can cause errors (Scheys et al., 2008). Using AnyBody Modelling System and the scaling technique, effect of changes in body weight, BW, (50-120 kg) and body height, BH, (150-200 cm) on spinal loads was investigated (Han et al., 2013b). Although spinal loads altered nearly linearly with changes in both BW and BH but the effect of the former on response was found to be much greater than that of the latter. In this model study, linear scaling was used in the model geometry and muscle cross-sectional areas. The corresponding effects of personal factors on spinal passive properties were not simulated. Recently, an optimization-based scaling method for dynamic tasks that require motion capture measurements have been proposed (Lund et al., 2015). Hajihosseinali et al. (2015) developed an automated anisotropic scaling method where the geometry (area and lever arm) of each muscle was altered in accordance with imaging data sets (Anderson et al., 2012) while accounting for variations only in the subject's BW. It is evident, hence, that a comprehensive, automated and accurate image-based method has not yet been introduced to personalize models. Moreover, existing scaling methods overlook expected crucial alterations in spinal passive properties as well as moment arms of muscles and gravity load at different levels as age, sex, BW and BH change.

Moreover and due to the importance of validation of model predictions and existence of *in vivo* data on the intradiscal pressure (IDP) during various activities (Nachemson, 1960; Sato et al., 1999; Wilke et al., 2001), it is important to compare estimated spinal compression forces to the corresponding IDP values measured *in vivo*. Shirazi-Adl and Drouin (1988) reported the effect of the axial compression when combined with some flexion moment on IDP at the L2-L3 level while Dreischarf, Rohlmann, Zhu, Schmidt, and Zander (2013) proposed a correction factor when estimating IDP from the compression force and L4-L5 disc area. Despite earlier attempts and based on results of a validated lumbar spine model under single and combined sagittal plane loading

(Shirazi-Adl, 2006), it is crucial to develop a comprehensive nonlinear regression equation relating the L4-L5 IDP not only to the compression force but the sagittal rotation as well.

The objectives of this study are, therefore, set to update and personalize, apply and validate the existing iterative nonlinear KD-FE model as well as to develop a nonlinear regression equation for compression force-sagittal rotation-IDP relation. For the former, following improvements are made: 1- The muscle architecture is extended, 2- A new technique of modeling rectus sheath and abdominal muscles is developed, 3- An additional deformable intervertebral disc (T11-T12) is added, and 4- A generic method to personalize the model based on BW, BH, age and sex is introduced. The presented method accounts for changes in both muscle geometries (length, area and lever arm) and passive properties of joints. A nonlinear regression equation is subsequently developed to estimate IDP as a function of the compression and the sagittal intersegmental angle. Estimated compression and muscle forces are validated by comparison with available *in vivo* measurements (Arjmand, Gagnon, Plamondon, Shirazi-Adl, & Lariviere, 2010; El Ouaaid, Shirazi-Adl, Plamondon, & Larivière, 2013b; Wilke et al., 2001).

3.2 Methods

3.2.1 Finite Element Model

A sagittally symmetric FE model of the spine (T1-S1), representing bony structures and soft tissues, is reconstructed in Abaqus (Simulia Inc., Providence, RI, USA). Original nodal coordinates are used for the spinal geometry (Figure 3.1) (Kiefer, Shirazi-Adl, & Parnianpour, 1998; Shirazi-Adl, El-Rich, Pop, & Parnianpour, 2005). Nonlinear passive responses of seven lower motion segments (including vertebrae, discs, facets and ligaments) are modeled by Timoshenko beam elements with quadratic displacement fields. In addition to T12-S1 motion segments with nonlinear passive properties (moment-curvature and force-strain) at three physiological planes (Figure 3.2) (Bazrgari, 2008; Shirazi-Adl, 1994a, 2006), the T11-T12 motion segment is also added with passive properties based on those of the T12-L1 motion segment (Oxland, Lin, & Panjabi, 1992) modulated according to their respective disc area and height using conventional beam theory. Furthermore, bending properties of the T11-T12 motion segment are subsequently increased by 20% to account for the rib cage stiffness (Brasiliense et al., 2011; Watkins et al., 2005). Deformable

beam elements are shifted 4 mm posteriorly to partially account for changes in the center of rotation under loads (Shirazi-Adl et al., 1986). Vertebrae and remaining T1-T11 motion segments are modeled by rigid elements. Trunk weight is distributed eccentrically and applied via rigid links to corresponding vertebrae (Pearsall, 1994); additionally, weights of upper arms, lower arms and head are applied at their centers of mass (De Leva, 1996).

3.2.2 Muscle Architecture and Wrapping

The existing muscle architecture (Arjmand & Shirazi-Adl, 2006b; El-Rich et al., 2004; Shirazi-Adl et al., 2005) is revised for the current study. New global fascicles of the longissimus and iliocostalis are added due to the addition of the T11-T12 motion segment (Stokes & Gardner-Morse, 1999). Muscle architecture of the quadratus lumborum and multifidus is refined by the addition of local and inter-segmental fascicles (Phillips, Mercer, & Bogduk, 2008; Stokes & Gardner-Morse, 1999). The intersegmental spinalis muscle is also introduced (Delp, Suryanarayanan, Murray, Uhlir, & Triolo, 2001; Gilroy et al., 2008). Furthermore, the geometry of abdominal muscles (rectus abdominis, internal oblique and external oblique) is updated (Stokes & Gardner-Morse, 1999) accounting for the geometry of the rib cage (Gayzik, Mao, Danelson, Slice, & Stitzel, 2008). The new sagittally-symmetric muscle architecture includes 126 muscles (Figure 3.1).

Muscles as deformable bodies develop contact forces with surrounding tissues and change line of action when wrap around vertebrae during trunk movements. This wrapping contact phenomenon is simulated by an algorithm which accounts both for the curved paths of the global extensor muscles as well as their contact forces (Arjmand et al., 2006).

3.2.3 Rectus Sheath

Some fascicles of the internal and external obliques are attached to the semilunar line (Brown, Ward, Cook, & Lieber, 2011; McGill, 1996). According to the muscle architecture, the uppermost fascicles of the external oblique and the lowermost fascicles of the internal oblique are inserted into the rectus sheaths (see Figure 3.1). The rectus sheaths, modelled separately on the left and the right side of RA, transfer tensile forces of muscle fascicles attached to them directly to the rib cage and pelvic bone. Forces of corresponding fascicles (F_{EO} and F_{IO}, Figure 3.1) are projected onto the rectus sheaths ($F_{EO}^{\parallel}$ and $F_{IO}^{\parallel}$, Figure 3.1) while remaining components ($F_{EO}^{\perp}$ and $F_{IO}^{\perp}$, Figure 3.1) on

both sides of rectus abdominis partially cancel each other in symmetric lifts or are assumed in general (symmetric and asymmetric lifts) to be counterbalanced by forces in transverse abdominal muscle (neglected in the current model) and intra-abdominal pressure (IAP). Besides, the upper rectus sheaths can transfer tension only; the projected force of the internal oblique minus that of the external oblique on the rectus sheath must be positive on each side pulling the rib cage downward ($F_{IO}^{\parallel} - F_{EO}^{\parallel} \geq 0$).

3.2.4 Muscle Force Calculation

For each iteration, known measured segmental and pelvic rotations (or equivalently angular velocities in dynamic simulations), $\boldsymbol{\omega}_i$ where $i \in \mathcal{I} \coloneqq \{T11, \dots, S1\}$, are iteratively prescribed into the FE model and associated required moments are used as equality equilibrium equations when estimating muscle forces (Eq. 3.1, see also the flowchart in Figure 3.3). Due to redundancy, an optimization algorithm with the cost function of quadratic sum of muscle stresses is used (Arjmand & Shirazi-Adl, 2006c) with equilibrium equations applied as equality constraints:

$$\sum_{\boldsymbol{i}} \left(\boldsymbol{r}_i^j - \boldsymbol{O}^j\right) \times \boldsymbol{f}_i^j = \boldsymbol{m}^j, \qquad \text{Eq. 3.1}$$

where $j \in \mathcal{J}$; $\boldsymbol{f}_i^j$ is the force vector of a muscle fascicle which is attached to the j^{th} vertebra. $\boldsymbol{r}_i^j$ and $\boldsymbol{O}^j$ are position vectors of the corresponding muscle force and j^{th} vertebra, respectively. Also, $\boldsymbol{m}^j$ is the required moment at j^{th} level evaluated iteratively by the nonlinear FE model. Besides, muscle forces are constrained to be positive and greater than their passive forces (Davis, Kaufman, & Lieber, 2003) and smaller than the sum of maximum active forces, 0.6 MPa × PCSA (physiological cross sectional area) (Winter, 2009), plus the passive forces. In more demanding activities simulated in this study such as tasks 3, 8 and 10-12 (Table 3.1), the maximum stress of 0.6 MPa was increased to 1.0 MPa to avoid excessive constraint on some muscle forces.

For the subsequent iterations, the updated muscle forces are applied onto their vertebrae as additional penalty forces and the analysis is repeated till convergence reached (no or < 1% changes in muscle forces between two successive iterations).

3.2.5 Simulated Tasks

The performance of the model is investigated in a number of tasks and estimated spinal loads and muscle activities are compared with corresponding measured IDPs and EMG data when available. IDPs in relaxed upright standing, flexed postures, asymmetric lifting and lateral bending are compared with *in vivo* measurements (Wilke et al., 2001). Furthermore, measured EMG activities (Arjmand et al., 2010; El Ouaaid et al., 2013b) are compared with estimated muscle activities during forward flexion and maximum voluntary exertions (MVEs) in flexion, extension and twisting (see Table 3.1).

3.2.6 Prescribed Rotations

To initially establish the upright standing posture under gravity alone as the reference condition in all tasks, prescribed rotations from the initial undeformed configuration are obtained from the following optimization problem (Shirazi-Adl, Sadouk, Parnianpour, Pop, & El-Rich, 2002):

$$\min_{\Omega} \sum_{i \in \mathcal{I}} \left| \boldsymbol{m}^{\boldsymbol{i}}(\Omega) \right| \qquad \text{Eq. 3.2}$$

where $\boldsymbol{m}$ is the required moment vector and $\Omega \coloneqq \{\boldsymbol{\omega}_{\alpha} | \, \alpha \in \mathcal{I}\}$. The initial guess, Ω_0, is made manually, and upper and lower bounds of the optimization problem are assumed to be $\pm 5°$ of Ω_0. The foregoing optimization problem is solved for each subject after the scaling (see the following section for scaling). In task 8, the trunk is rotated 5^{o} toward flexion in accordance with (Wilke et al., 2001), and in task 3, the following rotations are prescribed onto the undeformed initial posture (El-Rich & Shirazi-Adl, 2005) in accordance with (Wilke et al., 2001): -2.0^{o} at T11, 4.0^{o} at T12, 10.9^{o} at L1, 15.8^{o}, at L2, 14.5^{o} at L3, 9.9^{o} at L4 at, 4.9^{o} at L5, and 4.9^{o} at S1 where positive values are extension.

In flexion (tasks 4-7 in Table 3.1), the lumbopelvic rhythm is taken from *in vivo* measurements (Arjmand, Gagnon, Plamondon, Shirazi-Adl, & Lariviere, 2009; Arjmand et al., 2010). The total T11-S1 rotation, is then partitioned among T11-L5 vertebrae with 6.0% for T11-T12, 10.9% for T12-L1, 14.1% for L1-L2, 13.2% for L2-L3, 16.9% for L3-L4, 20.1% for L4-L5, and 18.7% for L5-S1 (Arjmand et al., 2009, 2010; Gercek et al., 2008; Hajibozorgi & Arjmand, 2015).

In lateral bending tasks (task 9 in Table 3.1), rotation proportions for the T11-T12 down to the L5-S1 levels are set to be 8.3%, 2.8%, 9.4%, 18.3%, 22.8%, 25.6% and 12.8%, respectively (Gercek et al., 2008; Rozumalski et al., 2008; Shirazi-Adl, 1994a). In accordance with (Paterson & Burn, 2012), the sacral lateral rotation varies linearly from 0^o to 2^o as the trunk lateral rotation reaches 20^o of lateral bending.

For extension and flexion MVE tasks rotations of 9^o and -13^o at the T11 and 16^o and 13^o at the S1 (positive: extension) are considered, respectively. These rotations are subsequently partitioned between the vertebrae (T11-S1) in accordance with aforementioned flexion rotation proportions. It is to be noted that the earlier proposed rotations (El Ouaaid et al., 2013b) were altered slightly when simulating semi-seated posture in the current model.

3.2.7 Model Scaling

Model scaling (personalization) is required since subjects with different individual parameters, i.e., sex, age, BH and BW, participated in various experimental studies (Arjmand et al., 2009, 2010; El Ouaaid et al., 2013b; Wilke et al., 2001). Biomechanical principles in conjunction with regression equations, derived from medical imaging databases (Anderson et al., 2012; Shi et al., 2014), are employed. Inputs of regression equations are the subject's personal parameters (sex, age, BW and BH). To find the reference personal parameters that best match with the reported regression equations (Anderson et al., 2012), a least absolute deviation (LAD) problem is initially solved:

$$\min_{\mathrm{F}} \left[\sum_{i \in \mathcal{M}} \left(\left| {}^{i}\overline{AP}^{Model} - {}^{i}\overline{AP}^{Reg}(F) \right| + \left| {}^{i}\overline{ML}^{Model} - {}^{i}\overline{ML}^{Reg}(F) \right| \right) \right], \qquad \text{Eq. 3.3}$$

where F is the personal parameter vector, $\mathrm{F} = [\mathrm{sex}, \mathrm{age}, \mathrm{BH}, \mathrm{BW}]$; $\mathcal{M}$ is the set containing all muscle groups, $\mathcal{M} \coloneqq \{\text{rectus abdominis}, \text{external oblique}, \dots, \text{longissimus}\}$. ${}^{i}\overline{AP}$ and ${}^{i}\overline{ML}$ denote average anterior-posterior and medio-lateral distances of i^{th} muscle ($i \in \mathcal{M}$) from vertebrae. $Model$ and Reg superscripts represent distances calculated in the reference model from the muscle architecture (Figure 3.1), and distances obtained from regression equations (Anderson et al., 2012), respectively. Results of the optimization process is sensitive to the lower bound of BH. Hence, 173 cm is assigned as the lower bound of BH because it is not rational that spine length

to BH becomes larger than 0.27 (estimated based on Keller, Colloca, Harrison, Harrison, and Janik (2005)).

Afterward, coordinates of the vertebrae, discs, head and arms alter proportionally with changes in BH (e.g., $(x, y, z)_{spine} \propto \mathrm{BH}/\mathrm{BH}_{\mathrm{Ref}}$, where $\mathrm{BH}_{\mathrm{Ref}}$ is obtained from Eq. 3.3). For the muscle architecture, z-coordinates (cranial-caudal) remain proportional to BH (e.g., $z_{Rectus\ Abdominis} \propto \mathrm{BH}/\mathrm{BH}_{\mathrm{Ref}}$). To adjust anterior-posterior and medio-lateral distances as well as PCSAs, the regression equations (Anderson et al., 2012) are first normalized to their reference counterparts (calculated from the reference personal parameters). Then, for the subject-specific model, the average anterior-posterior distances from vertebrae normalized to the reference values (Figure 3.1) are adapted according to the normalized regression equations. Similar process is performed for medio-lateral distances and PCSAs.

Furthermore, we utilize the conventional beam theory to alter passive joint properties (compression force-strain and moment-curvature relations). Three beam (or disc) parameters are used: 1- height, 2- area and 3- area moments. The disc height is assumed to be commensurate with BH (disc height $\propto \mathrm{BH}/\mathrm{BH}_{\mathrm{Ref}}$) (Han et al. 2013), and the disc area is changed in accordance with A/A_{Ref}, in which A is the maximum cross sectional area of the rib cage in the transverse plane for a given set of personal parameters (Shi et al., 2014); and A_{Ref} is the maximum cross sectional area of the rib cage in the transverse plane for the reference personal parameters (disc area $\propto A/A_{Ref}$) (Shi et al., 2014). Additionally, area moments are assumed to be proportional to the disc area squared (area moments $\propto \left(A/A_{Ref}\right)^2$).

3.2.8 Intra-Abdominal Pressure

Intra-abdominal pressure (IAP) is simulated in MVE tasks with concurrent activity in abdominal muscles. IAP is modeled as a follower load normal to the diaphragm reaching 10 kPa and 25 kPa (El Ouaaid et al., 2013b) while the diaphragm area is modified based on (Shi et al., 2014). The resultant force is transmitted to the T11 via a rigid link with an anterior lever arm of 5 cm (Arjmand & Shirazi-Adl, 2006b).

3.2.9 External Loads

In tasks 1-7 (Table 3.1), positions of upper arms, lower arms, head and the external load in hands are based on measurements. For asymmetric lifting (task 8), the external load is taken at 34 cm lateral and 0 cm anterior-posterior to the L5-S1 disc (Rajaee et al., 2015). A concentrated force applied at the T8 (task 10) or T6 (task 11) simulates MVE in extension or flexion, respectively (El Ouaaid et al., 2013). In the task 12 (Table 3.1), 78.3 Nm right axial torque with 21.1 right lateral and 16.7 flexion coupled moments are simultaneously applied at the T9 (Arjmand, Shirazi-Adl, & Parnianpour, 2008b; Ng, Parnianpour, Richardson, & Kippers, 2001; Ng, Richardson, Parnianpour, & Kippers, 2002).

3.2.10 IDP Estimation

A novel nonlinear regression equation for estimating IDP in the model is developed in this study. Inputs of this model are the compressive force (applied by a wrapping element) and the intersegmental rotation (under various sagittal moments) at the L4-L5 disc taken based on unpublished results (4 compressions levels at 16 intersegmental rotations each) of a validated lumbar spine FE model (Shirazi-Adl, 1994a, 1994b; Shirazi-Adl & Pamianpour, 1993). The quadratic regression equation is developed relating model output (i.e., IDP) to its inputs being compression force and sagittal rotation at the L4-L5 level.

3.2.11 Additional Constraints

A set of constraints is introduced for task 11 (see Table 3.1) to reduce excessively large required flexion moments at lumbar levels (Bazrgari, Shirazi-Adl, & Parnianpour, 2009; El Ouaaid et al., 2013b):

$$\sum \boldsymbol{f}_i^{T11} . \boldsymbol{t}_{AP}^{T11} = F_S^{T11}, \qquad \text{Eq. 3.4a}$$

$$\left[\sum \boldsymbol{f}_i^{T11} + \sum \boldsymbol{f}_i^{T12}\right] . \boldsymbol{t}_{AP}^{T12} = F_S^{T12}, \qquad \text{Eq. 3.4b}$$

where $\boldsymbol{f}_i^{T11}$ and $\boldsymbol{f}_i^{T12}$ denote muscle force vectors at the T11 and T12. $\boldsymbol{t}_{AP}^{T11}$ and $\boldsymbol{t}_{AP}^{T12}$ are unit vectors pointing toward anterior-posterior shear direction at the center of T11 and T12. F_S^{T11} and F_S^{T12}

represent required shear forces at the T11 and T12 levels to diminish flexion moments at local lumbar levels (Bazrgari et al., 2009); minimal values of F_S^{T11} and F_S^{T12} are found iteratively. In addition and based on recorded EMG at antagonist muscles (El Ouaaid et al., 2013), coactivation of antagonist muscles at flexion and extension MVE tasks are generated via additional constraints:

$$\sum_{a \in \mathcal{A}} (\boldsymbol{r}_a^{T11} - \boldsymbol{O}^{T11}) \times \boldsymbol{f}_a^{T11} = \boldsymbol{m}_A, \qquad \text{Eq. 3.5}$$

where $\mathcal{A}$ is the set including antagonist muscles attached to the T11, and $\boldsymbol{m}_A$ is the assumed antagonist moment generated antagonist muscles. It is to be noted that due to the symmetry in flexion and extension MVE tasks, only sagittal component of Eq. 3.5 is considered in this study.

3.3 Results

3.3.1 IDP Regression Equation

Regression analysis using unpublished results of the detailed FE model of the lumbar spine (Shirazi-Adl, 2006) for the L4-L5 motion segment yields the following quadratic equation:

$$\begin{aligned} \mathrm{IDP}(P,\theta) = {} & -1.556 \times 10^{-2} + 1.255P + 1.243 \times 10^{-2}\theta + 3.988 \times 10^{-2}P^2 \\ & - 1.212 \times 10^{-2}P\theta + 1.669 \times 10^{-3}\theta^2, \end{aligned} \qquad \text{Eq. 3.6}$$

where P (MPa) is the nominal pressure (compression/total disc cross sectional area) and θ (°, positive in flexion) is the intersegmental flexion rotation. The coefficient of determination, R^2, and root mean squared error (RMSE) of the regression equation are respectively 0.999 and 0.025 MPa showing the goodness of fit. It is noteworthy that we derived the appropriate set of data (P, θ) from (compression, θ) by considering the disc area of 1455 mm^2 (Shirazi-Adl, 1994a). Results of the detailed FE model (Shirazi-Adl, 2006), Eq. 3.6, Shirazi-Adl and Drouin (1988) under pure compresion, and Dreischarf et al. (2013) show differences that grow with the applied compression and segmental rotation (Figure 3.4). Hereafter, Eq. 3.6 is employed for IDP estimations.

3.3.2 Upright Neutral Standing Posture

Solving the optimization of required moments (Eq. 3.2) to set the upright neutral standing posture under gravity for 4 different personal parameters that are used in this study leads to sagittal rotations (from the initial unloaded geometry) presented in Table 3.2 using the reference personal parameters (Eq. 3.3) as sex = male, age = 41.8 year, BH = 173.0 cm, and BW = 75.1 kg.

3.3.3 Validation

For the simulated tasks, the correlation coefficient and RMSE between measured (Wilke et al., 2001) and estimated IDPs (Figure 3.5) are 0.984 and 0.14 MPa, respectively, demonstrating satisfactory IDP predictions both pattern-wise and magnitude-wise. In forward flexion (task 7), estimated activities of global longissimus and iliocostalis muscles follow trends similar to the measured EMG signals (Arjmand et al., 2010) (Figure 3.6a) and showing flexion relaxation phenomenon. The substantial drop in active force components accompany reverse trends in passive forces of these global extensor muscles as trunk flexion reaches its peak of 107^{o} (Figure 3.6b). At this full flexion, curved trajectory and large wrapping forces at different levels are computed in both global extensor muscles (Figure 3.6c).

Good agreement is also found in MVE tasks in extension under 242 Nm (Figure 3.7a) and in flexion under 151 Nm (Figure 3.7b) when comparing estimations of the model (personalized based on averaged parameters of all 12 subjects) versus mean of recorded EMG in 12 male subjects (with the average age, BW and BH of 25 years, 72.98 kg and 177.67 cm) for superficial back and abdominal muscles (El Ouaaid et al., 2013b). Applied IAPs, antagonistic coactivation moments (Eq. 3.5) and shear forces (Eq. 3.4) as well as correlation coefficients between estimated and measured muscle activities for MVE tasks are listed in Table 3.3. Additionally and under the reference upright posture, good agreements are noted in estimated muscle activities versus measured ones (Ng et al., 2001) on right (Figure 3.8a) and left (Figure 3.8b) sides for MVE in torsion.

3.3.4 Effects of Personal Parameters

The effect of changes in personalized parameters of subjects in earlier works (Arjmand et al., 2010; El Ouaaid et al., 2013b; Ng et al., 2002; Wilke et al., 2001) that are simulated here in this study on

compression and shear forces at the L4-L5 level is investigated (Figure 3.9) during forward flexion (task 7). Despite relatively small differences especially in BW (68-73 kg range) and BH (1.75-1.80 m range), relatively large differences are computed at larger flexion angles reaching peak differences of 21% in compression and 30% in shear.

3.4 Discussion

This study aimed to (1) markedly improve and personalize an existing trunk KD-FE musculoskeletal model and (2) develop a nonlinear regression equation to estimate IDP at the L4-L5 level as a function of its segmental compression force and sagittal rotation. The T11-T12 segment was added as a deformable body, the muscle architecture was updated with additional uni- and bi-articular muscles and a new model for the rectus sheath, and finally a novel automated scaling method was incorporated to personalize the entire model as subject sex, age, BW and BH change. This scaling framework modifies muscles geometry (i.e., length, area and lever arms), bony structures and passive joint properties. The personalized model was applied to a number of tasks and satisfactory agreement was found between predicted spinal IDPs and muscle activities with corresponding *in vivo* measurements (Arjmand et al., 2010; El Ouaaid et al., 2013b; Ng et al., 2002; Wilke et al., 2001).

3.4.1 Limitations and Methodological Issues

Since the model is driven by kinematics at different T11-S1 levels, the accuracy of measurements with motion capture camera systems and skin markers (due to the unavoidable inter skin-vertebrae and inter marker-skin movements) and subsequent partitioning of relative trunk-pelvis rotations among intervening T11-S1 levels remain of concern (Arjmand et al., 2010; Arjmand & Shirazi-Adl, 2006a; El-Rich et al., 2004). To be consistent with our pervious publications, we assumed maximum muscle stresses were 0.6 MPa despite using 1.0 MPa for demanding tasks. Stiffening the bending properties of the T11-T12 motion segment by 20% was assumed based on cadaver studies on the whole (Watkins et al., 2005) and upper (Brasiliense et al., 2011) thoracic spine as well as the consideration of a floating rib at this level. While IAP was simulated with a normal load to the diaphragm, the detailed mechanism relating the generated pressure to activity in surrounding abdominal muscles was not considered (Arjmand & Shirazi-Adl, 2006b). Likely effects of inter-

subject changes in initial spinal alignment and lordosis on results were neglected. Despite other imaging studies that report personalized moment arms and PCSAs (Chaffin, Redfern, Erig, & Goldstein, 1990; Jorgensen, Marras, Granata, & Wiand, 2001; Seo, Lee, & Kusaka, 2003; Wood, Pearsall, Ross, & Reid, 1996), we used here the data sets of Anderson et al. (2012) as they are comprehensive (100 females and males), not limited to the lumbar region and provide required regression equations accounting for sex, age, BH and BW; nevertheless, the R^2 value is low for some of the reported regression equations. Utilizing the conventional beam theory as the scaling rule for passive joint properties, though plausible, involves some approximations. It is to be noted that a detailed FE model of the spine can address this scaling issue, nonetheless, the computational burden would be significant. In personalization of the model, disc heights were assumed to change proportionally to the BH. Although no study has yet investigated the correlation between BH and disc heights, experimental (Dimitriadis et al., 2011) and modeling (Han et al., 2013b) studies indirectly support our relation. Despite studies suggesting the effect of obesity (that can be interpreted as BW) (Lidar et al., 2012; Urquhart et al., 2014) and aging (Videman, Battié, Gibbons, & Gill, 2014) on disc heights, we did not adjust disc heights as BW and age vary. For BW, however and due to associated increase in compression on discs, disc heights reduce more in heavier subjects. In older subjects, aging causes disc height loss (Videman et al., 2014) which should yield lower BH. Since we adjust disc heights with BH, the model accounts though indirectly for aging effects on disc heights. Disc areas were assumed to vary proportional to the area of the rib cage since no study has quantified the effects of changes in BH and BW on disc areas. Furthermore, in the development of the IDP regression equations, although the compression was normalized to the disc total cross-sectional area but this latter was constant in corresponding analyses. The disc total area and individual nucleus and annulus areas could play a role. Finally future sensitivity analyses should shed light on the relative effect of changes in various individual parameters on model predictions.

3.4.2 Data Analysis and Interpretation

Comparing estimated IDPs of a musculoskeletal model with measurements is frequently used for validation (Bruno et al., 2015; Han, Zander, Taylor, & Rohlmann, 2012; Mohammadi et al., 2015; Rajaee et al., 2015; Senteler, Weisse, Rothenfluh, & Snedeker, 2015). Although some studies

(Dreischarf et al., 2013; Shirazi-Adl & Drouin, 1988) provided a tool for such estimations, none explicitly incorporated the effect of intersegmental rotations, θ. Due to this simplification, those relations predict identical IDP for different values of θ (Figure 3.4). For instance, under pure moment with no axial force, no IDP is hence estimated in direct contrast to measurements and predictions. Furthermore, the effect of θ on the IDP is found to depend on the compression force as it diminishes at larger axial forces (Figure 3.4). Consequently, the intersegmental angle may be neglected with little loss of accuracy only at much larger compression forces. It is noteworthy that Shirazi-Adl and Drouin (1988) carried out simulations only on an L2-L3 motion segment. The FE model of (Shirazi-Adl, 2006) has smaller disc area (1455 mm^2) but larger nucleus area (653 mm^2) in comparison with those of (Dreischarf et al., 2013) (1480 mm^2 and 624 mm^2).

Validation of model predictions were performed under numerous tasks for which either IDP was available or surface EMG were collected in earlier studies. In addition, the considerations of forward flexion postures on the one hand and MVE tasks on the other were deliberately made to investigate the relative accuracy of both passive and active components in the model under diverse sets of large loads and movements. Results overall demonstrated satisfactory agreements in estimated IDP and hence associated muscle forces and spinal compression, flexion relaxation under large forward flexion angles, maximum strength in different planes, wrapping of global extensor muscles and activities of antagonist muscles. Some differences can be due to technical EMG issues such as electrode placement and crosstalk (Soderberg & Knutson, 2000; Türker, 1993) or the model limitations.

Detailed finite element studies of spinal motion segments (Meijer, Homminga, Veldhuizen, & Verkerke, 2011; Natarajan & Andersson, 1999; Niemeyer, Wilke, & Schmidt, 2012) and intervertebral discs (Cappetti, Naddeo, Naddeo, & Solitro, 2015) have demonstrated the substantial role of disc height and area in joint passive responses. Hence, to scale passive properties, we employed here the conventional beam theory that also yields results in general agreement with those based on the parametric FE model studies of the L3-L4 motion segment (Natarajan & Andersson, 1999). According to the proposed scaling scheme, variations in both disc height and disc area affect passive segmental stiffness. As an example, in comparison with the reference properties (Figure 3.2), angular and linear (axial) segmental stiffness values of a male subject with

BMI=25 kg/m^2 (the reference value) decreases by ~5% and 6% at shorter BH=160 cm but increases by ~8% and 9% at taller BH=190 cm, respectively.

The developed scaling method employed regression equations reported in imaging studies (Anderson et al., 2012; Shi et al., 2014) and biomechanical principles to modify the musculature and passive joint properties in the subject-specific models. The regression equations can present mean values for a cohort of subjects with the same sex, age, BW and BH. With these regression equations employed in our scaling, a cohort-specific trunk model is therefore generated in this work. In this study and for meaningful comparisons, we personalized the model for each simulation in accordance with the reported personal parameters of *in vivo* studies. Finally as a preliminary study to investigate the effect of changes in age, sex, BW and BH on results, forward flexion of 4 different subjects were considered (Figure 3.9). Despite relatively small changes in these parameters (i.e., 68-73 kg for BW, 1.74-1.80 cm for BH and 25-52 years for age), relatively large differences in spinal forces were estimated especially at larger trunk flexion angles. Maximum increases of 21% (410 N) in compression and 30% (72 N) in shear forces were found when the subject BH and BW increased only slightly from 1.75 m and 68 kg respectively to 1.80 m and 73 kg revealing the importance of the scaling. Utilizing a scaling algorithm along with the musculoskeletal modeling is therefore recommended in order to estimate more accurate results for individuals in a general population. Future studies will consider additional cases covering a comprehensive population with focus on the relative effect of greater changes in age, BW or BH when considered alone or combined.

In summary, we have presented a comprehensive personalized musculoskeletal trunk model and a novel regression equation relating IDP to normalized compression and sagittal rotation at the L4-L5 level. The model is an updated version of an existing one by adding a flexible level (T11-T12), extending muscle architecture and introducing the scaling concept. The described scaling framework modified muscles geometry and bony structures. Instead of personalizing solely geometric features, the scaling scheme altered passive joint properties as well for the first time. Moreover, by employing a detail FE model of the lumbar spine, we proposed a regression equation to estimate IDP at the L4-L5 disc as a function of the compression and the intersegmental angle. Predicted results were found in satisfactory agreement with reported IDP and surface EMG data under a number of tasks. Due to marked effects of personal parameters (e.g., stature, body weight)

on results of musculoskeletal models, future model studies should incorporate comprehensive scaling techniques for more accurate estimation of spinal forces and muscle activity.

3.5 Acknowledgements

This work was supported by the Institut de recherche Robert-Sauvé en santé et en sécurité du travail (IRSST-2014-0009) and the Natural Sciences and Engineering Research Council of Canada (RGPIN5596).

Table 3.1 Description of all simulated tasks

No.	*Description*
1	Standing relaxed posture with no load in hands
2	Standing posture while holding a 19.8 kg close to the body (Arjmand et al., 2011; Wilke et al., 2001)
3	Standing posture while holding a 19.8 kg away from the body (Arjmand et al., 2011; Wilke et al., 2001)
4	Trunk flexion at 50^o with no load in hands (Arjmand et al., 2011; Wilke et al., 2001)
5	Full trunk flexion (107.3^o) with no load in hands (Arjmand et al., 2011; Wilke et al., 2001)
6	Trunk flexion at 70^o with 19.8 kg load in hands (Arjmand et al., 2011; Wilke et al., 2001)
7	Forward flexion from the upright posture at 10^o intervals (Arjmand et al., 2009, 2010)
8	One-handed asymmetric lifting of 19.8 kg load (Rajaee et al., 2015)
9	Trunk lateral bendings at 10^o and 20^o with no load in hands (Wilke et al., 2001)
10	Maximum voluntary exertion (MVE) in extension under 242 Nm* extension moment (El Ouaaid et al., 2013b)
11	Maximum voluntary exertion (MVE) in flexion under 151 Nm* flexion moment (El Ouaaid et al., 2013b)
12	Maximum voluntary exertion (MVE) in torsion under 78.3 Nm right axial torque with 21.1 right lateral and 16.7 flexion moments (Arjmand et al., 2008b)

* Mean measured moments of 12 subjects (El Ouaaid et al., 2013b).

Table 3.2 Computed rotations (from undeformed geometry to construct the spinal configuration under gravity in the upright standing, positive values: extension) from the optimization of moments (Eq. 3.3) for 4 different personal parameters used in this study.

Personal Parameters	*Sex*	***Male***	***Male***	***Male***	***Male***
	Age	30	25	45	52
	BH	1.80	1.78	1.74	1.75
	BW	73	73	72	68
Rotations (°)	**T11**	-7.52	-7.69	-7.68	-7.65
	T12	-4.71	-4.70	-4.79	-4.80
	L1	-0.93	-0.80	-1.09	-1.16
	L2	2.55	2.29	2.49	2.42
	L3	5.01	5.12	5.21	5.10
	L4	6.77	6.80	6.78	6.90
	L5	8.04	8.00	8.09	8.22
	S1	9.59	10.04	9.65	9.70

Table 3.3 Considered IAPs and antagonistic coactivation moments as well as computed correlation coefficients between mean of estimated muscle activities (Figure 3.7) and measured EMG (for 12 subjects (El Ouaaid et al., 2013b)) and applied shear forces (Eq. 3.4) in MVE tasks.

Extension MVE Task		I	II	III	IV	V
	IAP (kPa)	0	0	0	10	10
	Co-Activation Moment (Nm)	0	10	20	10	20
	Correlation Coefficient	0.99	0.98	0.96	0.98	0.97
Flexion MVE Task		I	II	III	IV	V
	IAP (kPa)	0	0	0	25	25
	Co-Activation Moment (Nm)	0	15	30	15	30
	Correlation Coefficient	0.86	0.85	0.87	0.81	0.79
	F_S^{T11}/F_S^{T12} (N)	641/486	688/NA*	657/NA	288/NA	356/NA

* Not applied

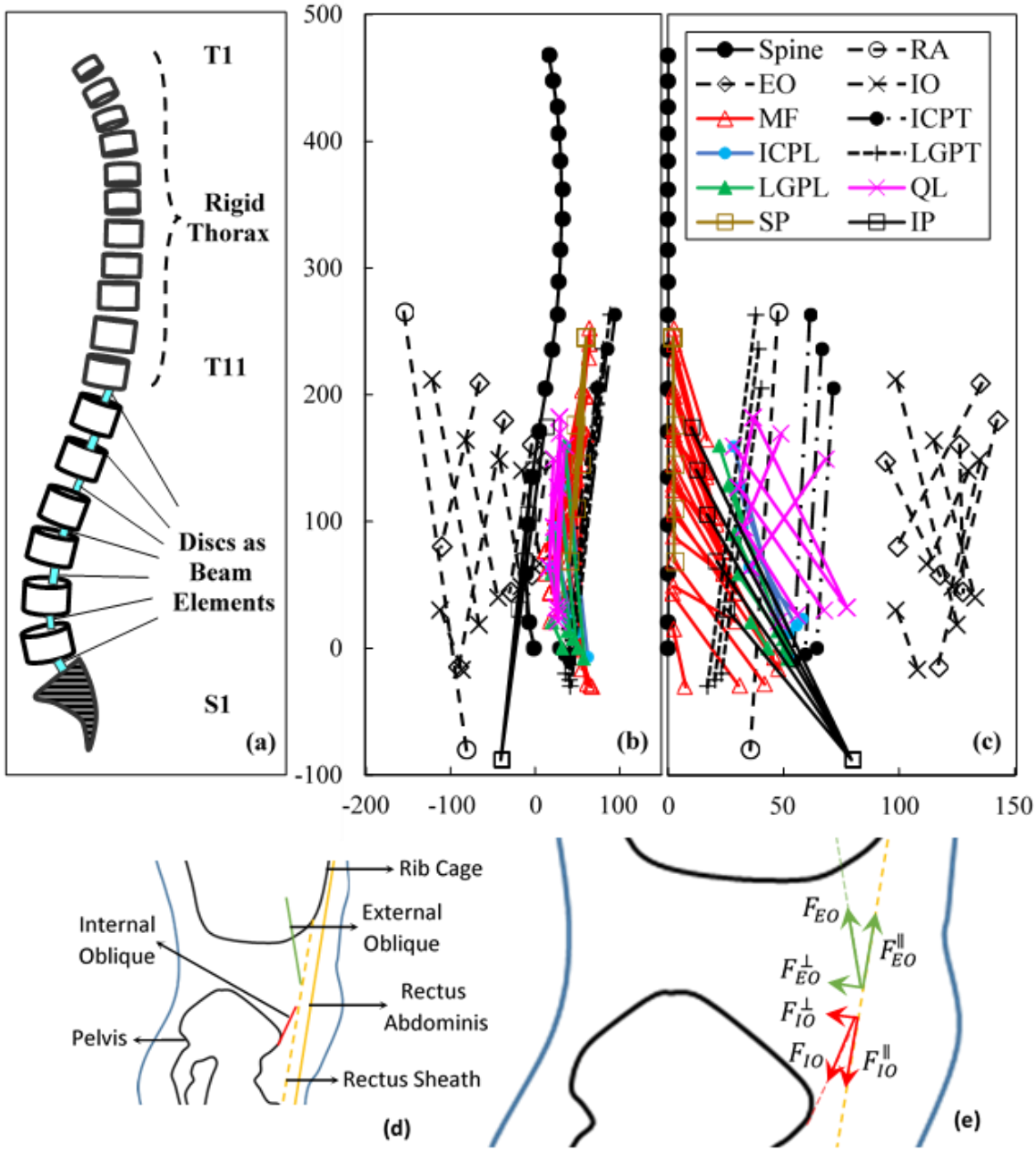

Figure 3.1 A schematic depiction of the (a) finite element model, (b) muscle architecture in the sagittal plane, (c) muscle architecture in the frontal plane, (d) rectus sheath anatomy in the sagittal plane, and (e) rectus sheath load interaction in the sagittal plane. ICPL: Iliocostalis Pars Lumborum; ICPT: Iliocostalis Pars Thoracic; IP: Iliopsoas; LGPL: Longissimus Pars Lumborum; LGPT: Longissimus Pars Thoracic; MF: Multifidus; QL: Quadratus Lumborum; IO: Internal Oblique; EO: External Oblique; RA: Rectus Abdominis; F_{EO}: force in the EO upper most fascicle; $F_{EO}^{\parallel}$: the projection of F_{EO} onto the rectus sheath; $F_{EO}^{\perp}$: the projection of F_{EO} onto the direction normal to the rectus sheath; F_{IO}: force in the IO upper most fascicle; $F_{IO}^{\parallel}$: the projection of F_{IO} onto the rectus sheath; $F_{IO}^{\perp}$: the projection of F_{IO} onto the direction normal to the rectus sheath.

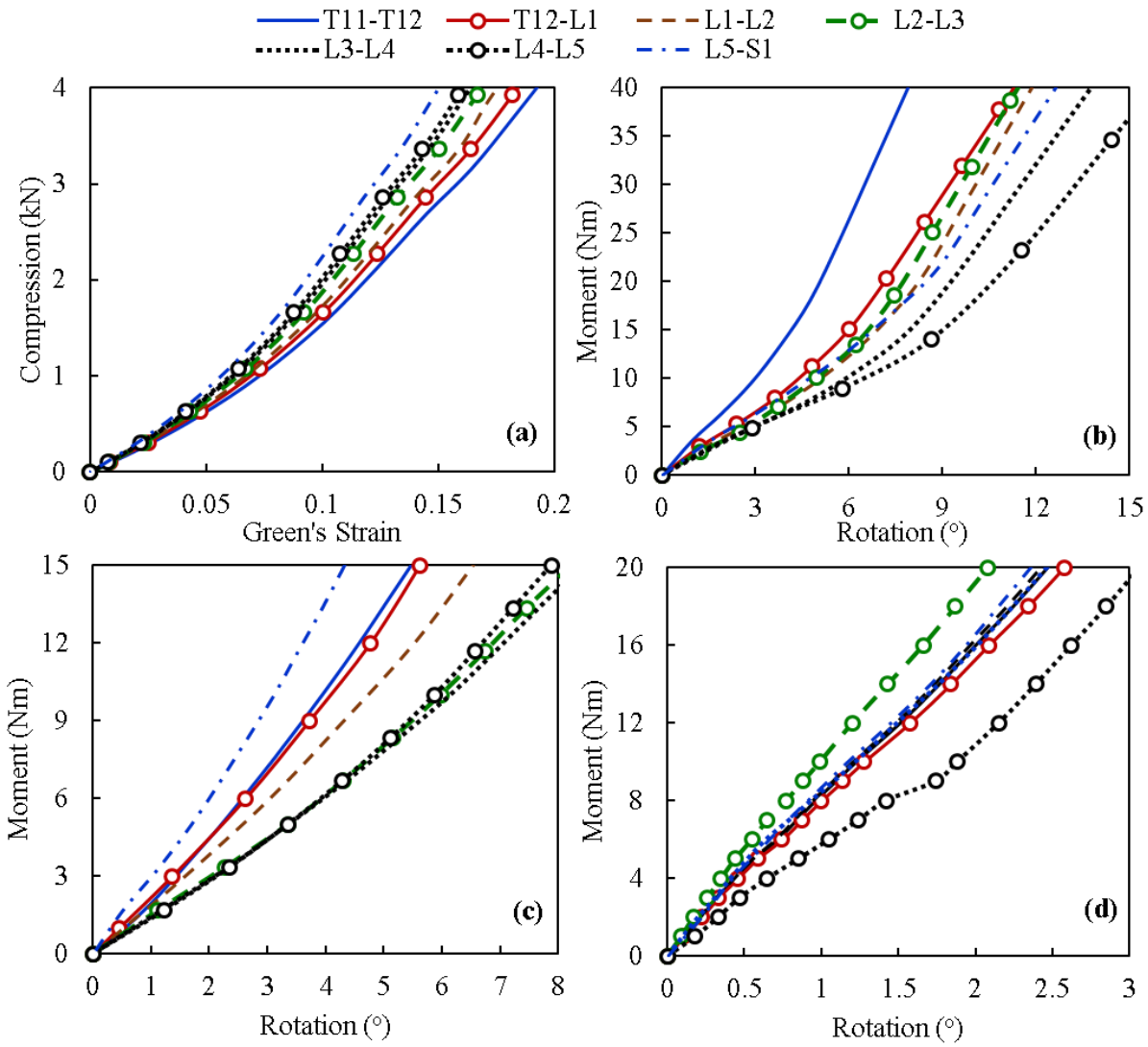

Figure 3.2 Passive property curves in (a) axial force (Shirazi-Adl 2006), (b) flexion moment (Shirazi-Adl 2006), (c) lateral moment (Shirazi-Adl 1994a), and (d) torsion (Shirazi-Adl 2006)

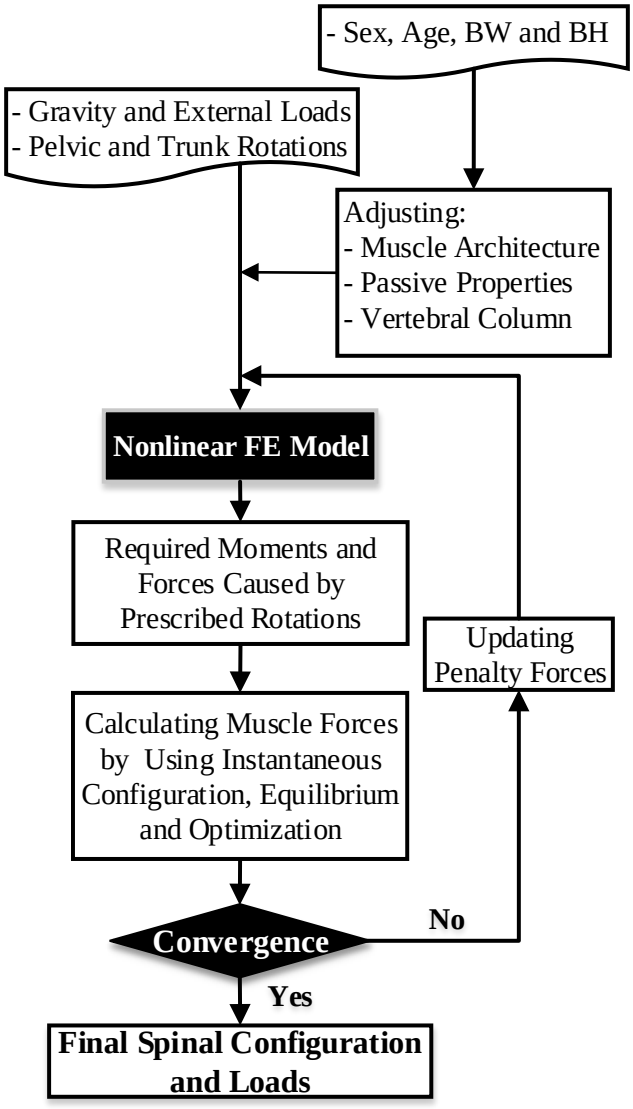

Figure 3.3 The flowchart of the kinematics-driven, nonlinear FE musculoskeletal model

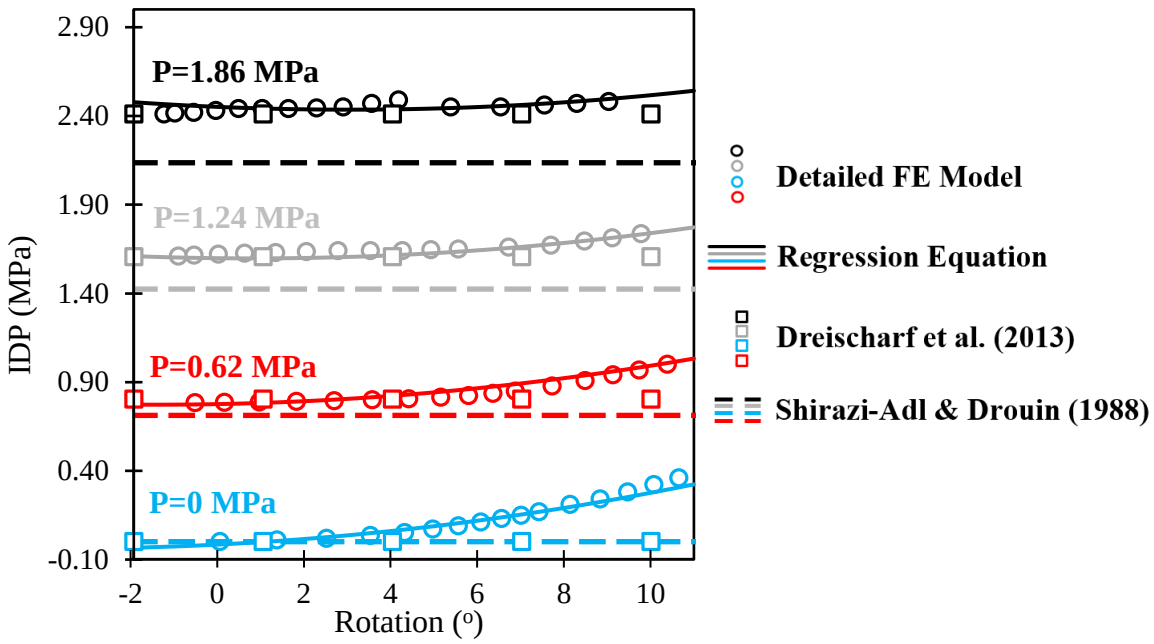

Figure 3.4 Estimated intradiscal pressures (IDPs) at the L4-L5 from the detailed FE model (Shirazi-Adl, 2006), regression equation (Eq. 3.6), proposed relation of (Dreischarf et al., 2013) (IDP=P/0.77), and proposed curve of (Shirazi-Adl & Drouin, 1988) (at the L2-L3) under pure axial force with the following color code: blue (bottom): P = 0 MPa; red: P = 0.62 MPa; grey: P = 1.24 MPa; black (top): P = 1.86 MPa, where P is the nominal pressure (compression/disc area) with the disc area of 1455 mm^2.

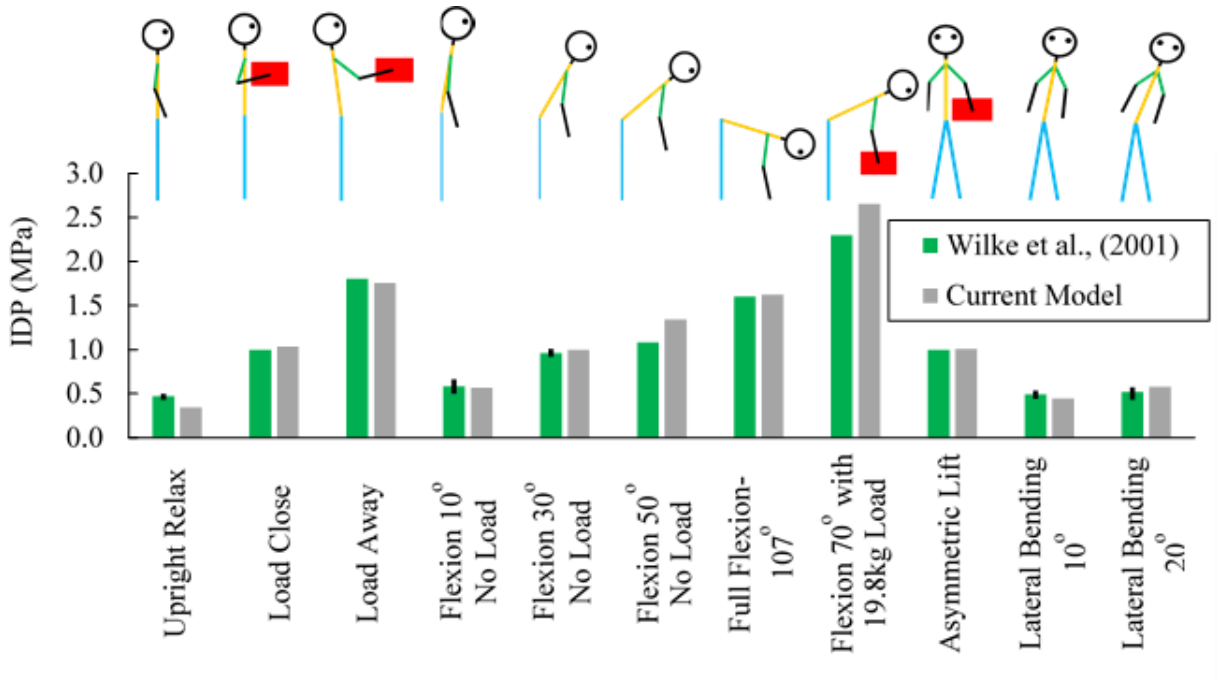

Figure 3.5 Measured intradiscal pressure (IDP) (Wilke et al. 2001) versus calculated IDPs of the model at the L4-L5 level; the model is personalized here to match the personal parameters of the subject participated in the *in vivo* study of Wilke et al. (2001): sex=male, age=45 years, BW=72 kg and BH=173.9 cm.

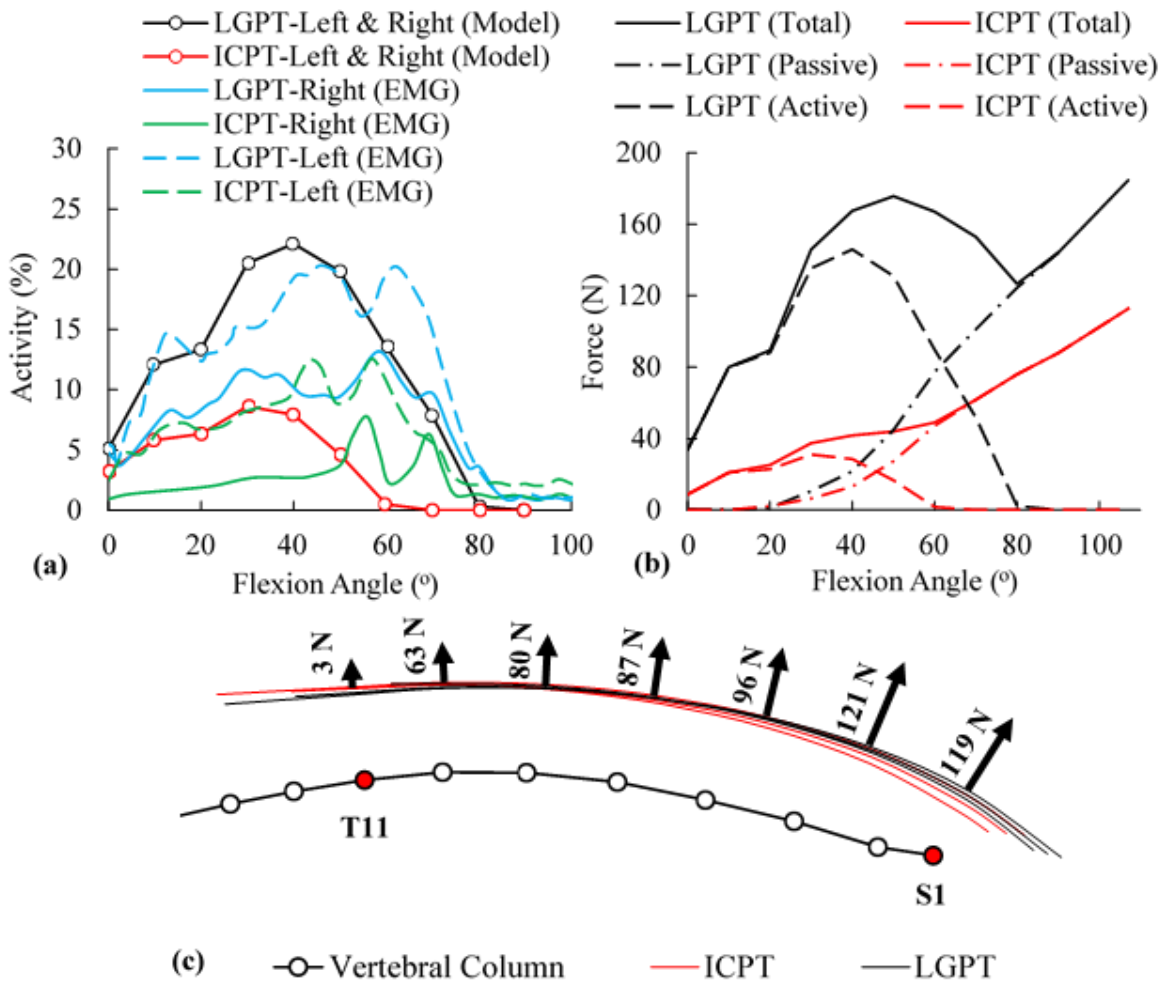

Figure 3.6 (a) Comparison between estimated activities (i.e., force divided by 0.6 MPa times PCSA) of right and left longissimus pars thoracic (LGPT) and iliocostalis pars thoracic (ICPT) muscles with normalized measured EMG signals (Arjmand et al. 2010); (b) computed passive, active and total forces of ICPT and LGPT for each side during forward flexion; (c) muscle wrapping for LGPT and ICPT at full-flexion with generated contact forces. Model parameters fitting the subject in measurements: sex=male, age=52 years, BW=68.4 kg and BH=174.5 cm.

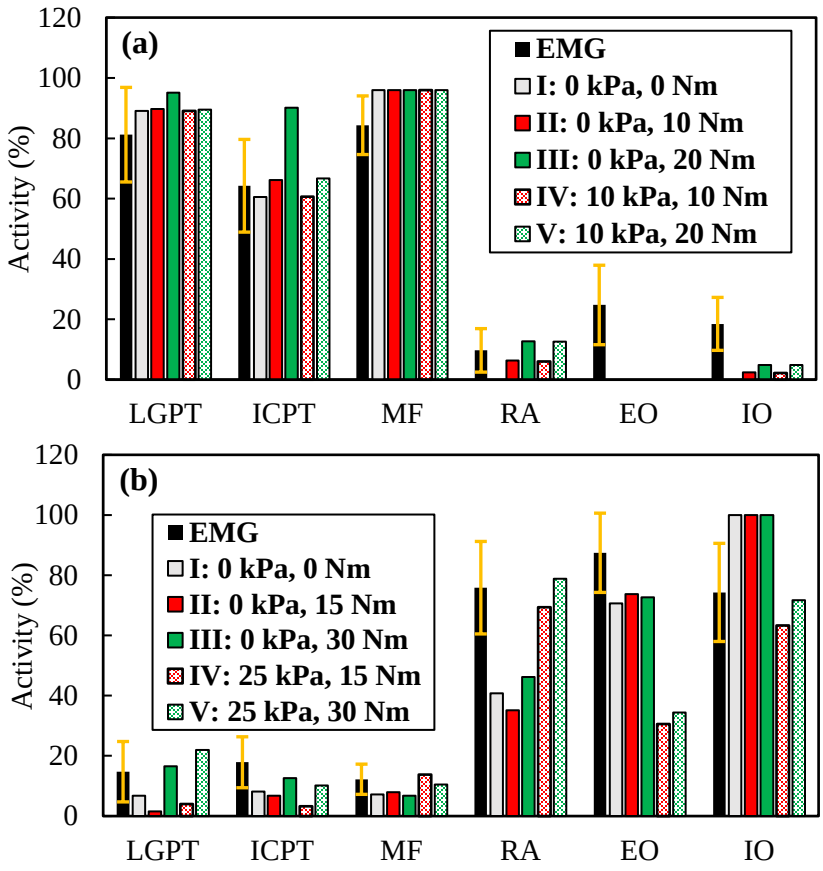

Figure 3.7 Calculated muscle activities at MVE tasks (a) under 242 Nm extension moment (average of 12 subjects) for different values of intra-abdominal pressure (IAP) (0 and 10 kPa) and antagonist moment (0, 10 and 20 Nm), Table 3, and (b) under 151 Nm flexion moment (average of 12 subjects) for different values of IAP (0 and 25 kPa) and antagonist moment (0, 15 and 30 Nm), Table 3, versus normalized EMG (El Ouaaid et al. 2013). Model parameters fitting mean of subjects: sex=male, age=25 years, BW=72.98 kg and BH=177.67 cm

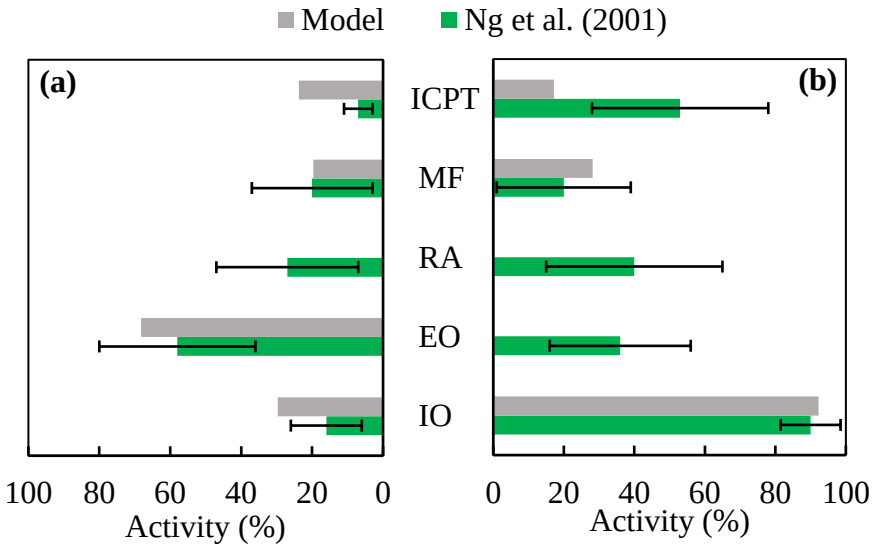

Figure 3.8 Estimated muscle activities for the MVE task in torsion at upright standing versus measured EMG signals on (a) left and (b) right sides under 78.3 Nm right axial torque along with 21.1 Nm right lateral moment and 16.7 Nm flexion moment (Ng et al. 2001). Fascicles with the maximum activity are shown for abdominal muscles. Model parameters used: sex=male, age=30 years, BW=73.00 kg and BH=179.90 cm.

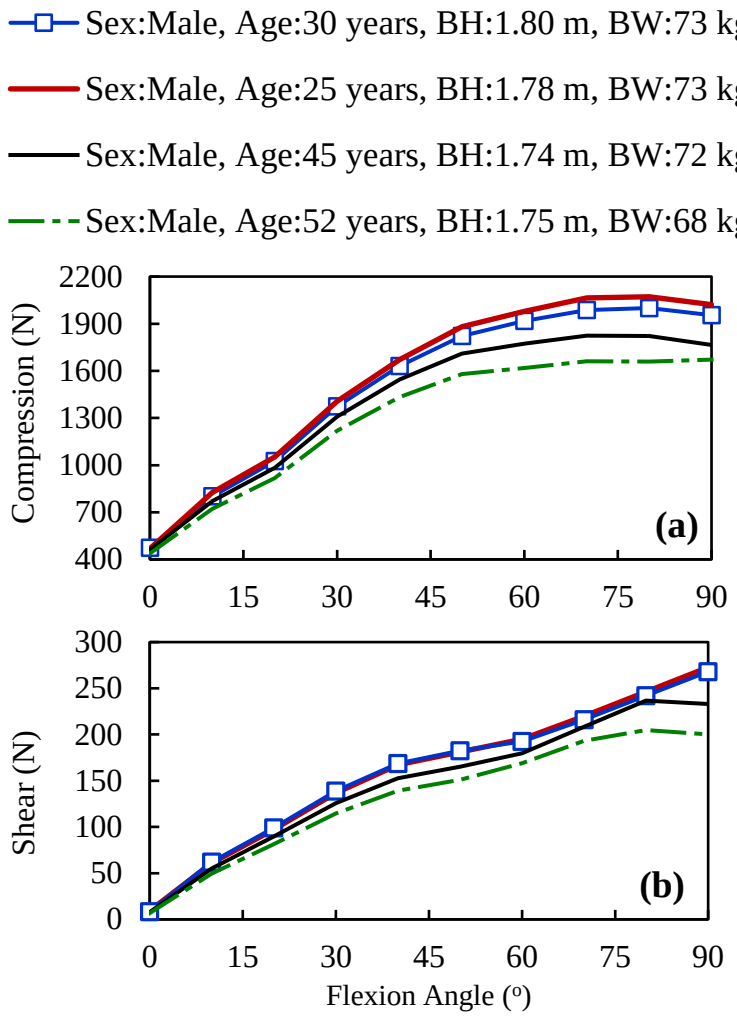

Figure 3.9 Predicted local (a) compression and (b) shear forces at the L4-L5 disc for 4 different personal parameters used in this study.

CHAPTER 4 ARTICLE 2: EFFECTS OF SEX, AGE, BODY HEIGHT AND BODY WEIGHT ON SPINAL LOADS: SENSITIVITY ANALYSES IN A SUBJECT-SPECIFIC TRUNK MUSCULOSKELETAL MODEL

Authors: F. Ghezelbash, A. Shirazi-Adl, N. Arjmand, Z. El-Ouaaid, A. Plamondon, and J.R. Meakin

Published in *Journal of Biomechanics* 49.14 (2016): 3492-3501

4.1 Introduction

Back pain is a prevalent health issue worldwide (Hoy et al., 2014; Hoy et al., 2010b) with significant social and economic burdens on individuals and society (Deyo, Cherkin, Conrad, & Volinn, 1991; Katz, 2006; Rapoport, Jacobs, Bell, & Klarenbach, 2004). Ageing (Hoy et al., 2012), obesity (Deyo & Bass, 1989) and body height (BH) (Leclerc, Tubach, Landre, & Ozguler, 2003) are recognized as risk factors. Ageing, for instance, increases the prevalence of back pain and alters its etiology (DePalma, Ketchum, & Saullo, 2011; Hoy et al., 2012; Hoy, Brooks, Blyth, & Buchbinder, 2010a). While back pain in younger individuals has often discogenic origins, it is in older individuals mainly from facets and sacroiliac joint (DePalma et al., 2011; DePalma, Ketchum, & Saullo, 2012; Dionne, Dunn, & Croft, 2006). As a rising global health problem (Flegal, Carroll, Kit, & Ogden, 2012; Wang et al., 2011), obesity has also been associated with back pain (Deyo & Bass, 1989; Heuch, Hagen, Heuch, Nygaard, & Zwart, 2010; Koyanagi et al., 2015; Leboeuf–Yde et al., 1999; Shiri et al., 2009; Shiri, Lallukka, Karppinen, & Viikari-Juntura, 2014; Smuck et al., 2014; Webb et al., 2003). These studies define obesity based on body mass index (BMI) whereas waist to hip ratio (Han, Schouten, Lean, & Seidell, 1997a; Yip, Ho, & Chan, 2001), waist circumference (Lean, Han, & Seidell, 1998a; Shiri et al., 2013; Taanila et al., 2012) and body weight (BW) (Croft & Rigby, 1994; Heuch, Heuch, Hagen, & Zwart, 2015b) have also been used. As a risk factor, greater BH can also cause back pain in females (Heuch, Heuch, Hagen, & Zwart, 2015a; Yip et al., 2001), males (Walsh, Cruddas, & Coggon, 1991) or both (Hershkovich et al., 2013). Though some studies question the likely role of BH (Han et al., 1997a), others suggest that taller stature could predispose individuals to back pain (Coeuret-Pellicer, Descatha, Leclerc, & Zins, 2010). Correlation between gender and back pain has been reported (DePalma et al., 2012;

Schneider, Randoll, & Buchner, 2006). Though personalized factors have been indicated in back pain, underlying mechanisms remain yet unknown.

The above factors likely alter spinal loads. To estimate loads on spine, *in vivo* studies, though valuable, are costly, limited and invasive (Dreischarf et al., 2015a; Rohlmann et al., 2013b; Sato et al., 1999). Musculoskeletal models have emerged as robust and relatively accurate alternatives. Hajihosseinali et al. (2015) applied an image-based anisotropic scaling method to modify musculature morphology in a musculoskeletal trunk model while investigating the effects of changes in BW on spinal loads. They reported that BW substantially influences spinal loads particularly at flexed postures. Using a linear and isotropic scaling scheme in AnyBody Modelling System (Damsgaard et al., 2006), Han et al. (2013b) found that the spinal shear and compression forces change linearly with BH and BW though the effect of BW is more pronounced. To investigated age-related hyperkyphosis by a static model of the spine, Bruno, Anderson, D'Agostino, and Bouxsein (2012) considered three spinal configurations (hyperkyphosis alone, with pelvic tilt or with increased lordosis) and reported that changes in both kyphosis and spinal posture affect spinal loads. Nevertheless, to-date no study has comprehensively investigated the likely effects of all subject-specific parameters of age, sex, BH and BW on spinal loads.

Computing spinal forces by multi-joint trunk musculoskeletal models, especially when BW changes, requires an accurate segmental weight distribution along the spine (T1 to L5). Pearsall et al. (Pearsall, 1994; Pearsall, Reid, & Livingston, 1996) evaluated this distribution in lean individuals using CT imaging. For overweight and obese individuals, however, available studies have estimated only the total trunk mass center by MR images (Matrangola, Madigan, Nussbaum, Ross, & Davy, 2008), X-ray absorptiometry scans (Chambers, Sukits, McCrory, & Cham, 2010) and 3D body scans (Pryce & Kriellaars, 2014). Consequently, the required segmental weight distribution in overweight and obese individuals has not yet been estimated.

We aim to comprehensively investigate the effects of alterations in age, sex, BH and BW on spinal loads. To adequately account for the overweight and obese individuals, we initially develop a novel technique to estimate segmental weight distribution along the trunk (T1 to L5) as BW alters.

Moreover, using an updated validated nonlinear finite element (FE) subject-specific trunk musculoskeletal model (Ghezelbash, Shirazi-Adl, Arjmand, El-Ouaaid, & Plamondon, 2016b) (Chapter 3) in conjunction with personalized spinal kinematics (with respect to age and sex) (Pries, Dreischarf, Bashkuev, Putzier, & Schmidt, 2015), we evaluate spinal loads and sensitivities therein as individual parameters alter in a full factorial simulation (90 cases) taking 4 independent factors (age, sex, BH and BW) in five sagittally symmetric tasks. In accordance with earlier studies, we hypothesize that spinal loads are much more sensitive to variations in BW than in sex, BH and age.

4.2 Methods

4.2.1 Musculoskeletal Model of Trunk

The development and validation of a nonlinear FE, subject-specific, musculoskeletal model of the trunk for symmetric-asymmetric tasks are reported elsewhere (Ghezelbash et al., 2016b) (Chapter 3). The model includes a comprehensive sagittally-symmetric muscle architecture (126 muscle fascicles) and spinal motion segments (T11-T12 to L5-S1) that are simulated as shear-deformable beam elements with nonlinear properties (Shahvarpour et al., 2016; Shirazi-Adl, 2006). To estimate muscle forces, the musculoskeletal trunk model is driven by measured kinematics while minimizing sum of squared muscle stresses (Arjmand et al., 2010; Arjmand & Shirazi-Adl, 2006a). Moreover, to adjust the model in accordance with subject's personal parameters (age, sex, BH and BW), we use a physiological-based scaling method that modifies both muscle architecture (geometry and area of muscles) and passive joint properties in accordance with imaging studies (Anderson et al., 2012; Shi et al., 2014) and biomechanical principles (Ghezelbash et al., 2016b) (Chapter 3).

4.2.2 Body Weight Distribution

For BMI<25 kg/m^2, upper trunk BW (head, arms and trunk) is distributed based on the literature (De Leva, 1996; Pearsall, 1994) and similar to our earlier works (Arjmand et al., 2010; El Ouaaid et al., 2015; Shahvarpour et al., 2015a). However, for BMI>25 kg/m^2, a new approach described

below, is developed since the existing data, collected on lean individuals, cannot accurately be extended to obese and overweight ones.

4.2.2.1 3D Reconstruction from 2D Images

3D body shapes of subjects are initially reconstructed (e.g., by spline curves) using available 2D image datasets of thousands of human laser scans (BMI Visualizer, Perceiving Systems Department, Max Planck Institute for Intelligent Systems, Germany) in the sagittal and frontal planes (Allison, Thomas, & Zhang, 2013). BW of each reconstructed 3D body is then estimated and calibrated based on a reported regression equation (Velardo & Dugelay, 2010).

4.2.2.2 Placement of the Vertebral Column

We employ a standing MR image of a male subject (BMI=26 kg/m^2) produced from data acquired in a previous study (Meakin, Smith, Gilbert, & Aspden, 2008b) including images of the lumbar and thoracic spines to position the spinal column within foregoing body images by fitting the boundaries of the MR and body scan images. With feet and head fixed as landmarks (Figure 4.1), it is assumed that the spine preserves its relative position to landmarks as BMI varies. To validate the 3D reconstruction and this positioning algorithm of the spine within images, estimated segmental masses and mass centers as well as the total trunk mass in lean subjects are subsequently compared to those reported in supine based on CT images (Pearsall, 1994; Pearsall et al., 1996).

4.2.2.3 Calculation of Mass Centers for Obese and Overweight Subjects

For these subjects (BMI>25 kg/m^2), BW is initially partitioned into two parts:

$$BW = BW_R + BW_A, \qquad \text{Eq. 4.1}$$

where BW_R is the reference body weight assuming a BMI=25 kg/m^2 and BW_A is the additional body weight. While the reference body weight (BW_R) is distributed in accordance with the available data for lean subjects (De Leva, 1996; Pearsall, 1994), the additional body weight (BW_A) is assumed to be made of adipose tissue (yellow areas in Figure 4.1) with distribution based on

reconstructed 3D shapes. This procedure is carried out at BMI=25, 30, 35 and 40 kg/m^2 at BH=173 cm and then scaled for other BHs. Segmental masses of adipose tissue are scaled proportional to BW_A, and the mass centers are adjusted proportional to BH. Additional masses of the head and arms are estimated from the reconstructed 3D surface images with mass center locations reported in the literature (De Leva, 1996). To evaluate the validity of foregoing partitioning approach, we compared the estimated density of the additional material (yellow areas in Figure 4.1) with the reported density of adipose tissue (919.6 kg/m^3 (Farvid, Ng, Chan, Barrett, & Watts, 2005)).

4.2.2.4 Sensitivity Analysis

The foregoing method of estimating weight along the spine represents general obese population. Therefore, to investigate the likely effects of extreme weight distributions on spinal loads at BMI=35 kg/m^2, BH=173 cm and age=47.5 years, we replace segmental weights at lumbar levels with those of either 30 kg/m^2 (less weight around the waist) or 40 kg/m^2 (more weight around the waist) while keeping the BW constant by proportionally adjusting segmental weights in the upper thorax region. Flexion at 20^o and 50^o are simulated with no load in hands.

4.2.3 Full Factorial Design

A full factorial simulation with 4 independent factors (2 sexes × 3 ages × 3 BHs × 5 BWs=90 cases, Table 4.1) is considered. All 90 cases are simulated under five sagittally symmetric tasks (in total 450 simulations): 1- upright standing holding 5 kg in hands anteriorly, 2- and 3- trunk flexion at 20^o and 50^o with no load in hands, 4- flexion at 20^o with 10 kg in hands, and 5- flexion at 50^o with 5 kg in hands. In each analysis, initially the reference subject-specific upright standing posture under gravity alone is sought from corresponding personalized undeformed (unloaded) configuration by a moment optimization approach in which the sum of sagittal moments at the T11-L5 levels is minimized under upper body gravity loads (Shirazi-Adl et al., 2002). Subsequently, in each flexed posture, total thoracolumbar (T11-L5) and sacral (S1) rotations are determined in accordance with reported measured lumbopelvic ratios that are personalized for sex and age (Pries et al., 2015). Thoracolumbar (T11-S1) rotations in each task are partitioned between

its motion segments; 6.0% at the T11-T12, 10.9% at the T12-L1, 14.1% at the L1-L2, 13.2% at the L2-L3, 16.9% at the L3-L4, 20.1% at the L4-L5, and finally 18.7% at the L5-S1 (Gercek et al., 2008; Ghezelbash et al., 2016b; Hajibozorgi & Arjmand, 2015).

4.2.3.1 Statistical Analysis

Main effect plots are utilized to investigate the effects of various factors and analyses of variance (ANOVA) are carried out to determine relative importance of various factors (Dar, Meakin, & Aspden, 2002; Meakin, Shrive, Frank, & Hart, 2003). Each response (shear and compression forces at the L4-L5 and L5-S1 levels) are considered separately with interactions neglected (reduced order model).

4.3 Results

4.3.1 Body Weight Distribution

For the reference case (BMI=25 kg/m^2), the correlation coefficient (Pearson's r) and root-mean-square error (RMSE) between the predicted (as described earlier in Methods) and reported (Pearsall, 1994) locations of the segmental mass center at various spinal levels are 0.92 and 6.8 mm, respectively. The correlation coefficient and RMSE for segmental weights (from T1 to L5) are 0.83 and 3.2 N, respectively. Besides, the absolute relative error between the predicted and reported (Pearsall, 1994) whole trunk mass is 9.0%. Low errors in combination with high correlation coefficients indicate the relative accuracy in our body weight distributions and positioning of the spine in each case within the reconstructed personalized body shape images.

In overweight and obese cases (BMI=30, 35 and 40 kg/m^2), mass center locations of the additional weights are found relatively close to each other (Figure 4.2a). Additional segmental weights vary along the spine (Figure 4.2b). Absolute relative error of the predicted density of the adipose tissue for different BHs (150–190 cm) and BMIs (30-40 kg/m^2) is 6.6 ± 3.8% (mean± standard deviation).

4.3.2 Spinal Loads

Changes in BW, sex and BH influence spinal loads. Increasing BW from 55 to 120 kg nearly doubles compression forces at the L4-L5 and L5-S1 levels (Figure 4.3 and Figure 4.4). Based on the results of all simulations and under identical parameters, females experience slightly larger (~4.7% in compression and ~8.7% in shear) loads than males. With no load in hands, BW-normalized spinal loads increase with BW (Figure 4.5). However, these trends reverse when a load is added in hands (Figure 4.5). BH-normalized spinal loads drop linearly with BH for all loading conditions (Figure 4.6), except for the largest BW at lower BH values. Loads in females are slightly larger than their male counterparts. Also, sensitivity analyses on weight distribution of obese individuals at BMI=35 kg/m^2, BH=173 cm and age=47.5 years show relatively small differences in spinal loads (peaks of 7.5% in shear and 6.2% in compression).

4.3.3 Statistical Analysis

Main effect plots (for all analyses, Figure 4.7) reveal that the spinal loads at the L5-S1 increase nearly proportionally with BW. For identical age, BW and BH, males have lower spinal loads than females with larger differences in shear than in compression. BH and age, on the other hand, do not noticeably affect spinal loads. Similar trends are obtained for spinal loads at the L4-L5 disc. According to the analyses of variance (Table 4.2), BW (~98.9% for compression and 96.1% for shear) is the main contributing factor while sex (~0.7% for compression and 2.1% for shear), BH (~0.4% for compression and 1.5% for shear) and age (<5.4%) have much less effects.

4.4 Discussion

In this study, we investigated the sensitivity of spinal loads at the L4-L5 and L5-S1 levels to changes in personalized factors (age, sex, BW and BH) under 5 different sagittal-symmetric loads. Proper accounts of gravity distribution along the spine in obese subjects and of initial posture of spine under gravity were made. In confirmation of our hypothesis, changes in BW (means of 98.9% in compression and 96.1% in shear) influenced to a great extent the spinal loads whereas the role

of sex (0.7% in compression and 2.1% in shear), BH (0.4% in compression and 1.5% in shear) and age (<5.4%) (Table 4.2) were much smaller. In comparison to males, females (at identical age, BH and BW) experienced greater spinal loads (~4.7% in compression and ~8.7% in shear).

4.4.1 Model Evaluation

4.4.1.1 Novelties

Segmental weight distribution for overweight and obese individuals was presented in this study for the first time. It was also applied (utilizing a subject-specific model of the trunk with scaled muscle geometry and passive joint properties along with personalized kinematics) to the investigation of the effects of age, sex, BH and BW on spinal loads. The initial posture in upright standing under gravity alone was also personalized for each subject.

4.4.1.2 Shortcomings

Apart from limited *in vivo* studies available for validation (Dreischarf, Shirazi-Adl, Arjmand, Rohlmann, & Schmidt, 2016a) and the limitations (e.g., neglecting intra-abdominal pressure and coactivity) noted elsewhere (Arjmand et al., 2006; El-Rich et al., 2004; Ghezelbash et al., 2015; Ghezelbash et al., 2016b) (Chapter 3), the model did not converge for taller, older, obese and female individuals with load in hands (≥5 kg) at large flexion angles (≥70^{o}) since in contrast to spinal loads, the contribution of BH to the required moments is not negligible, and muscles in females could not counterbalance the induced required moments. In accordance with the input data used (Anderson et al., 2012; Pries et al., 2015; Shi et al., 2014) and to avoid spinal disorders observed at older ages, we chose the range of 35-60 years that also covers active working ages. The proposed method of estimating segmental weights involves some simplifying assumptions: reconstruction of the 3D body from 2D images (Allison et al., 2013), placement of the spine in the reconstructed body, homogenous distribution of density (Pryce & Kriellaars, 2014), scaling weight distribution of adipose tissue and extrapolation of weight distribution for three cases (BH=150 cm at BMI=46.1 and 53.3 kg/m^2; BH=170 cm at BMI=41.5 kg/m^2) due to limitations in the available database (BMI

Visualizer, Perceiving Systems Department, Max Planck Institute for Intelligent Systems, Germany). Nonetheless, the method yielded results in satisfactory agreement with the distribution of gravity loads along the spine in lean subjects (Pearsall, 1994; Pearsall et al., 1996) and the density of additional adipose tissue (Farvid et al., 2005). Moreover, for an extreme underweight case (BMI=15.2 kg/m^2), we used the mass distribution similar to normal weight individuals. Only sagittally symmetric tasks were simulated here; the sensitivity of spinal loads to personalized factors may alter in asymmetric tasks although conclusions likely remain unchanged. Changes in the thoracic kyphosis angle or alterations in the initial lordosis (Meakin, Gregory, Smith, Gilbert, & Aspden, 2008a) could influence results.

4.4.2 Comparisons

4.4.2.1 Age

No study has investigated changes in age while employing a detailed trunk musculoskeletal model; existing studies (Boocock, Mawston, & Taylor, 2015; Shojaei, Vazirian, Croft, Nussbaum, & Bazrgari, 2016; Song & Qu, 2014) employed link-segment models (for limitations and shortcomings see (Rajaee et al., 2015). In contrast to our findings, Shojaei et al. (2016) reported significantly lower shear force at the L5-S1 in younger participants. The use of a dynamic link-segment model with no muscles and passive spine, different anthropometric input data and age groups (22-68 years versus 35-60 years) as well as asymmetry in tasks could be some likely sources for different findings.

4.4.2.2 Sex

Marras et al. (Marras, Davis, & Jorgensen, 2003; Marras et al., 1995) estimated lower spinal loads in females (except the anterior-posterior shear at the L5-S1 disc (Marras et al., 1995)). In those studies, however, male participants were, in average, heavier and taller than females. These differences in BH and BW along with using a single level EMG-driven model without a comprehensive scaling algorithm (Dreischarf et al., 2016a) can play a role in lower estimations of

spinal loads in females. In agreement with our findings, Shojaei et al. (2016) computed larger shear forces (~6%) in females.

4.4.2.3 BW and BH

In accordance with our findings, Hajihosseinali et al. (2015) and Han et al. (2013b) found also that BW markedly affects spinal loads and Han et al. (2013b) reported that BH has less effects on spinal loads. Moreover, obese individuals experience more spinal shrinkage (Yar, 2008) and implant subsidence (Behrbalk et al., 2013).

4.4.3 Interpretations

Among various parameters, spinal loads are particularly sensitive to passive joint properties, muscle moment arms, lumbopelvic ratio and net external moments. Greater passive joint stiffness as well as muscle moment arms markedly reduce muscle forces and consequently spinal loads. Likewise, increasing the lumbopelvic ratio (at a given posture) reduces spinal loads by accentuating the load-carrying role of the passive spine (Tafazzol, Arjmand, Shirazi-Adl, & Parnianpour, 2014). Finally, greater net moment at a spinal level, being due to larger external/gravity load or changes in the posture, tends to increase muscle forces and spinal loads. Subject specific factors affect spinal loads by altering the foregoing parameters. For instance, at identical age, BH and BW, female spines experience greater loads due to associated smaller muscle moment arms and passive joint contributions (Table 4.3). Results indicate that changes in age hardly influence spinal loads that could be due to opposing trends in the lumbopelvic ratio and passive contributions/muscle moment arms (Table 4.3). By increasing external moments, BW markedly influence spinal loads while the increase in external moments due to BH is almost counterbalanced by the larger muscle moment arms and passive joint contributions (Table 4.3).

With no load in hands, the BW-normalized spinal loads further increase with BW in both sexes and particularly at higher BHs (Figure 4.5). This highlights the accentuating role of BW in increasing spinal loads especially in obese individuals. It further demonstrates the exponential increase in spinal loads with BW. This trend, however, disappears in conditions with a load in

hands (Figure 4.5) with larger decreases under greater loads in hands which indicates the substantial effect of external loads on spinal forces. BH-normalized spinal loads decreased in all loading conditions with BH for all BWs (except and in particular in shear forces at larger BWs and smaller BHs, Figure 4.6). This drop in BH-normalized spinal forces when compared to the opposite increase in BW-normalized loads versus BW further suggests the important role of BW on spinal loads.

Due to the controversial relation between the lumbar lordosis and age, sex, BH and BW (or alternatively BMI) (Been & Kalichman, 2014), the initial (undeformed) lumbar lordosis was kept constant in all models. Some studies found no association between the lordosis and age (Kalichman, Li, Hunter, & Been, 2011; Murrie, Dixon, Hollingworth, Wilson, & Doyle, 2003) while others reported age-related decrease (Amonoo-Kuofi, 1992) or increase (Tüzün, Yorulmaz, Cindaş, & Vatan, 1999) in the lordosis. In a preliminary study (not reported here) simulating forward flexion, however, the initial L1-S1 lordosis Cobb's angle was increased by 10^{o} (from 46^{o}) while preserving the kyphosis angle and the sacral plumb line in agreement with the literature (Endo, Suzuki, Tanaka, Kang, & Yamamoto, 2010; Jackson, Peterson, McManus, & Hales, 1998; Park et al., 2013). Results demonstrated that it primarily influences the relative ratio of shear and compression forces especially at the L5-S1 under larger flexion angles. Factors such as age and sex could, therefore, potentially influence spinal loads indirectly through alterations in lordosis.

Excessive spinal loads have been recognized as a risk factor of back pain (Bovenzi, Schust, Menzel, Hofmann, & Hinz, 2015; Coenen et al., 2013; Marras et al., 1995) and disc degeneration (Adams et al., 2000; Rannou et al., 2004; Stokes & Iatridis, 2004). Thus, greater BWs that yield larger (BW normalized) spinal loads and fat accumulation at the (upper) trunk in comparison with more weight around and below the waist can predispose individuals to higher risk of back disorders. It is to be noted that consideration of loads when normalized to subject's BW is more appropriate since unlike absolute loads, BW-normalized loads to some extent automatically take account of anthropometric differences. Overall, increase in spinal loads (Singh, Park, Hwang, & Levy, 2015), reduction in postural stability (Corbeil, Simoneau, Rancourt, Tremblay, & Teasdale, 2001; Hue et al., 2007),

fall due to slipping (Allin, Wu, Nussbaum, & Madigan, 2016), limitations in goal-oriented movements (Berrigan, Simoneau, Tremblay, Hue, & Teasdale, 2006) and metabolic changes (Samartzis, Karppinen, Cheung, & Lotz, 2013) due to obesity increase back pain risk of injury while some alterations such as the associated decrease in the ranges of motion (Park, Ramachandran, Weisman, & Jung, 2010; Vismara et al., 2010), adaptation (Porter, Adams, & Hutton, 1989), physical activity (Smuck et al., 2014) and the unloading role of IAP (due to increased diaphragm area (Shi et al., 2014)) could influence this risk. Pregnant females are also susceptible to injury as a result of additional spinal loads due to the weight gain (~10-15 kg (Noon & Hoch, 2012; Schieve et al., 2000; Yaktine & Rasmussen, 2009)) although radical hormonal changes during pregnancy and their likely effects on biomechanical factors are additional influential factors. According to our findings, slightly higher spinal loads in females (at identical BH, BW and age) combined likely with other risk factors (e.g., psychological factors, physical ability, different job assignments (Bielby & Baron, 1986)) could play a role in greater prevalence of low back pain in females reported in some studies (DePalma et al., 2012; Schneider et al., 2006). Although current results suggest that age (in the range of 35-60 years) does not affect spinal loads, ageing could reduce damage tolerance threshold of intervertebral discs making them more susceptible to injury (Adams, Lama, Zehra, & Dolan, 2015; Adams & Roughley, 2006).

In summary, using an image-based scaling algorithm for the trunk musculature and passive properties as well as prescribed (based on available *in vivo* measurements) spinal kinematics and lumbopelvic rhythm (based on sex and age) in conjunction with a novel technique of estimating trunk weight distribution in overweight and obese individuals, we investigated the effect of various personal factors (i.e., age, sex, BH and BW) on spine loads. Variations in BW have the greatest influence on spinal loads followed by those in sex, BH and age. With no load in hands, the rate of increase in spinal loads actually exceeds that in BW which highlights the exponential increase in spinal loads and hence risk of injury with BW especially in obese individuals. At identical BH and BW, spinal loads are slightly larger (~4.7% in compression and ~8.7% in shear) in females than in males.

4.5 Acknowledgement

This work was supported by the institut de recherche Robert-Sauvé en santé et en sécurité du travail (IRSST-2014-0009).

Table 4.1 Personalized factors and corresponding levels in the full factorial simulation design

Factors	*Unit*	*Levels*
Sex	-	Female – Male
Age	year	35 – 47.5 – 60
BH	cm	150 – 170 – 190
BW	kg	55 – 71.25 – 87.5 – 103.75 – 120

Table 4.2 Contribution (%) of each factor for various simulated tasks to the total sum of spinal loads squared.

Task	*Response*	*Sex*	*Age*	*BH*	*BW*
Standing with 5 kg load	L4-L5 Compression	0.2	0.3	0.4	99.2
	L5-S1 Compression	0.2	0.3	0.5	98.9
	L4-L5 Shear	13.6	5.4	32.0	49.0
	L5-S1 Shear	0.5	0.4	0.0	99.1
Flexion at 20^o with no load	L4-L5 Compression	0.2	0.0	0.0	99.8
	L5-S1 Compression	0.6	0.0	0.1	99.2
	L4-L5 Shear	4.3	0.3	3.4	92.0
	L5-S1 Shear	1.1	0.1	0.5	98.3
Flexion at 50^o with no load	L4-L5 Compression	0.1	0.0	0.1	99.7
	L5-S1 Compression	0.5	0.0	0.3	99.2
	L4-L5 Shear	4.3	0.4	4.4	91.0
	L5-S1 Shear	1.0	0.1	0.9	98.0
Flexion at 20^o with 10 kg load	L4-L5 Compression	0.9	0.0	0.8	98.3
	L5-S1 Compression	1.5	0.0	1.0	97.5
	L4-L5 Shear	3.7	0.8	2.2	93.2
	L5-S1 Shear	2.4	0.6	1.5	95.5
Flexion at 50^o with 5 kg load	L4-L5 Compression	0.7	0.1	0.9	98.3
	L5-S1 Compression	1.3	0.0	1.2	97.4
	L4-L5 Shear	3.7	0.9	2.6	92.8
	L5-S1 Shear	2.2	0.6	1.8	95.4
All tasks	L4-L5 Compression	0.5	0.0	0.3	99.2
	L5-S1 Compression	1.0	0.0	0.5	98.5
	L4-L5 Shear	4.1	0.6	3.2	92.2
	L5-S1 Shear	1.6	0.2	1.1	97.1
Overall	Compression	0.7	0.0	0.4	98.9
	Shear	2.1	0.3	1.5	96.1

Table 4.3 Effects of changing personal parameters (sex, age, BH and BW) on model parameters (Anderson et al., 2012; Ghezelbash et al., 2016b; Shi et al., 2014) (Chapter 3)

Parameter	*Passive Joint Properties*	*Muscle Moment Arms*	*Lumbopelvic Ratio*	*External Moment*
Sex*	↘	↘	↘ or ↗	No Change
Age↗	↗	↗	↘	No Change
BH↗	↗♱	↗	No Change	↗
BW↗	↗	↗	No Change	↗

↗: Increase

↘: Decrease

* Here, sex is altered from male to female

♱ Increasing BH stiffens passive properties when BMI is kept constant.

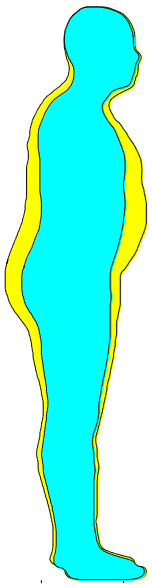

Figure 4.1 Schematic body shape of an obese person (outer contour) versus a lean person (inner contour) in the sagittal plane (BMI Visualizer, Perceiving Systems Department, Max Planck Institute for Intelligent Systems, Germany).

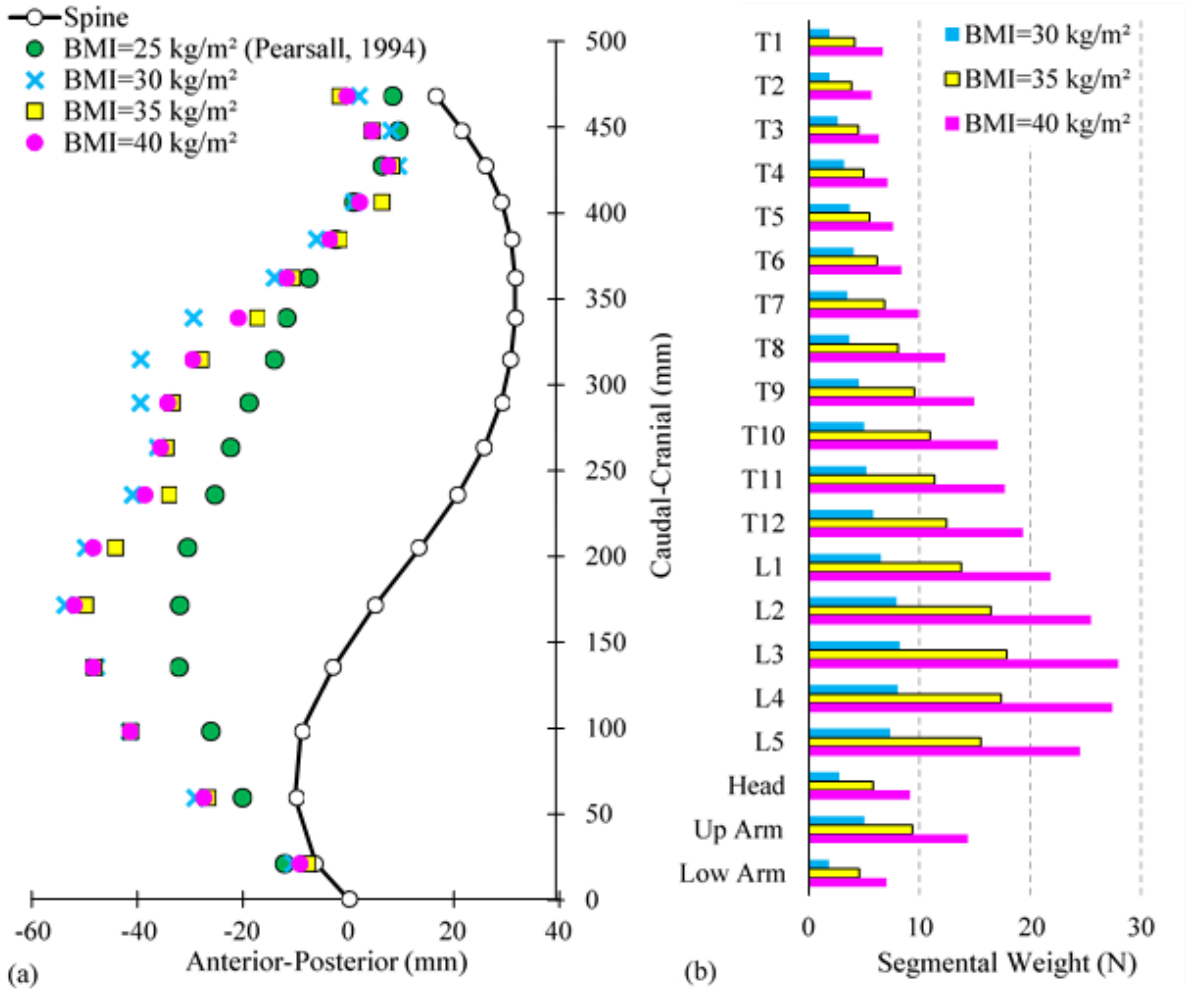

Figure 4.2 Calculated (a) mass centers for BMI=25 kg/m^2 and for the additional trunk fat in cases with BMI>25 kg/m^2 and (b) additional (on top of those for BMI=25 kg/m^2) segmental weights of the trunk, arms (on each side and applied in the model onto the T3 level) and head (applied in the model onto the T1 level) for the overweight and obese cases with BH=173 cm.

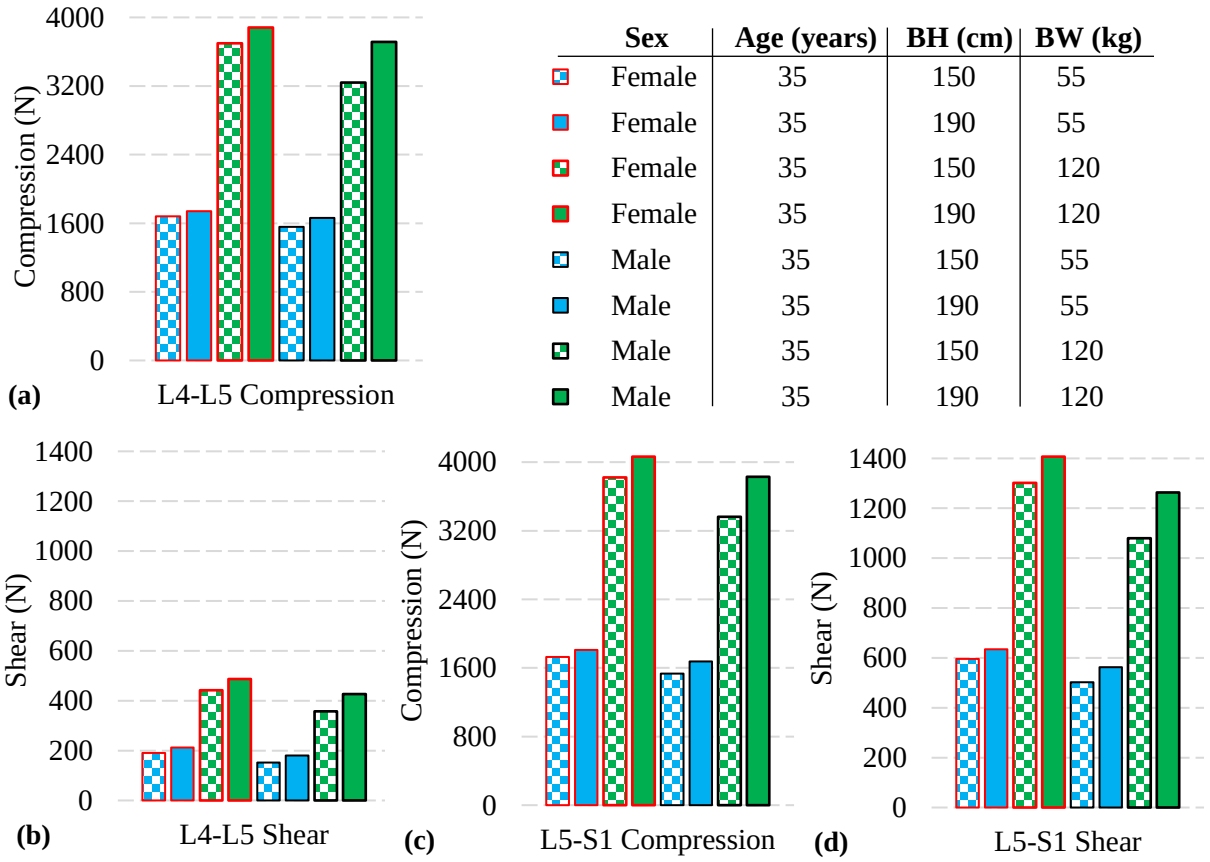

Sex	Age (years)	BH (cm)	BW (kg)
Female	35	150	55
Female	35	190	55
Female	35	150	120
Female	35	190	120
Male	35	150	55
Male	35	190	55
Male	35	150	120
Male	35	190	120

Figure 4.3 Local shear and compression forces at the L4-L5 and L5-S1 levels with 5 kg load in hands at the trunk flexion of 50^{o} for various individuals of 35 years age.

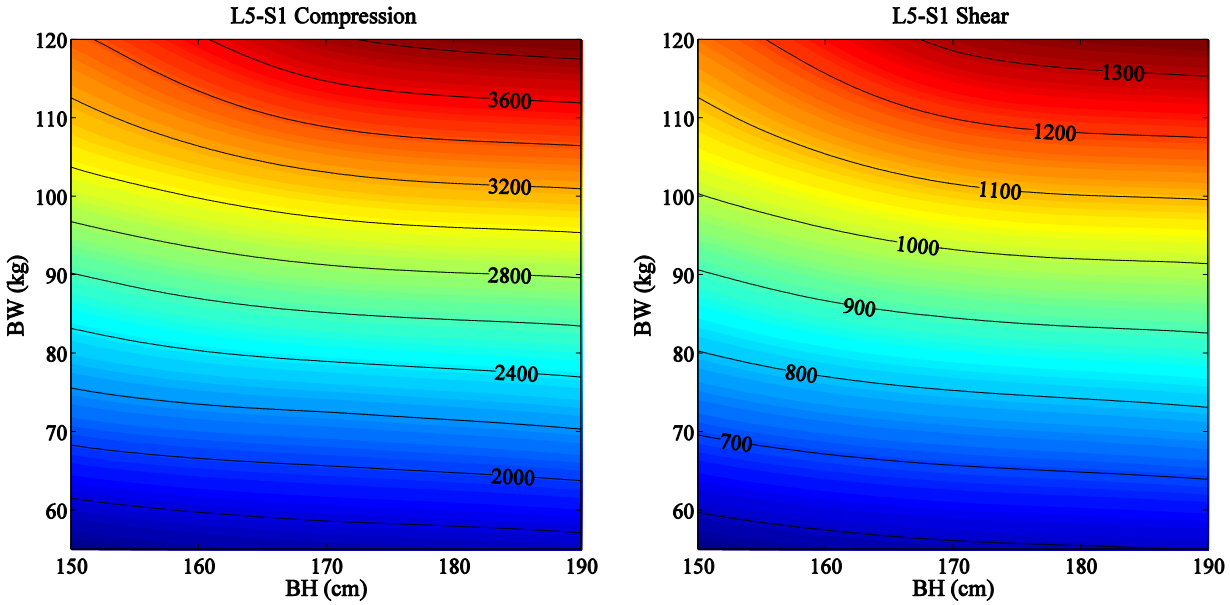

Figure 4.4 The contour plot of local compression (left) and shear (right) forces at the L4-L5 (top) and L5-S1 (bottom) levels at 50^{o} flexion with 5 kg load in hands. Age and sex are set constant at 47.5 years and male.

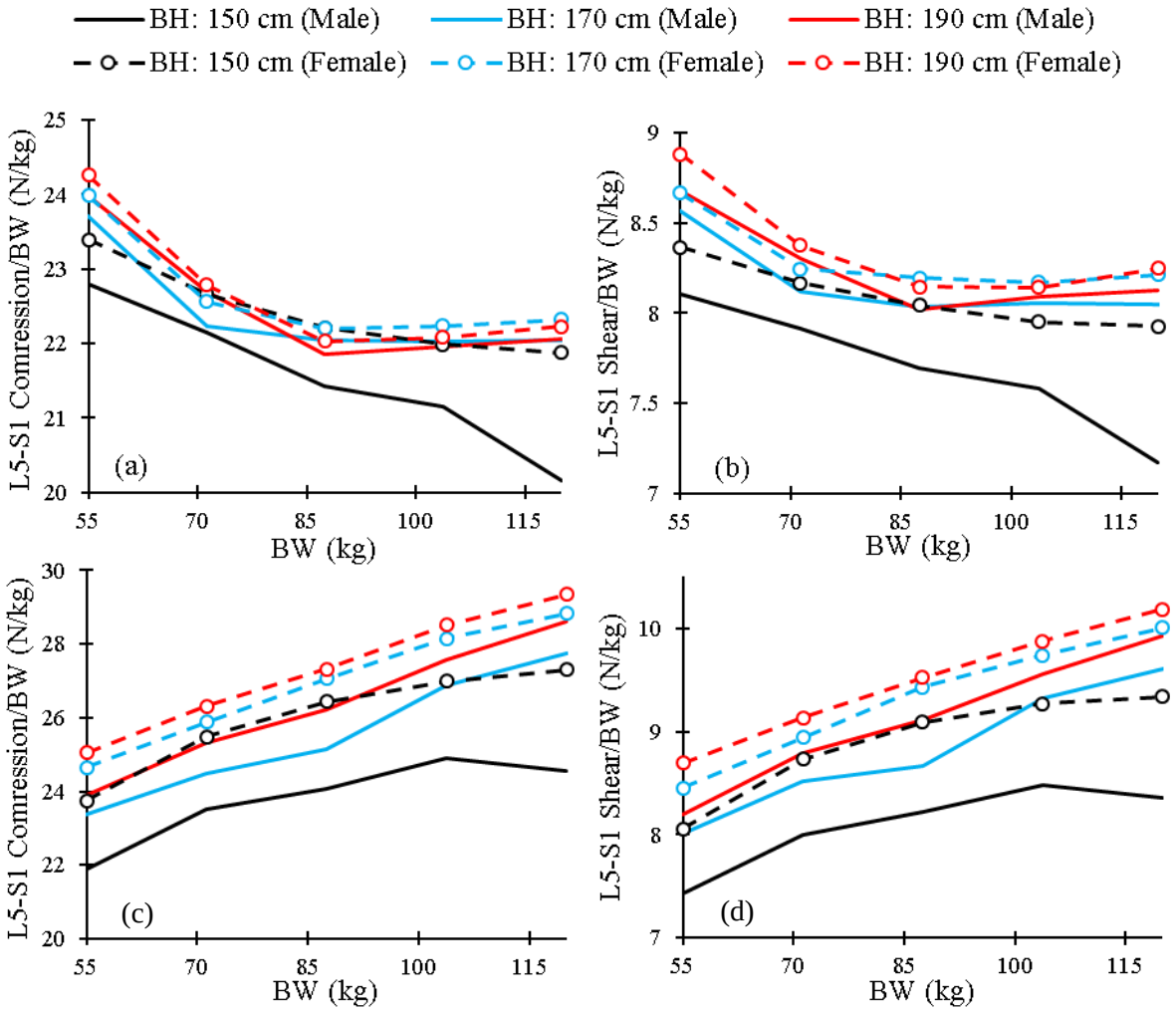

Figure 4.5 BW-normalized local compression (left) and shear (right) forces at the L5-S1 level for 3 different BHs and 2 sexes under (a,b) 20^{o} flexion with 10 kg load in hands and (c,d) 50^{o} flexion without external load. Age is set at 47.5 years.

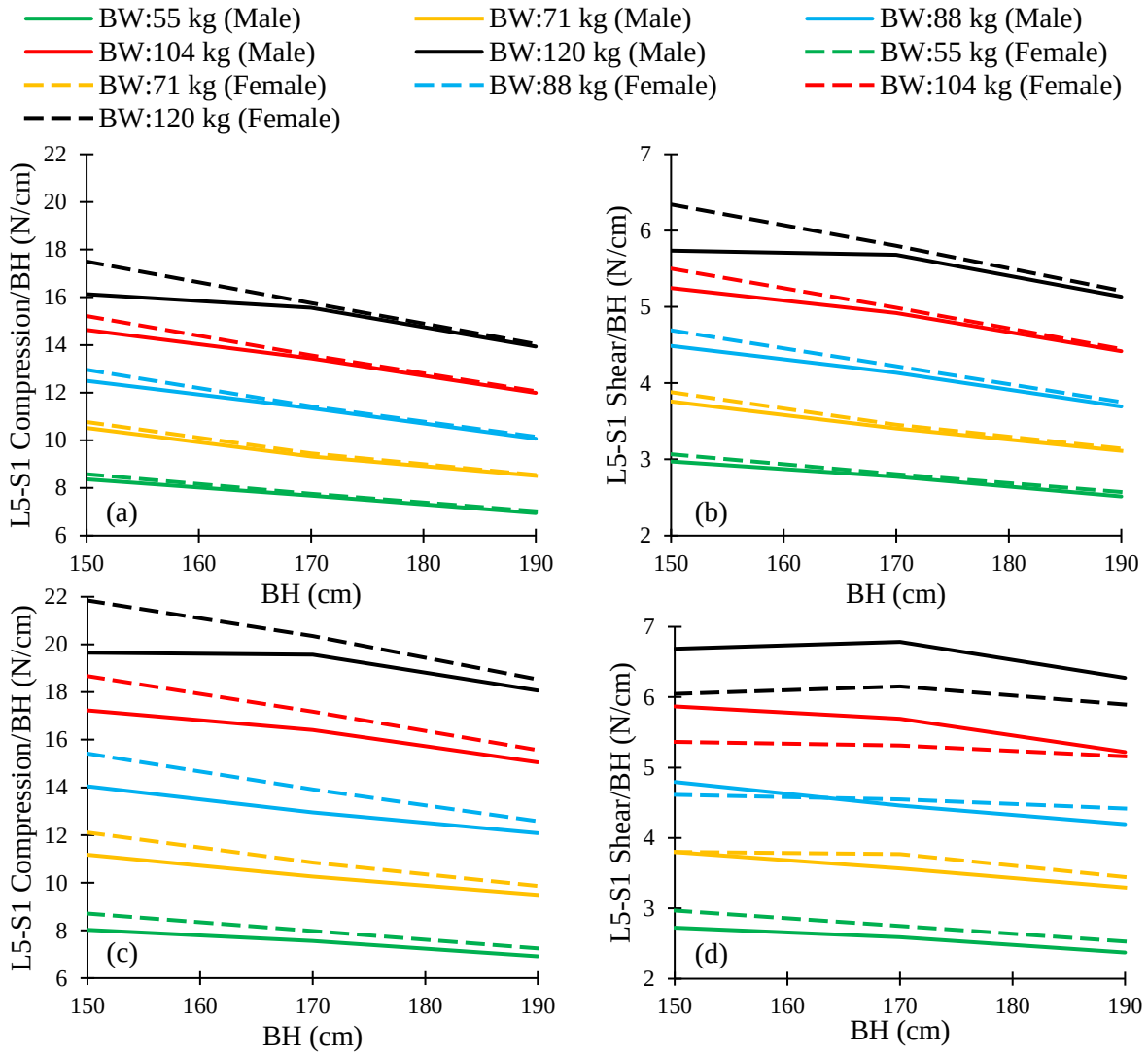

Figure 4.6 BH-normalized local compression (left) and shear (right) forces at the L5-S1 level for 5 different BWs and 2 sexes under (a,b) 20^{o} flexion with 10 kg load and (c,d) 50^{o} flexion without load. Age is set at 47.5 years.

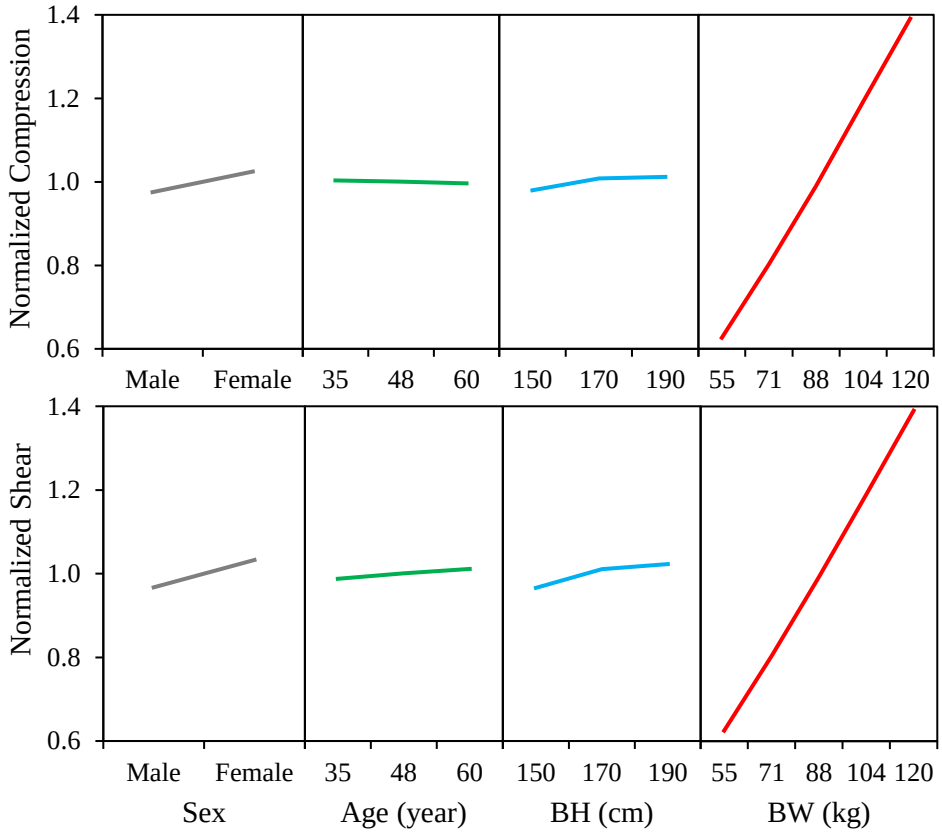

Figure 4.7 Main effect of all simulations plots for compression (top) and shear (bottom) forces normalized to the mean values at each task at the L5-S1 discs.

CHAPTER 5 ARTICLE 3: OBESITY AND OBESITY SHAPE MARKEDLY INFLUENCE SPINE BIOMECHANICS: A SUBJECT-SPECIFIC RISK ASSESSMENT MODEL

Authors: F. Ghezelbash, A. Shirazi-Adl, A. Plamondon, N. Arjmand, and M. Parnianpour

Published in *Annals of Biomedical Engineering* 45.10 (2017): 2373-2382

5.1 Introduction

Obesity (body mass index, BMI> 30 kg/m^2) is at spotlight due to an alarming increase in its growth and health care consequences. World Health Organization has recognized obesity as an "escalating global epidemic" (WHO, 2016a). In the US and UK, the prevalence of obesity has been estimated to reach as high as ~30-60% of adult population by 2030 (Wang et al., 2011), yet obesity is not limited only to the developed countries (WHO, 2016b). Previous studies have indicated that obesity increases the risk of disc degeneration (Liuke et al., 2005; Takatalo et al., 2013), vertebral fracture (Gonnelli, Caffarelli, & Nuti, 2014; Kim, Shin, Lee, Im, & Lee, 2010) and back pain (Heuch et al., 2010; Smuck et al., 2014; Webb et al., 2003). Nonetheless and despite their crucial role in effective prevention and treatment managements, the underlying mechanisms relating obesity to low back disorders have not yet been well understood. Adequate subject-specific investigation of the spine biomechanics in the obese population is needed to pave the way toward proper evaluation of risks involved and subsequent engineering of novel personalized treatments that has been recognized as one of the grand engineering challenges of this century (Perry et al., 2008). The issue is however involved and complex since even at identical body height (BH) and body weight (BW) (or BMI), the risk of back injury likely depends on the adipose tissue distribution along the body that varies much from one obese individual to another.

Three conditions, amongst others, are known as causal biomechanical factors for higher risk of spinal injury and low back pain: 1- over-loading in which the threshold strength of constituent materials are exceeded, 2- spinal instability where loads and/or muscles cause hypermobility

(abnormal laxity) in spinal joints and 3- cyclic (or fatigue) loading under rather smaller but repetitive loading conditions where the rate of damage propagation exceeds that of healing. For the first two conditions, the risks can be assessed by accurate examination of the mechanical equilibrium and its stability of the trunk neuromusculoskeletal system during various daily and occupational activities. As for the third condition, one may use recently proposed, based on compression fracture tests on human vertebrae, subject-specific fatigue-failure criterion (Huber et al., 2016b) which accounts for the spinal compression load, endplate area and bone mineral density (BMD). The foregoing considerations within a subject-specific framework appear promising in advancing our knowledge of the trunk functional and failure biomechanics toward a comprehensive subject-specific risk assessment.

The current study aims to investigate spine biomechanics and the risk of injury in obese population using a subject-specific framework. Employing the extensive database of National Health and Nutrition Examination Survey (NHANES) (including thousands of obese individuals), we initially perform the principal component (PC) analysis on a number of body measures of obese individuals to identify influential PCs and quantify various obesity shapes. Then, to accurately incorporate segmental mass distribution of these upper-body shapes in our validated subject-specific musculoskeletal model (Ghezelbash, Shirazi-Adl, Arjmand, El-Ouaaid, & Plamondon, 2016a; Ghezelbash et al., 2016b) (Chapter 3; Chapter 4) we perform regression analysis on the associated results of double-energy X-ray absorptiometry (DXA). Spinal loads, cycles to failure and trunk stability of different obesity shapes are computed during a free-style (static and symmetric) forward flexion task (in standing with and without a hand-load) for various BWs and obesity shapes. In accordance with earlier observations (Kim et al., 2010), we hypothesize that the obesity and obesity shape, markedly influences spinal loads and the risk of spinal fatigue injury.

5.2 Materials and Methods

5.2.1 Obesity Shapes

Fat distribution in obese individuals is commonly categorized into apple and pear body shapes. Such body attributes remain however qualitative as existing measures (like waist-to-hip ratio and waist circumference) overlook likely concurrent changes in other regions (such as arms, feet and head). To quantitatively identify various fat distributions, we initially carried out PC analysis on five body anthropometric measures (i.e., body height and calf/thigh/waist/upper arm circumferences) using the NHANES database of 5,852 obese individuals (18-85 years) (National Center for Health Statistics, 1999-2014). Variations of the third PC represented two different obesity shapes (apple and pear) at identical BH (Figure 5.1), and PCs (instead of direct body measures) takes account of concurrent changes in other regions of the body. In the foregoing representation, however, BW (as an influential spinal load determinant (Ghezelbash et al., 2016a; Han et al., 2013b) (Chapter 4)) varies from one shape to another, so the extreme shapes with maximum and minimum waist circumferences were developed based on an optimization process that took account of concurrent changes in various measures at constant BW. Three obesity shapes were then sought: 1- mean obesity, 2- with maximum waist (abdominal) circumference and 3- with minimum waist circumference. Mean obesity represents the average shape of all individuals with similar BW and BH; to select the individuals with similar BH and BW from the entire population (5852 individuals), we considered an interval with ±2.5% variations in BH and BW. Maximum and minimum waist circumferences are defined as apple- and pear-shaped obesities, respectively. The waist circumference was set as the cost function based on the 3 primary contributing PCs:

$$\text{Waist Circumference} = \alpha_1 PC1 + \alpha_2 PC2 + \alpha_3 PC3, \quad \text{Eq. 5.1}$$

PCi (i=1,2 and 3) are the principal components and α_i represent their eigenvector coefficients for the waist circumference (α_1=0.781, α_2=-0.476 and α_3=-0.389; see Table 5.1). PCi (i=1,2 and 3) in Eq. 5.1 were constrained to be within $\pm$3SD (standard deviation) of PC scores of individuals with

similar (within ±2.5% variations) BW and BH (within the interval of ±2.5% variation in BH and BW); this guaranties that the obtained solution (body shape) is within physiological boundaries. To constrain BW in the optimization process, we developed a linear regression equation (BW (kg) = 98.45 + 1.23 PC1 + 0.06 PC2 + 0.60 PC3; see Eq. 5.3), correlating BW and primary contributing PCs (the first three PCs which can describe 96.7% of variation in the data; see Results). Since BW substantially affects spinal loads (Ghezelbash et al., 2016a; Han et al., 2013b) (Chapter 4) we considered in this work three BWs (86, 98 and 109 kg) at a single BH=167 cm (average of the entire population) corresponding to BMI=30.8, 35.1 and 39.1 kg/m^2.

5.2.2 Subject-Specific Upper-Body Weights

Evaluating spinal loads in a subject-specific framework requires an accurate estimation of the upper extremity segmental masses (trunk, arms and head). Therefore, using the DXA of the total body from 1,462 obese individuals (18-85 years) (National Center for Health Statistics, 1999-2014), we developed regression equations to correlate these segmental masses with the body anthropometric measures (calf/thigh/waist/upper arm circumferences, body height and BW). Estimated arm masses (lower and upper arms) were then proportionally partitioned (Matrangola et al., 2008) and applied at their corresponding mass centers (De Leva, 1996; Ghezelbash et al., 2016b) (Chapter 3). Segmental masses along the spine at each level (T1 to L5) were rigidly attached onto the corresponding vertebra, and after the calculation of total trunk mass (Table 5.2), spinal segmental masses were proportionally partitioned while mass centers were scaled based on BH (see Fig. 2 in (Ghezelbash et al., 2016b) (Chapter 3)). For more details on gravity load partitioning see Appendix B.

5.2.3 Spinal Loads

To estimate spinal loads, our validated (for intradiscal pressure comparisons see Fig. 5 in (Ghezelbash et al., 2016b) (Chapter 3); for comparisons between estimated and measured back muscle activities during flexion see Fig. 6 in (Ghezelbash et al., 2016b) (Chapter 3); for comparisons between estimated and measured muscle activities maximum voluntary contractions

see Figs 7 and 8 in (Ghezelbash et al., 2016b) (Chapter 3) subject-specific nonlinear (both geometric and material) finite element musculoskeletal model which represents the entire compliance/rigidity of T11-T12 to L5-S1 motion segments (by separate shear deformable beams attached between rigid vertebrae) and 126 muscle fascicles was used. Both muscle architecture and nonlinear ligamentous spine were scaled in this model based on imaging databases (Anderson et al., 2012; Shi et al., 2014) and biomechanical principles (Ghezelbash et al., 2016b) (Chapter 3) description of the scaling algorithm is presented in Appendix C. Along with the physiological partitioning of the upper BW at different levels and wrapping of global muscles, muscle forces were computed using an iterative optimization- and kinematics-driven algorithm accounting for a gender- and age-specific lumbopelvic rhythm (Pries et al., 2015) during forward flexion from the upright standing to 90^o with and without a 5 kg held symmetrically in hands in front close to the body. Further details on the model and scaling approach are available elsewhere (Ghezelbash et al., 2016a, 2016b) (Chapter 3; Chapter 4).

5.2.4 Stability Analyses

After the evaluation of muscle forces and spinal loads (i.e., equilibrium phase), each muscle was replaced by a spring with a stiffness linearly proportional to its current force (F) and inversely proportional to its current length (l) as $k = qF/l$ where q denotes a dimensionless coefficient (Bergmark, 1989; Cholewicki & McGill, 1996). After verifications (i.e., identical results in this stability phase as those in prior equilibrium phase), the stability margin of the trunk was assessed by buckling analyses at the final deformed configurations. At each given load and posture, we defined the system stable if the additional buckling load (reserve margin computed from the linear buckling analysis) was greater than zero. Dimensionless muscle coefficient (q) was gradually reduced from a large value (say 100) down to a threshold at which the reserve load reached zero; the corresponding dimensionless muscle coefficient q_{cr} (critical q) was identified (Arjmand, Shirazi-Adl, & Parnianpour, 2008a; Ghezelbash et al., 2015).

5.2.5 Vertebral Fatigue Fracture

To estimate the risk of vertebral fracture due to cyclic loading at a given posture and external load condition, we employed a subject-specific regression equation which were developed based on the fatigue test of human cadaver specimens (Huber et al., 2016b):

$$Log_{10}(N) = 27.93 - 7.14\ log_{10}(F_{norm}), \quad \text{Eq. 5.2}$$

where N is the estimated cycles to failure, and F_{norm} denotes the compression force normalized by the subject-specific vertebral volumetric BMD and endplate area. Since DXA reported in the available dataset provides the areal BMD which is significantly correlated with the volumetric BMD,(Melton et al., 2007; Wang et al., 2012a) we estimated volumetric BMD from the proposed regression equation by (Wang et al., 2012a). The vertebral BMD for each obesity shape was subsequently estimated from DXA of 4,470 obese individuals (National Center for Health Statistics, 1999-2014) (1,954 individuals of this sample were a subset of foregoing 5,852 obese individuals (see section 5.2.1), but the rest are new individuals since NHANES did not measure spinal BMD and all anthropometric parameters in all years) at our assigned BW, BH and waist circumference (within $\pm$5% variations). We scaled the reference endplate area (14.55 cm^2) based on BH, BW, age and sex (not obesity shapes) assuming that the endplate area of the reference model (BH=173.0 cm, BW=75.1 kg, age=41.8 years and sex=male) varies proportionally to the maximum ribcage area at the transverse plane (see Appendix C) (Ghezelbash et al., 2016b) (Chapter 3). Personalized ribcage geometry was reconstructed based on proposed regression equations for given BH, BW, sex and age.(Shi et al., 2014)

5.3 Results

Five PCs were computed (Table 5.1) of which the first three explained 96.7% of variations in the data. The first PC was linearly correlated with the body weight (correlation coefficient, R=0.94), Figure 5.1 First principal component (PC1) versus body weight (BW) calculated for 5,852 obese individuals (National Center for Health Statistics, 1999-2014). The third PC represented various

obesity shapes at nearly identical BH showing quite different distributions of adipose tissue, Figure 5.2. The first three PCs could also satisfactorily predict the body weight (R=0.97; relative error ± SD=3.43%±2.80%):

$$BW\ (kg) = 98.45 + 1.23\ PC1 + 0.06\ PC2 + 0.60\ PC3. \quad \text{Eq. 5.3}$$

Besides, body measures (e.g., BH, BW, waist circumference) could accurately predict segmental masses, Table 5.2.

Additional BW by 12 kg increased local compression (~11.2%) and shear (~12.5%) loads at lower lumbar levels. At identical BH, BW and hence BMI, spinal loads varied with obesity shapes by as much as 11.0% at BW=86 kg, 17.7% at BW=98 kg and 14.8% at BW=109 kg in the L4-L5 compression (Figure 5.3) and 15.1% at BW=86 kg, 13.1% at BW=98 kg and 11.0% at BW=109 kg in the L5-S1 shear (Figure 5.4). Various obesity shapes (maximum versus minimum waist circumferences) at identical BH, BW and BMI substantially affected the vertebral fatigue cycle to compression fracture at the L4 level by nearly 3, 5 and 7 times, respectively at BW=86, 98 and 109 kg (Figure 5.5). However, increasing BWs improved spinal stability though only at the standing posture (Figure 5.6). Larger forward flexion stabilized the spine while having negligible effects on its fatigue failure cycles (>60^{o}).

5.4 Discussion

Using a complex and validated subject-specific musculoskeletal model of the trunk along with large and comprehensive datasets, the effect of obesity and its shape on the spinal loads, vertebral fatigue cycles to compression fracture and trunk stability were investigated under upright standing and flexion postures with and without a hand-load. Results confirmed the hypothesis that both obesity and obesity shape (greater waist circumference or abdominal obesity) substantially increases spinal loads and risk of fatigue failure, that further increase at larger BWs. This highlights the important role of not only BW and BMI but the adipose tissue distribution in spinal

biomechanics that should be considered for effective prevention, rehabilitation and treatment programs of low back disorders.

5.4.1 Limitations

Although we characterized our model to be validated, it was meant in a relative sense as no such complex biomechanical musculoskeletal model could be considered entirely validated. To estimate muscle forces, we used an optimization algorithm (quadratic sum of muscle stresses) that despite its satisfactory performance (Arjmand & Shirazi-Adl, 2006c) neglects inter- and intra-personal variability and antagonist coactivity. Spine shape (Meakin et al., 2008b; Pavlova et al., 2016) and muscle architecture were taken the same for different obesity shapes at identical BWs while scaling the model with subject's BW, BH, sex and age. Endplate area was assumed to be proportional to the maximum ribcage area in the transverse plane and was scaled based on BH, BW, sex and age (not obesity shapes), which can affect estimated cycles to failure. Passive spine properties were scaled based on BH, BW, age and sex (Appendix C) and not on obesity shapes. The effect of uncertainties in the estimation of passive properties were however small since when all passive properties (force-strain and moment-curvature) were altered by 5%, changes in spinal loads (at the L4-L5 and L5-S1 levels) remained <1.6%. Total segmental masses along the spine were rigidly connected to the corresponding vertebra despite the likely error especially at the abdominal levels filled with internal soft organs. Moreover, although scaling the total trunk weight were based on the obesity shape, we did not consider likely differences in segmental weights of different obesity shapes, though our earlier sensitivity analyses demonstrated that changes in spinal loads (at L4-L5 and L5-S1 levels) remained <7.5% when smaller lumbar masses were replaced with larger thoracic masses (Ghezelbash et al., 2016b) (Chapter 3). Lumbar lordosis remained constant in all subjects since no study has explored likely association between lumbar lordosis and obesity shapes, but sensitivity analyses showed that increasing lumbar lordosis by 10^{o} reduced the compression force (at the L5-S1) up to 12% and increased the shear force (at the L5-S1) up to 29%. Spine kinematics (lumbopelvic rhythm) in our model (based on reported measurements on skin) took account of sex and age but not of BW and obesity shape due to the unavailability of data. Earlier sensitivity

analyses on lumbopelvic ratio have demonstrated that a substantial alteration in this ratio from 0.5 to 3 reduces L5-S1 compression and shear forces by up to ~21% and ~45% (Tafazzol et al., 2014). Though muscle areas were scaled, changes in other muscle parameters (e.g., maximum muscle stress, muscle fat content) were not taken into account due again to the paucity in available data (Tomlinson, Erskine, Morse, Winwood, & Onambélé-Pearson, 2015). Due to the crucial role of alterations in BW on the spinal loads when compared to those in BH, sex and age (Ghezelbash et al., 2016a) (Chapter 4), the effect on results of only BW at three levels was considered. Due to limitations of DXA in accurate measurement of muscle mass (Maden-Wilkinson, Degens, Jones, & McPhee, 2013), the defined apple- and pear-shaped obesities may not exactly take account of all differences between two obesity shapes. In the fatigue failure analysis, we estimated volumetric BMD from areal BMD using a linear regression equation (Wang et al., 2012a).

5.4.2 Interpretations

5.4.2.1 Body Shapes

Though proposed in as early as 1940 (Sheldon, Stevens, & Tucker, 1940), the notion of body shape (or "somatotype" (Sheldon et al., 1940)) has overwhelmingly been neglected in earlier clinical and biomechanical studies; the main reason being likely the lack of data and proper approach to categorize body shapes (Streuber et al., 2016). The use of BMI, as the most popular parameter, tends to oversimplify obesity. The use of waist-to-hip ratio (Han, Schouten, Lean, & Seidell, 1997b) or waist circumference (Lean, Han, & Seidell, 1998b; Shiri et al., 2013) alone limits the attention and overlooks likely effects on results of concurrent changes in thigh, calf and arm. The current proposed method, however, addressed such shortcomings and qualified android/gynoid or apple/pear-shaped obesities which are two descriptive extreme body attributes (Seo, Cordier, & Magnenat-Thalmann, 2003) as maximum and minimum waist circumferences. Computed PCs were also found to be correlated with BW and body fat distributions (Figure 5.1 and Figure 5.2) with the former expressed as a dependent variable (Eq. 5.3).

5.4.2.2 Risk of Injury

At constant BW and BH and hence BMI, greater concentration of weight in the upper-body, in obese individuals with larger waist (abdominal) circumference, noticeably increased the loads on spine (Figure 5.3 and Figure 5.4). This effect further grew at larger BW; for example, at 90^{o} forward flexion without a hand-load, L4-L5 compression increased by 166 N (10.9%) at BW=86 kg but by 273 N (17.3%) at BW=109 kg as the waist circumference altered from its minimum to its maximum (Figure 5.3). Interestingly, the alteration in spinal forces was found greater when, at a constant BW, the waist circumference changed between its extremes than when, at the same waist circumference, BW altered from a level to another; for example from 86 kg to 98 kg (Figure 5.3 and Figure 5.4). This translates in the estimation of larger spinal forces even at smaller BW; for example when comparing mean waist circumference at BW=86 kg with minimum waist circumference at higher BW=98 kg and mean waist circumference at BW=109 kg with maximum waist circumference at lower BW=98 kg. In other words, extreme changes in waist circumference alter spinal forces to the extent of ~20 kg change in BW.

Damages to vertebrae (e.g. fracture) or discs can lead to perturbation in nutrient supply (Urban, Smith, & Fairbank, 2004), cell apoptosis (Haschtmann, Stoyanov, Gédet, & Ferguson, 2008), inflammation (Ulrich, Liebenberg, Thuillier, & Lotz, 2007), additional innervation (Fagan et al., 2010) and subsequent degeneration and pain (Adams & Roughley, 2006; Dudli, Ferguson, & Haschtmann, 2014; Marras et al., 1995; van Dieën, Weinans, & Toussaint, 1999; Vergroesen et al., 2015b; Wang, Videman, & Battié, 2012b). As a result of marked increases in compression and shear forces, the risk of over-load and fatigue failure (in annulus (Green, Adams, & Dolan, 1993a) and/or vertebra (Brinckmann, Biggemann, & Hilweg, 1988)) substantially increased especially at greater waist circumferences that tended to accentuate the corresponding effect of BW as well (Figure 5.5). Gains in BW, by increasing simultaneously both the spinal forces and BMD (Hamilton, Fisher, Roy, Gower, & Hunter, 2013; Khosla, Atkinson, Riggs, & Melton, 1996), appear to play opposing roles in the risk of vertebral injury. Our results, however, demonstrated that the aggravating effect of larger spinal loads subdued the shielding role of accompanying

increase in BMD resulting in a substantial drop in cycles to fatigue compression fracture (i.e., increased risk of fracture) at higher waist circumferences. In contrast, however, the risk of vertebral fracture remained the same at smaller waist circumference irrespective of changes in BW considered here (Figure 5.5). In corroboration with these findings, the favorable effect of BW on BMD (Hamilton et al., 2013; Khosla et al., 1996) has been reported to even reverse in obesity with large waist circumferences (Kim et al., 2010) which would further increase the risk to fracture. Based on our findings, BMD and BMI cannot hence be used as sole surrogate measures of the risk of vertebral fatigue fracture since body shape also plays a substantial role.

Consideration of BMI alone in some earlier studies (El Maghraoui et al., 2015; Laslett, nee Foley, Quinn, Winzenberg, & Jones, 2012; Pirro et al., 2010) may therefore have concealed the role of obesity in vertebral fractures that remain still controversial. On the other hand and in agreement with our findings, Kim et al. (2010) found greater prevalence of vertebral fracture among female obese individuals with higher body fat ratio and waist circumference. It should be noted that various factors play a role in vertebral fracture. Although obesity can improve BMD by stimulating bone formation through increased mechanical loads, insulin secretion, increased sex hormone level and androgens to estrogens conversion; obesity reduces BMD due to increases in cytokines (mainly IL and TNF-α which have lower levels in subcutaneous fat than in abdominal adipose tissue) and leptin (Gonnelli et al., 2014).

Unlike foregoing increases in the risk of injuries associated with larger spinal loads, increases in BW irrespective of the obesity shape improved the spinal stability though only at the upright standing posture. This points to the favorable effect of gain in BW in increasing the passive ligamentous and musculature stiffness contributions despite deteriorating effect of associated compression forces at larger magnitudes. Overall, greater risk of over-loading and fatigue fracture along with the reported reduction in global postural balance (Corbeil et al., 2001; Hue et al., 2007), increase in fall [(Allin et al., 2016)], limitations in goal-directed movements (Berrigan et al., 2006) and adipokines release (Samartzis et al., 2013) tend to predispose the obese population to additional

injuries whereas the reduction in the range of motion (Park et al., 2010; Vismara et al., 2010) and physical activity (Smuck et al., 2014) might mitigate this risk.

5.4.2.3 Bone Formation

Bone formation increases BMD and strengthens vertebrae (Bruno et al., 2014; Crawford, Cann, & Keaveny, 2003); however, not all physical activities offer the potential to stimulate bone formation unless some threshold values (i.e., dead zone) are reached and exceeded. Notwithstanding relative paucity in available data on the effect of various stimulus characteristics on bone formation, future works should incorporate subject-specific considerations in comprehensive prevention, rehabilitation and treatment programs (such as designing subject-specific exercise programs which minimize injury risk and stimulate bone formation for individuals with osteopenia and osteoporosis).

5.5 Conclusion

We estimated the risk of spinal injury (by over-load, repetitive loading and instability) during various activities in upright and forward flexion tasks for different obesity types (i.e., different BMIs, apple- and pear-shaped) in a subject-specific framework where musculature, passive ligamentous spine, segmental weights, trunk kinematics and BMD were personalized. In obese individuals and in contrast to BH, sex and age (Ghezelbash et al., 2016a) (Chapter 4), changes in BW and obesity shape markedly influenced spinal loads. At identical BW and BH, obese individuals with larger waist circumference (i.e., abdominal obesity) experienced greater loads equivalent to those with ~20 kg additional BW. Greater waist circumferences being associated with larger spinal loads and lower BMD substantially boosted the risk of vertebral fracture by ~3-7 times. This study should be considered as the first attempt to explore the role of body shape (or obesity shape or somatotypes) by combining various available databases. Caution should be exercised when extending these findings in clinical applications. It took account of crucial failure modes while employing a subject-specific trunk musculoskeletal. Moreover, consideration of bone

formation potential, as a risk mitigation factor, demonstrate the future potential of such approaches in design and management of subject-specific rehabilitation programs (Ross et al., 2000).

5.6 Acknowledgments

This work was supported by the institut de recherche Robert-Sauvé en santé et en sécurité du travail (IRSST-2014-0009) and the fonds de recherche du Québec en nature et technologies (FRQNT; merit scholarship program for foreign students - 200564).

Table 5.1 Computed eigenvalues and eigenvectors of principal components (PCs) evaluated from the dataset of 5,852 obese subjects (18-85 years) (National Center for Health Statistics, 1999-2014)

Body Parameters		***PC1***	***PC2***	***PC3***	***PC4***	***PC5***
Eigenvalues (λ_i)		191.9	77.2	45.6	5.9	4.9
Eigenvecto	Calf Circumference (cm)	0.178	-0.014	0.362	-0.026	0.915
	Arm Circumference (cm)	0.195	-0.083	0.237	0.942	-0.107
	Waist Circumference (cm)	0.781	-0.476	-0.389	-0.107	-0.008
	Thigh Circumference (cm)	0.283	-0.119	0.810	-0.317	-0.386
	Body Height (cm)	0.490	0.867	-0.074	-0.013	-0.053

Table 5.2 Coefficients of regression equations for various body part masses (gram), plus correlation coefficients (R) and relative errors of the regression equations evaluated from DXA of the total body of 1,462 obese individuals (18-85 years) (National Center for Health Statistics, 1999-2014)

Body Parts	***Regression Equation Coefficients***							***R***	***Relative Error % (SD)***
	Constant (gram)	Body Weight (gram/kg)	Body Height (gram/cm)	Thigh Circum.† (gram/cm)	Waist Circum. (gram/cm)	Arm Circum. (gram/cm)	Gender* (gram)		
Trunk**	1.73E4	593.09	-67.09	-370.01	110.05	-136.26	-	0.98	3.08 (2.46)
Arm	-5.08E3	48.77	21.79	-33.76	-2.23	129.29	-	0.95	5.78 (4.82)
Head	3.61E3	20.32	-	-	-	-2.83	-611.34	0.78	6.83 (5.27)

† Circumference

* Male=0; Female=1

** As an example: Trunk Mass (gram) = 1.73×10^4 + 593.09×[Body Weight (kg)] – 67.09×[Body Height (cm)] – 370.01×[Thigh Circumference (cm)] + 110.05×[Waist Circumference (cm)] – 136.26×[Arm Circumference (cm)]

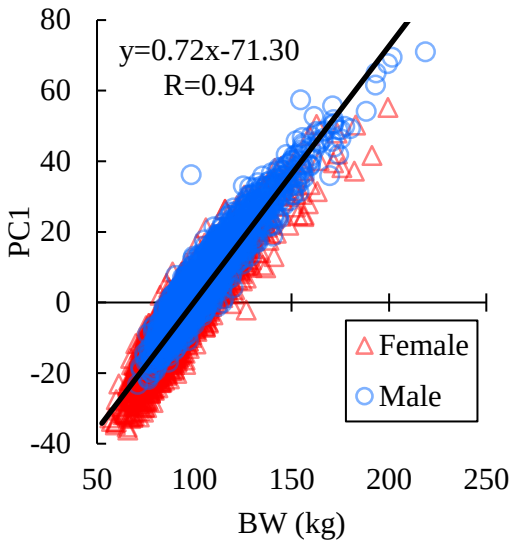

Figure 5.1 First principal component (PC1) versus body weight (BW) calculated for 5,852 obese individuals (National Center for Health Statistics, 1999-2014)

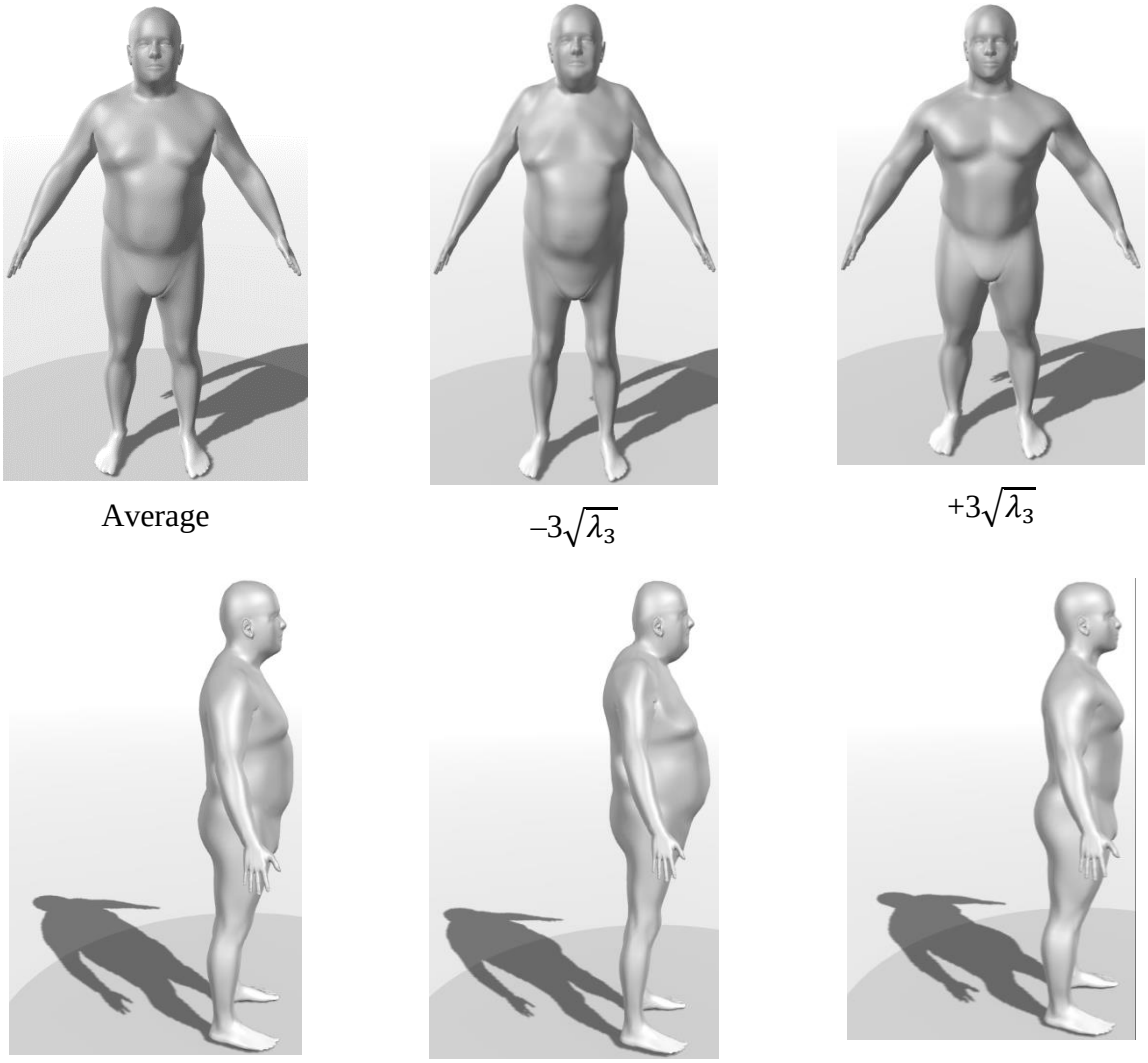

Figure 5.2 Schematic representation of the mean obesity (5,852 obese individuals) and body shape variations described by the third PC (with limits applied at $\pm 3\sqrt{\lambda_3}$, where λ_3 denotes the third principal eigenvalue) in frontal (top) and sagittal (bottom) planes (Black, 2015)

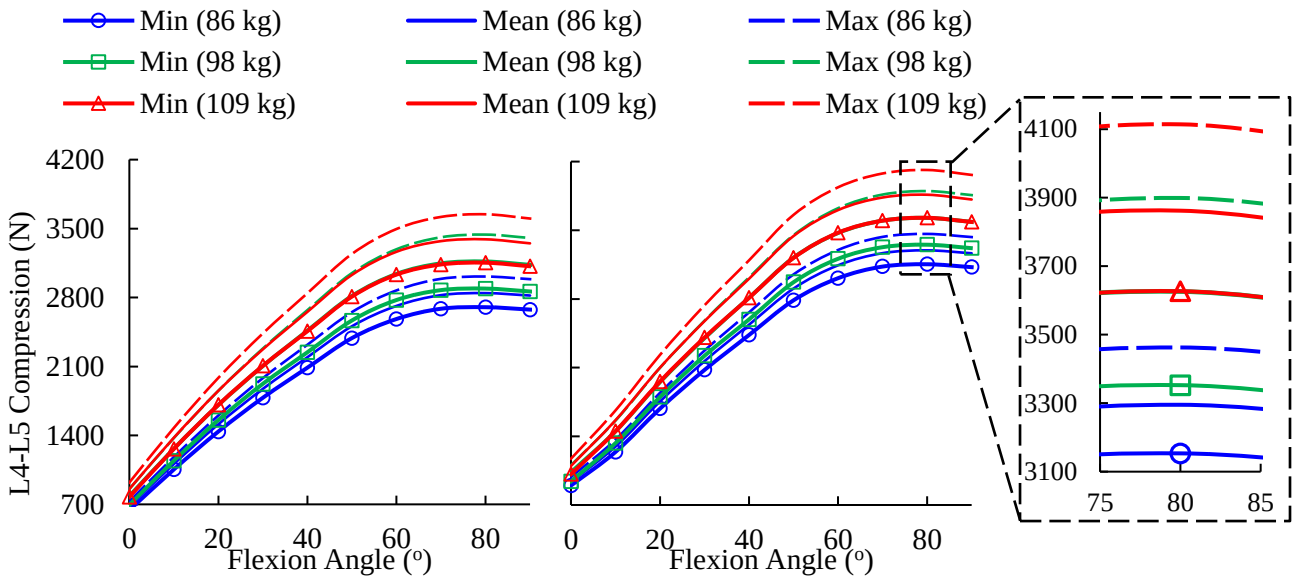

Figure 5.3 Local spinal compression force at the L4-L5 disc during flexion without load (left) and with 5 kg weight in hands (right) for three different body weights three obesity shapes (maximum, mean and minimum waist circumferences) at BH=167 cm, sex=male and age=42 years

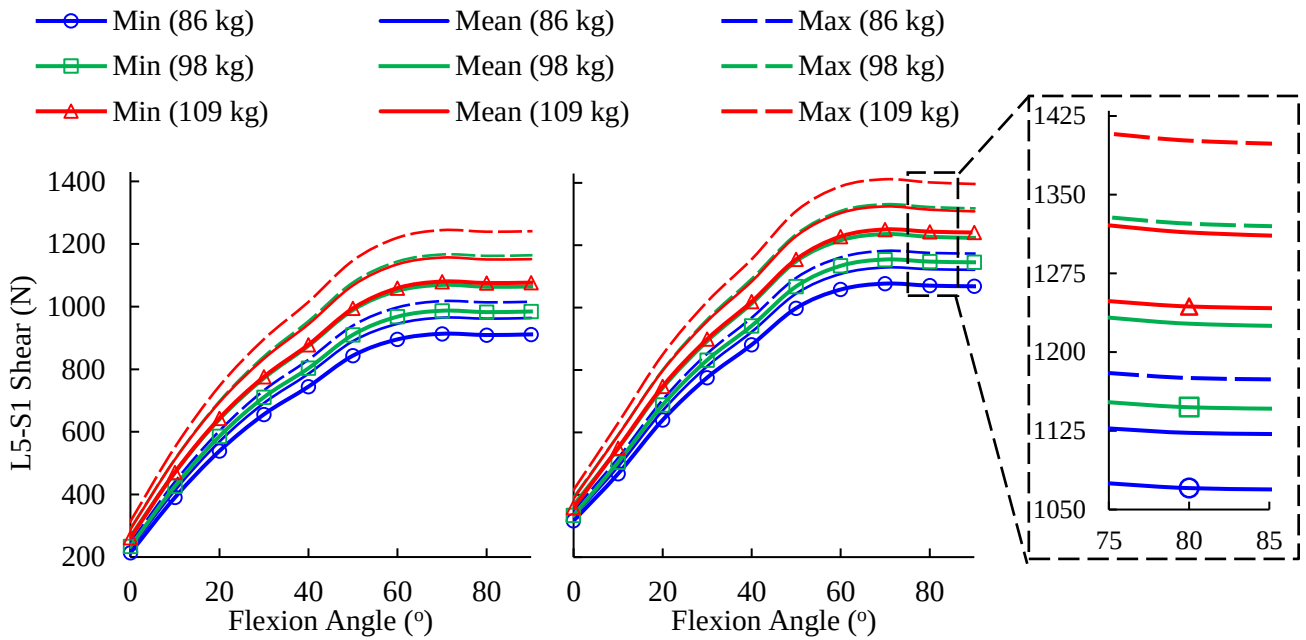

Figure 5.4 Local spinal shear force at the L5-S1 disc during flexion without load (left) and with 5 kg weight in hands (right) for three different body weights and three obesity shapes (maximum, mean and minimum waist circumferences) at BH=167 cm, sex=male and age=42 years

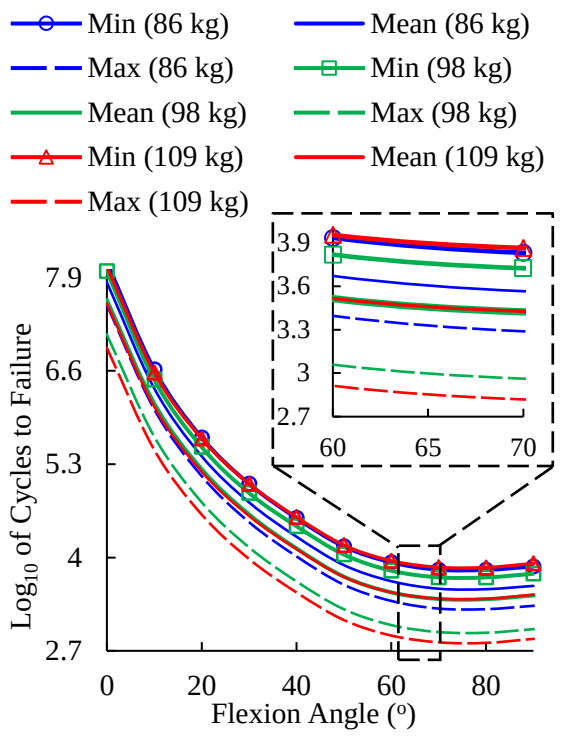

Figure 5.5 Estimated cycles to failure of the L4 vertebra during flexion for three different body weights and three obesity shapes (maximum, mean and minimum waist circumferences) at BH=167 cm, sex=male and age=42 years

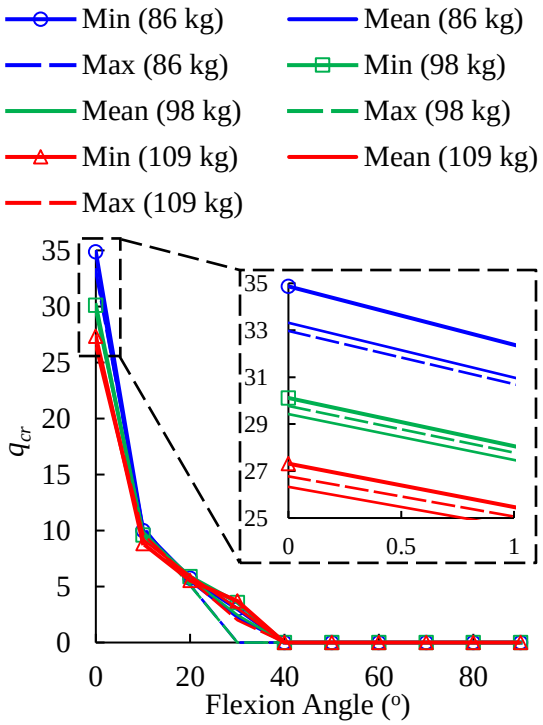

Figure 5.6 Computed minimum (critical) muscle stiffness coefficient (q_{cr}) required to maintain trunk stability during flexion for three different body weights and three obesity shapes (maximum, mean and minimum waist circumferences) at BH=167 cm, sex=male and age=42 years

CHAPTER 6 ARTICLE 4: EFFECTS OF MOTION SEGMENT SIMULATION AND JOINT POSITIONING ON SPINAL LOADS IN TRUNK MUSCULOSKELETAL MODELS

Authors: F. Ghezelbash, A.H. Eskandari, A. Shirazi-Adl, N. Arjmand, Z. El-Ouaaid, and A. Plamondon

Published in *Journal of Biomechanics* 70 (2018): 149-156.

6.1 Introduction

Under mechanical loads and motions in various daily activities, spinal motion segments display complex nonlinear and transient responses that alter with time, preloads and load/motion directions/magnitudes (Gardner-Morse & Stokes, 2004a; Panjabi, Oxland, Yamamoto, & Crisco, 1994). Detailed finite element (FE) models, as predictive tools, can satisfactorily replicate these responses in static (Dreischarf et al., 2014; Naserkhaki, Jaremko, Adeeb, & El-Rich, 2016; Shirazi-Adl, 1994a, 1994b), viscoelastic (Jones & Wilcox, 2008; Wang, Parnianpour, Shirazi-Adl, & Engin, 2000; Wang et al., 1997) and poroelastic (Argoubi & Shirazi-Adl, 1996; Schmidt, Shirazi-Adl, Galbusera, & Wilke, 2010; Schroeder, Wilson, Huyghe, & Baaijens, 2006) conditions. However, due to the substantial computational burden of such detailed FE models especially in iterative algorithms (Schmidt, Galbusera, Rohlmann, & Shirazi-Adl, 2013; Toumanidou & Noailly, 2015), musculoskeletal models of the trunk commonly employ more simplified approaches to take account of the intervertebral joints (including intervertebral discs, ligaments and facet joints) and the spinal passive responses. Proper representation of the intervertebral joints and passive stiffness contributions are crucial in accurate estimation of both muscle forces and hence internal spinal loads and trunk stability margin (Dreischarf, Shirazi-Adl, Arjmand, Rohlmann, & Schmidt, 2016b). Some models use spherical joints (ball and socket or hinge joints) with fixed centers of rotation along with rotational springs (with linear or nonlinear stiffness properties) (Bruno et al., 2015; Cholewicki & McGill, 1996) while others employ beams (stiffness matrices or bushing elements) that take into account translational degrees of freedom (Christophy, Curtin, Senan, Lotz, & O'Reilly, 2013; Ignasiak et al., 2016a; Malakoutian et al., 2016) and coupled terms as well (El-Rich et al., 2004; Meng et al., 2015; Stokes & Gardner-Morse, 2016). Although foregoing rather

simplified models have extensively been employed in earlier studies, their relative accuracy in representing joint kinematics and kinetics remains yet unknown.

Some important concerns regarding these rather simplified models of motion segments include the type of model (beam element versus spherical joint), the use of linear mechanical properties (rotational springs or beams) or none at all (frictionless spherical joints) to simulate passive responses of motion segments and their placement within the spinal joints (cranial-caudal and anterior-posterior). According to the approximation theory, linearizing nonlinear responses of motion segments remains valid only in the neighbourhood of the linearization point, yet the validity domain of utilizing linearized elements has not been explored. Furthermore, some earlier studies carried out sensitivity analyses on the anterior-posterior (Han, Kim, Park, Lim, & Kim, 2013a; Zander, Dreischarf, & Schmidt, 2016) and cranial-caudal (Ghezelbash et al., 2015) positioning of spherical joints and reported marked effects on computed muscle forces and spinal loads. In this regard, changes in the position of the joint center in musculoskeletal models with frictionless spherical joint has been found to have substantial effects on model predictions (Zander et al., 2016). For accurate results, the joint center should coincide with the joint "center-of-reaction" that however neither is known a priori nor remains constant under applied loads and motions (Zander et al., 2016). No comprehensive sensitivity analyses have yet been carried out on the effects of alterations in anterior-posterior positioning of (shear deformable, linear and nonlinear) beam elements or moment resisting spherical joints on predictions of trunk musculoskeletal models.

We, therefore, aim here to investigate the relative performance and accuracy of the simplified models (i.e., spherical joints and shear deformable beams), the effects of using linearized passive properties (instead of the more accurate nonlinear properties) and the role of positioning of the simplified models when predicting trunk kinematics and kinetics. To do so, we initially compare displacements-flexion moment responses of a detailed lumbar spine FE model (Shirazi-Adl, 1994a, 1994b) with those of the simplified models (employing beams or spherical joints with linear and nonlinear stiffness properties). Subsequently, using a validated nonlinear subject-specific FE musculoskeletal model of the trunk (Ghezelbash et al., 2016b) (Chapter 3), foregoing

linear/nonlinear beam elements and spherical joints (representing the entire motion segments) are shifted at all levels in the anterior-posterior direction and muscle forces as well as spinal loads are computed. Estimated intradiscal pressures (IDPs) at the L4-L5 are also compared versus available in vivo measured IDPs (Wilke et al., 2001) during flexed and standing tasks with/without a load in hands. It is hypothesized that the trunk active-passive kinematics-kinetics response is substantially influenced by both the simplification in the model (particularly linear ones) employed and its anterior-posterior position. Based on the characteristic of the center-of-reaction at which no moment resistance exists, it is also hypothesized that for a unique estimation of muscle forces and internal loads as the joint center shifts posteriorly, the simulated passive moment resistance of the motion segments should increase.

6.2 Methods

Here, we compared passive ligamentous spine (without muscles) responses of simplified models (beams/spherical joints with linear/nonlinear stiffness) versus those of a detailed lumbar spine FE model (Shirazi-Adl, 1994a, 1994b) to determine which simplified approach estimated kinematic responses of the lumbar spine accurately and to identify likely deviations in responses from the detailed FE model. Then, the corresponding musculoskeletal model of each simplified ligamentous spine model were developed by adding the same musculature.

6.2.1 Ligamentous Spine

To investigate the performance of and accuracy in utilizing beams and moment resisting spherical joints in the trunk musculoskeletal models when simulating the ligamentous spine (isolated spine without muscles), we initially compared their predictions with those (displacements- flexion moment and L1 instantaneous center of rotation (ICoR)) of a detailed lumbar spine FE model (Figure 6.1a) under 20 Nm flexion moment and 2.7 kN follower compression load (Shirazi-Adl, 2006). The lumbar spine model (L1 to S1) were previously developed based on CT scans of a cadaver and included intervertebral discs, curved facet surfaces, ligaments and vertebrae (which were modeled each as two rigid bodies interconnected with two deformable beams to account for

vertebral compliance) (Shirazi-Adl, 1994a, 1994b). In the beam and spherical joint models, responses were simulated under similar moment and compression follower load (i.e., a load that causes nearly zero vertebral rotations when no moment is applied) passing through beams/spherical joints (from the upper endplate to the lower one) with the L1-L5 vertebrae completely free but the S1 fixed. Simplified models are described as follows:

- **Nonlinear beam model:** In this model Figure 6.1b), vertebrae were assumed rigid and motion segments were replaced with shear deformable beams (representing discs, ligaments and facets) with nonlinear properties running between adjacent vertebral endplate centers (offset=0 mm, Figure 6.1e). Nonlinear moment-curvature (level-dependent and different in flexion than in extension) and compression force-strain (level dependent) properties of beams were assigned and verified to match those of the detailed FE model (Shirazi-Adl, 2006) under similar external loading and boundary conditions (see curves in (Ghezelbash et al., 2016b) (Figure 3.2)). Nonlinear moment-curvature and compression force-strain properties of beams were assigned (Shirazi-Adl et al., 2002) and verified to match results of the detailed FE model under similar external loading and boundary conditions (Shirazi-Adl, 2006). Additional models were developed by rigidly shifting beams at all levels perpendicular to their disc mid-height planes (parallel to their reference orientations) (i.e., offset= –2, 2, 4 and 8 mm, Figure 6.1e).

- **Linear beam model:** The nonlinear passive properties (moment-curvature and compression force-strain) of the foregoing nonlinear beam model with offset at 4 mm were linearized at and around the origin (up to ~600 N compression and 4 Nm flexion moment) of the load-displacement curves.

- **Nonlinear spherical joint model:** Each beam in the beam models was replaced with a spherical joint (Figure 6.1c) placed at its midpoint of corresponding beam when offset=0 mm, Figure 6.1e. To account for the nonlinear stiffness of the passive ligamentous spine, we reinforced these joints with nonlinear rotational springs (representing the stiffness of intervertebral discs, ligaments and facet joints) with moment-rotation curves matching those

of the detailed FE model (Shirazi-Adl, 2006). Additional models were developed by shifting these joints along the disc mid-height anteriorly by -2 mm or posteriorly by +4 mm.

- **Linear spherical joint model:** The nonlinear rotational springs in the spherical joint model with offset at 4 mm were linearized at and around the origin (up to ~4 Nm flexion moment) of the moment-rotation curve. Translational degrees of freedom are naturally neglected in spherical joint models.

6.2.2 Musculoskeletal Model

We used our nonlinear subject-specific FE model of the trunk which includes 7 deformable (beams or spherical joints) spinal levels (T11-T12 to L5-S1) and takes account of 126 sagittally-symmetric muscle fascicles to compute muscle forces and spinal loads in an optimization- and kinematics-driven framework (Ghezelbash et al., 2015; Ghezelbash et al., 2016b). At each task, required (reaction) moments at various vertebral levels (T11 to L5) were obtained from the nonlinear FE model. An optimization algorithm estimated muscle forces to minimize the sum of quadratic muscle stresses (as the objective function) along with moment equilibrium equations at all vertebral levels imposed as equality constraints and muscle forces bounded to be greater than the passive force component (Davis et al., 2003) and less than the sum of the passive force component plus $PCSA \times \sigma_{max}$ (where $PCSA$ and σ_{max} = 1 MPa are physiological cross sectional area and maximum muscle stress). At the subsequent iteration, estimated muscle forces were applied to the corresponding vertebra as additional external forces and the iteration repeated until convergence (i.e., muscle forces remaining almost the same in two consequent iterations). Upper body gravity loads were partitioned along the spine (T1 to L5) (Pearsall et al., 1996) as well as arms, head-neck and hands (De Leva, 1996). T11 and S1 rotations were estimated based on sex- and age-specific lumbopelvic rhythm (Pries et al., 2015), and then the total T12-L5 rotations were partitioned by 6.0% at T11–T12, 10.9% at T12- L1, 14.1% at L1–L2, 13.2% at L2–L3, 16.9% at L3–L4, 20.1% at L4–L5, and 18.7% at L5-S1 (Ghezelbash et al., 2016b) (Chapter 3). Further details on the model and the scaling algorithm are available elsewhere (Ghezelbash et al., 2016b) (Chapter 3).

Once more here we shifted (rigidly displaced parallel to its reference orientation) nonlinear and linear beams/spherical joints (representing the entire motion segment: disc, ligaments and facets) at all 7 levels (T11-T12 to L5-S1) from 2 mm anterior to -8 mm posterior from the reference position (offset=0 mm, Figure 6.1e). Furthermore, as an extreme case, we removed passive elements (rotational springs) and simulated joints as pure frictionless spherical joints with zero offset. In each case, neutral standing posture under gravity alone was initially sought through an optimization process (Shirazi-Adl et al., 2002). Within a kinematics- and optimization-driven framework, muscle forces were then computed in various static standing and forward flexion tasks with/without load (19.8 kg mass) in hands similar to those considered in in vivo studies (Wilke et al., 2001). We evaluated spinal loads using force equilibrium equations and estimated IDPs by employing a quadratic regression equation ($\mathrm{IDP}(P,\theta) = -1.556\times10^{-2} + 1.255P + 1.243\times10^{-2}\theta + 3.988\times10^{-2}P^2 - 1.212\times10^{-2}P\theta + 1.669\times10^{-3}\theta^2$ where P (MPa) denotes the nominal pressure (compression (N)/total disc cross sectional area (mm^2)) and θ (°, positive in flexion) is the intersegmental flexion rotation (Ghezelbash et al., 2016b) (Chapter 3)). After the computation of muscle forces (F) during forward flexion, passive (F_p) and active (F_a) muscle forces of global back muscles were estimated taking $F = F_a + F_p$, with F_p estimated from the muscle elongation (Davis et al., 2003). In the current study, the model was adjusted to fit the subject participated in the IDP measurement study (age= 42, sex=male, body height=173.9 cm and body weight=72 kg) since those personal parameters and particularly the body weight substantially affect spinal loads and hence IDP estimations (Ghezelbash et al., 2016a) (Chapter 4).

6.3 Results

6.3.1 Ligamentous Spine

Under 2700 N follower compression preload and up to 20 Nm flexion moment, L1 (at vertebral center) rotation- and translations-moment responses of the nonlinear beam agreed well with those of the detailed FE model (Figure 6.2). On the contrary, linear and nonlinear spherical joint models of the passive ligamentous spine deviated from the detailed FE model, particularly in the axial Z-

translation (Figure 6.2c). In contrast to (linear/nonlinear) spherical joints, the nonlinear beam models with posterior offsets up to +4 mm satisfactorily simulated the path of the L1 centroid, Figure 6.3. The instantaneous center of rotation (ICoR) of the L1 was also best simulated by both nonlinear beam elements (correlation coefficient=0.91, mean absolute error of 1.4 mm at -2 mm offset and 3.6 mm at 4 mm offset) as well as the nonlinear spherical joints (correlation coefficient=1.00, mean absolute error of 2.8 mm at -2 mm offset and 4 mm at 4 mm offset) at -2 mm to +4 mm offset; on the other hand, linear spherical joints model (and to a lesser extent the linear beam model) could not replicate the ICoR path either pattern- or magnitude-wise (Figure 6.3).

6.3.2 Musculoskeletal Model

The models and the anterior-posterior placement of joints markedly affected spinal loads, especially under greater flexion angles. Using linear (instead of nonlinear) passive properties increased shear and compression forces, at peak flexion, by 26.3% (174 N) and 17.0% (296 N) in the beam model whereas 18.7% (111 N) and 6.1% (125 N) in the spherical joint model, respectively (Figure 6.4). As an extreme case, neglecting passive properties (joint stiffnesses) in the spherical joint model ("No Passive" model in Figure 6.4 and Figure 6.6) substantially increased L5-S1 shear and compression forces (at peak flexion by 63.0% and 32.3% or equivalently by 330 N and 665 N, respectively), Figure 6.4. At the joint offset of +4 mm and in forward flexion, estimated L5-S1 local compression and shear forces increased from their values at the reference case (i.e., 0 mm) by as much as 10.9% and 15.7% in the nonlinear beam model, and 11.4% and 12.4% in the nonlinear spherical joint model, respectively (Figure 6.4). Likewise and in accordance with the variations in computed compression forces, when linearized passive properties were utilized (or neglected in the spherical joint model) and when the joints shifted posteriorly, the estimated IDPs markedly increased especially in the heavier tasks with load in hands (Figure 6.5). Location of joint in both beam and spherical joints substantially affected the force partitioning between passive and active muscle components. As joints shifted posteriorly, the active component of back muscles

increased (e.g., by 137 N in the global iliocostalis muscle) while at the same time the passive component dropped (e.g., by 107 N in the global iliocostalis muscle) (Figure 6.6).

6.4 Discussion

In the current study, we explored the relative performance and validity of various rather simplified models of spinal motion segments regularly used in trunk musculoskeletal models. In particular, spherical joints were compared to beam elements using matched linear and nonlinear stiffness properties with locations varying from the anterior to the posterior of the disc geometric centers. The predictions were compared in a ligamentous lumbar spine model versus a detailed L1-S1 FE model under follower compression and flexion moment and in a trunk musculoskeletal model in forward flexion with and without load in hands versus reported in vivo disc pressure measurements. Equivalent stiffness properties of nonlinear beam as well as spherical joint models were initially set by matching global displacements under combined flexion-compression with those of an existing detailed FE model. Hypotheses were confirmed in finding substantial effects of modeling, especially when using linear stiffness properties or no stiffness at all in frictionless spherical joints, and joint position on spine kinematics and kinetics. Muscle forces and spinal loads increased as joints shifted posteriorly. Finally, for identical predictions on muscle forces and spinal loads, one is needed to increase passive properties (joint stiffnesses) to counterbalance the added moment of external/gravity loads as well as the reduced resisting moment of back muscles as joint position shifts posteriorly.

6.4.1 Limitations:

Kinematics were matched only under flexion moments up to 20 Nm in the presence of a 2700 N follower compression preload. While considering the stiffening role of the compressive preload in flexion (Shirazi-Adl, 2006; Stokes, Gardner-Morse, Churchill, & Laible, 2002) and the nonlinear responses in flexion and compression, the employed nonlinear shear deformable beam model should be considered only as a rather simplified replicate of a detailed FE model of the motion segment. Nonlinear beam and spherical joint musculoskeletal models with the offsets at 0 (in peak

flexion and for the spherical joint only) and -2 mm (in 90^{o} and peak flexions) did not converge due to excessive flexion moments at the lower lumbar levels. Likewise, linearized models did not converge in upright posture holding a 19.8kg load away. The current study focused only on sagittally symmetric tasks (both posture and loading). Although nonlinear beam and spherical joint models demonstrated satisfactory performances in such conditions, extension of findings to asymmetric tasks should await future studies. Presented results with alterations at all levels cannot identify the relative effects of changes in individual segments on results that would require a sensitivity analyses on each joint positioning. Other limitations and shortcomings related to the musculoskeletal modeling are presented elsewhere (Arjmand & Shirazi-Adl, 2006a; Ghezelbash et al., 2015; Shahvarpour et al., 2015b).

6.4.2 Interpretation and Comparison

Unlike the nonlinear beam model, the nonlinear spherical joint model did not as accurately predict cranial-caudal translation (Figure 6.2c) due to the lack of translational degrees of freedom. This model overlooks the compliances under shear and axial compression forces and as such its response predictions deteriorate further under greater loads. Another variable in spherical joint modeling, unlike the beam simulation, is the cranial-caudal location of the joint. Here we placed these joints at the disc mid-heights at all levels and analyses. Our earlier studies, however, demonstrated that changing the center of spherical joints from the mid-disc height in the cranial-caudal direction within upper and lower endplates would yield up to ~15% and ~30% differences in the computed compression and shear forces, respectively (Ghezelbash et al., 2015).

Posterior joint offsets in both beam and spherical joints locations in the musculoskeletal models substantially affected muscle forces and spinal loads. For example, L5-S1 spinal loads increased up to 20.1% in compression and 23.1% in shear as the beam shifted from the disc center posteriorly by 8 mm. Spinal loads however dropped by 9.7% and 18.2% as the joint shifted anteriorly by 2 mm. Foregoing alterations in muscle forces and spinal loads are due directly to the combined effects of changes in the net external moments, lever arms of muscles evaluated at the updated position of joints and alterations in extensor muscle passive forces. As the joint (beam or spherical

model) shifts posteriorly, the net external moment of gravity and load in hands increase while the lever arm of extensor muscles decrease resulting both in larger muscle forces and hence spinal loads. Reverse trends occur as the joint shifts anteriorly instead. At flexion>70^{o}, increases in muscle lengths and thus passive muscle forces noticeably decreased as joints shifted posteriorly (Fig. 6), and since at full flexion, passive muscle forces are a major contributor to spinal loads, computed IDPs at full flexion by different beam models remained almost the same (Figure 6.5). In agreement with our findings, Zander et al. (2016) and Han et al. (2013a) also computed larger (smaller) spinal loads when joints shifted posteriorly (anteriorly).

In other words and as schematically illustrated in Figure 6.6, when joint locations shift posteriorly at all levels (from point 1 to 2 or 3), muscle forces increased resulting in larger compression forces. Alternatively and in order to keep muscle forces and hence joint loads at constant magnitudes irrespective of the joint location, passive resistance of the joint should increase as the joint location shifts posteriorly. This condition is shown in Figure 6.7 where although there is no internal moment required when the joint center instantaneously coincides with the joint "center-of-reaction", the internal resistant moment should increase as the joint center shifts from the point 1 to 2 and further to 3; $M_3 > M_2 > M_1 \sim 0$. In addition and compared to the beam model at identical locations, the spherical joint model even with nonlinear properties overestimated compression forces (or equivalently IDPs) in demanding tasks (e.g., lifting 19.8 kg load at flexion 70^{o}, Figure 6.5) due mainly to overlooking the stiffening role of the compressive force on the passive responses. Neglecting this factor particularly in demanding tasks reduced the load-carrying role of the passive spine and increased muscle activities (Arjmand & Shirazi-Adl, 2005). Overall, best agreements were found in beam models with smaller joint offsets. In this study, we shifted joints along the corresponding disc mid-height plane, which is more reasonable. Additional analyses with joint offsets carried out in global horizontal direction (X) did however demonstrate only negligible changes in spinal forces (<1% smaller in compression and <4% greater in shear).

Variations in joint offset altered spinal kinematics and therefore active-passive muscle force partitioning and net moment resistant contributions. As joints shifted anteriorly, net moments and

the active component of back muscles both decreased (Figure 6.6); thus, at early- to mid-flexion points, larger spinal loads in models with posteriorly placed joints were mainly due to larger active components in muscle forces. However, anterior joint placement also markedly increased the elongation in extensor muscles and hence their passive forces (Figure 6.6) so much so that at flexions>70^{o}, these passive muscle forces and resulting spinal loads increased significantly in models at greater anterior offsets counterbalancing the effects of reduction in active muscle forces (Figure 6.5 and Figure 6.6). Featured by a substantial drop in extensor muscle activities, flexion-relaxation angle (defined as the trunk forward flexion at which extensor muscles become silent) was delayed from ~60^{o} to ~90^{o} as joints shifted from -2 to 8 mm. This occurred since anterior offset in joints tended to substantially and concurrently increase passive but decrease active force contributions of back muscles. It is interesting to note that, in counterbalancing the excessive resistant moment generated by large passive forces in extensor muscles, anterior disc offset tends also to further increase antagonistic activities in abdominal muscles initiated in larger trunk flexion angles.

Linearization of passive properties as an approximation of the nonlinear response remains valid only in the neighborhood of the linearization point. The further one deviates from the reference linearization point; the more divergence is expected in results away from the original nonlinear system; thus, using linear passive properties (constant joint stiffnesses) (as the mainstream modeling technique (Bruno et al., 2017; De Zee et al., 2007; Delp et al., 2007)) seems reasonable only in a small range. At the extreme in the frictionless spherical joint with no passive resistance, due to marked load-carrying role of the passive ligamentous spine, muscles alone will resist the moments of external loads resulting in greater muscle forces and internal loads, especially in heavier tasks with larger trunk rotations. Thus, in musculoskeletal modeling software (such as AnyBody and OpenSim (Christophy et al., 2012; De Zee et al., 2007; Delp et al., 2007)), we recommend to use nonlinear intervertebral joint stiffness in tasks with large flexion angles (>40^{o}) or to use linear joint stiffness only when flexion angles remain relatively small (<40^{o}). One valid but cumbersome alternative option is to continuously update the linear stiffness properties

depending on the current load magnitude considered in an analysis. Passive elements (rotational springs) should however never be neglected.

One should consider both kinematics and kinetics of the spine and their likely interactions while positioning intervertebral joints. To accurately capture kinematics responses, one can place spherical joints at or near corresponding ICoRs; however, according to the current and earlier (Ghezelbash et al., 2015) results, using reported ICoR values (e.g., ~ 16 mm posterior to disc centers (Liu et al., 2016) or near lower endplates (Staub, Holman, Reitman, & Hipp, 2015)) without proper adjustments in passive properties (joint stiffnesses) adversely influences the kinetics (i.e., muscle forces and spinal loads). During flexion and relative to the lower vertebra, a spherical joint considers a fixed ICoR whereas a shear deformable beam accounts for some translations in ICoR. (~ 0.6 mm during flexion under 2.7 kN follower preload). In this study, the simplified nonlinear models estimated the ICoR locus of the L1 fairly well during its overall (global) motion. It should be noted that the center of rotation (i.e., a point that has no instantaneous velocity under applied loads) does not fall on the "center of reaction" (i.e., a point in which the net moment vanishes (Gracovetsky, Zeman, & Carbone, 1987; Zander et al., 2016), so moment equilibrium equations about the center of rotation should not overlook the internal moment (Figure 6.7). Alternatively, one can write equilibrium equations about the "center of reaction" with no net (internal) moment. Although the "center of reaction" introduces significant computational simplicity, this point is not known a priori and displaces during deformation.

Results of this study have implications in biomechanics of total disc replacements that should be considered in future designs. Anterior-posterior placement of these implants, passive resistance they offer and the nonlinearity in their stiffnesses under increasing compression and rotations should be carefully considered and examined as they all influence spinal kinematics, muscle forces and hence internal loads.

In summary, we explored the accuracy and validity, in sagittally symmetric tasks, of modeling spinal motion segments as spherical joints (with and without rotational springs) and beams both with linear/nonlinear passive properties while their location shifted in the anterior-posterior

directions. Estimated kinematics by these simplified models (spherical joint/beam) were compared with a detailed FE model of the lumbar spine under a 2.7 kN follower load and 20 Nm moment. Introducing foregoing simplified models into a subject-specific musculoskeletal model, we predicted active-passive components of muscle forces and local spinal loads at various lifting tasks and compared the computed IDP with available in vivo measurements (Wilke et al., 2001). Nonlinear shear deformable beams and nonlinear spherical joints with joint offset at -2 to 4 mm range predicted kinematics (in comparison with the detailed FE) and spinal loads (in comparison with the in vivo measurements) accurately although the nonlinear spherical joint model failed to accurately estimate the axial displacements. Shifting joints posteriorly in general increased spinal loads (up to 17% in compression and 26% in shear) and delayed flexion relaxation (by 40^o) during forward flexion. Employing linear rotational springs or beams remained valid only at relatively small flexion angles ($<40^o$). Due to the substantial role of the ligamentous spine in resisting external moments especially in heavier tasks, overlooking rotational springs (i.e., in frictionless spherical joints) should be avoided as it would yield marked overestimation of compression (32%) and shear (63%) forces.

6.5 Acknowledgments

This work was supported by the institut de recherche Robert-Sauvé en santé et en sécurité du travail (IRSST-2014-0009) and fonds de recherche du Québec en nature et technologies (FRQNT-200564).

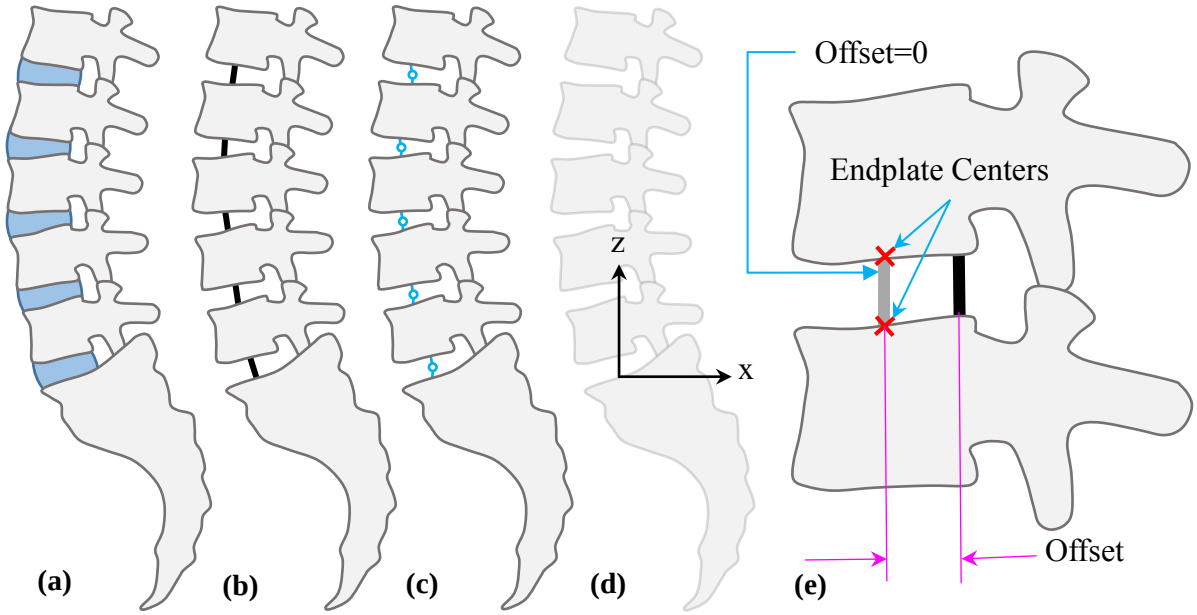

Figure 6.1: Schematic illustration of the (a) detailed FE model (with intervertebral disc, facet joints and ligaments at all levels), (b) beam model, (c) spherical joint model (d) global coordinate system and (e) beam positioning and offset (+ posterior; - anterior) at a typical motion segment.

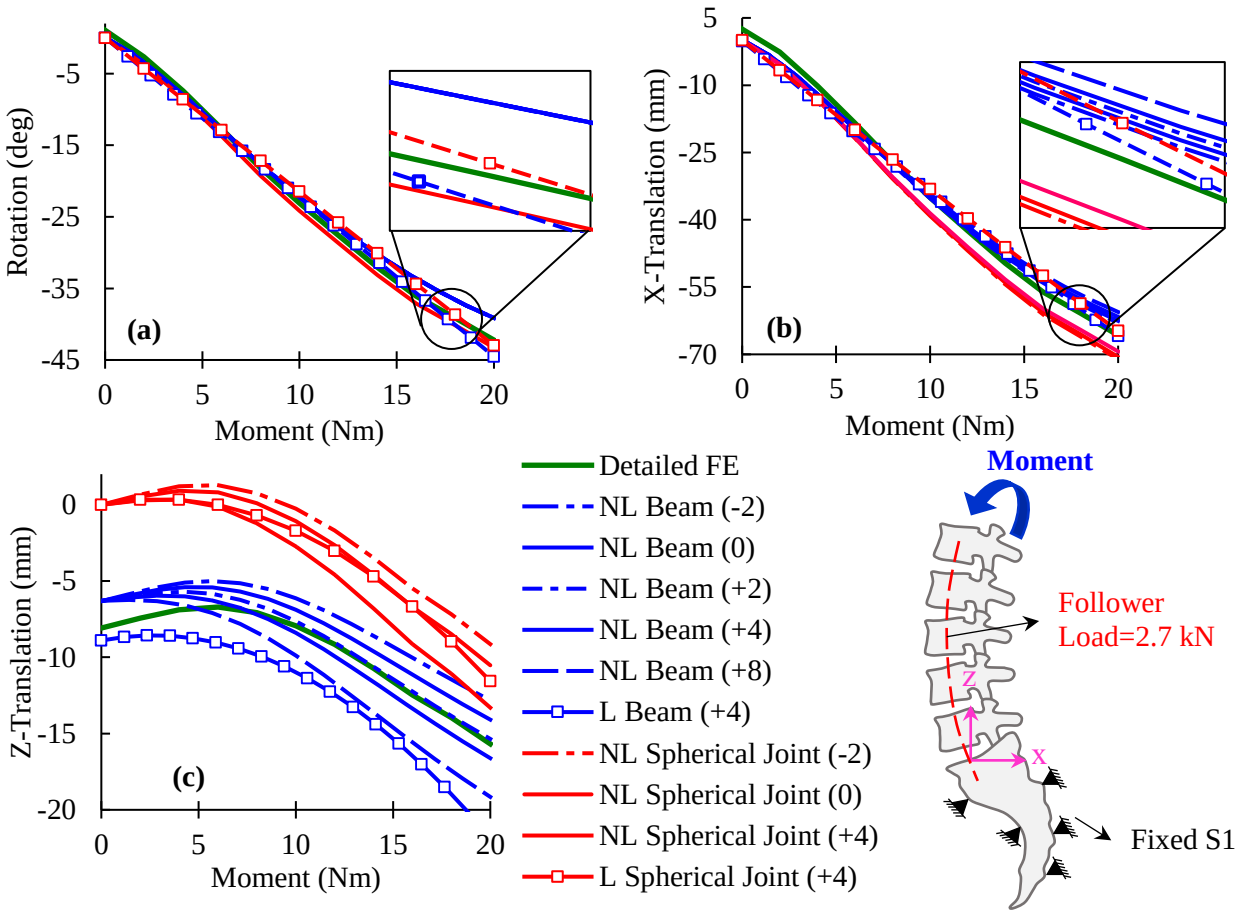

Figure 6.2: (a) Flexion rotation, (b) X-translation and (c) Z- translation of the L1 vertebra in different models (detailed FE, beam and spherical joint) under 20 Nm flexion moment and 2700 N follower preload. Values in parentheses denote joint offset (+ posterior; -anterior) (see Figure 6.1e).

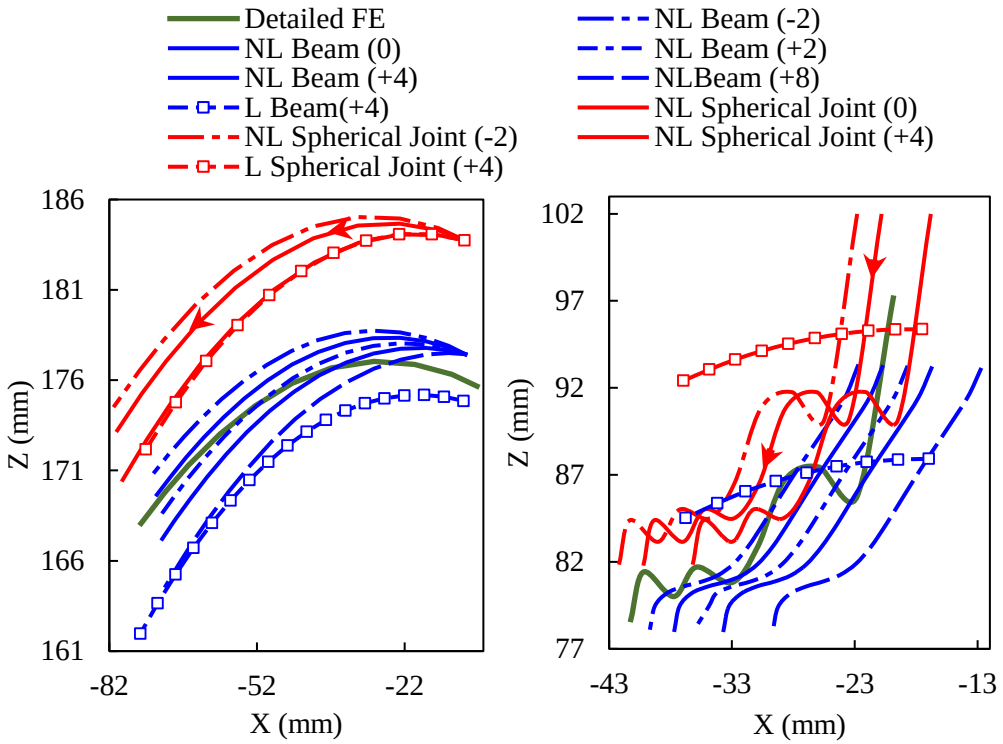

Figure 6.3: Path of the center the L1 (left) and ICoR of the L1 (right) during forward flexion (from right to left) for different joint types and offset magnitudes

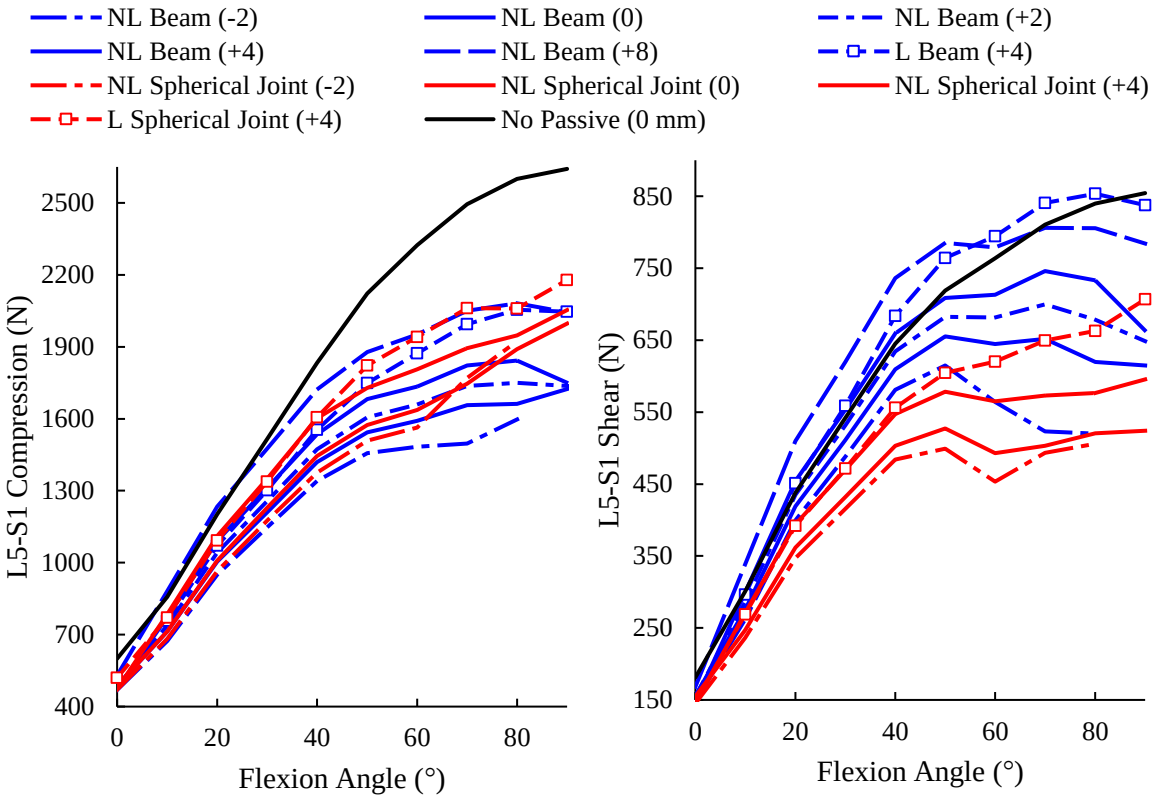

Figure 6.4: Computed local L5-S1 compression (left) and shear (right) forces in different flexed postures without hand load for different joint types and offset values (+ posterior; - anterior) (see Fig.1e). Personal parameters of the model were set at sex=male, body height=173.9 cm, body weight=72.0 kg and age=42.0 years. Values in the parentheses denote joint offset (+ posterior; - anterior).

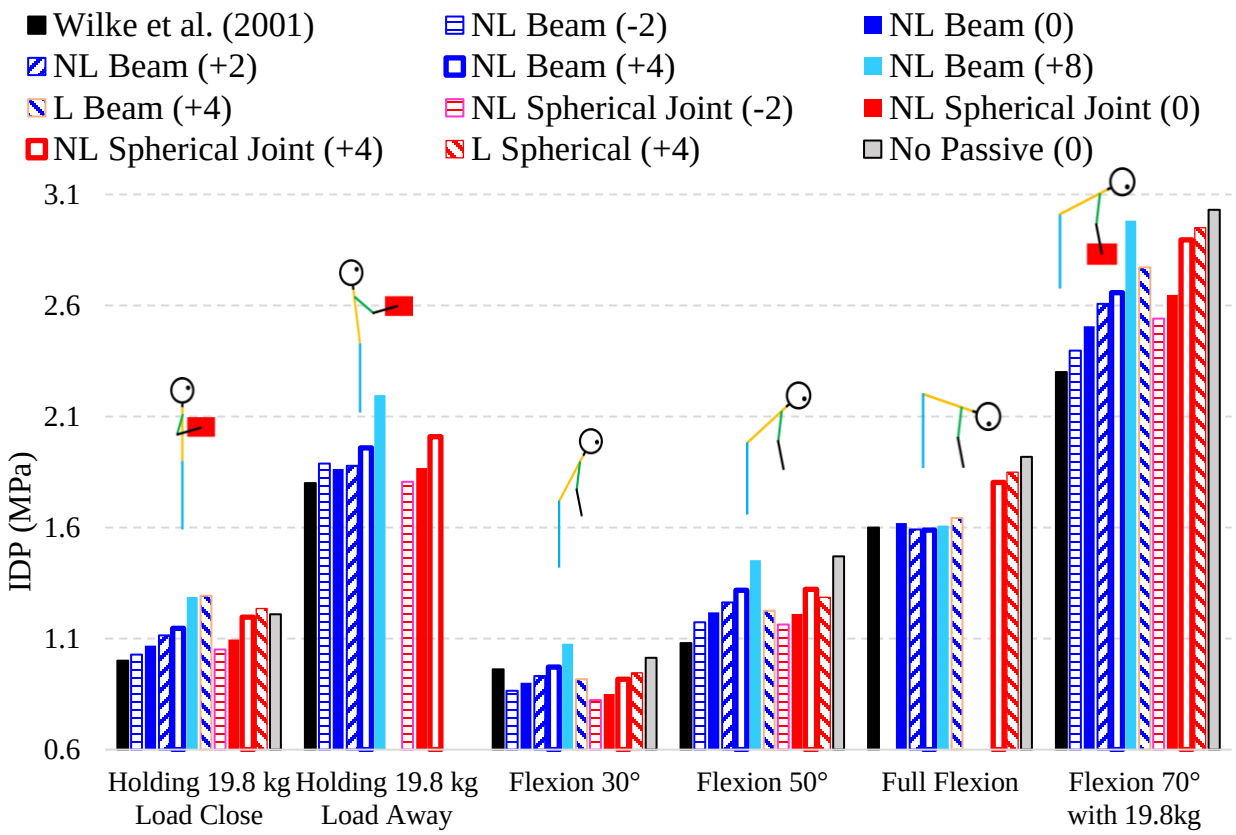

Figure 6.5: Measured (Wilke et al., 2001) and estimated IDPs (using the compression-IDP-flexion rottaion relation proposed in (Ghezelbash et al., 2016b) (Eq. 3.6)) during various tasks. Values in the parentheses denote joint offset (+ posterior; -anterior) (see Figure 6.1).

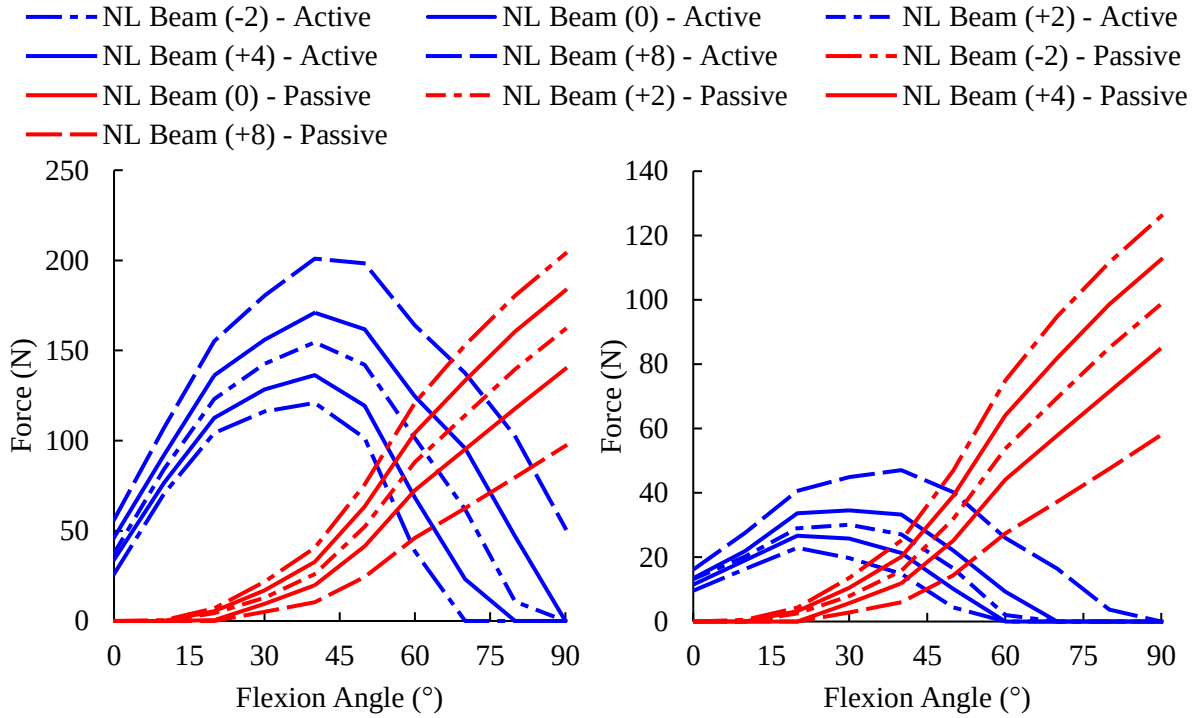

Figure 6.6: Active and passive muscle force components in right/left global longissimus (left) and iliocostalis (right) pars thoracic muscles during forward flexion with no load in hands in the nonlinear beam model at different offsets (see Figure 6.1e). Drop and disappearance of active muscle forces denote the flexion relaxation phenomenon in forward flexion.

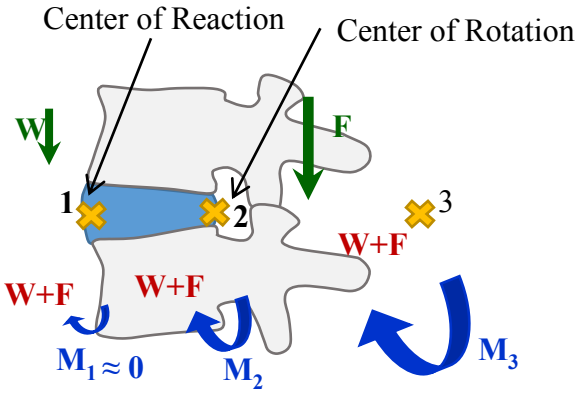

Figure 6.7: Schematic illustration of joint positioning kinetics. W: external (in hands) and gravity forces; F: extensor muscle forces; M_1, M_2 and M_3: resultant free-body diagram moments at the plane of cut ($M_1<M_2<M_3$)

CHAPTER 7 ARTICLE 5: TRUNK MUSCULOSKELETAL RESPONSE IN MAXIMUM VOLUNTARY EXERTIONS: A COMBINED MEASUREMENT-MODELING INVESTIGATION

Authors: F. Ghezelbash, Z. El Ouaaid, A. Shirazi-Adl, A. Plamondon, and N. Arjmand

Published in *Journal of Biomechanics* 70 (2018): 124-133

7.1 Introduction

Maximum voluntary exertion (MVE) measurements aim to quantify trunk (and muscle) strength in various planes serving both clinical and biomechanical objectives (Azghani, Farahmand, Meghdari, Vossoughi, & Parnianpour, 2009; Larivière, Bilodeau, Forget, Vadeboncoeur, & Mecheri, 2010; Roy, De Luca, & Casavabt, 1989; Tsao, Galea, & Hodges, 2008). The database of MVE moments (for both females and males) can be a helpful tool in risk of injury assessment, selection or exclusion of manual workers, functional diagnosis, performance evaluation/enhancement, rehabilitation and treatment evaluations. Fear of pain, however, results in lower MVE moments in patients with back pain and injuries that limits its application (Dankaerts, O'Sullivan, Burnett, Straker, & Danneels, 2004; Demoulin et al., 2013). Determination of maximal EMG in MVEs is also needed for the normalization of muscle activities to improve the use and reliability within and in between subjects (Sousa & Tavares, 2012).

Previous measurements have recorded highest isometric trunk strength in extension and lowest in axial twist with those in flexion and lateral bending falling in between (Azghani et al., 2009; Larivière, Gagnon, & Genest, 2009); peak moments exceeding 350 Nm have been reported in extension (Gravel, Gagnon, Plamondon, & Desjardins, 1997; Kumar, 1996; Larivière et al., 2009). The measured MVE moments alter with posture (Gravel et al., 1997; Kumar, 1996; O'sullivan et al., 2006), with gender (smaller in females) (Kumar, 1996; Lee & Kuo, 2000; Plamondon et al., 2014), with low-back pain (Dankaerts et al., 2004; Larivière et al., 2003; Ng et al., 2002) and 2 months after spinal surgery (Arja, Tiina, Pt, & Jari, 2003). Complex activity patterns are recorded in trunk muscles during maximal exertions, especially in lateral bending and axial torque with much higher EMG activities in agonists than in antagonists (Cholewicki et al., 1995; Ng et al., 2002; Song & Chung, 2004). Though most studies have reported only the measured primary

moments, coupled moments are important and non-negligible especially in lateral and axial MVEs unless cable-harness (Oddsson & De Luca, 2003) or visual feedback (Larivière et al., 2009) systems are considered in measurements. Rather small coupled moments have been recorded in flexion and extension MVEs (~10% of the primary moments). In contrast, coupled moments can exceed 50% of the primary moment during lateral and axial MVEs (Larivière et al., 2009; Ng et al., 2002).

In musculoskeletal (MS) models, apart from load-carrying role of ligamentous spine and posture, muscle areas and maximum muscle stress (which limits maximum muscle forces) as well as muscle moment arms influence the trunk isometric strength and as such should be individualized as much to obtain accurate results in a musculoskeletal model study. The estimation of trunk muscle forces, internal loads and maximum muscle stress in maximal exertions, however, requires biomechanical MS models that adequately account for both active and passive structures of the trunk. Some studies used EMG-driven (Cholewicki et al., 1995), optimization-driven (Gardner-Morse, Stokes, & Laible, 1995; Gatton, Pearcy, & Pettet, 2011; Jamshidnejad & Arjmand, 2015; Song & Chung, 2004) and kinematics-driven (Arjmand et al., 2008b; El Ouaaid et al., 2013b) models to investigate internal loads, spinal stability and muscle activities during MVE tasks while others employed MS models to estimate maximum muscle stresses at jaw (Pruim, De Jongh, & Ten Bosch, 1980), elbow (Buchanan, 1995; Kawakami, Abe, Kuno, & Fukunaga, 1995), wrist (Goislard, Rao, Gay, Berton, & Vigouroux, 2017), ankle (Fukunaga, Roy, Shellock, Hodgson, & Edgerton, 1996) and trunk (only in extension) (Burkhart, Bruno, Bouxsein, Bean, & Anderson, 2017) MVEs. However as yet, no study has either investigated trunk responses (internal loads and muscle activities) during MVEs for both females and males or estimated the maximum muscle stress of trunk muscles considering MVEs in all directions.

In the present study, we aim to simulate MVE tasks in a subject-specific model, compare predicted muscle activities with measured EMGs, compute maximum muscle stresses and finally investigate likely differences between females and males in exerted MVE moments and spinal loads. We initially carry out isometric MVE experiments in extension, flexion, lateral and axial directions on

19 asymptomatic young right-handed female and male subjects while recording EMGs of superficial muscles. Furthermore, to explore the accuracy of our geometrically subject-specific nonlinear MS FE model, we simulate MVE tasks, estimate maximum muscle stresses and compare estimated activities of select muscles with measured EMGs.

7.2 Methods

7.2.1 Experiments

With approval from our institutional review board and written consent from participants, healthy young right-handed females (9 females; height=163.4±3.7 cm; weight=61±4.5 kg; age=24.1±4.3 years) and males (10 males; height=174.6±4.2 cm; weight=72.2±8.7 kg; age=30.6±6.5 years) performed two trials of flexion, extension, lateral and axial isometric MVEs in a dynamometer at a semi-seated posture (Larivière et al., 2001). During trials (lasting ~8 s), subjects were verbally encouraged to exert their maximal effort while their pelvic and legs were fixed, and their hands were held crossed on the chest. Each trial afterward followed by a two-minute rest. Three triaxial force platforms (Advanced Mechanical Technology Incorporated, model MC6-6-1000, Watertown, MA, USA) collected dynamometer signals at 128 Hz frequency. An EMG acquisition device (model DE-2.3, DelSys Inc., Wellesley, MA) recorded EMG signals of 12 superficial muscles (longissimus, iliocostalis pars thoracic/lumborum, multifidus, external oblique, internal oblique and rectus abdominis) at the frequency of 1024 Hz via surface electrodes placed bilaterally, Figure 7.1 (De Foa, Forrest, & Biedermann, 1989; McGill, 1991). A band-pass filter (30 - 450 Hz) reduced the effects of noises and artifacts from EMG signals, and subsequently, root mean squared envelopes of EMG amplitudes were normalized to their recorded maximum root mean squared values during MVE tasks. Data of the trial with the larger primary moment were considered in these and subsequent analyses.

7.2.2 MS Modeling

We simulated MVE tasks in all 6 directions for all 19 subjects in our geometrically subject-specific nonlinear finite element MS trunk model (Ghezelbash et al., 2016a, 2016b) (Chapter 3; Chapter 4). The model includes 126 sagittally-symmetric muscles and computes muscle forces in an optimization- and kinematics-driven framework while taking account of seven individual (T11-T12 to L5-S1) motion segments as shear-deformable beams. Each deformable beam attaches two adjacent rigid vertebrae and represents the stiffness (moment-curvature and force-strain) of an entire motion segment (disc, facets, ligaments and vertebrae). For a given set of prescribed thoracolumbar (T11 to S1) rotations (for details see below), required moments at each vertebral level were initially determined from the nonlinear FE model. An optimization algorithm (with quadratic sum of muscle stresses as the cost function and moment equilibrium equations (at T11 to L5 levels) as equality constraints) then estimated muscle forces that counterbalanced computed required moment at each vertebral level (T1-T11 as a single rigid body, T12, L1, L2, L3, L4 and L5). To obtain physiologically valid muscle forces, we constrained muscle forces (F_i) to be greater than the passive force component (F_i^p) (Davis et al., 2003) and less than the sum of the passive force component plus the maximal active component:

$$F_i^p \leq F_i \ \leq F_i^p + \ PCSA_i \ \sigma_{max}, \qquad \text{Eq. 7.1}$$

in which $PCSA_i$ and σ_{max} respectively denote physiological cross sectional area (of i^{th} muscle) and the upper bound of maximum muscle stress. To evaluate σ_{max} needed for convergence at each MVE task, we increased maximum muscle stresses (σ_{max}) starting from 0.2 MPa with the increment of 0.1 MPa. In this manner, required σ_{max} was calculated in each subject and each MVE task.

For subsequent comparison with recorded normalized EMGs in select muscles under a specific MVE of a subject, relative muscle activities were evaluated by normalizing their computed active forces ($F_i \ - F_i^p$) to their maximum active forces ($^{max}F_i^a$) computed during all 6 MVE tasks:

$$^{max}F_i^a = max(\,^{F}F_i^a,\,^{E}F_i^a,\,^{RL}F_i^a,\,^{LL}F_i^a,\,^{RAx}F_i^a,\,^{LAx}F_i^a) = PCSA_i\,\sigma_i, \qquad \text{Eq. 7.2}$$

where $^{j}F_i^a$ denotes computed active muscle force ($^{j}F_i = {}^{j}F_i^p + {}^{j}F_i^a$) of i^{th} muscle at j^{th} task (i.e., extension (E), flexion (F), right lateral (RL), left lateral (LL), right axial (RAx) and left axial (LAx) MVEs). σ_i represents the peak muscle stress reached in i^{th} muscle under all MVEs of that subject. It should be noted that the use of foregoing σ_i ensures the appropriateness of comparisons between estimated and recorded relative muscle activities as a similar procedure was carried out when normalizing recorded EMGs.

Upper body gravity loads and their position were proportionally adjusted to the body weight and height, respectively, and partitioned along the spine (T1 to L5) (Pearsall et al., 1996) as well as arms, head-neck and hands (De Leva, 1996). The scaling algorithm adjusted both muscle architecture and passive spine responses based on imaging databases (Anderson et al., 2012; Shi et al., 2014) and biomechanical principles (Ghezelbash et al., 2016b). For more details on the model and the scaling algorithm see Figure 7.2, Chapter 3 and (Ghezelbash et al., 2016b). The nonlinear elastostatic analyses were carried out using ABAQUS (version 6.14, Simulia, Inc., Providence, RI, USA) finite element package program, and MATLAB (Optimization Toolbox) was used in the optimization algorithm.

At the interface between each subject and the dynamometer harness, identified visually in each task, equivalent forces (generating exactly the same moments recorded about the S1) were evaluated and applied on each model at respective contact points. During extension, flexion and lateral MVEs, contact points were located at the cranial-caudal heights situated respectively at the T8, T6 and shoulder joint and were offset out of the primary plane to generate measured moments (primary and coupled) about the S1. In the axial torque, the recorded axial MVE moment was applied at the T4. In addition and in order to reproduce accompanying coupled moments about the S1, required forces in the transverse plane were also calculated and applied to the T4.

To simulate the semi-seated posture of subjects during exertion tests and in accordance with the visual observation of subjects' configurations and radiological studies of individuals in seated posture, we reduced the lumbar lordosis (Bae, Jang, Lee, & Kim, 2012; De Carvalho, Soave, Ross, & Callaghan, 2010). Thus, we prescribed 9^o (backward extension) and −13^o (forward flexion) at the T11 in addition to 16^o and 13^o backward extensions at the S1 in extension and flexion MVEs, respectively, resulting in much smaller lordosis in the flexion tasks (by 7^o in extension and 26^o in flexion). Foregoing rotations were subsequently partitioned among intervening T11-S1 segments based on our earlier works (El Ouaaid et al., 2013b; Ghezelbash et al., 2016b). In lateral and axial MVEs, we reduced the lumbar lordosis by 11^o (+10^o rotation at the S1 and -1^o at the L1) that was then partitioned proportional to neutral standing rotations (Ghezelbash et al., 2016b) (Chapter 3). In flexion MVEs and in order to diminish large required flexion moments at local lumbar levels that cannot be supported by the trunk musculature, an additional constraint was applied via a posterior shear force (to be generated by abdominal oblique muscles in order to reduce flexion moments at lumbar levels) at thoracic levels (T11 and T12) in accordance with earlier studies (Bazrgari et al., 2009; El Ouaaid et al., 2013b; Ghezelbash et al., 2016b).

7.2.3 Statistical Analysis

We employed the analysis of variance (ANOVA) to compare exerted primary and coupled moments and estimated spinal loads (shear and compression) between females and males.

7.3 Results

In our measurements, females produced lower mean MVE moments in the primary plane in comparison with their male counterparts (Figure 7.3); the differences were statistically significant in all MVEs except flexion, Table 7.1. While in flexion and extension MVEs, mean coupled moments were small (~9%), coupled moments were rather large in axial and lateral MVEs reaching in average to as high as ~50% of primary moments, Table 7.2.

Estimated muscle activities in extension and flexion MVEs were strongly correlated (Pearson's r=0.69 and r=0.76, respectively) with measured muscle activities (Figure 7.4). However, estimated muscle activities in lateral and axial MVEs were very weakly correlated (Pearson's r=0.27 and 0.13, respectively) with measured EMGs (Figure 7.5 and Figure 7.6). Largest spinal forces were computed in both sexes in extension MVEs (Figure 7.7). In lateral and axial MVEs, however, compression and shear spinal loads can reach large values of ~5500 N and ~1700 N in average, respectively. Smallest spinal forces were computed in both sexes in flexion MVEs (Figure 7.7), and sex (p=0.03 in shear and compression) and MVE direction (p<0.001) significantly affected spinal loads. The predicted σ_{max} (Eq. 7.1) required to reach convergence under the measured moments were affected by MVE direction (Figure 7.8a). The peak muscle stress (σ_i) used in Eq. 7.2 for normalization of calculated muscle forces varied from one muscle group to another with the least value computed in rectus abdominis (0.40$\pm$0.22 MPa) and the largest in external oblique (0.99$\pm$0.30 MPa). Almost all estimated σ_i (96% of muscles among all participants) remained less than 1.5 MPa (Figure 7.8b). The average maximum muscle stresses (σ_i) was 0.80$\pm$0.42 MPa.

7.4 Discussion

A dataset of measured MVE moments of individuals is potentially helpful to clinicians, ergonomists, occupational health and safety professionals in estimating maximum acceptable effort during cyclic loadings (Potvin, 2012), assessing rehabilitation outcomes (Stokes, 2011) and identifying patients with back injury and pain (Burkhart et al., 2017). Simulating MVE tasks, furthermore, is an effective way of evaluating MS models; some models can fail predicting reasonable maximum muscle stresses (when maximum moments are prescribed otherwise predicting accurate maximum moments when maximum muscle stress is input) and muscle activities if not having realistic and accurate muscle architecture, muscle force estimation protocol, passive properties and scaling algorithms. Our measured moments were found in general agreement with earlier studies. The differences in measured moments between females and males reached significance levels in all MVEs (except flexion); females exerted smaller primary moments. All MVE tasks were simulated in a geometrically subject-specific MS model. The

predicted muscle activities were in qualitative agreement with measured EMGs in flexion and extension MVEs; however, in lateral and axial MVEs, agreements were very weak. Very large compression and shear forces in average ~5867 N and ~2144 N, respectively, were estimated at the L5-S1 level of the spine during MVE extension tasks. Maximum muscle stress (in average 0.80±0.42 MPa) varied among muscles from 0.40±0.22 MPa in rectus abdominis to 0.99±0.30 MPa in external oblique.

7.4.1 Limitations and Methodological |Issues

Collected EMGs were limited to specific select locations of superficial muscles. Recorded EMG is susceptible to technical issues (e.g., electrode placement for long, flat and/or deep muscles, difficulties in capturing internal oblique and multifidus activities with surface electrodes (Stokes, Henry, & Single, 2003)) and signal contaminations (e.g., muscle cross-talk, power line noise, motion artifacts) (De Luca, Gilmore, Kuznetsov, & Roy, 2010; Soderberg & Knutson, 2000; Türker, 1993). Choice of the muscles in the model used for comparison of activity with a specific surface EMG recording (Figure 7.1) influences comparisons. Spinal kinematics were assumed based on visual observation of postures due to technical limitations of using motion capture camera with the dynamometer (El Ouaaid et al., 2013b). Locations of subject-machine interfaces to apply contact forces during MVEs were also approximate as identified visually. Unlike fully articulated spine models (Bruno et al., 2015; Ignasiak et al., 2016a), the thorax (T1 to T11) was simulated as a rigid body. The effect however is expected to be small due to negligible bending deformations expected in the upper thorax under MVE tasks with large internal compression forces (Figure 7.7) (Ignasiak, Ferguson, & Arjmand, 2016b; Sis et al., 2016). We personalized the MS model based on available generic imaging databases using subjects' personal parameters (that are body height, body weight, sex and age); some variations between subjects and the scaled (or personalized) models are expected that could influence predictions. Further modeling limitations are stated elsewhere Chapter 3, Chapter 5 and (Arjmand et al., 2009; Ghezelbash et al., 2016b; Ghezelbash, Shirazi-Adl, Plamondon, Arjmand, & Parnianpour, 2017b).

7.4.2 Interpretations and Data Analysis

Measured MVE moments in different directions were in agreement with mean of those reported in earlier studies although female subjects in our study compared to others in average exerted greater moments (Figure 7.3). Nonetheless and in absolute terms, females applied lower mean primary moments (reaching significance except in flexion MVE) in comparison with males (Table 7.1 and Table 7.2). Due to approximately sagittally symmetric musculature as well as likely asymmetry in posture and nearly balanced activities of bilateral muscles during symmetric tasks (Oddsson & De Luca, 2003), flexion and extension MVEs had the least coupled moments when compared to lateral and axial MVEs. The direction of coupled moments were consistent between two trials in nearly all subjects but among subjects. For example, in the left axial MVE, 9 subjects exerted extension moments (versus 10 flexion moments) and 16 exerted left lateral moments (versus 3 right lateral moments).

Musculature (muscle moment arms and PCSAs) and maximum muscle stresses limit the trunk strength. As a result and since MS models are personalized prior to analyses, evaluation of maximum muscle stresses and comparison of the estimated muscle activities with EMG data can evaluate the accuracy of the muscle architecture, scaling (or personalization) scheme, passive properties and muscle force estimation algorithm. Estimated maximum muscle stresses were in agreement with earlier studies (Buchanan, 1995; Burkhart et al., 2017; Pruim et al., 1980), a finding that highlights the relative accuracy of the employed scaling scheme since participants were selected from both sexes with varying body heights and weights. Very large/small maximum muscle stresses would have been estimated had inaccurate personalized geometric musculature been employed. Estimated muscle activities strongly agreed with recorded EMGs in flexion (Pearson's r=0.72) and extension (Pearson's r=0.69) MVEs (Figure 7.4), but not in lateral (Pearson's r=0.44) and axial (Pearson's r=0.34) MVEs (Figure 7.5 and Figure 7.6). Comparisons are however affected, amongst others, by the accuracy of collected EMG and its position on skin especially in large flat and deep abdominal oblique muscles as well as the abdominal musculature in the model. Optimization-driven methods, especially when not driven by measured kinematics,

overlook existing differences in muscle recruitment strategies among individuals. In the current MVE tasks, alterations in the cost function would likely have minor effects on muscle force estimations since a considerable number of agonist muscles are (totally or nearly) saturated that tends to limit the available redundancy or solution space. Alternatively, hybrid approaches (such as EMG assisted optimization (Arjmand et al., 2010; Mohammadi et al., 2015) and utilizing muscle synergies (for dimensionality reduction) (Fregly et al., 2012; Walter et al., 2014)) may potentially improve muscle activity estimations. However, hybrid approaches require EMG measurements (which are susceptible to contamination), remain sensitive to initial gain value (Mohammadi et al., 2015) and use some optimization to satisfy equilibrium.

Large spinal forces were estimated in MVEs, with the maximum in extension and minimum in flexion (Figure 7.7). Maximum spinal loads were reached in the extension MVEs due both to the larger moments applied and smaller lever arms of extensor muscles that resist them. Nonetheless, estimated spinal loads in lateral and axial MVEs were also rather large and were significantly influenced by MVE direction ($p<0.001$) (Figure 7.7). Greater MVE moments reaching significance in all directions (except extension), Table 7.1, yielded significant differences between spinal loads in females and males ($p=0.03$ for shear and compression forces). This suggests that similar to bodyweight and external loads (Ghezelbash et al., 2016a) (Chapter 3), sex markedly affects spinal loads in MVE tasks particularly due to differences in exerted moments.

One can estimate the maximum muscle stress (or specific muscle tension) through musculoskeletal modeling of MVE tasks (Burkhart et al., 2017; Goislard et al., 2017; Pruim et al., 1980). We found that the maximum muscle stresses, σ_{max}, varied across MVE tasks and subjects (Buchanan, 1995; Fukunaga et al., 1996). Almost all computed maximum muscle stresses (~95%) remained less than 1.5 MPa (Buchanan, 1995) though in few cases (5%), they reached 1.5-1.8 MPa similar to those reported in jaw muscles (Pruim et al., 1980). It is to be noted that the scaling algorithm used in this work adjusted muscle moment arms and PCSAs with participants' personalized anthropometric parameters based on generic imaging datasets (Anderson et al., 2012; Shi et al., 2014) (Figure 7.2) and not on direct measurements of participants. Since muscle moment arms and PCSAs influence

maximum muscle stress estimations, such approximations (along with posture predictions) likely affect estimations. The upper bound of 1.5 MPa (Buchanan, 1995) for the maximum muscle stress may be taken for the general healthy and young populations. Furthermore, due to dependency on MVE task, current results indicate that an accurate estimation of the maximum muscle stress requires consideration of MVEs in all directions.

In summary, we measured MVE moments of 19 young right-handed heathy individuals (9 females and 10 males) in primary directions (flexion, extension, lateral and axial) while collecting EMG signals of 12 superficial muscles. Females exerted significantly less moments in comparison with their male counterparts in all directions except in flexion MVEs. Coupled moments were larger in axial and lateral MVEs. Estimated muscle activities were in strong (in flexion and extension MVEs) to very weak (in lateral and axial MVEs) correlations with measured EMGs. Estimated maximum muscle stresses in almost all cases (95% of muscles in all participants) remained less than 1.5 MPa which is in agreement with (Buchanan, 1995). Very large spinal loads were computed with maximum values in extension and minimum values in flexion MVEs. To estimate maximum muscle stress and muscle activities in a musculoskeletal model during MVE tasks, one should consider MVE tasks in all direction along with the primary moments and coupled moments.

7.5 Acknowledgments

This work was supported by the institut de recherche Robert-Sauvé en santé et en sécurité du travail (IRSST-2014-0009) and fonds de recherche du Québec en nature et technologies (FRQNT-200564).

Table 7.1: Computed p-values from ANOVA of recorded primary (shown in boldface) and coupled moments in MVE tests when comparing females and males

Moment Direction	*Flexion MVE*	*Extension MVE*	*Right Lateral MVE*	*Left Lateral MVE*	*Right Axial MVE*	*Left Axial MVE*
Flexion Moment	**0.1711**	**0.0294***	0.1900	0.4732	0.6400	0.2337
Lateral Moment	0.8558	0.8534	**0.0207***	**0.0017***	0.0900	0.3422
Axial Moment	0.3620	0.9069	0.6811	0.2316	**0.0034***	**0.0070***

* Significant difference ($p<0.05$)

Table 7.2 Mean and standard deviation of measured MVE primary (in bold) and coupled moments (N.m) in different directions and their normalized values to the primary moments (in parentheses). Results for each MVE are separately listed in each column.

Study	*Direction*	*Flexion MVE*	*Extension MVE*	*Right Lateral MVE*	*Left Lateral MVE*	*Right Axial MVE*	*Left Axial MVE*
Present Study 9 Females	*Flexion*	**124±17 (100%)**	**-190±45 (100%)**	-25±31 (-21%)	-49±49 (48%)	-21±69 (-33%)	10±47 (-14%)
	Right Lateral	9±11 (7%)	17±21 (-9%)	**117±31 (100%)**	**-103±36 (100%)**	-21±45 (-33%)	33±36 (-45%)
	Right Axial	-11±6 (-9%)	-10±23 (5%)	-23±26 (-20%)	8±29 (-8%)	**64±19 (100%)**	**-74±20 (100%)**
Present Study 10 Males	*Flexion*	**144±38 (100%)**	**-236±39 (100%)**	-53±56 (-35%)	-34±41 (22%)	-39±96 (-40%)	-23±66 (23%)
	Right Lateral	8±15 (6%)	19±26 (-8%)	**151±28 (100%)**	**-156±26 (100%)**	-53±30 (-55%)	48±33 (-47%)
	Right Axial	-5±17 (-3%)	-12±19 (5%)	-18±33 (-12%)	27±36 (-17%)	**97±23 (100%)**	**-102±20 (100%)**
Ng et al. (2001) 12 Males	*Flexion*	**119±38 (100%)**	**-169±37 (100%)**	3±24 (2%)	-2±16 (1%)	17±30 (22%)	11±33 (-14%)
	Right Lateral	3±12 (3%)	-17±19 (10%)	**129±32 (100%)**	**-138±36 (100%)**	21±26 (27%)	-52±41 (67%)
	Right Axial	1±11 (1%)	-6±11 (4%)	19±17 (15%)	-18±15 (13%)	**78±25 (100%)**	**-78±19 (100%)**
Lariviere et al. (2009)* 20 Males	*Flexion*	**186±34 (100%)**	**270±70 (100%)**	68±27 (34%)	66±32 (35%)	74±32 (56%)	80±51 (61%)
	Right Lateral	16±11 (9%)	25±16 (9%)	**199±32 (100%)**	**190±40 (100%)**	59±22 (45%)	63±23 (48%)
	Right Axial	15±12 (8%)	32±21 (12%)	37±16 (19%)	35±12 (18%)	**132±31 (100%)**	**131±31 (100%)**

* Lariviere et al. (2009) reported absolute values

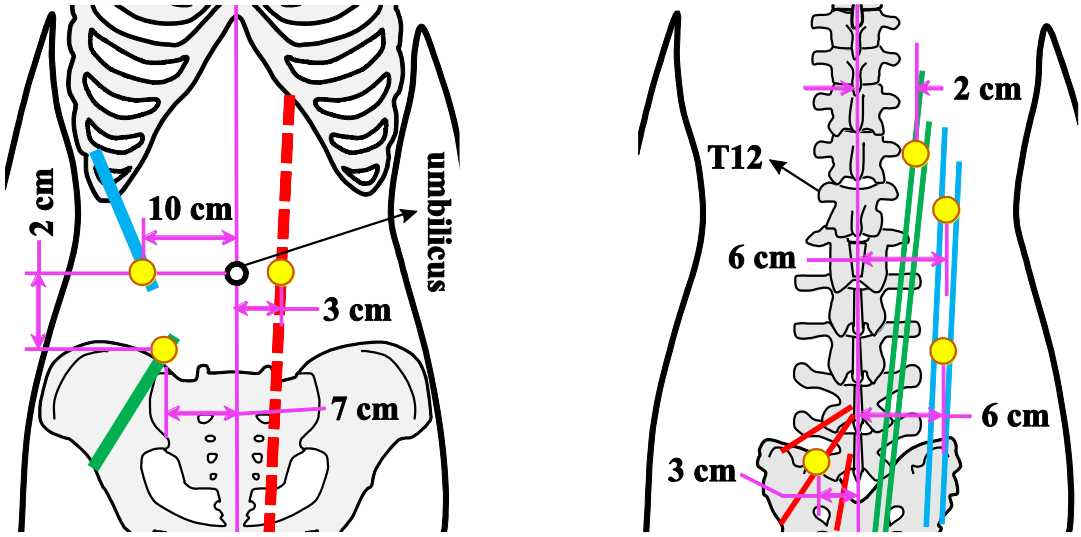

(a) (b)

Figure 7.1 Schematic illustration of EMG electrodes (yellow circles) of (a) abdominal muscles (rectus abdominis: red; external oblique: blue; internal oblique: green) and (b) back muscles (iliocostalis at two levels: blue; longissimus: green; multifidus: red) and corresponding underlying muscles in the MS model.

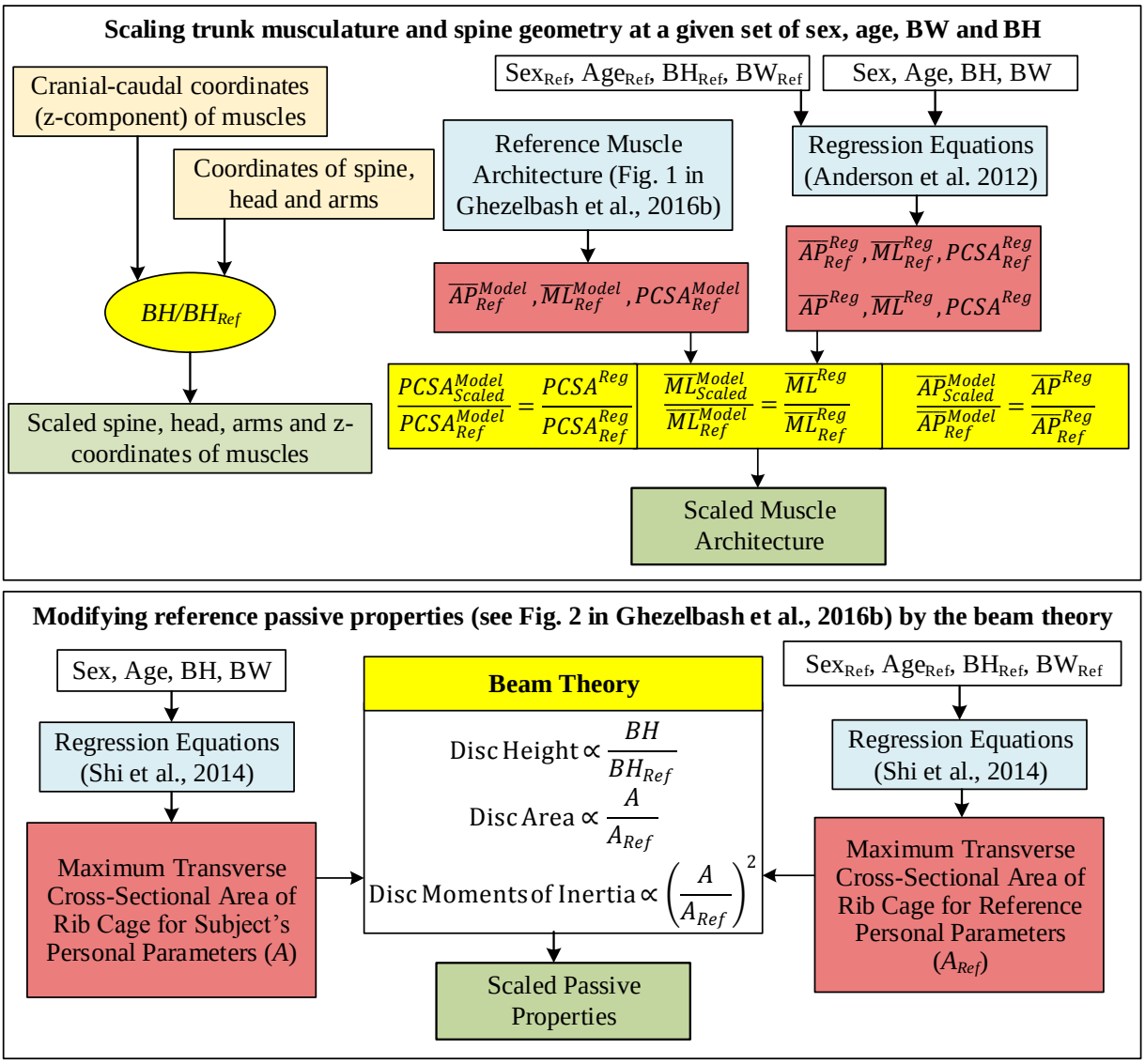

Figure 7.2 The flowchart of the scaling algorithm. BH: body height; BW: body weight; PCSA: physiological cross-sectional area; $\overline{AP}$: average anterior-posterior distance of a muscle centroid (when cut by a transverse plane at the corresponding vertebral height) from vertebrae; $\overline{ML}$: average medio-lateral distance of a muscle centroid (when cut by a transverse plane at the corresponding vertebral height) from vertebrae; A: maximum transverse cross-sectional area of the rib cage; subscript "Ref": values from the reference configuration; subscript "Scaled": values from the patient-specific model; superscript "Reg": values calculated from regression equations. Reference personal parameters are sex_{ref}=male, age_{ref}=41.8 year, BH_{ref}=173.0 cm, and BW_{ref}=75.1 kg (Ghezelbash et al., 2016b) (Chapter 3).

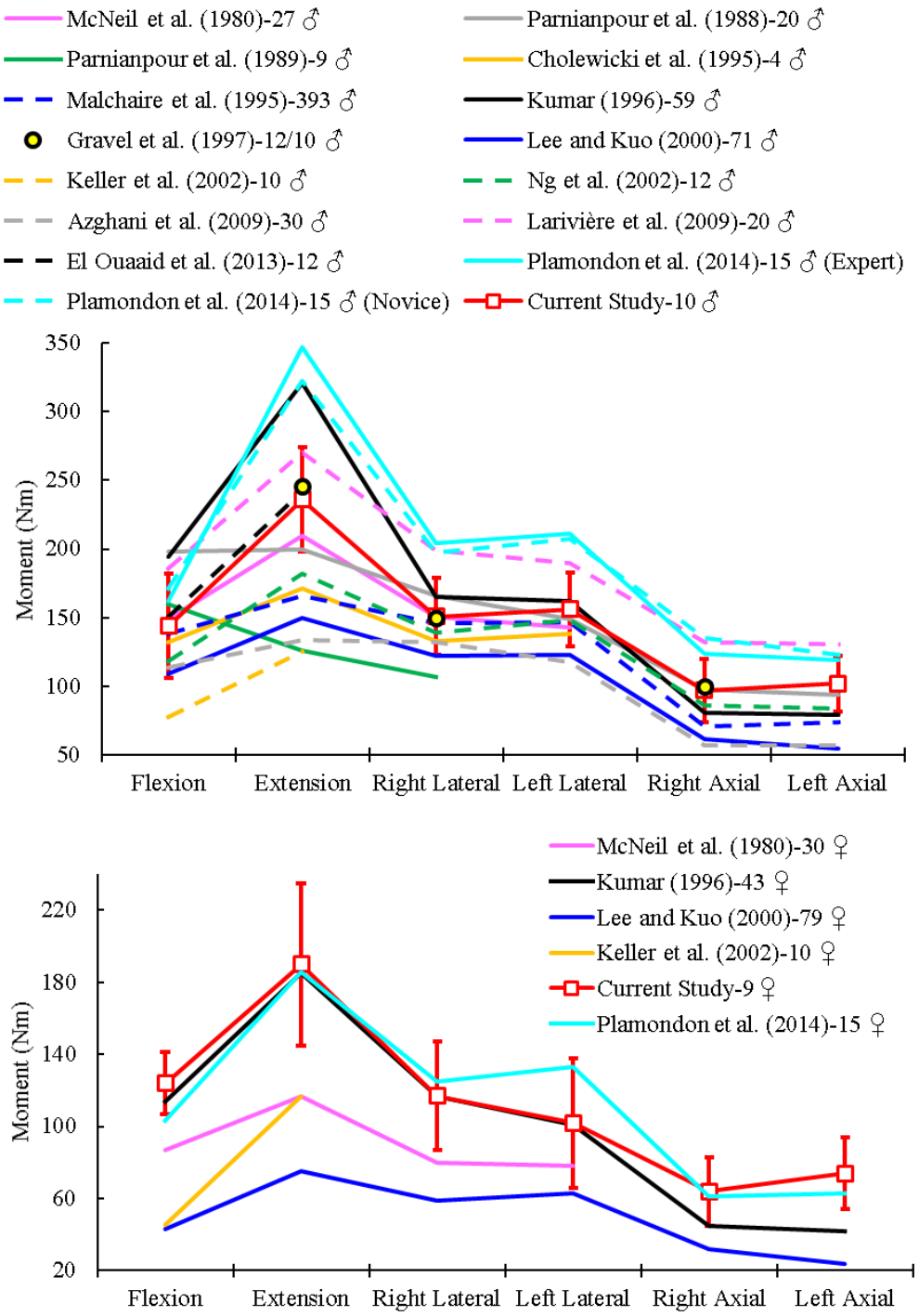

Figure 7.3 Average measured primary MVE moments (Nm) of male (top) and female (bottom) individuals versus earlier studies in different directions. Number of subjects in each study is also indicated. (Azghani et al., 2009; Cholewicki et al., 1995; El Ouaaid et al., 2013b; Gravel et al., 1997; Kumar, 1996; Larivière et al., 2009; Lee & Kuo, 2000; Malchaire & Masset, 1995; Mcneill, Warwick, Andersson, & Schultz, 1980; Ng et al., 2001; Ng et al., 2002; Parnianpour, Li, Nordin, & Frankel, 1988; Parnianpour, Nordin, Kahanovitz, & Frankel, 1988; Plamondon et al., 2014)

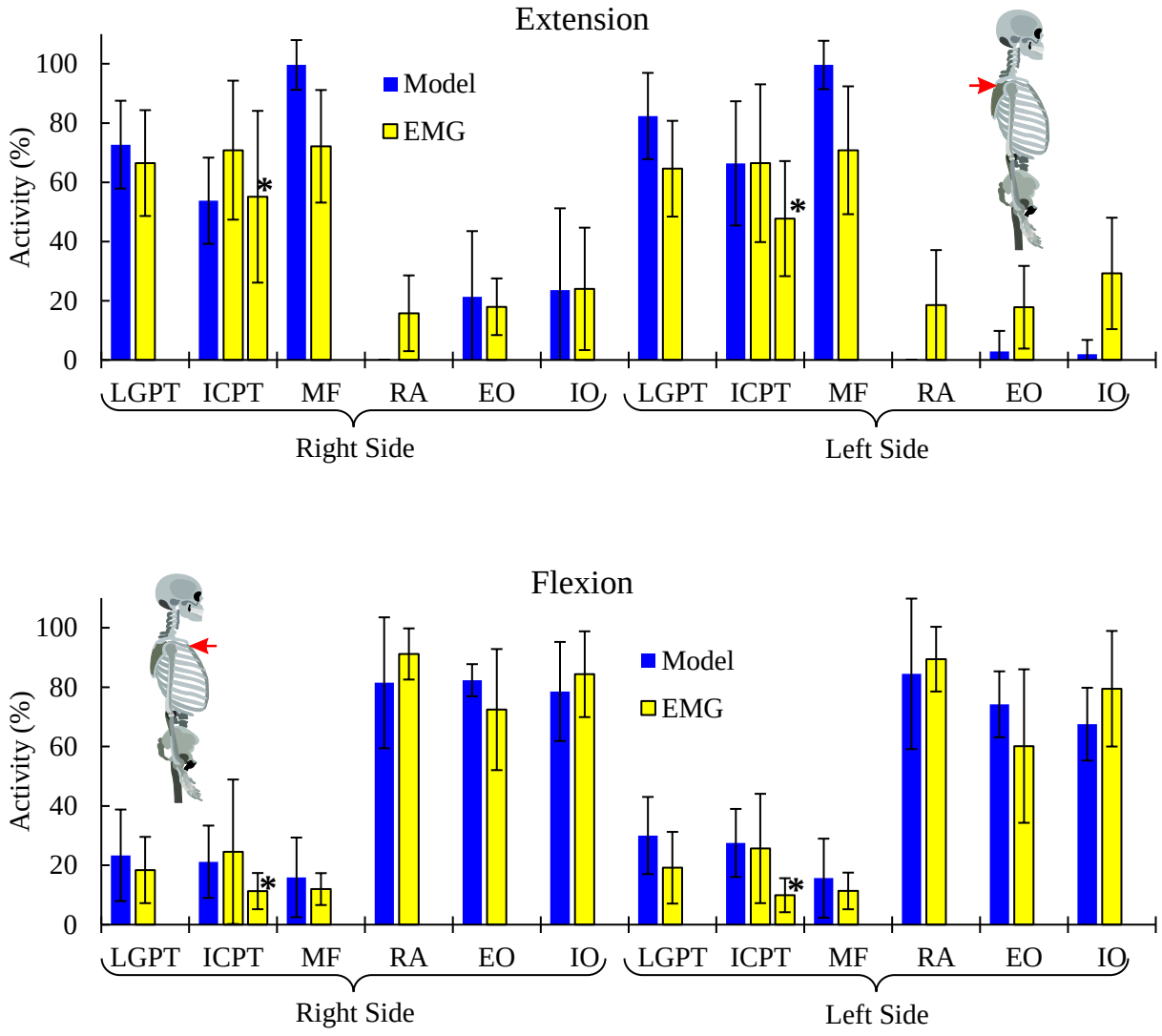

Figure 7.4 Measured versus estimated normalized muscle activities in extension (top) and flexion (bottom) MVE tasks. Bars marked by asterisk (*) present the ICPT EMGs collected at the L3. (LGPT: longissimus pars thoracic; ICPT: iliocostalis pars thoracic; MF: multifidus; RA: rectus abdominis; EO: external oblique; IO: internal oblique)

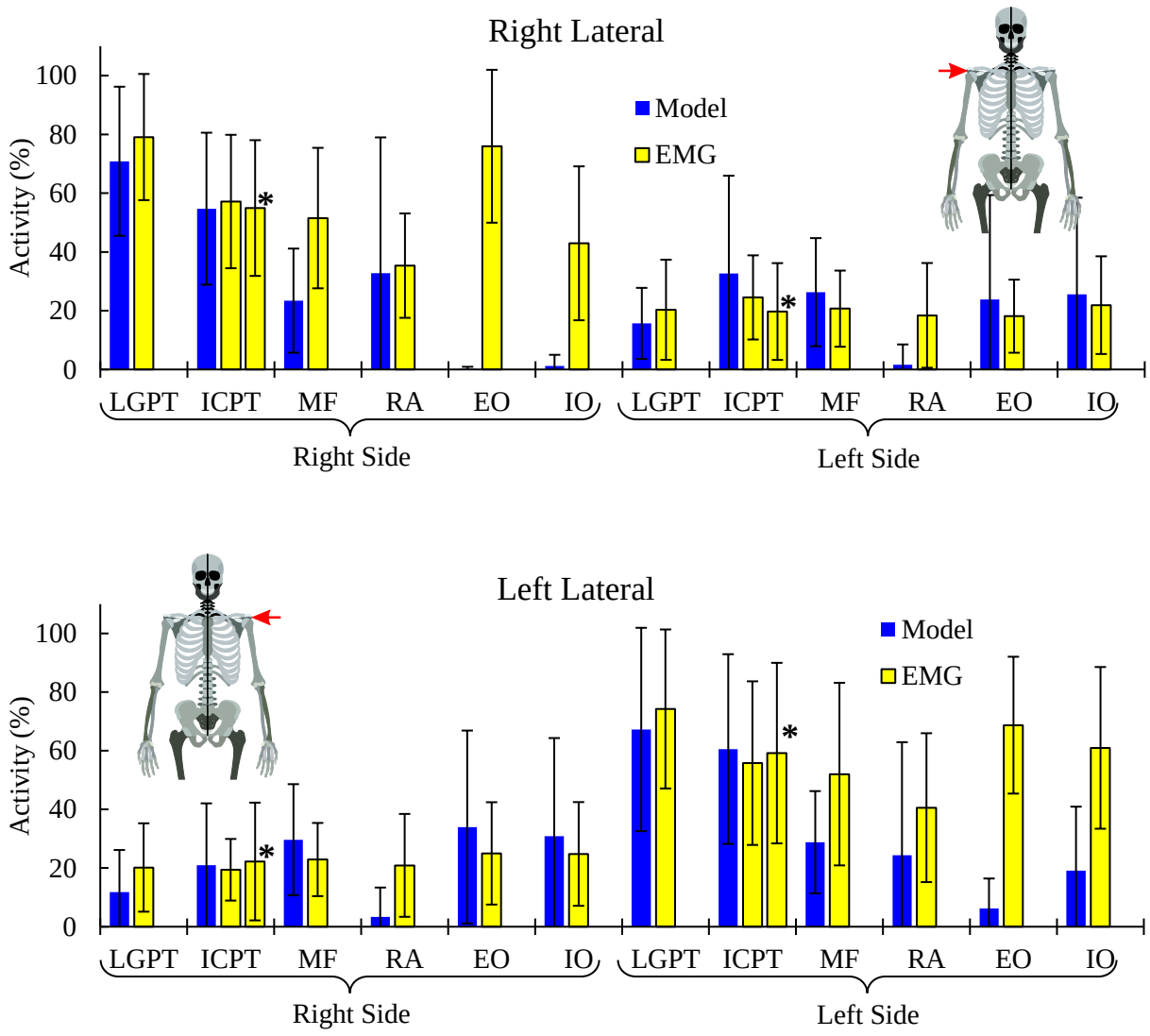

Figure 7.5 Measured versus estimated normalized muscle activities in right (top) and left (bottom) lateral MVE tasks. Bars marked by asterisk (*) present the measured ICPT EMGs collected at the L3. (LGPT: longissimus pars thoracic; ICPT: iliocostalis pars thoracic; MF: multifidus; RA: rectus abdominis; EO: external oblique; IO: internal oblique)

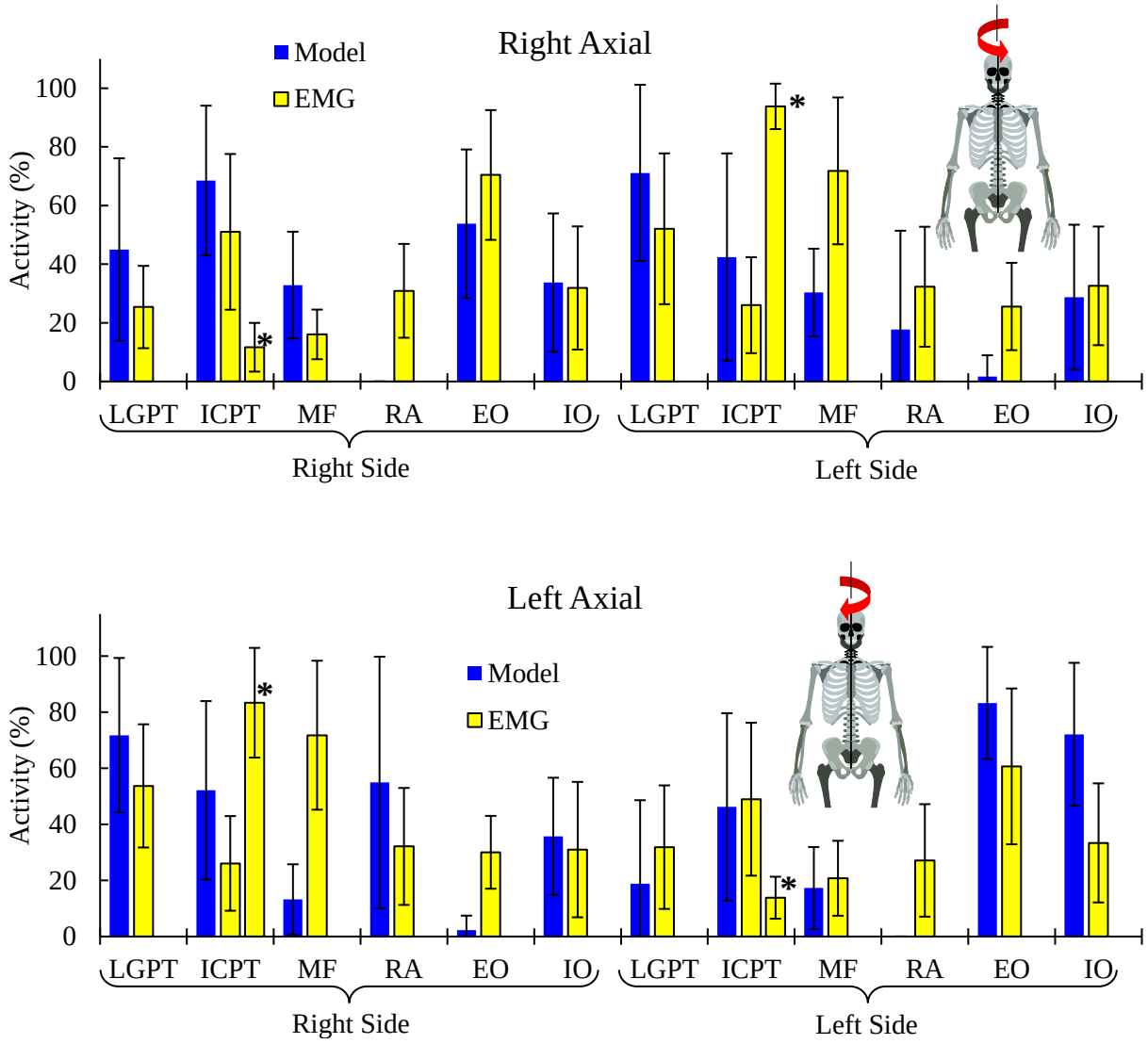

Figure 7.6 Measured versus estimated normalized muscle activities in right (top) and left (bottom) axial MVE tasks. Bars marked by asterisk (*) present the measured ICPT EMGs collected at the L3. (LGPT: longissimus pars thoracic; ICPT: iliocostalis pars thoracic; MF: multifidus; RA: rectus abdominis; EO: external oblique; IO: internal oblique)

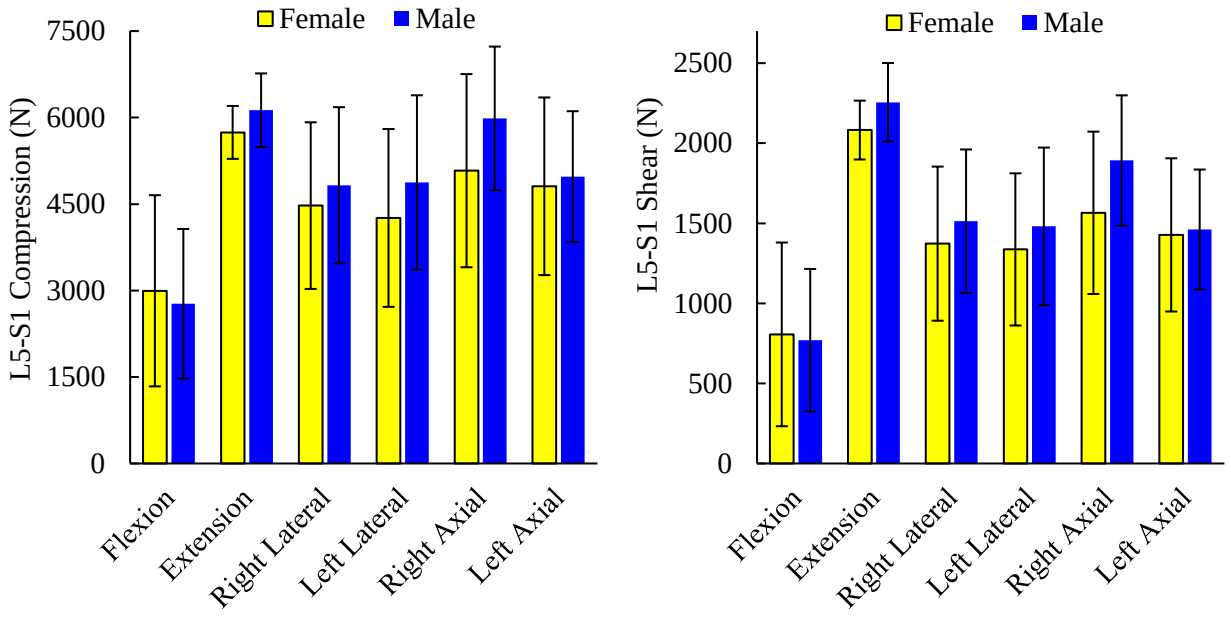

Figure 7.7 Computed local L5-S1 compression (left) and shear (right) forces in all female and male subjects during various MVEs. Both sex and MVE direction significantly affected spinal loads ($p<0.03$).

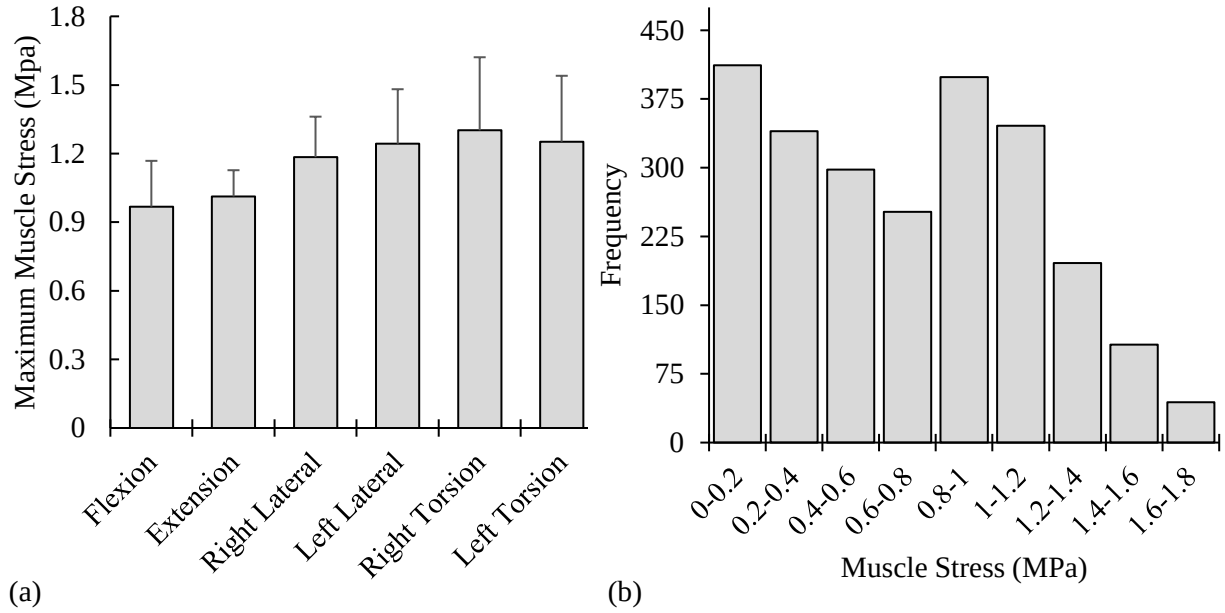

Figure 7.8 (a) The computed maximum muscle stress (σ_{max} in Eq. 7.1; mean + standard deviation) required to reach convergence in various MVE directions, and (b) histogram of estimated peak muscle stresses (σ_i; Eq. 7.2) in all muscles and participants (in total 2394=126 muscles × 19 participants)

CHAPTER 8 ARTICLE 6: SUBJECT-SPECIFIC REGRESSION EQUATIONS TO ESTIMATE LOWER SPINAL LOADS DURING SYMMETRIC AND ASYMMETRIC STATIC LIFTING

Authors: F.Ghezelbash, A.Shirazi-Adl, Z. El-Ouaaid, A. Plamondon, and N.Arjmand

Accepted in *Journal of Biomechanics*, 2019

8.1 Introduction

Work-related musculoskeletal injuries and disorders have been identified as one of the most frequent and costly impairments. Back pain as the leading cause of disability tops this list (Hoy et al., 2012; Hoy et al., 2014). Excessive and/or cumulative loads on the lumbar spine are recognized to play a causative role in the back pain (Adams et al., 2000; Adams & Roughley, 2006). Accurate estimation of muscle forces and loads on the spine in various daily and occupational activities is therefore crucial in effective prevention, workplace design as well as treatment and management of back disorders. Since no direct technique of measuring spinal loads exists, and indirect methods (i.e., intradiscal pressure (IDP) measurements (Nachemson, 1960; Wilke et al., 1999), instrumented vertebral replacements (Dreischarf et al., 2015b; Rohlmann et al., 2013a)) are invasive and limited, trunk musculoskeletal models (in spite of their limitations) are recognized as viable and complementary alternatives.

A number of tools with different degrees of complexity and accuracy have been developed and applied to estimate loads on the spine (Rajaee et al., 2015). 3DSSPP software (University of Michigan, Center for Ergonomics) is a user-friendly program, but it does not take account of muscle wrapping (Arjmand et al., 2006), translational degrees of freedom at spinal joints (Ghezelbash et al., 2015), comprehensive muscle architecture and satisfaction of equilibrium equations at all spinal levels (Arjmand et al., 2007), which can yield erroneous results. AnyBody Modelling System (Bassani et al., 2017; Damsgaard et al., 2006) and OpenSim (Bruno et al., 2015; Bruno et al., 2017; Delp et al., 2007) are generic musculoskeletal modeling programs with comprehensive muscle architectures, muscle wrapping algorithms and multi-joint passive spine.

They, however, commonly neglect translational degrees of freedom at discs, assume fixed centers of rotation in spherical joints and overlook nonlinear behavior of the ligamentous spine, which adversely affect spinal load predictions (Arshad, Zander, Dreischarf, & Schmidt, 2016; Ghezelbash et al., 2015; Ghezelbash et al., 2018b) (Chapter 6). Generic rather than physiological-based approaches are also employed to scale musculoskeletal models (Rasmussen et al., 2005). In addition, efficient application of these programs requires sufficient prior training and knowledge of their capabilities.

Regression equations and artificial neural networks (ANNs) (Arjmand, Ekrami, Shirazi-Adl, Plamondon, & Parnianpour, 2013), on the other hand, are simple, accurate and practical alternatives in ergonomics when based on more complex musculoskeletal models. However, existing regression equations and ANNs are limited to symmetric postures (Arjmand et al., 2011; Arjmand et al., 2012; Merryweather et al., 2008; Potvin, 1997), spinal loads (i.e., only compression and not shear) at one spinal level (McGill et al., 1996; Merryweather et al., 2008; Potvin, 1997), overlook external load magnitude, location and direction (McGill et al., 1996), and/or employ a simplified trunk model (Merryweather et al., 2008; Potvin, 1997). Additionally, although anthropometric differences among subjects (particularly body weight (Ghezelbash et al., 2016a; Hajihosseinali et al., 2015) and waist circumference (Ghezelbash et al., 2017b) (Chapter 5)) markedly affect spinal loads, none of existing regression equations utilize a physiological-based personalization method to take account of such factors (Arjmand et al., 2011; Arjmand et al., 2012; McGill et al., 1996; Merryweather et al., 2008; Potvin, 1997).

Thus, we aim to develop subject-specific regression equations to estimate lower spinal loads during asymmetric static lifting tasks. After recording whole body kinematics and surface electromyography (EMG) of 19 healthy individuals during various symmetric and asymmetric static lifting tasks, we simulated the foregoing and additional tasks using our subject-specific nonlinear finite element musculoskeletal (FE-MS) model of trunk driven by measured kinematics for different body heights (BHs), body weights (BWs) and sex. Quadratic regression equations were developed to estimate L4-L5 and L5-S1 shear and compression loads by using FE-MS model

outputs for various subject-specific inputs. For validation, estimated muscle activities and L4-L5 IDPs were compared with our own recorded surface EMG data and reported in vivo IDP measurements, respectively.

8.2 Methods

8.2.1 Experiments

After obtaining approval of the institutional ethics committee and consent of subjects, 9 female (height=163.4±3.7 cm; weight=61±4.5 kg; age=24.1±4.3 years) and 10 male (174.6±4.2 cm; 72.2± 8.7 kg; 30.6±6.5 years) asymptomatic participants performed various symmetric and asymmetric lifting tasks. Subjects held four hand-loads (2, 6, 10 and 14 kg) at four different heights (mid-tibia, knee, mid-femur and umbilicus levels) and asymmetry angles (A=0, 30, 60 and 90^{o}; performed to the left side of participants; Figure 8.1) at a fixed horizontal distance from feet (0.2×BH). Kinematics (anatomical joint centers and rotations) was measured with Optotrak system (Northern Digital, Canada) by using 12 clusters (feet, thighs, upper arms and forearms, pelvis, T11, C7 and head) with four LED markers glued on each cluster. We recorded EMG signals of 14 muscles by skin surface electrodes (longissimus thoracis pars thoracis and lumborum, iliocostalis pars thoracis and lumborum, multifidus, external oblique, internal oblique and rectus abdominis). Raw motion signals were filtered by a lowpass filter (corner frequency at 10 Hz). EMG signals were initially band-pass filtered (30-450 Hz) followed by the evaluation of the root mean square values of the signal (50 ms window). Subjects performed lifting tasks once. Data was collected while subjects statically held the hand-load in a predefined location (height and asymmetry angle) without bending their knees. Average EMG and kinematics data over this period were taken in following analyses. EMGs were normalized to their maximal root mean square values at maximum isometric voluntary exertions (flexion, extension, lateral and axial directions) (Ghezelbash, El Ouaaid, Shirazi-Adl, Plamondon, & Arjmand, 2018a) (Chapter 7).

8.2.2 Subject-Specific FE-MS Model

The nonlinear subject-specific FE-MS model of the trunk included 7 joints (T11-T12 to L5-S1) simulated with shear deformable nonlinear beams (representing the entire motion segments: intervertebral discs, vertebrae, facet joints and ligaments) and took account of the rest of the upper trunk (T1 to T11) as a single rigid body with identical rotations. Muscle forces in all 148 sagittally-symmetric muscles (external oblique, Iliocostalis (lumbar and thoracic), iliopsoas, internal oblique, latissimus dorsi, longissimus (lumbar and thoracic), multifidus, quadratus lumbarum, serratus posterior inferior, spinalis, and rectus abdominis) were computed in a combined optimization- and kinematics-driven framework (Ghezelbash et al., 2016b) (Chapter 3).

For each task, measured vertebral rotations (T11 to S1) were prescribed and associated reaction moments at each level (T11 to S1) were determined from the nonlinear finite element model. Due to the joint redundancy, we employed an optimization algorithm with minimization of quadratic sum of muscle stresses as the cost function. The optimization problem was constrained to satisfy moment equilibrium equations at all T11 to S1 levels and anatomical planes/directions, and muscle forces were bounded to vary within their physiological limits (greater than the passive force (Davis et al., 2003) and less than the sum of the passive force component plus the active component (Buchanan, 1995; Ghezelbash et al., 2018a; Pruim et al., 1980) (Chapter 7)). At each iteration and in the instantaneous configuration, muscle penalty forces (i.e., vector sum of muscle forces attached to a vertebra) were applied as additional forces to the corresponding vertebra until convergence was reached (i.e., slight changes (<2%) in muscle forces between two consecutive steps). In this manner, equilibrium equations of all T11-L5 vertebrae in all force and moment directions (6 degrees-of-freedom) and at deformed posture were satisfied under the action of upper body weight, external load in hands and estimated muscle forces. Local spinal loads were subsequently computed based on the force equilibrium requirements.

T11 and S1 rotations were assigned in accordance with our in vivo kinematics measurements. To compare estimated muscle activities with measured EMGs, we used recorded kinematics of each subject specifically while to develop regression equations, we employed average kinematics of all

subjects at each load elevation. In addition, intersegmental (T12 to L5) rotations were partitioned based on measured kinematics by linear interpolation of T11 and S1 rotation vectors (i.e., $\boldsymbol{v} = \theta \boldsymbol{k}$ in which θ and $\boldsymbol{k}$ denote angle magnitude and unit vector along the axis of rotation) by 6.0% at T11–T12, 10.9% at T12- L1, 14.1% at L1–L2, 13.2% at L2–L3, 16.9% at L3–L4, 20.1% at L4–L5, and 18.7% at L5-S1 (Ghezelbash et al., 2016b) (Chapter 3). Gravity loads in the trunk (Pearsall et al., 1996), lower/upper arms (De Leva, 1996), and the head (De Leva, 1996) were distributed after being scaled proportional to the subject BW. The scaling algorithm personalized the spine geometry, gravity loads, muscle architecture and passive properties for given BW, BH, age and sex parameters using available imaging databases (Anderson et al., 2012; Shi et al., 2014) and biomechanical principles (Ghezelbash et al., 2016b) (Chapter 3). More details of the FE-MS model and scaling algorithm are provided elsewhere (Ghezelbash et al., 2016b) (Chapter 3), Appendix C.

8.2.3 Simulations

We performed two sets of simulations to develop regression equations (at upright standing and flexed postures) and to compare EMGs with model predictions. To develop regression equations during flexed postures, we simulated all permutations (in total 3840 cases) of different load elevations (equivalent to the trunk flexion, F; Appendix D), external load distance from the shoulder joints (D), asymmetry angle (A), external load magnitude (M), body height (BH), sex (male=0 and female=1) and body mass index (BMI; equivalent to BW at a given BH to avoid extremely thin – BMI<19 kg/m^2 – or obese – BMI>30kg/m^2 – cases) (Table 8.1 and Figure 8.1). To develop regression equations, we used average kinematics of subjects during various lifting activities (64 tasks) while BH, BW and sex were altered, Table 8.1. Subjects held different hand-loads at different heights (mid-tibia, knee, mid-thigh and navel level) and measured trunk kinematics (3D rotations of T11 and S1) were applied to the model; at each task, load-height and flexion angle (F; Figure 8.1) are dependent variables. Because at the upright posture, hand reach is greater than that in the flexed posture, additional simulations with greater range of D (25 to 60 cm) were performed (1440 cases), and regression equations were developed separately for the upright standing (Table 8.1). Furthermore, to compare estimated muscle activities with measured EMGs,

we exactly simulated tasks performed by each subject in our experiments (64x19=1216 cases in total) by employing recorded load and arms locations as well as trunk kinematics after adjusting the model in accordance with subjects' anthropometric parameters.

8.2.4 Regression Analyses

We performed regression analysis to identify likely associations between average measured rotation vectors (at T11 and S1) and surrogate predictors (flexion (F) and asymmetric (A) angles). To correlate inputs (Table 8.1) with outputs (shear and compression at L4-L5 and L5-S1), regression equations were developed using backward elimination. Since flexion angle (F; Figure 8.1) and load height (H; Figure E.1; Appendix E) are dependent variables, we proposed two sets of regression equations, which take either flexion angle (F; presented in Results) or load height (H; presented in Appendix E) as inputs. Additionally, to further reduce regression equations, sex and BH that slightly affect spinal loads are removed and a simplified set of regression equations are presented in Appendix F. The relative importance of inputs to spinal loads in a linear regression analysis were estimated by using dominance analysis (Azen & Budescu, 2003).

8.2.5 EMG and IDP Comparisons

To evaluate the performance of FE-MS model and associated regression equations, we compared predicted muscle activities with our measured EMGs and also compared estimated and measured L4-L5 IDPs considering participants' BH, BW and sex (Sato et al., 1999; Takahashi, Kikuchi, Sato, & Sato, 2006; Wilke et al., 2001). The L4-L5 IDP (MPa) was estimated using the following equation (Ghezelbash et al., 2016b) (Eq. 3.6):

$$\begin{aligned}\mathrm{IDP}(P,\theta) = {} & -1.556\times10^{-2} + 1.255P + 1.243\times10^{-2}\theta + 3.988\times10^{-2}P^2 \\ & - 1.212\times10^{-2}P\theta + 1.669\times10^{-3}\theta^2\end{aligned} \qquad \text{Eq. 8.1}$$

and

$$P = \frac{C_{L4-L5}}{DA} \qquad \text{Eq. 8.2}$$

in which θ (^{o}) denotes intersegmental angle in the sagittal plane, and C_{L4-L5} and DA represent personalized L4-L5 compression (N) and disc area (mm^2), respectively.

8.3 Results

After the evaluation of measured kinematics, pelvic rotations of four subjects (one female and thee males) were excluded (due to marker detachment and/or slippage). Flexion (F) and asymmetric (A) angles explained ~94% of the variation in T11 and S1 rotation vector components (Table 8.2). The musculoskeletal model did not converge in 363 cases (out of 5280) when developing regression equations and in 210 cases (out of 1216) when simulating our experiments (due mainly to large lumbar axial rotation in some cases as discussed later). Low average relative error (<11%) and high R^2 (>0.92) demonstrated satisfactory performance of regression equations (i.e., goodness of fit) in estimating L4-L5 and L5-S1 shear and compression forces, Table 8.3 and Table 8.4.

Based on the dominance analysis (Azen & Budescu, 2003), trunk flexion angle (45%), hand-load weight (22%), hand-load moment arm (12%), body weight (11%) and asymmetry angle (8%) were the most influential predictors while the effects of sex and BH were minor (<2%); Figure 8.2 and Figure 8.3. Large compression (>3500 N) and shear (>1200 N) forces were computed at the lowermost L5-S1 level for some demanding tasks simulated here. Notwithstanding missing or imprecise recording and report of trunk and pelvic rotations in in vivo studies and approximate nature of IDP-compression relationship that inevitably affect comparisons, predicted IDPs were found in strong agreement with reported measurements (R^2=0.85; Figure 8.4). Estimated muscle activities were in moderate (for extensor muscles; R^2=0.40) to weak (for abdominal muscles; R^2=0.02) qualitative agreement with our measured normalized EMGs (Figure 8.5 and Figure 8.6).

8.4 Discussion

Accurate subject-specific spinal load estimation is an integral part of workplace safety, personalized treatment design and back pain prevention programs. Due to the lack of reliable non-invasive approaches, regression equations which have been constructed based on the results of complex and accurate musculoskeletal models are straightforward and robust alternatives. Here, we developed personalized regression equations to estimate shear and compression forces at the L4-L5 and L5-S1 levels during static asymmetric lifting tasks using our nonlinear FE-MS model of the trunk. Muscle activity predictions of the personalized model had moderate (for back muscles) to weak (for abdominal muscles) agreement with our measured EMGs. Estimated IDPs were in strong agreement with reported in vivo measurements (R^2=0.85).

8.4.1 Limitations

Regression equations were limited to two-hand lifting tasks, and we assumed that the hand-load and thorax were in the same asymmetric plane (Figure 8.1), so the equations do not predict spinal loads during all asymmetric tasks such as pure lateral bending (Dempsey & Fathallah, 1999). Optimization-based muscle force estimation algorithm (driven by measured subject-specific kinematics) is sensitive to the choice of cost function (Arjmand & Shirazi-Adl, 2006c; Stokes & Gardner-Morse, 2001) and overlooks likely inter- and intra-subject variabilities in muscle activities (that does not affect collected kinematics) as well as coactivity in muscle activities. Existing alternatives (Cholewicki & McGill, 1994; Gerus et al., 2013; Mohammadi et al., 2015; Walter et al., 2014), however, require extensive EMG measurements and could not be utilized as a stand-alone tool. Besides, EMGs are limited to few superficial muscles, with unknown relations to force, and susceptible to cross-talk, power line hum and motion artifacts (De Luca et al., 2010; Soderberg & Knutson, 2000; Türker, 1993). Since the effects of sex, BH and BW on lordosis is controversial (Been & Kalichman, 2014), initial lordosis angle was kept identical in all analyses. The scaling algorithm used regression equations (developed based on CT scans of 100 individuals (Anderson et al., 2012)) to adjust muscle architecture (moment arms and PCSA) despite rather weak

coefficients of determination in some equations. Trunk weight along the spine was distributed among corresponding vertebrae via rigid beams in spite of likely errors in such an assumption particularly at lower abdominal levels. Average kinematics of 15 subjects during various tasks were used along with alterations in BW, BH and sex (Table 8.1) when regression equations were developed. Since we did not measure trunk kinematics with 20 kg hand-load, we used trunk kinematics measured at 14 kg hand-load. Due to the relatively large stiffness of the ligamentous lumbar spine in torsion, computed results in more extreme asymmetric positions were found sensitive to the prescribed vertebral axial rotations. At some simulations with large rotations, convergence difficulty was encountered as muscles were not able to generate required large axial moments. Developed regression equations estimate spinal loads during quasi-static tasks which remain accurate for dynamic tasks with intermediate lifting speeds as well (Bazrgari et al., 2008). Proposed regression equations were developed based on measured kinematics of young healthy subjects with no experience in manual handling of loads. Extension to patients with back pain and to experienced workers requires caution. For further limitations on the musculoskeletal model see earlier works (Ghezelbash, Shiraz-Adl, Plamondon, Arjmand, & Parnianpour, 2017a; Ghezelbash et al., 2016b) (Chapter 3; Chapter 5).

8.4.2 Interpretations

Rajaee et al. (2015) compared various lifting tools and rated AnyBody software and the regression equations developed by Arjmand et al. (Arjmand et al., 2011; Arjmand et al., 2012) as the most comprehensive tools in satisfactory agreement with IDP measurements (Wilke et al., 2001). Foregoing tools, however, either neglect the substantial role of anthropometric parameters (Arjmand et al., 2011; Arjmand et al., 2012) or utilize simplistic scaling algorithms (Rasmussen et al., 2005). Furthermore, the performance of earlier tools has not been evaluated by comparison with both EMG and IDP measurements during numerous lifting tasks. In comparison, our proposed regression equations (Table 8.3 and Table 8.4) take account of major anthropometric parameters using imaging databases (Anderson et al., 2012; Shi et al., 2014) and biomechanical principles (Ghezelbash et al., 2016a, b) (Chapter 3; Chapter 4).

After adjusting the model and regression equations in accordance with subjects' anthropometric parameters in our EMG and reported IDP experiments, we compared estimated muscle activities and IDPs against measurements. In symmetric tasks (A=0^o), there was a satisfactory agreement between estimated muscle activities and measured EMGs; however, in asymmetric tasks, estimations were in moderate to weak agreement with measured EMGs. This can partly be due to intrinsic problems with EMG signals (e.g., cross-talk, susceptibility to contamination, normalization) especially in the large and deep abdominal oblique muscles. Substantial differences were noted even among surface EMG recordings on the same extensor muscle at two different locations (see quite different iliocostalis EMG at the T11 and L3 levels, Figure 8.5). Besides, the EMG-force relation, maximum muscle force used for normalization of estimated forces, and limitations in the FE-MS model (see above) should also be considered. Incorporation of personalized muscle recruitment patterns either by EMG-assisted approaches (Cholewicki & McGill, 1994; Mohammadi et al., 2015) or by introducing muscle synergies (Gerus et al., 2013; Walter et al., 2014) would substantially complicate the application of regression equations. Estimated IDPs had strong agreement with different measurements (R^2=0.85) (Sato et al., 1999; Takahashi et al., 2006; Wilke et al., 2001) showing the relative accuracy of developed regression equations in spinal load estimation.

Although asymmetry is found to markedly affect spinal loads (Figure 8.2 and Figure 8.3), prior regression equations have been limited to symmetric postures (Arjmand et al., 2011; Arjmand et al., 2012; Merryweather et al., 2008; Potvin, 1997). Larger asymmetry angle (A) increases spinal loads (especially at smaller flexion angles F<50^o), and thus, under identical conditions (BH, BW, sex, F, M and D), the safest posture with the least spinal loads is a sagittally symmetric one (A=0^o). In lifting, it is hence suggested to face as much as possible towards the load. For example, when other inputs were set at F=20^o, M=5 kg, D=0 cm, BW=75 kg, BH=175 cm and sex=male, L5-S1 compression and shear forces substantially increased, respectively, from 1137 N and 395 N at A=0^o to 2531 N (by 123%) and 927 N (by 135%) at A=70^o.

Simulation of an asymmetric task is much more complex than a sagittally-symmetric one. In a static symmetric task only two angular parameters (T11 and S1 rotations in the sagittal plane) are required to define and prescribe trunk kinematics while in an asymmetric task, required parameters increase to six (three trunk T11 rotations and three pelvic S1 rotations). To subsequently partition intersegmental rotations (at T12-L5 levels and based on proportions given earlier) from measured spatial T11 and S1 rotations, multiple choices are available: 1- linear interpolation of associated Euler angles at T11 and S1 levels, 2- linear interpolation of rotation vectors, 3- linear interpolation of rotation matrices, and 4- spherical linear interpolation (SLERP) of rotation quaternions (Dam, Koch, & Lillholm, 1998). Although foregoing approaches during symmetric tasks yield identical results, they could markedly affect spinal loads and model convergence in asymmetric tasks. For example, at F=87^o, A=70^o, M=5 kg, D=0 cm, BW=70 kg, BH=175 cm and sex=male, L5-S1 compression was calculated at 2724 N with linear interpolation of Euler angles, 2660 N with linear interpolation of rotation vectors, 2895 N with linear interpolation of a rotation matrix, and 2520 N for SLERP. Besides, only linear interpolation of rotation vectors and SLERP of rotation quaternions yielded model convergence in most asymmetric tasks. In our study and to develop regression equations, we used the linear interpolation of rotation vectors at the S1 (pelvis) and T11 (trunk) levels (i.e, Rodriguez parameters) to determine intersegmental rotations (T12 to L5) based on proportions listed earlier in Methods. Nevertheless, finding the best technique to distribute intersegmental rotations in asymmetric tasks requires further imaging and modeling studies.

In current regression equations, the identification of the posture during an asymmetric lift requires only two distinct parameters: flexion (F) and asymmetry (A) angles (Figure 8.1). Although in general, six rotation components (three trunk T11 rotations and three pelvic S1 rotations) are required to determine kinematics along the spine, regression analyses showed that F and A alone can satisfactorily be used as surrogate measures to predict all six rotation components (R^2>0.94 and root mean squared error<3.1^o; Table 8.2). Therefore, instead of measuring multiple rotations at trunk and pelvic (requiring a video-camera system or gyro sensors), these angles (F and A) can approximately be estimated in the workplace and be applied into regression equations with some variations to investigate the likely effects on spinal loads. For completeness and in analogy with

the revised NIOSH lifting equations (Waters et al., 1993), another set of regression equations are provided in "Supplementary Materials 3", which takes horizontal and vertical load locations as well as asymmetric angle (A) as input variables.

Trunk flexion angle (45%), hand-load weight (22%), hand-load moment arm (12%), body weight (11%) and asymmetry angle (8%) were most influential in spinal loads. Since the effect of sex and BH were minor (<1%), we developed a simplified version of regression equations by removing sex and BH (as independent variables) and by considering only significant terms ($p<0.05$) ("Supplementary Materials 4"). Removing the number of predictors in regression analysis slightly reduced R^2; estimated IDPs reached satisfactory agreement with measurements at $R^2=0.81$. Simplified regression equations are practical and relatively accurate alternatives to full regression equations.

Injury or damage to spine due to mechanical overload or cyclic loading can start a cascade of events toward disc degeneration and probably pain (Adams et al., 2000; Adams & Roughley, 2006) in lumbar discs (especially at L4-L5 and L5-S1) (Cheung et al., 2009; Hadjipavlou, Tzermiadianos, Bogduk, & Zindrick, 2008; Jang et al., 2016).To perform an individualized biomechanical risk assessment of a task, the primary step is the estimation of spinal loads using proposed regression equations. Based on the risk of compression fracture, NIOSH proposed, using rather simple models, the safe limit of 3400 N in compression. Future works should, when attempting to improve estimations of safe compression limits, consider also the role of fatigue and tissue response (mechanobiology, inflammation and healing).

In summary, we developed subject-specific regression equations to predict shear and compression spinal loads at L4-L5 and L5-S1 levels during symmetric-asymmetric static lifting by employing an optimization- and kinematics-driven personalized musculoskeletal model of the trunk. To estimate kinematics along the spine during an asymmetric task, three trunk T11 and three pelvic rotations are required. We proposed instead two surrogate flexion (F) and asymmetric (A) angles that can accurately replace them ($R^2>0.94$). Developed regression equations predicted personalized spinal loads in satisfactory agreement with various IDP measurements ($R^2=0.85$) (Sato et al., 1999;

Takahashi et al., 2006; Wilke et al., 2001). Computed muscle activities in the personalized musculoskeletal models were in moderate to weak agreement with our measured EMGs of 19 young and healthy participants. Spinal loads were most influenced by changes in the trunk flexion, hand-load weight, hand-load lever arm, BW and asymmetry angle whereas least affected by sex and BH.

8.5 Acknowledgements

This work was supported by the institut de recherche Robert-Sauvé en santé et en sécurité du travail (IRSST-2014-0009) and fonds de recherche du Québec en nature et technologies (FRQNT-200564).

Table 8.1 Levels of load elevation (equivalent to trunk flexion, F; ^{o}), external load horizontal distance from the shoulder joints (D; cm), asymmetry angle (A; ^{o}), external load magnitude (M; kg), sex (female=1; male=0), body height (BH; cm) and body mass index (BMI; kg/m^2) considered in the development of regression equations (see Figure 8.1).

Parameters	*Upright*	*Flexion*
Load Elevation	35 cm above L5-S1	Mid-Tibia, Knee, Mid-Femur and Umbilicus Levels
D (cm)	25 - 42.5 – 60	0 – 30
A(^{o})	4 Levels between 0^{o} to 70^{o} Based on Kinematic Measurements	
M (kg)	2 – 6 – 10 – 14 – 20	
Sex	Female (1) - Male (0)	
BH (cm)	160 – 175 – 190	
BMI (kg/m^2)	19 - 22.7 - 26.3 – 30	

Table 8.2 Computed coefficients, p-values, root mean squared error (RMSE) and R^2 from regression analysis on average measured trunk T11 and pelvic S1 rotation vectors (i.e., $\boldsymbol{v} = \theta\boldsymbol{k} = (\alpha, \beta, \gamma)$ in which θ and $\boldsymbol{k}$ denote angle magnitude and unit vector along the axis of rotation; α, β and γ are components of $\boldsymbol{v}$ in the global coordinate system; see Figure 8.1-top left) during flexion with asymmetric angle (A; Figure 8.1) and flexion angle (F; Figure 8.1) as predictors; significant p-values (<0.05) were shown in boldface.

Parameters			*Constant*	*A*	*F*	*A×F*	*RMSE*	*R^2*
T11 Rotation Vector ($\boldsymbol{v}$; deg)	α	Coefficient	-1.62681	0.00399	0.01563	0.00935	1.347	0.996
		p-value	**0.00560**	0.80994	**0.03709**	**0.00000**		
	β	Coefficient	7.77428	-0.03188	-1.01957	0.00293	1.424	0.998
		p-value	**0.00000**	0.07298	**0.00000**	**0.00000**		
	γ	Coefficient	1.94587	1.14017	-0.02221	-0.00495	2.396	0.986
		p-value	0.05791	**0.00000**	0.09346	**0.00000**		
S1 Rotation Vector ($\boldsymbol{v}$; deg)	α	Coefficient	0.47939	-0.06038	-0.00521	0.00348	1.341	0.964
		p-value	0.39833	**0.00052**	0.47763	**0.00000**		
	β	Coefficient	0.07832	0.00545	-0.36600	0.00087	3.146	0.944
		p-value	0.95294	0.88822	**0.00000**	0.07220		
	γ	Coefficient	2.20352	0.82977	-0.02181	-0.00096	1.888	0.990
		p-value	**0.00728**	**0.00000**	**0.03780**	**0.00144**		

Table 8.3 Computed regression coefficients, R^2, root mean squared error (RMSE) and p-values at upright standing

Parameter	*L4-L5*				*L5-S1*			
	Compression		Shear		Compression		Shear	
	Coef.*	p-value	Coef.*	p-value	Coef.*	p-value	Coef.*	p-value
Constant	-752.375	0.0015	-45.6541	0.1499	-915.245	0.0011	-213.087	0.105556
Sex†	-34.2617	0.0298	2.213731	0.4284	-31.217	0.0946	-27.1718	0.0017
BH	4.036604	0.0092	-0.17664	0.4033	4.922405	0.0073	0.732533	0.4120
BW	2.801715	0.0072	0.49574	0.0015	1.839903	0.1363	1.246567	0.0579
M	100.1808	<0.0001	13.71772	<0.0001	105.2327	<0.0001	38.30302	<0.0001
A	29.51852	<0.0001	5.015594	<0.0001	34.76647	<0.0001	13.38083	<0.0001
D	21.04534	<0.0001	1.363474	<0.0001	21.24288	<0.0001	7.913065	0.0004
Sex×BH	-	-	-	-	-	-	-	-
Sex×BW	-	-	-	-	-	-	-	-
Sex×M	3.444643	0.0046	-	-	5.382006	0.0002	2.274996	0.0006
Sex×A	-2.54159	<0.0001	-0.39249	<0.0001	-2.99263	<0.0001	-1.05515	<0.0001
Sex×D	-	-	-	-	-	-	-	-
BH×BW	-	-	-	-	-	-	-	-
BH×M	-0.48814	<0.0001	-0.0555	0.0006	-0.53138	<0.0001	-0.15533	<0.0001
BH×A	-0.09225	<0.0001	-0.01959	<0.0001	-0.11433	<0.0001	-0.04389	<0.0001
BH×D	-0.10352	0.0002	-	-	-0.11285	0.0005	-0.0346	0.0213
BW×M	-	-	-0.03536	0.0031	-	-	-0.06353	0.0153
BW×A	0.122158	<0.0001	0.032099	<0.0001	0.14919	<0.0001	0.066209	<0.0001
BW×D	0.089068	<0.0001	-	-	0.109336	<0.0001	0.033575	0.0026
M×A	-	-	0.035849	<0.0001	-	-	-	-
M×D	1.494802	<0.0001	0.183764	<0.0001	1.661007	<0.0001	0.587299	<0.0001
A×D	0.043595	<0.0001	0.010119	0.0001	0.063209	<0.0001	0.023537	<0.0001
R^2	0.976		0.950		0.975		0.966	
RMSE (N)	125.97		31.97		149.29		69.04	
Mean (N)	2086.15 ± 822.37		256.35 ± 143.01		2192.24 ± 929.80		858.38 ± 372.67	

* Coef.: Coefficient

† Female =1; Male = 0

Table 8.4 Computed regression coefficients, R^2, root mean squared error (RMSE) and p-values at flexed postures

Parameter	*L4-L5*				*L5-S1*			
	Compression		Shear		Compression		Shear	
	Coef.*	p-value	Coef.*	p-value	Coef.*	p-value	Coef.*	p-value
Constant	37.22059	0.7989	-71.9487	<0.0001	-1.75693	0.9901	41.2652	0.5349
Sex†	-338.104	<0.0001	5.412437	0.0697	-217.864	<0.0001	-19.0914	0.0659
BH	1.909076	0.0369	-	-	1.457613	0.0777	-0.61484	0.1706
BW	6.116562	<0.0001	1.316494	<0.0001	8.206912	<0.0001	4.365337	<0.0001
M	-11.8938	0.0022	3.106165	<0.0001	-8.93808	0.0222	4.1331	<0.0001
A	31.64569	<0.0001	3.088134	<0.0001	33.00651	<0.0001	12.15568	<0.0001
F	-4.78868	<0.0001	0.187397	0.0356	-7.42666	<0.0001	-3.88622	<0.0001
D	13.76692	0.0037	0.899799	<0.0001	14.80836	0.0018	9.048787	<0.0001
Sex×BH	-	-	-	-	-	-	-	-
Sex×BW	2.683103	<0.0001	-	-	1.618418	0.0032	-	-
Sex×M	7.612364	<0.0001	-	-	6.336128	<0.0001	1.425617	0.013136
Sex×A	-3.12525	<0.0001	-0.52792	<0.0001	-3.99728	<0.0001	-1.18111	<0.0001
Sex×F	2.848695	<0.0001	0.570002	<0.0001	3.442527	<0.0001	0.911929	<0.0001
Sex×D	2.171282	0.0003	0.220941	0.0071	2.593731	<0.0001	0.809314	0.0005
BH×BW	-	-	-	-	-	-	-	-
BH×M	-	-	-	-	-	-	-	-
BH×A	-0.08315	<0.0001	-	-	-0.06053	<0.0001	-0.02459	<0.0001
BH×F	-	-	-	-	-	-	0.025913	<0.0001
BH×D	-0.14364	<0.0001	-	-	-0.1373	<0.0001	-0.05908	<0.0001
BW×M	0.087833	0.0498	-0.02079	0.0006	0.123601	0.0059	-	-
BW×A	0.024035	0.0428	-	-	-	-	0.017099	0.0002
BW×F	0.231384	<0.0001	0.034375	<0.0001	0.242496	<0.0001	0.055798	<0.0001
BW×D	0.118724	<0.0001	-	-	0.120693	<0.0001	0.038626	<0.0001
M×A	-0.05777	0.0212	-0.03358	<0.0001	-0.1649	<0.0001	-0.04489	<0.0001
M×F	0.914314	<0.0001	0.109374	<0.0001	0.922464	<0.0001	0.220514	<0.0001
M×D	2.473507	<0.0001	0.304779	<0.0001	2.596952	<0.0001	1.00079	<0.0001
A×F	-0.09588	<0.0001	-0.02111	<0.0001	-0.09849	<0.0001	-0.0663	<0.0001
A×D	-0.02157	0.0346	-0.01119	<0.0001	-0.06065	<0.0001	-0.0125	0.0015
F×D	0.051812	<0.0001	-0.0037	0.0009	0.026435	0.0014	-0.01553	<0.0001
R^2	0.949		0.956		0.949		0.928	
RMSE (N)	273.24		37.13		274.15		105.72	
Mean (N)	2925.21 ± 1211.28		388.59 ± 175.63		3032.31 ± 1205.98		1056.23 ± 392.21	

* Coef.: Coefficient

† Female =1; Male = 0

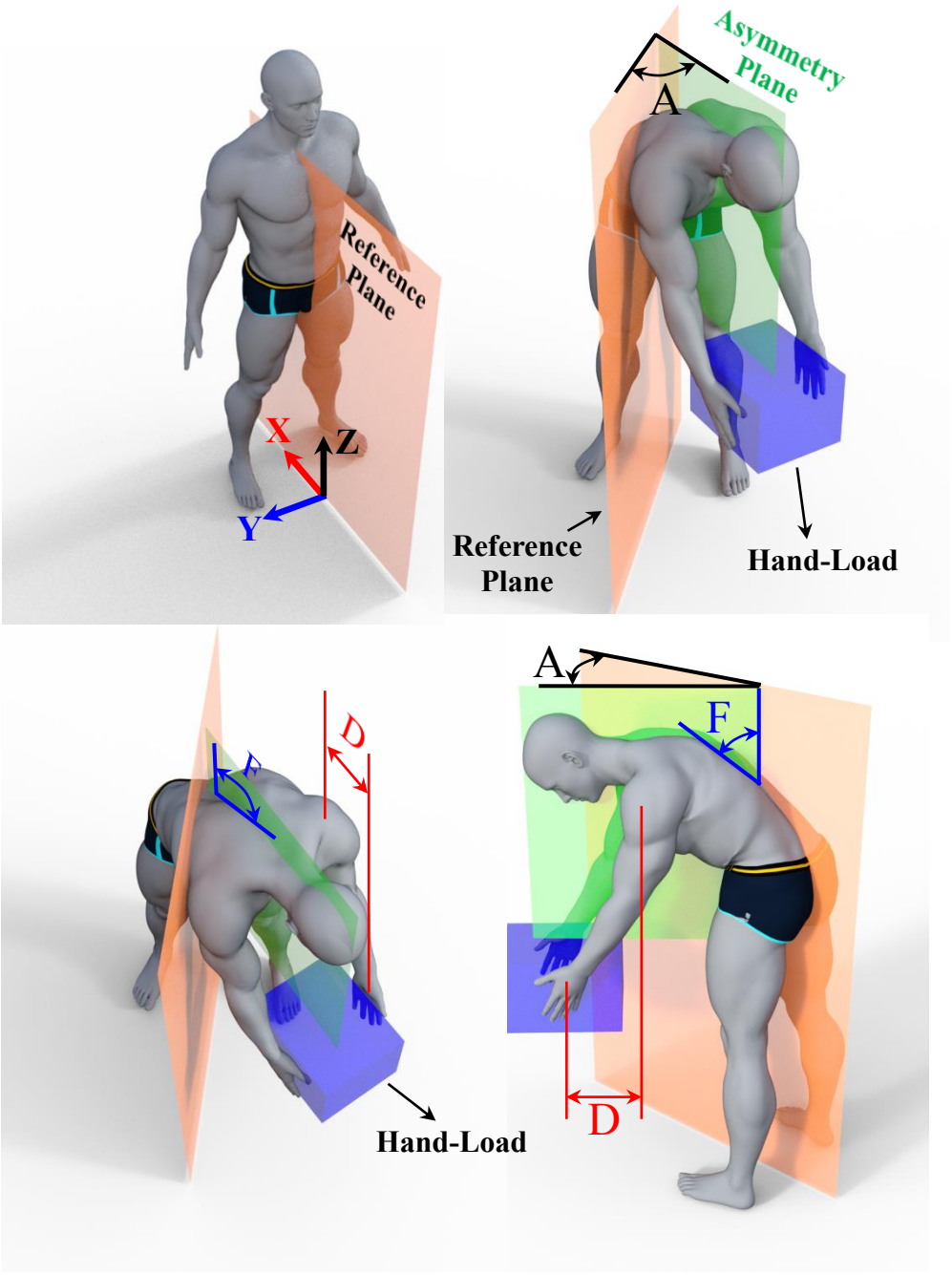

Figure 8.1 Schematic representation of the global coordinate system and an asymmetric lifting task (A: asymmetry angle; F: flexion angle; D: moment arm from the shoulder joint). The asymmetry plane (perpendicular to the transverse plane - highlighted in green) is defined to pass through thorax and hand-load in the deformed posture. The angle between Z-axis and the tangent plane to the trunk at T11 is defined as F. For more details on angles F and A see Appendix D.

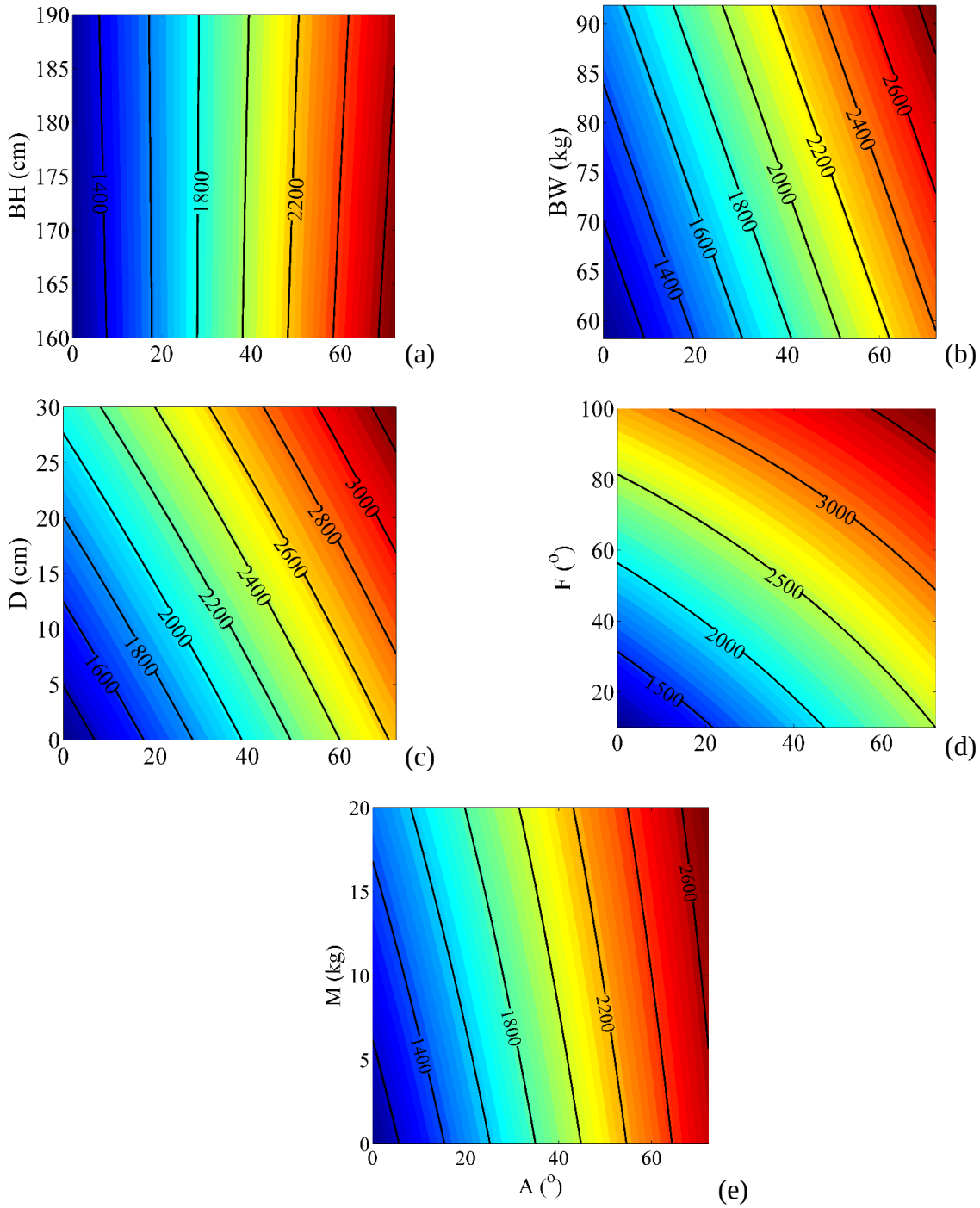

Figure 8.2 L5-S1 compression forces (N) computed from regression equations during asymmetric flexion with variations in (a) body height (BH), (b) body weight (BW), (c) horizontal distance of the external load from the shoulder joint (D), (d) flexion angle (F) and (e) external load magnitude (M) versus asymmetry angle (A). If not acting as an independent variable, regression parameters in this figure were set at sex=male (0), D=0 cm, M=10 kg, BW=75 kg, BH=175 cm and F=20°.

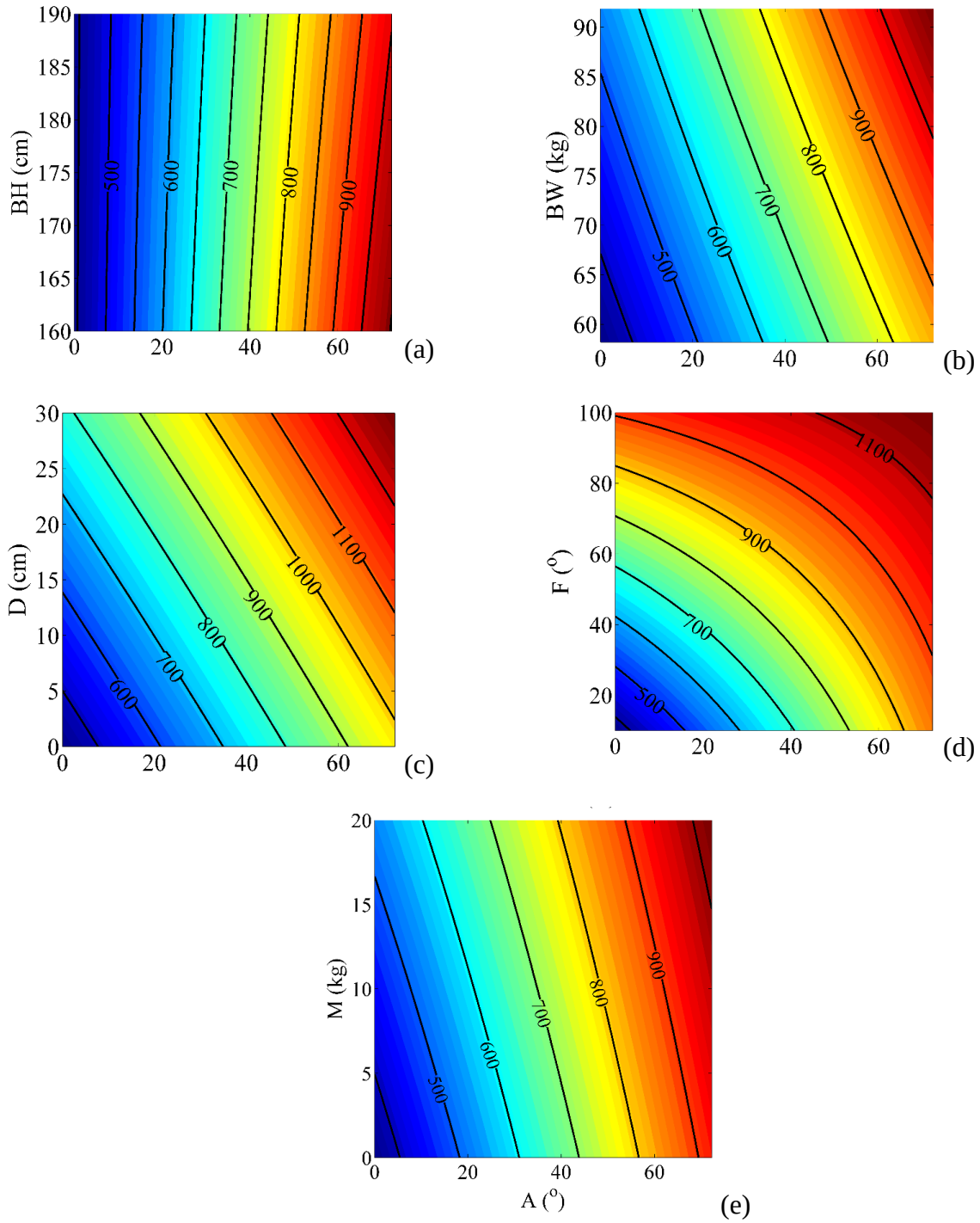

Figure 8.3 L5-S1 shear forces (N) computed from regression equations during asymmetric flexion with variations in (a) body height (BH), (b) body weight (BW), (c) horizontal distance of the external load from the shoulder joint (D), (d) flexion angle (F) and (e) external load magnitude (M) versus asymmetry angle (A). If not acting as an independent variable, regression parameters in this figure were set at sex=male (0), D=0 cm, M=10 kg, BW=75 kg, BH=175 cm and F=20°.

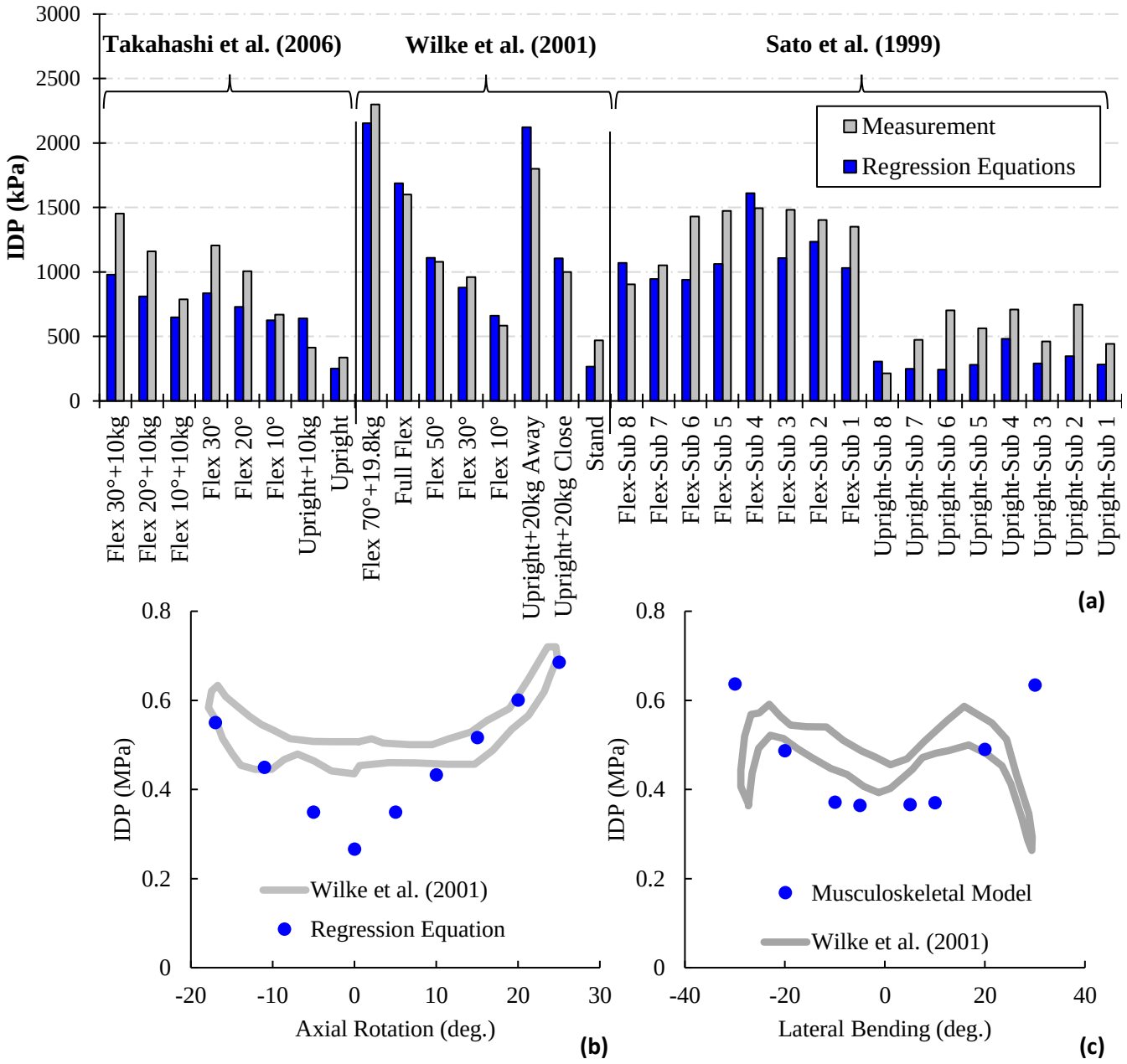

Figure 8.4 Estimated IDPs from regression equations (a and b) and FE-MS model (c) versus measurements during sagittally symmetric tasks (a; Flex: Flexion; Sub: Subject – Sato et al. (1999) measured IDP of 8 subjects), axial rotation (b) and lateral bending (c; proposed regression equations cannot estimate spinal loads during pure lateral bending; we, therefore, used the FE-MS model driven with reported kinematics (Narimani & Arjmand, 2018) to estimate spinal loads.)

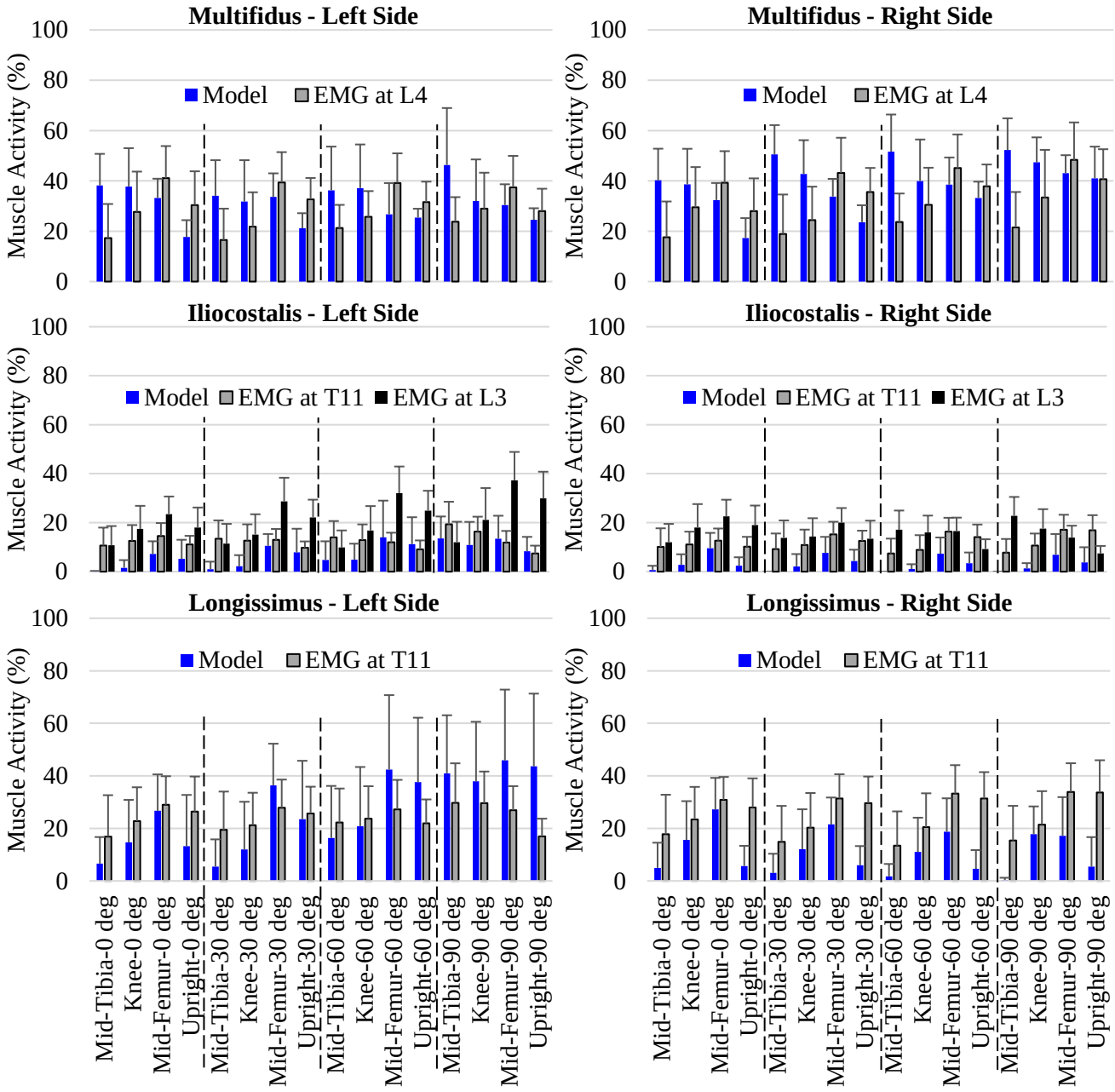

Figure 8.5 Average (bars denote one SD) estimated muscle activities (average of muscles closest to the corresponding EMG electrodes) and measured EMGs of 19 subjects in right and left back muscles during various lifting activities at different load elevations (upright, mid-femur, knee and mid-tibia) and asymmetry angles (A=0, 30, 60, 90^{o}) with 14 kg hand-loads

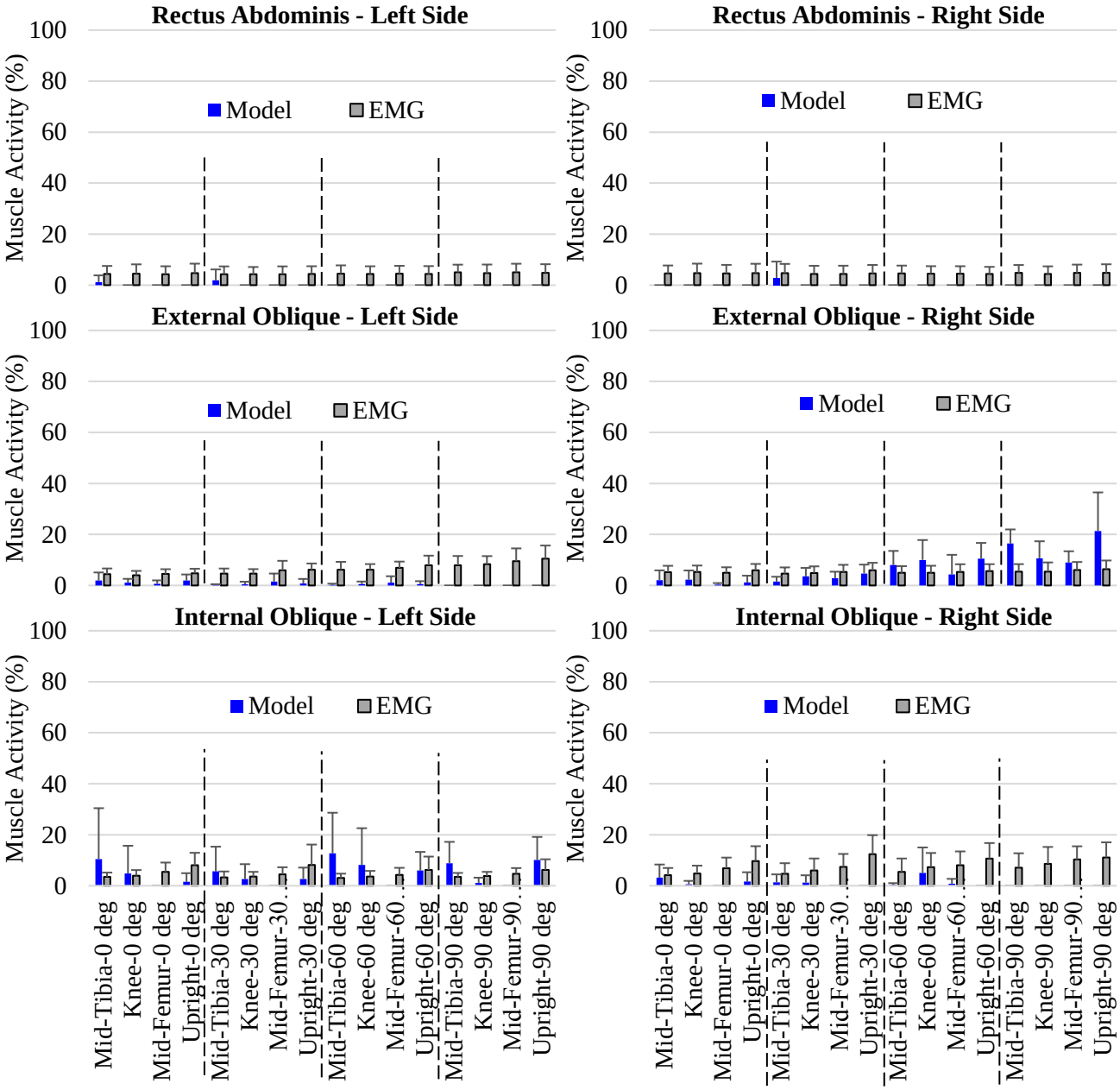

Figure 8.6 Average (bars denote one SD) estimated muscle activities (average of muscles closest to the corresponding EMG electrodes) and measured EMGs of 19 subjects in right and left abdominal muscles during various lifting activities at different load elevations (upright, mid-femur, knee and mid-tibia) and asymmetry angles (A=0, 30, 60, 90^{o}) with 14 kg hand-loads

CHAPTER 9 GENERAL DISCUSSION

An existing KD-FE musculoskeletal model of the trunk has been upgraded by refining the muscle architecture, adding a new deformable disc (T11-T12) and introducing a scaling algorithm to explore the effects of variations in age, sex, BW and BH on spine biomechanics and spinal loads. The scaling algorithm adjusts the muscle architecture (muscle moment arms and cross-sectional areas), spine geometry, passive properties of the ligamentous spine and gravity loads based on subject's sex, age, BH and BW. A full-factorial sensitivity analysis on model inputs showed that BW and obesity (as an extreme case) substantially affected spinal loads while the effects of other contributing factors (BH, sex and age) remained relatively small. Obesity shape (i.e., variations in the distribution of adipose tissue along the body) at identical BMI (or BH and BW) affected spinal loads; obese individuals with greater waist circumference experienced greater spinal loads and the risk of vertebral fatigue fracture. Moreover, personalized regression equations were developed to estimate spinal loads during various symmetric and asymmetric lifting tasks. The performance and validity of the model were evaluated by comparing estimated IDPs with *in vivo* measurements and estimated muscle activities (during MVE and lifting tasks) with measured EMGs (Ghezelbash et al., 2018a; Ghezelbash, Shiraz-Adl, El Ouaaid, Plamondon, & Arjmand, 2019) (Chapter 7; Chapter 8). Using beams and spherical joints with nonlinear passive properties (to represent ligamentous spine) satisfactorily predicted spine kinematics, spinal loads and muscle activities.

9.1 Novelties

A new deformable disc (T11-T12) was added to an existing musculoskeletal model of the trunk and the muscle architecture was refined. The proposed scaling algorithm adjusts muscle moment arms, muscle cross-sectional areas, spine geometry, gravity loads and passive properties of ligamentous spine to incorporate likely effects of sex, age, BH and BW based on imaging datasets (Anderson et al., 2012; Shi et al., 2014) and biomechanical principles, Figure 7.2. Including subject-specific kinematics and material properties, the model could comprehensively account for the effects of individual differences on spine biomechanics. Obesity and obesity shapes (apple- and pear-shaped, or android and gynoid) were realistically simulated by estimating mass distribution along the body (calves, thighs, waist, arms and head) in different obesity types based on available measurements on thousands of obese individuals (National Center for Health Statistics, 1999-

2014). Maximum muscle stresses of different muscle groups in each subject's trunk were calculated by simulating MVE tasks in different directions. Validity and accuracy of using simplified joint models (i.e., beams/spherical joints with linear/nonlinear passive properties) in predicting kinematics of the passive spine, muscle forces and spinal loads have been investigated. Easy-to-use subject-specific regression equations were developed to estimate spinal loads during asymmetric tasks.

9.2 Limitations

Muscle forces were estimated by using an optimization criterion, which overlooks inter- and intra-subject variability as well as coactivation in antagonist muscles (Arjmand & Shirazi-Adl, 2006c; Stokes & Gardner-Morse, 2001); coactivation in antagonist muscles can however be introduced by imposing stability or coactivity constraints (El Ouaaid et al., 2013a; Mohammadi et al., 2015). Muscles were modeled as 1D elements (i.e., vectors with linear or multi-linear trajectories that simulate wrapping muscles) with constant activity along the length in spite of the fact that muscles are 3D objects (Blemker & Delp, 2005); however, simulating muscles as 3D objects significantly increases the computational burden. Gravity loads along the trunk were applied off-center via rigid beams attached to the corresponding vertebrae although this modeling technique may not be accurate particularly at around the abdominal cavity. In the scaling algorithm, lumbar lordosis was not changed based on subject's BH, BW, age and sex since the association between lordosis and foregoing anthropometric parameters are controversial (Been & Kalichman, 2014). The model was scaled based on subject's BH, BW, age and sex, but all subject-specific differences cannot be described by those factors alone; for example, regression equations employed to adjust muscle moment arms and cross-sectional areas have in some cases poor coefficient of determination (Anderson et al., 2012), and this indicates that this approach does not explain all variations in the data. Disc cross-sectional areas were assumed to be proportional to the maximum ribcage area in the transverse plane, but more recently, new regression equations have been proposed to correlate disc areas also with BH, BW, age and sex (Tang et al., 2019). Estimated IDPs should be considered as approximate measures since under a constant compressive force, IDP varies with time and

location in the nucleus pulposus (Schmidt & Shirazi-Adl, 2018). Although IAP is proportional to muscle activities (Cresswell, Grundström, & Thorstensson, 1992; McGill & Sharratt, 1990; Tayashiki, Takai, Maeo, & Kanehisa, 2016), it was overlooked in most analyses while taking it into account unloads the spine and alters muscle activity predictions of abdominal muscles (Arjmand & Shirazi-Adl, 2006b; Stokes, Gardner-Morse, & Henry, 2010). Vertebral rotations (T11 and S1) were estimated (in measurements whose data were used to drive current model studies) from skin markers; although skin measurements explain >85% of variance in forward flexion, they are less accurate during asymmetric tasks (explaining ~59% of data) (Mörl & Blickhan, 2006). Passive properties of the ligamentous spine were scaled based on geometric parameters and beam theory (which is accurate in comparison with detailed FE models (Natarajan & Andersson, 1999)) while material properties were not scaled. Although some studies have highlighted the role of facia on spine biomechanics (Gracovetsky, 2008; Macintosh, Bogduk, & Gracovetsky, 1987), lumbar facia was not taken into account due to the paucity of the literature on its anatomy and material properties as well as inconsistent findings on the role of facia (Ranger, Newell, Grant, Barker, & Pearcy, 2017).

9.3 Validation

Validating a musculoskeletal model should be performed at different levels; all constituents of the model (muscle architecture, passive spine and scaling algorithm) as well as overall responses need to be included. In the upgraded model, the muscle architecture (insertion points and PCSAs) was based on detailed cadaver studies (Delp et al., 2001; Phillips et al., 2008; Stokes & Gardner-Morse, 1999), Appendix A, and was subsequently scaled based on available imaging datasets, Appendix B (Anderson et al., 2012). Nonlinear passive properties of the ligamentous spine were based on a validated detailed FE model of the lumbar spine, Figure 3.1 (Dreischarf et al., 2014; Shirazi-Adl, 1994a, 2006).Simulation of the motion segments as nonlinear shear deformable beams accurately replicated mechanical responses of the detailed model, Figure 6.2 and Figure 6.3 (Ghezelbash et al., 2018b). Scaling passive properties based on the conventional beam theory (Figure 7.2) yields

satisfactory results in comparison with detailed FE results (Natarajan & Andersson, 1999), Figure 9.1.

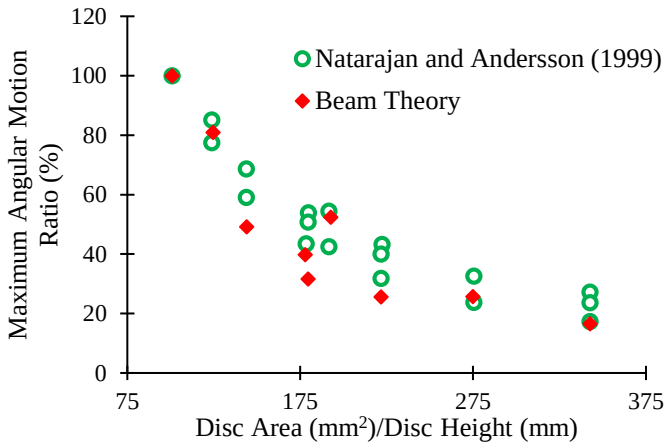

Figure 9.1 Results of the beam theory against those of an FE model of L3-L4 motion segment (Natarajan & Andersson, 1999) for different values of disc height (5.5, 8.8 and 10.5 mm) and disc area (1060, 1512 and 1885 mm^2).

Estimated subject-specific IDPs had satisfactory agreement with available *in vivo* measurements (Sato et al., 1999; Takahashi et al., 2006; Wilke et al., 2001) during various symmetric and asymmetric activities (Figure 3.5 and Figure 8.4). Since IDP is proportional to compression (Brinckmann & Grootenboer, 1991; Dreischarf et al., 2015b), and since individualized IDPs were computed in accordance with participants' anthropometric parameters (BH, BW, age, sex and disc area), the agreement between measurements and estimations demonstrates the accuracy of calculated spinal loads and the scaling algorithm employed in this work. It is to be noted that *in vivo* IDP measurements during asymmetric lifting tasks are very limited.

Qualitative comparison between estimated muscle activities and EMG measurements shows the accuracy of active-passive responses as well as the muscle force estimation algorithm. Flexion-relaxation is observed in back muscles during larger forward flexion when passive responses of muscles and ligamentous spine alone counterbalance the required external moment with no need for muscle activation; also, passive muscle forces and joint positioning (Figure 6.6) substantially

affect the flexion-relaxation point; therefore, accurate prediction of this phenomenon demonstrates the validity of force estimation algorithm and passive responses, Figure 3.6. The model accurately predicted muscle activities during MVE tasks in flexion and extension (Figure 3.7 and Figure 7.4) as well as various symmetric lifting tasks (Figure 8.5 and Figure 8.6). During asymmetric lifting activities, the agreement was moderate (back muscles; Figure 8.5) to weak (abdominal muscles; Figure 8.6). This can be due to intrinsic problems of surface EMG especially on large muscles (e.g., contamination, cross-talk, uncertainty in EMG-force relation (De Luca et al., 2010; Türker, 1993)) as well as modeling limitations.

9.4 Interpretations

9.4.1 Personalized Differences

Evaluating the effects of personalized differences on spine biomechanics requires an accurate subject-specific model along with a comprehensive scaling algorithm. The full factorial sensitivity analysis on the individualized musculoskeletal model showed that BW contributed 99% to compression and 96% to shear spinal loads while the effects of BH, sex and age remained relatively small (Figure 4.7 and Table 4.2). At identical BH, BW and waist circumference, females had slightly greater spinal loads (5% in compression; 9% in shear), but in general, females have smaller BW in comparison with males and therefore smaller spinal loads. The contribution of age alone to spinal loads remained less than 5%, but if the effects of ageing on BW, BH, waist circumference and posture are taken into account, age (or ageing) could substantially influence spinal loads (Ghezelbash, Shiraz-Adl, Plamondon, & Arjmand, 2018c). Due to ageing (21 years vs 70 years), median compression at L5-S1 increased by 28% (613 N vs 785 N at flexion<50^o) in females and by 21% (810 N vs 979 N at flexion<30^o) in males (Ghezelbash et al., 2018c).

Obesity has been identified as one of the risk factors of back pain (Leboeuf–Yde et al., 1999; Shiri et al., 2009). Despite the prevalence of 27% in Canada and Quebec (Statistics Canada, 2019) and the estimated rise in the coming 20 years (Bancej et al., 2015), underlying biomechanical roots of obesity-associated back pain remain still unknown. Obesity significantly affects spinal loads; for

instance, L4-L5 compression increased by 16% (2820 N vs 3350 N) in forward flexion without a hand-load when at identical BH, BMI increased from 31 kg/m^2 to 39 kg/m^2.

Apart from BMI, obesity shape or the distribution of adipose tissue along the body influences spinal loads. To explain different obesity shapes, various qualitative descriptions (apple- and pear-shaped or android and gynoid) as well as quantitative parameters (e.g., waist to hip ratio and waist circumference) have been proposed. Unlike existing measures, the proposed method (section 5.2.1) of reconstructing 3 distinct obesity shapes (corresponding to minimum, mean and maximum waist circumference) not only quantitatively describes various obesity types but also accounts for the distribution of adipose tissue along the body (including calves, thighs, waist and arms), Table 5.1 and Figure 5.2. At identical BH and BW, greater waist circumference (apple shaped) increased spinal loads to the extent of gaining 20 kg additional BW and the risk of vertebral fatigue fracture up to 7 times.

9.4.2 Joint Simulation

Accurate simulation of the passive ligamentous spine (as a primary component of a trunk musculoskeletal model) is of great importance. Detailed FE models of the spine accurately capture time-dependent, complex and nonlinear responses of the spine. Due to the computational burden of detailed FE models, however, simplified models (i.e., spherical joints/beams with linear/nonlinear passive properties) are commonly used in the trunk musculoskeletal models. Unlike beam elements, spherical joints overlooked translational degrees of freedom; therefore, such elements did not accurately estimate kinematics of the lumbar spine particularly in the cranial-caudal direction, Figure 6.2 and Figure 6.3. Shear deformable beams with nonlinear passive properties and spherical joints with nonlinear rotational springs accurately predicted spinal loads while linear beams/spherical joints yielded valid results only in small to moderate flexion angles ($<40^o$), Figure 6.4 and Figure 6.5. Ligamentous spine (as a passive element) partially counterbalances external loads, and in the absence of passive elements, active components (muscles) should carry the entire external loads, so the musculoskeletal model without passive properties (i.e., frictionless spherical joints and no rotational springs) overestimated compression

force (by 32%) and shear force (by 63%) (Figure 6.4 and Figure 6.5). Passive properties of ligamentous spine (e.g., moment-rotation) should therefore be properly incorporated in trunk musculoskeletal models.

Anterior-posterior positioning of simplified joints markedly affected spinal loads and active/passive muscle forces. Shifting simplified elements posteriorly (8 mm) increased spinal loads by ~20% (compression and shear) while an anterior shift (2 mm) decreased spinal loads by 10% and 18% in compression and shear, respectively. By evaluating muscle moment arms at disc centers, offsetting simplified joint models posteriorly decreases moment arms of back muscles, so the activity of back muscles (agonist) should increase as a result to compensate the moment arm reduction. In addition, this increases net external moments by increasing moment arms of external forces (gravity and loads in hands), which further increases the activity of back muscles and consequently spinal loads. Reverse trends are computed when the joint model shifts anteriorly instead. Joint positioning alters spine kinematics, muscle lengths and hence passive muscle forces; moving joints in the posterior direction reduced passive muscle forces while increasing their active components delaying thus the flexion-relaxation. Simplified elements should be located in -2 to +4 mm (+: posterior) range from the disc center for accurate predictions of spinal loads and active/passive muscle forces.

To accurately capture spine kinematics, one can place spherical joints at their instantaneous center of rotation based on experiments (Pearcy & Bogduk, 1988; Yoshioka, Tsuji, Hirano, & Sainoh, 1990). Though addressing kinematic issue, such an approach can adversely affect kinetics. For example, some experiments estimated instantaneous center of rotation at 12 mm posterior to the disc center during lifting (Liu et al., 2016), but such joint positioning substantially increases spinal loads (Figure 6.4) if passive properties are not modified accordingly. To discard moment-rotation passive properties of joints, spherical joints can be placed at corresponding centers of reaction (i.e., a point in which the joint resultant moment vector disappears, Figure 6.7); however, the location of the centers of reaction at different levels is not known before the analysis and muscle force calculation.

9.4.3 Regression Equations

Existing regression equations and lifting analysis tools either entirely neglect the effects of personal parameters (e.g., BW, BH) on spinal loads (Arjmand et al., 2011; Arjmand et al., 2012; McGill, 1992) or use heuristic and simplistic approaches to take account of those factors (Damsgaard et al., 2006; Delp et al., 2007; Rasmussen et al., 2005). The performance of existing lifting analysis tools, furthermore, have not been assessed by comparing both estimated muscle activities and spinal loads with measured EMGs and IDPs (Rajaee et al., 2015). Proposed regression equations, on the other hand, have addressed foregoing shortcomings by taking into account effects of anthropometric parameters based on a physiological approach (imaging datasets and biomechanical principles (Ghezelbash et al., 2016b) (Appendix C)), and by evaluating the performance of the model in comparison with EMG (Figure 8.5 and Figure 8.6) and IDP (Figure 8.4) measurements.

Apart from BH and sex, which slightly affected spinal loads, other inputs (i.e., BW, asymmetry angle, flexion angle as well as hand-held mass and moment arm) markedly affected spinal compression (Figure 8.2) and shear (Figure 8.3) forces. Existing regression equations neglect the effects of anthropometric factors and posture asymmetry (Arjmand et al., 2011; Arjmand et al., 2012; Merryweather et al., 2008) although these factors can substantially alter spinal loads. For example, changing BW from 70 kg to 90 kg increased L5-S1 compression and shear forces by 26% (1534 N versus 1936 N) and 25% (543 N versus 681 N) (sex=male; BH=175 cm; M=5 kg; A=0^o; F=50^o; D=0 cm), and at BW=75 kg, F=30^o, M=10 kg and D=0 cm, changing asymmetry angle from 0^o to 60^o increased compression by 63% (1501 N vs 2454 N) and shear by 66% (539 N vs 897 N) at L5-S1 level. It should be noted that task asymmetry increasingly augments spinal loads; sagittally symmetric tasks have thus smaller spinal loads in comparison with asymmetric ones and as a results lower risk of injury.

Spinal injury (particularly to the disc) due to a cyclic loading or overloading can initiate disc degeneration and back pain (Adams et al., 2000; Adams & Roughley, 2006; Iatridis & Gwynn, 2004; Vergroesen et al., 2015a). Biomechanical safety assessment of a lifting task requires subject-specific estimation of spinal loads, which can be performed using proposed regression equations.

NIOSH considers tasks with a spinal compression <3400 N to be biomechanically safe (Waters et al., 1993). Based on NIOSH criterion, heavier individuals have thus greater risk of injury although some epidemiological studies suggest otherwise since a greater BW may also play a protective role (Videman, Gibbons, Kaprio, & Battié, 2010). This discrepancy may be due to the fact that NIOSH criterion overlooks likely differences in individualized damage tolerance thresholds. Furthermore, cyclic loads much smaller than a tissue ultimate strength can cause structural damage and failure (Green, Adams, & Dolan, 1993b; Iatridis, MacLean, & Ryan, 2005). Predicting cycles to failure based on estimated spinal loads and existing failure methods (Brinckmann, Biggemann, & Hilweg, 1989; Gallagher & Schall, 2016; Gallagher, Sesek, Schall Jr, & Huangfu, 2017; Huber et al., 2016a) provides a more adequate quantitative measure of accumulated damage due to fatigue. It is nevertheless to be noted that the existing fatigue-failure risk assessment tools are based on in vitro studies and neglect the healing ability of the tissue particularly in vertebrae which can partly or totally reverse damage accumulation.

CHAPTER 10 CONCLUSION AND RECOMMANDATIONS

An existing KD-FE musculoskeletal model of the trunk has been improved by updating the muscle architecture, adding an additional deformable level (T11-T12) and introducing a novel and physiological scaling algorithm to investigate subject-specific spine biomechanics. The scaling algorithm adjusts muscle architecture, spine geometry, gravity loads and passive properties of spine by using biomechanical principals and reported imaging datasets. The performance of the individualized model was evaluated by comparing estimated IDPs and muscle activities with available *in vivo* measurements during various symmetric and asymmetric tasks. Estimated muscle activities (in symmetric lifting and MVE tasks) and IDPs had satisfactory agreement with measurements while in asymmetric lifting and MVE tasks, the agreement between reported EMGs (Ghezelbash et al., 2018a; Ghezelbash et al., 2019) and estimations were weak (abdominal muscles) to moderate (back muscles). BW and obesity substantially affected spinal loads while the effects of BH, sex and age remained relatively small. At identical BH and BW, changes in the distribution of adipose tissue along the body substantially affected spinal loads (to the extent of gaining 20 kg additional BW in an example) and the risk of vertebral fatigue fracture (up to ~7 times). Although at identical BW, BH and waist circumference, effects of sex and age on spinal loads were small, when concurrent changes in BW, BH and waist circumference due to ageing and likely associations between sex and foregoing parameters are taken into account, ageing and sex could also significantly alter spinal loads (Ghezelbash et al., 2018c). Proposed subject-specific regression equations accurately predicted spinal loads during various symmetric and asymmetric tasks and can be used for personalized biomechanical risk assessment of a lifting task. The accuracy and validity of using simplified (i.e., linear/nonlinear beams/spherical joints) elements and their anterior-posterior positioning in estimating kinematics of the ligamentous spine, muscle forces and spinal loads were investigated. Simplified joint models with nonlinear passive properties should be located in -2 to +4 mm (+: posterior) range from the disc centers for accurate predictions of spinal loads and active/passive muscle forces.

10.1 Future Works

Future works may address existing shortcomings:

- The proposed scaling algorithm can be employed to scale the upgraded musculoskeletal model based on medical images (e.g., CT scan, MRI). This approach addresses some limitations of the current study such as variations in spinal shape and muscle architecture among individuals, which cannot be explained by BW, BH, age and sex.
- Diffusion imaging tensor techniques can be employed to estimate material properties of tissues (collagen fibers orientation, collagen content and porosity) and to realistically personalize both geometrical parameters and material properties.
- Developing a hybrid musculoskeletal model of trunk by incorporating a detailed FE model of the lumbar spine along with a subject-specific spine geometry and muscle architecture to resolve the issue of using simplified models as intervertebral joints and their positioning. This modeling approach provides us with new outputs (e.g., strain/stress field in discs, ligaments, facet forces) and paves the way toward musculoskeletal simulations of surgical interventions and the implementation of complex failure constitutive models.
- Subject-specific criteria may be developed to biomechanically assess the personalized risk of injury due to overloading and cyclic loading.
- Muscles are 3D objects, and muscle activity varies within the muscle volume; however, musculoskeletal models consider muscles as 1D elements (vectors) and assume that muscle activity is constant throughout the muscle. The accuracy of using 1D elements instead of 3D elements is still unknown and require investigations.
- Apart from the above-mentioned technical issues, the fundamental question is whether biomechanics alone substantially contributes to the disc degeneration and pain or not. Multiple epidemiological studies (particularly on twins) have found that genetics is the main risk factor for the disc degeneration while biomechanics and other factors play a minor role (Wang & Battié, 2014). The role of mechanical environment in tissue damage and inflammatory response as well as subsequent cascade of events require further investigations.

REFERENCES

Adams, M. A. (2015). Intervertebral Disc Tissues *Mechanical Properties of Aging Soft Tissues* (pp. 7-35): Springer.

Adams, M. A., Freeman, B. J., Morrison, H. P., Nelson, I. W., & Dolan, P. (2000). Mechanical initiation of intervertebral disc degeneration. *Spine, 25*(13), 1625-1636.

Adams, M. A., Lama, P., Zehra, U., & Dolan, P. (2015). Why do some intervertebral discs degenerate, when others (in the same spine) do not? *Clin Anat, 28*(2), 195-204.

Adams, M. A., & Roughley, P. J. (2006). What is intervertebral disc degeneration, and what causes it? *Spine, 31*(18), 2151-2161.

Alkalay, R. (2002). The material and mechanical properties of the healthy and degenerated intervertebral disc *Integrated Biomaterials Science* (pp. 403-424): Springer.

Allin, L. J., Wu, X., Nussbaum, M. A., & Madigan, M. L. (2016). Falls resulting from a laboratory-induced slip occur at a higher rate among individuals who are obese. *J Biomech, 49*(5), 678-683.

Allison, D., Thomas, O., & Zhang, C. (2013). Systems and methods for estimating body composition. U.S. Patent: US 13/992,070.

Amonoo-Kuofi, U. (1992). Changes in the lumbosacral angle, sacral inclination and the curvature of the lumbar spine during aging. *Cells Tissues Organs, 145*(4), 373-377.

Anderson, D. E., D'Agostino, J. M., Bruno, A. G., Manoharan, R. K., & Bouxsein, M. L. (2012). Regressions for estimating muscle parameters in the thoracic and lumbar trunk for use in musculoskeletal modeling. *J Biomech, 45*(1), 66-75.

Antoniou, J., Steffen, T., Nelson, F., Winterbottom, N., Hollander, A. P., Poole, R. A., . . . Alini, M. (1996). The human lumbar intervertebral disc: evidence for changes in the biosynthesis and denaturation of the extracellular matrix with growth, maturation, ageing, and degeneration. *Journal of Clinical Investigation, 98*(4), 996.

Argoubi, M., & Shirazi-Adl, A. (1996). Poroelastic creep response analysis of a lumbar motion segment in compression. *Journal of biomechanics, 29*(10), 1331-1339.

Arja, H., Tiina, K., Pt, T. U., & Jari, Y. (2003). Trunk muscle strength in flexion, extension, and axial rotation in patients managed with lumbar disc herniation surgery and in healthy control subjects. *Spine, 28*(10), 1068-1073.

Arjmand, N., Amini, M., Shirazi-Adl, A., Plamondon, A., & Parnianpour, M. (2015). Revised NIOSH Lifting Equation May generate spine loads exceeding recommended limits. *International Journal of Industrial Ergonomics, 47*, 1-8.

Arjmand, N., Ekrami, O., Shirazi-Adl, A., Plamondon, A., & Parnianpour, M. (2013). Relative performances of artificial neural network and regression mapping tools in evaluation of spinal loads and muscle forces during static lifting. *Journal of biomechanics, 46*(8), 1454-1462.

Arjmand, N., Gagnon, D., Plamondon, A., Shirazi-Adl, A., & Lariviere, C. (2009). Comparison of trunk muscle forces and spinal loads estimated by two biomechanical models. *Clin Biomech, 24*(7), 533-541.

Arjmand, N., Gagnon, D., Plamondon, A., Shirazi-Adl, A., & Lariviere, C. (2010). A comparative study of two trunk biomechanical models under symmetric and asymmetric loadings. *J Biomech, 43*(3), 485-491.

Arjmand, N., Plamondon, A., Shirazi-Adl, A., Lariviere, C., & Parnianpour, M. (2011). Predictive equations to estimate spinal loads in symmetric lifting tasks. *J Biomech, 44*(1), 84-91.

Arjmand, N., Plamondon, A., Shirazi-Adl, A., Parnianpour, M., & Larivière, C. (2012). Predictive equations for lumbar spine loads in load-dependent asymmetric one-and two-handed lifting activities. *Clinical Biomechanics, 27*(6), 537-544.

Arjmand, N., & Shirazi-Adl, A. (2005). Biomechanics of changes in lumbar posture in static lifting. *Spine, 30*(23), 2637-2648.

Arjmand, N., & Shirazi-Adl, A. (2006a). Model and in vivo studies on human trunk load partitioning and stability in isometric forward flexions. *J Biomech, 39*(3), 510-521.

Arjmand, N., & Shirazi-Adl, A. (2006b). Role of intra-abdominal pressure in the unloading and stabilization of the human spine during static lifting tasks. *Eur Spine J, 15*(8), 1265-1275.

Arjmand, N., & Shirazi-Adl, A. (2006c). Sensitivity of kinematics-based model predictions to optimization criteria in static lifting tasks. *Med Eng Phys, 28*(6), 504-514.

Arjmand, N., Shirazi-Adl, A., & Bazrgari, B. (2006). Wrapping of trunk thoracic extensor muscles influences muscle forces and spinal loads in lifting tasks. *Clin Biomech, 21*(7), 668-675.

Arjmand, N., Shirazi-Adl, A., & Parnianpour, M. (2007). Trunk biomechanical models based on equilibrium at a single-level violate equilibrium at other levels. *Eur Spine J, 16*(5), 701-709.

Arjmand, N., Shirazi-Adl, A., & Parnianpour, M. (2008a). Relative efficiency of abdominal muscles in spine stability. *Comput Method Biomec, 11*(3), 291-299.

Arjmand, N., Shirazi-Adl, A., & Parnianpour, M. (2008b). Trunk biomechanics during maximum isometric axial torque exertions in upright standing. *Clin Biomech, 23*(8), 969-978.

Arshad, R., Zander, T., Dreischarf, M., & Schmidt, H. (2016). Influence of lumbar spine rhythms and intra-abdominal pressure on spinal loads and trunk muscle forces during upper body inclination. *Medical Engineering & Physics, 38*(4), 333-338.

Azen, R., & Budescu, D. V. (2003). The dominance analysis approach for comparing predictors in multiple regression. *Psychological methods, 8*(2), 129.

Azghani, M., Farahmand, F., Meghdari, A., Vossoughi, G., & Parnianpour, M. (2009). Design and evaluation of a novel triaxial isometric trunk muscle strength measurement system.

Proceedings of the Institution of Mechanical Engineers, Part H: Journal of Engineering in Medicine, 223(6), 755-766.

Bae, J. S., Jang, J.-S., Lee, S.-H., & Kim, J. U. (2012). A comparison study on the change in lumbar lordosis when standing, sitting on a chair, and sitting on the floor in normal individuals. *Journal of Korean Neurosurgical Society, 51*(1), 20-23.

Bancej, C., Jayabalasingham, B., Wall, R., Rao, D., Do, M., De Groh, M., & Jayaraman, G. (2015). Trends and projections of obesity among Canadians. *Health promotion and chronic disease prevention in Canada: research, policy and practice, 35*(7), 109.

Bassani, T., Stucovitz, E., Qian, Z., Briguglio, M., & Galbusera, F. (2017). Validation of the AnyBody full body musculoskeletal model in computing lumbar spine loads at L4L5 level. *Journal of biomechanics, 58*, 89-96.

Bazrgari, B. (2008). *Biodynamic of the human spine.* (PhD), École Polytechnique de Montréal, Canada (Montreal).

Bazrgari, B., & Shirazi-Adl, A. (2007). Spinal stability and role of passive stiffness in dynamic squat and stoop lifts. *Comput Method Biomec, 10*(5), 351-360.

Bazrgari, B., Shirazi-Adl, A., & Kasra, M. (2008). Computation of trunk muscle forces, spinal loads and stability in whole-body vibration. *Journal of Sound and Vibration, 318*(4), 1334-1347.

Bazrgari, B., Shirazi-Adl, A., & Parnianpour, M. (2009). Transient analysis of trunk response in sudden release loading using kinematics-driven finite element model. *Clin Biomech, 24*(4), 341-347.

Bean, J. C., Chaffin, D. B., & Schultz, A. B. (1988). Biomechanical model calculation of muscle contraction forces: a double linear programming method. *Journal of biomechanics, 21*(1), 59-66.

Been, E., & Kalichman, L. (2014). Lumbar lordosis. *Spine J, 14*(1), 87-97.

Behrbalk, E., Uri, O., Parks, R. M., Musson, R., Soh, R. C. C., & Boszczyk, B. M. (2013). Fusion and subsidence rate of stand alone anterior lumbar interbody fusion using PEEK cage with recombinant human bone morphogenetic protein-2. *Eur Spine J, 22*(12), 2869-2875.

Bergmark, A. (1989). Stability of the lumbar spine: a study in mechanical engineering. *Acta Orthop Scand Suppl, 60*(sup230), 1-54. doi: 10.3109/17453678909154177

Berrigan, F., Simoneau, M., Tremblay, A., Hue, O., & Teasdale, N. (2006). Influence of obesity on accurate and rapid arm movement performed from a standing posture. *Int J Obesity, 30*(12), 1750-1757.

Berthet-Colominas, C., Miller, A., Herbage, D., Ronziere, M.-C., & Tocchetti, D. (1982). Structural studies of collagen fibres from intervertebral disc. *Biochimica et Biophysica Acta (BBA)-Protein Structure and Molecular Enzymology, 706*(1), 50-64.

Bielby, W. T., & Baron, J. N. (1986). Men and women at work: Sex segregation and statistical discrimination. *Am J Sociology*, 759-799.

Black, M. (2015). BMI Visualizer. from http://bmijs.is.tuebingen.mpg.de/

Blemker, S. S., & Delp, S. L. (2005). Three-dimensional representation of complex muscle architectures and geometries. *Ann Biomed Eng, 33*(5), 661-673.

Boocock, M. G., Mawston, G. A., & Taylor, S. (2015). Age-related differences do affect postural kinematics and joint kinetics during repetitive lifting. *Clin Biomech, 30*(2), 136-143.

Bottasso, C. L., Prilutsky, B. I., Croce, A., Imberti, E., & Sartirana, S. (2006). A numerical procedure for inferring from experimental data the optimization cost functions using a multibody model of the neuro-musculoskeletal system. *Multibody System Dynamics, 16*(2), 123-154.

Bovenzi, M., Schust, M., Menzel, G., Hofmann, J., & Hinz, B. (2015). A cohort study of sciatic pain and measures of internal spinal load in professional drivers. *Ergonomics, 58*(7), 1088-1102.

Brasiliense, L. B., Lazaro, B. C., Reyes, P. M., Dogan, S., Theodore, N., & Crawford, N. R. (2011). Biomechanical contribution of the rib cage to thoracic stability. *Spine, 36*(26), E1686-E1693.

Brinckmann, P., Biggemann, M., & Hilweg, D. (1988). Fatigue fracture of human lumbar vertebrae. *Clin Biomech, 3*, i-S23. doi: 10.1016/S0268-0033(88)80001-9

Brinckmann, P., Biggemann, M., & Hilweg, D. (1989). Prediction of the compressive strength of human lumbar vertebrae. *Clinical Biomechanics, 4*, iii-27.

Brinckmann, P., & Grootenboer, H. (1991). Change of disc height, radial disc bulge, and intradiscal pressure from discectomy. An in vitro investigation on human lumbar discs. *Spine, 16*(6), 641-646.

Brown, S. H., & Potvin, J. R. (2005). Constraining spine stability levels in an optimization model leads to the prediction of trunk muscle cocontraction and improved spine compression force estimates. *Journal of biomechanics, 38*(4), 745-754.

Brown, S. H., Ward, S. R., Cook, M. S., & Lieber, R. L. (2011). Architectural analysis of human abdominal wall muscles: implications for mechanical function. *Spine, 36*(5), 355.

Bruno, A. G., Anderson, D. E., D'Agostino, J., & Bouxsein, M. L. (2012). The effect of thoracic kyphosis and sagittal plane alignment on vertebral compressive loading. *J Bone Miner Res, 27*(10), 2144-2151.

Bruno, A. G., Bouxsein, M. L., & Anderson, D. E. (2015). Development and validation of a musculoskeletal model of the fully articulated thoracolumbar spine and rib cage. *Journal of biomechanical engineering, 137*(8), 081003.

Bruno, A. G., Broe, K. E., Zhang, X., Samelson, E. J., Meng, C. A., Manoharan, R., . . . Bouxsein, M. L. (2014). Vertebral size, bone density, and strength in men and women matched for age and areal spine BMD. *J Bone Miner Res, 29*(3), 562-569. doi: 10.1002/jbmr.2067

Bruno, A. G., Mokhtarzadeh, H., Allaire, B. T., Velie, K. R., De Paolis Kaluza, M., Anderson, D. E., & Bouxsein, M. L. (2017). Incorporation of CT-based measurements of trunk anatomy into subject-specific musculoskeletal models of the spine influences vertebral loading predictions. *Journal of orthopaedic research*.

Buchanan, T. (1995). Evidence that maximum muscle stress is not a constant: differences in specific tension in elbow flexors and extensors. *Medical Engineering & Physics, 17*(7), 529-536.

Burkhart, K. A., Bruno, A. G., Bouxsein, M. L., Bean, J. F., & Anderson, D. E. (2017). Estimating Apparent Maximum Muscle Stress of Trunk Extensor Muscles in Older Adults using Subject-Specific Musculoskeletal Models. *Journal of orthopaedic research*.

Cappetti, N., Naddeo, A., Naddeo, F., & Solitro, G. (2015). Finite elements/Taguchi method based procedure for the identification of the geometrical parameters significantly affecting the biomechanical behavior of a lumbar disc. *Computer methods in biomechanics and biomedical engineering*, 1-8.

Cassinelli, E. H., Hall, R. A., & Kang, J. D. (2001). Biochemistry of intervertebral disc degeneration and the potential for gene therapy applications. *The Spine Journal, 1*(3), 205-214.

Chaffin, D. B. (1969). A computerized biomechanical model—development of and use in studying gross body actions. *Journal of biomechanics, 2*(4), 429-441.

Chaffin, D. B., Redfern, M. S., Erig, M., & Goldstein, S. A. (1990). Lumbar muscle size and locations from CT scans of 96 women of age 40 to 63 years. *Clin Biomech, 5*(1), 9-16.

Chambers, A. J., Sukits, A. L., McCrory, J. L., & Cham, R. (2010). The effect of obesity and gender on body segment parameters in older adults. *Clin Biomech, 25*(2), 131-136.

Cheung, K. M., Karppinen, J., Chan, D., Ho, D. W., Song, Y.-Q., Sham, P., . . . Luk, K. D. (2009). Prevalence and pattern of lumbar magnetic resonance imaging changes in a population study of one thousand forty-three individuals. *Spine, 34*(9), 934-940.

Cholewicki, J., & McGill, S. M. (1994). EMG assisted optimization: a hybrid approach for estimating muscle forces in an indeterminate biomechanical model. *Journal of biomechanics, 27*(10), 1287-1289.

Cholewicki, J., & McGill, S. M. (1996). Mechanical stability of the in vivo lumbar spine: implications for injury and chronic low back pain. *Clin Biomech, 11*(1), 1-15.

Cholewicki, J., McGill, S. M., & Norman, R. W. (1995). Comparison of muscle forces and joint load from an optimization and EMG assisted lumbar spine model: towards development of a hybrid approach. *Journal of biomechanics, 28*(3), 321-331.

Cholewicki, J., van Dieën, J., Lee, A. S., & Reeves, N. P. (2011). A comparison of a maximum exertion method and a model-based, sub-maximum exertion method for normalizing trunk EMG. *Journal of Electromyography and Kinesiology, 21*(5), 767-773.

Christophy, M., Curtin, M., Senan, N. A. F., Lotz, J. C., & O'Reilly, O. M. (2013). On the modeling of the intervertebral joint in multibody models for the spine. *Multibody System Dynamics, 30*(4), 413-432.

Christophy, M., Senan, N. A. F., Lotz, J. C., & O'Reilly, O. M. (2012). A musculoskeletal model for the lumbar spine. *Biomec Model Mechan, 11*(1-2), 19-34.

Coenen, P., Kingma, I., Boot, C. R., Twisk, J. W., Bongers, P. M., & van Dieën, J. H. (2013). Cumulative low back load at work as a risk factor of low back pain: a prospective cohort study. *J Occup Rehabil, 23*(1), 11-18.

Coeuret-Pellicer, M., Descatha, A., Leclerc, A., & Zins, M. (2010). Are tall people at higher risk of low back pain surgery? A discussion on the results of a multipurpose cohort. *Arthrit Care Res, 62*(1), 125-127.

Corbeil, P., Simoneau, M., Rancourt, D., Tremblay, A., & Teasdale, N. (2001). Increased risk for falling associated with obesity: mathematical modeling of postural control. *IEEE Trans Neural Sys Rehabil Eng, 9*(2), 126-136.

Coyte, P. C., Asche, C. V., Croxford, R., & Chan, B. (1998). The economic cost of musculoskeletal disorders in Canada. *Arthritis & Rheumatism: Official Journal of the American College of Rheumatology, 11*(5), 315-325.

Crawford, R. P., Cann, C. E., & Keaveny, T. M. (2003). Finite element models predict in vitro vertebral body compressive strength better than quantitative computed tomography. *Bone, 33*(4), 744-750.

Cresswell, A., Grundström, H., & Thorstensson, A. (1992). Observations on intra-abdominal pressure and patterns of abdominal intra-muscular activity in man. *Acta Physiologica Scandinavica, 144*(4), 409-418.

Crisco, J., Panjabi, M., Yamamoto, I., & Oxland, T. (1992). Euler stability of the human ligamentous lumbar spine. Part II: Experiment. *Clinical Biomechanics, 7*(1), 27-32.

Croft, P. R., & Rigby, A. S. (1994). Socioeconomic influences on back problems in the community in Britain. *J Epidemiol Commun H, 48*(2), 166-170.

Crowninshield, R. D., & Brand, R. A. (1981). A physiologically based criterion of muscle force prediction in locomotion. *Journal of biomechanics, 14*(11), 793-801.

da Costa, B. R., & Vieira, E. R. (2010). Risk factors for work-related musculoskeletal disorders: a systematic review of recent longitudinal studies. *Am J Ind Med, 53*(3), 285-323.

Dam, E. B., Koch, M., & Lillholm, M. (1998). *Quaternions, interpolation and animation* (Vol. 2): Citeseer.

Damsgaard, M., Rasmussen, J., Christensen, S. T., Surma, E., & de Zee, M. (2006). Analysis of musculoskeletal systems in the AnyBody Modeling System. *Simul Model Pract Th, 14*(8), 1100-1111.

Dankaerts, W., O'Sullivan, P. B., Burnett, A. F., Straker, L. M., & Danneels, L. A. (2004). Reliability of EMG measurements for trunk muscles during maximal and sub-maximal voluntary isometric contractions in healthy controls and CLBP patients. *Journal of Electromyography and Kinesiology, 14*(3), 333-342.

Dar, F. H., Meakin, J. R., & Aspden, R. M. (2002). Statistical methods in finite element analysis. *J Biomech, 35*(9), 1155-1161.

Davis, J., Kaufman, K. R., & Lieber, R. L. (2003). Correlation between active and passive isometric force and intramuscular pressure in the isolated rabbit tibialis anterior muscle. *J Biomech, 36*(4), 505-512.

De Carvalho, D. E., Soave, D., Ross, K., & Callaghan, J. P. (2010). Lumbar spine and pelvic posture between standing and sitting: a radiologic investigation including reliability and repeatability of the lumbar lordosis measure. *Journal of manipulative and physiological therapeutics, 33*(1), 48-55.

De Foa, J. L., Forrest, W., & Biedermann, H. (1989). Muscle fibre direction of longissimus, iliocostalis and multifidus: landmark-derived reference lines. *J Anat, 163*, 243.

De Leva, P. (1996). Adjustments to Zatsiorsky-Seluyanov's segment inertia parameters. *J Biomech, 29*(9), 1223-1230.

De Luca, C. J., Gilmore, L. D., Kuznetsov, M., & Roy, S. H. (2010). Filtering the surface EMG signal: Movement artifact and baseline noise contamination. *Journal of biomechanics, 43*(8), 1573-1579.

De Zee, M., Hansen, L., Wong, C., Rasmussen, J., & Simonsen, E. B. (2007). A generic detailed rigid-body lumbar spine model. *J Biomech, 40*(6), 1219-1227.

Delp, S. L., Anderson, F. C., Arnold, A. S., Loan, P., Habib, A., John, C. T., . . . Thelen, D. G. (2007). OpenSim: open-source software to create and analyze dynamic simulations of movement. *IEEE T Bio-Med Eng, 54*(11), 1940-1950.

Delp, S. L., Suryanarayanan, S., Murray, W. M., Uhlir, J., & Triolo, R. J. (2001). Architecture of the rectus abdominis, quadratus lumborum, and erector spinae. *J Biomech, 34*(3), 371-375.

Demoulin, C., Huijnen, I. P., Somville, P.-R., Grosdent, S., Salamun, I., Crielaard, J.-M., . . . Volders, S. (2013). Relationship between different measures of pain-related fear and

physical capacity of the spine in patients with chronic low back pain. *The Spine Journal, 13*(9), 1039-1047.

Dempsey, P. G., & Fathallah, F. A. (1999). Application issues and theoretical concerns regarding the 1991 NIOSH equation asymmetry multiplier. *International Journal of Industrial Ergonomics, 23*(3), 181-191.

DePalma, M. J., Ketchum, J. M., & Saullo, T. (2011). What is the source of chronic low back pain and does age play a role? *Pain Med, 12*(2), 224-233.

DePalma, M. J., Ketchum, J. M., & Saullo, T. R. (2012). Multivariable analyses of the relationships between age, gender, and body mass index and the source of chronic low back pain. *Pain Med, 13*(4), 498-506.

Deyo, R. A., & Bass, J. E. (1989). Lifestyle and low-back pain: the influence of smoking and obesity. *Spine, 14*(5), 501-506.

Deyo, R. A., Cherkin, D., Conrad, D., & Volinn, E. (1991). Cost, controversy, crisis: low back pain and the health of the public. *Annu Rev Publ Health, 12*(1), 141-156.

Dimitriadis, A., Papagelopoulos, P., Smith, F., Mavrogenis, A., Pope, M., Karantanas, A., . . . Katonis, P. (2011). Intervertebral disc changes after 1 h of running: a study on athletes. *J Int Med Res, 39*(2), 569-579.

Dionne, C. E., Dunn, K. M., & Croft, P. R. (2006). Does back pain prevalence really decrease with increasing age? A systematic review. *Age Ageing, 35*(3), 229-234.

Dreischarf, M., Albiol, L., Zander, T., Arshad, R., Graichen, F., Bergmann, G., . . . Rohlmann, A. (2015a). In vivo implant forces acting on a vertebral body replacement during upper body flexion. *J Biomech, 48*(4), 560-565.

Dreischarf, M., Albiol, L., Zander, T., Arshad, R., Graichen, F., Bergmann, G., . . . Rohlmann, A. (2015b). In vivo implant forces acting on a vertebral body replacement during upper body flexion. *Journal of biomechanics, 48*(4), 560-565.

Dreischarf, M., Rohlmann, A., Zhu, R., Schmidt, H., & Zander, T. (2013). Is it possible to estimate the compressive force in the lumbar spine from intradiscal pressure measurements? A finite element evaluation. *Med Eng Phys, 35*(9), 1385-1390.

Dreischarf, M., Shirazi-Adl, A., Arjmand, N., Rohlmann, A., & Schmidt, H. (2016a). Estimation of loads on human lumbar spine: a review of in vivo and computational model studies. *J Biomech, 49*(6), 833-845.

Dreischarf, M., Shirazi-Adl, A., Arjmand, N., Rohlmann, A., & Schmidt, H. (2016b). Estimation of loads on human lumbar spine: a review of in vivo and computational model studies. *Journal of biomechanics, 49*(6), 833-845.

Dreischarf, M., Zander, T., Shirazi-Adl, A., Puttlitz, C., Adam, C., Chen, C., . . . Labus, K. (2014). Comparison of eight published static finite element models of the intact lumbar spine:

Predictive power of models improves when combined together. *J Biomech, 47*(8), 1757-1766.

Dudli, S., Ferguson, S. J., & Haschtmann, D. (2014). Severity and pattern of post-traumatic intervertebral disc degeneration depend on the type of injury. *Spine J, 14*(7), 1256-1264. doi: 10.1016/j.spinee.2013.07.488

Dufour, J. S., Marras, W. S., & Knapik, G. G. (2013). An EMG-assisted model calibration technique that does not require MVCs. *Journal of Electromyography and Kinesiology, 23*(3), 608-613.

Dul, J., Johnson, G., Shiavi, R., & Townsend, M. (1984). Muscular synergism—II. A minimum-fatigue criterion for load sharing between synergistic muscles. *Journal of biomechanics, 17*(9), 675-684.

El-Rich, M., & Shirazi-Adl, A. (2005). Effect of load position on muscle forces, internal loads and stability of the human spine in upright postures. *Comput Method Biomec, 8*(6), 359-368.

El-Rich, M., Shirazi-Adl, A., & Arjmand, N. (2004). Muscle activity, internal loads, and stability of the human spine in standing postures: combined model and in vivo studies. *Spine, 29*(23), 2633-2642.

El Maghraoui, A., Sadni, S., El Maataoui, A., Majjad, A., Rezqi, A., Ouzzif, Z., & Mounach, A. (2015). Influence of obesity on vertebral fracture prevalence and vitamin D status in postmenopausal women. *Nutrition Metabol, 12*(1), 1. doi: 10.1186/s12986-015-0041-2

El Ouaaid, Z., Arjmand, N., Shirazi-Adl, A., & Parnianpour, M. (2009). A novel approach to evaluate abdominal coactivities for optimal spinal stability and compression force in lifting. *Comput Method Biomec, 12*(6), 735-745.

El Ouaaid, Z., Shirazi-Adl, A., Arjmand, N., & Plamondon, A. (2013a). Coupled objective function to study the role of abdominal muscle forces in lifting using the kinematics-driven model. *Computer methods in biomechanics and biomedical engineering, 16*(1), 54-65.

El Ouaaid, Z., Shirazi-Adl, A., & Plamondon, A. (2015). Effects of variation in external pulling force magnitude, elevation, and orientation on trunk muscle forces, spinal loads and stability. *J Biomech*.

El Ouaaid, Z., Shirazi-Adl, A., Plamondon, A., & Larivière, C. (2013b). Trunk strength, muscle activity and spinal loads in maximum isometric flexion and extension exertions: A combined in vivo-computational study. *J Biomech, 46*(13), 2228-2235.

Endo, K., Suzuki, H., Tanaka, H., Kang, Y., & Yamamoto, K. (2010). Sagittal spinal alignment in patients with lumbar disc herniation. *Eur Spine J, 19*(3), 435-438.

Fagan, A. B., Sarvestani, G., Moore, R. J., Fraser, R. D., Vernon-Roberts, B., & Blumbergs, P. C. (2010). Innervation of anulus tears: an experimental animal study. *Spine, 35*(12), 1200-1205.

Farvid, M., Ng, T., Chan, D., Barrett, P., & Watts, G. (2005). Association of adiponectin and resistin with adipose tissue compartments, insulin resistance and dyslipidaemia. *Diabetes Obes Metab, 7*(4), 406-413.

Ferguson, S., & Marras, W. (1997). A literature review of low back disorder surveillance measures and risk factors. *Clin Biomech, 12*(4), 211-226.

Flegal, K. M., Carroll, M. D., Kit, B. K., & Ogden, C. L. (2012). Prevalence of obesity and trends in the distribution of body mass index among US adults, 1999-2010. *Jama, 307*(5), 491-497.

Fregly, B. J., Besier, T. F., Lloyd, D. G., Delp, S. L., Banks, S. A., Pandy, M. G., & D'lima, D. D. (2012). Grand challenge competition to predict in vivo knee loads. *Journal of orthopaedic research, 30*(4), 503-513.

Freivalds, A., Chaffin, D. B., Garg, A., & Lee, K. S. (1984). A dynamic biomechanical evaluation of lifting maximum acceptable loads. *Journal of biomechanics, 17*(4), 251-262.

Fukunaga, T., Roy, R., Shellock, F., Hodgson, J., & Edgerton, V. (1996). Specific tension of human plantar flexors and dorsiflexors. *Journal of Applied Physiology, 80*(1), 158-165.

Gagnon, D., Arjmand, N., Plamondon, A., Shirazi-Adl, A., & Larivière, C. (2011). An improved multi-joint EMG-assisted optimization approach to estimate joint and muscle forces in a musculoskeletal model of the lumbar spine. *J Biomech, 44*(8), 1521-1529.

Gallagher, S., & Schall, M. (2016). *The Biomechanical Relevance of Stress Range and Mean Stress in the Analysis of Variable Loading on Musculoskeletal Tissues.* Paper presented at the Proceedings of the Human Factors and Ergonomics Society Annual Meeting.

Gallagher, S., Sesek, R. F., Schall Jr, M. C., & Huangfu, R. (2017). Development and validation of an easy-to-use risk assessment tool for cumulative low back loading: The Lifting Fatigue Failure Tool (LiFFT). *Applied ergonomics, 63*, 142-150.

Gardner-Morse, M. G., & Stokes, I. A. (2004a). Structural behavior of human lumbar spinal motion segments. *Journal of biomechanics, 37*(2), 205-212.

Gardner-Morse, M. G., & Stokes, I. A. (2004b). Structural behavior of human lumbar spinal motion segments. *J Biomech, 37*(2), 205-212.

Gardner-Morse, M., Stokes, I. A., & Laible, J. P. (1995). Role of muscles in lumbar spine stability in maximum extension efforts. *Journal of orthopaedic research, 13*(5), 802-808.

Gatton, M. L., Pearcy, M. J., & Pettet, G. J. (2011). Computational model of the lumbar spine musculature: implications of spinal surgery. *Clinical Biomechanics, 26*(2), 116-122.

Gayzik, F. S., Mao, M. Y., Danelson, K. A., Slice, D. E., & Stitzel, J. D. (2008). Quantification of age-related shape change of the human rib cage through geometric morphometrics. *J Biomech, 41*(7), 1545-1554.

Gercek, E., Hartmann, F., Kuhn, S., Degreif, J., Rommens, P. M., & Rudig, L. (2008). Dynamic angular three-dimensional measurement of multisegmental thoracolumbar motion in vivo. *Spine, 33*(21), 2326-2333.

Gerus, P., Sartori, M., Besier, T. F., Fregly, B. J., Delp, S. L., Banks, S. A., . . . Lloyd, D. G. (2013). Subject-specific knee joint geometry improves predictions of medial tibiofemoral contact forces. *J Biomech, 46*(16), 2778-2786.

Ghezelbash, F., Arjmand, N., & Shirazi-Adl, A. (2015). Effect of intervertebral translational flexibilities on estimations of trunk muscle forces, kinematics, loads, and stability. *Comput Method Biomec, 18*(16), 1760-1767.

Ghezelbash, F., El Ouaaid, Z., Shirazi-Adl, A., Plamondon, A., & Arjmand, N. (2018a). Trunk musculoskeletal response in maximum voluntary exertions: a combined measurement-modeling investigation. *Journal of biomechanics, 70*, 124-133.

Ghezelbash, F., Eskandari, A., Shirazi-Adl, A., Arjmand, N., El-Ouaaid, Z., & Plamondon, A. (2018b). Effects of motion segment simulation and joint positioning on spinal loads in trunk musculoskeletal models. *J Biomech, 70*, 149-156.

Ghezelbash, F., Shiraz-Adl, A., El Ouaaid, Z., Plamondon, A., & Arjmand, N. (2019). Subject-specific regression equations to estimate lower spinal loads during symmetric and asymmetric static lifting. *J Biomech, Under Review*.

Ghezelbash, F., Shiraz-Adl, A., Plamondon, A., & Arjmand, N. (2018c). *Subject-specific risk assessment of obesity and ageing in spine biomechanics.* Paper presented at the 15th International Symposium on Computer Methods in Biomechanics and Biomedical Engineering, lisbon.

Ghezelbash, F., Shiraz-Adl, A., Plamondon, A., Arjmand, N., & Parnianpour, M. (2017a). Obesity and obesity shape both matter in spine biomechanics: a subject-specific risk assessment model. *Submitted to Annals of Biomedical Engineering*.

Ghezelbash, F., Shirazi-Adl, A., Arjmand, N., El-Ouaaid, Z., & Plamondon, A. (2016a). Effects of sex, age, body height and body weight on spinal loads: sensitivity analyses in a subject-specific trunk musculoskeletal model. *J Biomechanics*.

Ghezelbash, F., Shirazi-Adl, A., Arjmand, N., El-Ouaaid, Z., & Plamondon, A. (2016b). Subject-specific biomechanics of trunk: musculoskeletal scaling, internal loads and intradiscal pressure estimation. *Biomechanics and modeling in mechanobiology, 15*(6), 1699-1712.

Ghezelbash, F., Shirazi-Adl, A., Plamondon, A., Arjmand, N., & Parnianpour, M. (2017b). Obesity and Obesity Shape Markedly Influence Spine Biomechanics: A Subject-Specific Risk Assessment Model. *Annals of biomedical engineering*.

Gilroy, A. M., MacPherson, B. R., Ross, L. M., Schünke, M., Schulte, E., Schumacher, U., . . . Wesker, K. (2008). *Atlas of anatomy*. Stuttgart: Thieme.

Goislard, d. M. B., Rao, G., Gay, A., Berton, E., & Vigouroux, L. (2017). A scaling method to individualise muscle force capacities in musculoskeletal models of the hand and wrist using isometric strength measurements. *Medical & biological engineering & computing*.

Gonnelli, S., Caffarelli, C., & Nuti, R. (2014). Obesity and fracture risk. *Clin Cases Miner Bone Metab, 11*(1), 9-14. doi: 10.11138/ccmbm/2014.11.1.009

Gracovetsky, S. (2008). Is the lumbodorsal fascia necessary? *Journal of bodywork and movement therapies, 12*(3), 194-197.

Gracovetsky, S., Zeman, V., & Carbone, A. (1987). Relationship between lordosis and the position of the centre of reaction of the spinal disc. *Journal of biomedical engineering, 9*(3), 237-248.

Granata, K., & Marras, W. (1993). An EMG-assisted model of loads on the lumbar spine during asymmetric trunk extensions. *Journal of biomechanics, 26*(12), 1429-1438.

Granata, K., & Marras, W. (1995). An EMG-assisted model of trunk loading during free-dynamic lifting. *J Biomech, 28*(11), 1309-1317.

Granata, K., & Wilson, S. (2001). Trunk posture and spinal stability. *Clinical Biomechanics, 16*(8), 650-659.

Gravel, D., Gagnon, M., Plamondon, A., & Desjardins, P. (1997). Development and application of predictive equations of maximal static moments generated by the trunk musculature. *Clinical Biomechanics, 12*(5), 314-324.

Green, T., Adams, M., & Dolan, P. (1993a). Tensile properties of the annulus fibrosus. *Eur Spine J, 2*(4), 209-214. doi: 10.1007/BF00299448

Green, T., Adams, M., & Dolan, P. (1993b). Tensile properties of the annulus fibrosus. *European Spine Journal, 2*(4), 209-214.

Hadjipavlou, A., Tzermiadianos, M., Bogduk, N., & Zindrick, M. (2008). The pathophysiology of disc degeneration: a critical review. *The Journal of bone and joint surgery. British volume, 90*(10), 1261-1270.

Hajibozorgi, M., & Arjmand, N. (2015). Sagittal range of motion of the thoracic spine using inertial tracking device and effect of measurement errors on model predictions. *J Biomech, 49*(6), 913-918.

Hajihosseinali, M., Arjmand, N., & Shirazi-Adl, A. (2015). Effect of body weight on spinal loads in various activities: A personalized biomechanical modeling approach. *J Biomech, 48*(2), 276-282.

Hajihosseinali, M., Arjmand, N., Shirazi-Adl, A., Farahmand, F., & Ghiasi, M. (2014). A novel stability and kinematics-driven trunk biomechanical model to estimate muscle and spinal forces. *Med Eng Phys, 36*(10), 1296-1304.

Hamilton, K. C., Fisher, G., Roy, J. L., Gower, B. A., & Hunter, G. R. (2013). The effects of weight loss on relative bone mineral density in premenopausal women. *Obesity, 21*(3), 441-448. doi: 10.1002/oby.20052

Han, K.-S., Kim, K., Park, W. M., Lim, D. S., & Kim, Y. H. (2013a). Effect of centers of rotation on spinal loads and muscle forces in total disk replacement of lumbar spine. *Proceedings of the Institution of Mechanical Engineers, Part H: Journal of Engineering in Medicine, 227*(5), 543-550.

Han, K.-S., Rohlmann, A., Zander, T., & Taylor, W. R. (2013b). Lumbar spinal loads vary with body height and weight. *Med Eng Phys, 35*(7), 969-977.

Han, K.-S., Zander, T., Taylor, W. R., & Rohlmann, A. (2012). An enhanced and validated generic thoraco-lumbar spine model for prediction of muscle forces. *Med Eng Phys, 34*(6), 709-716.

Han, T., Schouten, J., Lean, M., & Seidell, J. (1997a). The prevalence of low back pain and associations with body fatness, fat distribution and height. *Int J Obesity, 21*(7), 600-607.

Han, T., Schouten, J., Lean, M., & Seidell, J. (1997b). The prevalence of low back pain and associations with body fatness, fat distribution and height. *Int J Obes, 21*(7), 600-607. doi: 10.1038/sj.ijo.0800448

Happee, R., de Bruijn, E., Forbes, P. A., & van der Helm, F. C. (2017). Dynamic head-neck stabilization and modulation with perturbation bandwidth investigated using a multisegment neuromuscular model. *Journal of biomechanics, 58*, 203-211.

Haschtmann, D., Stoyanov, J. V., Gédet, P., & Ferguson, S. J. (2008). Vertebral endplate trauma induces disc cell apoptosis and promotes organ degeneration in vitro. *Eur Spine J, 17*(2), 289-299. doi: 10.1007/s00586-007-0509-5

Hayashibe, M., & Guiraud, D. (2013). Voluntary EMG-to-force estimation with a multi-scale physiological muscle model. *Biomedical engineering online, 12*(1), 86.

Heneweer, H., Staes, F., Aufdemkampe, G., van Rijn, M., & Vanhees, L. (2011). Physical activity and low back pain: a systematic review of recent literature. *Eur Spine J, 20*(6), 826-845.

Hershkovich, O., Friedlander, A., Gordon, B., Arzi, H., Derazne, E., Tzur, D., . . . Afek, A. (2013). Associations of body mass index and body height with low back pain in 829,791 adolescents. *Am J Epidemiol, 178*(4), 603-609.

Heuch, I., Hagen, K., Heuch, I., Nygaard, Ø., & Zwart, J.-A. (2010). The impact of body mass index on the prevalence of low back pain: the HUNT study. *Spine, 35*(7), 764-768.

Heuch, I., Heuch, I., Hagen, K., & Zwart, J.-A. (2015a). Association between body height and chronic low back pain: a follow-up in the Nord-Trøndelag Health Study. *BMJ open, 5*(6), e006983.

Heuch, I., Heuch, I., Hagen, K., & Zwart, J.-A. (2015b). A Comparison of Anthropometric Measures for Assessing the Association between Body Size and Risk of Chronic Low Back Pain: The HUNT Study. *PloS one, 10*(10), e0141268.

Heuer, F., Schmidt, H., & Wilke, H.-J. (2008). Stepwise reduction of functional spinal structures increase disc bulge and surface strains. *Journal of biomechanics, 41*(9), 1953-1960.

Hoy, D., Bain, C., Williams, G., March, L., Brooks, P., Blyth, F., . . . Buchbinder, R. (2012). A systematic review of the global prevalence of low back pain. *Arthritis Rheum, 64*(6), 2028-2037.

Hoy, D., Brooks, P., Blyth, F., & Buchbinder, R. (2010a). The epidemiology of low back pain. *Best Pract Res Cl Rh, 24*(6), 769-781.

Hoy, D., March, L., Brooks, P., Blyth, F., Woolf, A., Bain, C., . . . Barendregt, J. (2014). The global burden of low back pain: estimates from the global burden of disease 2010 study. *Ann Rheum Dis*, annrheumdis-2013-204428.

Hoy, D., March, L., Brooks, P., Woolf, A., Blyth, F., Vos, T., & Buchbinder, R. (2010b). Measuring the global burden of low back pain. *Best Pract Res Cl Rh, 24*(2), 155-165.

Huber, G., Nagel, K., Skrzypiec, D. M., Klein, A., Püschel, K., & Morlock, M. M. (2016a). A description of spinal fatigue strength. *Journal of biomechanics, 49*(6), 875-880.

Huber, G., Nagel, K., Skrzypiec, D. M., Klein, A., Püschel, K., & Morlock, M. M. (2016b). A description of spinal fatigue strength. *J Biomech, 49*(6), 875-880. doi: 10.1016/j.jbiomech.2016.01.041

Hue, O., Simoneau, M., Marcotte, J., Berrigan, F., Doré, J., Marceau, P., . . . Teasdale, N. (2007). Body weight is a strong predictor of postural stability. *Gait posture, 26*(1), 32-38.

Hughes, R. E., & Chaffin, D. B. (1988). Conditions under which optimization models will not predict coactivation of antagonist muscles. *Journal of biomechanics, 21*(10), 862.

Iatridis, J. C., & Gwynn, I. (2004). Mechanisms for mechanical damage in the intervertebral disc annulus fibrosus. *Journal of biomechanics, 37*(8), 1165-1175.

Iatridis, J. C., MacLean, J. J., & Ryan, D. A. (2005). Mechanical damage to the intervertebral disc annulus fibrosus subjected to tensile loading. *Journal of biomechanics, 38*(3), 557-565.

Ignasiak, D., Dendorfer, S., & Ferguson, S. J. (2016a). Thoracolumbar spine model with articulated ribcage for the prediction of dynamic spinal loading. *Journal of biomechanics, 49*(6), 959-966.

Ignasiak, D., Ferguson, S. J., & Arjmand, N. (2016b). A rigid thorax assumption affects model loading predictions at the upper but not lower lumbar levels. *Journal of biomechanics, 49*(13), 3074-3078.

Inerot, S., & Axelsson, I. (1991). Structure and composition of proteoglycans from human annulus fibrosus. *Connective tissue research, 26*(1-2), 47-63.

Jackson, R. P., Peterson, M. D., McManus, A. C., & Hales, C. (1998). Compensatory spinopelvic balance over the hip axis and better reliability in measuring lordosis to the pelvic radius on standing lateral radiographs of adult volunteers and patients. *Spine, 23*(16), 1750-1767.

Jamshidnejad, S., & Arjmand, N. (2015). Variations in trunk muscle activities and spinal loads following posterior lumbar surgery: A combined in vivo and modeling investigation. *Clinical Biomechanics, 30*(10), 1036-1042.

Jang, T.-W., Ahn, Y.-S., Byun, J., Lee, J.-I., Kim, K.-H., Kim, Y., . . . Yoon, J.-H. (2016). Lumbar intervertebral disc degeneration and related factors in Korean firefighters. *BMJ open, 6*(6), e011587.

Jia, B., Kim, S., & Nussbaum, M. A. (2011). An EMG-based model to estimate lumbar muscle forces and spinal loads during complex, high-effort tasks: Development and application to residential construction using prefabricated walls. *Int J Ind Ergonom, 41*(5), 437-446.

Jones, A. C., & Wilcox, R. K. (2008). Finite element analysis of the spine: towards a framework of verification, validation and sensitivity analysis. *Medical Engineering & Physics, 30*(10), 1287-1304.

Jorgensen, M., Marras, W., Granata, K., & Wiand, J. (2001). MRI-derived moment-arms of the female and male spine loading muscles. *Clin Biomech, 16*(3), 182-193.

Kalichman, L., Li, L., Hunter, D. J., & Been, E. (2011). Association between computed tomography–evaluated lumbar lordosis and features of spinal degeneration, evaluated in supine position. *Spine J, 11*(4), 308-315.

Katz, J. N. (2006). Lumbar disc disorders and low-back pain: socioeconomic factors and consequences. *J Bone Joint Surg Am, 88*(suppl 2), 21-24.

Kaufman, K. R., Au, K.-N., Litchy, W. J., & Chao, E. (1991). Physiological prediction of muscle forces—II. Application to isokinetic exercise. *Neuroscience, 40*(3), 793-804.

Kawakami, Y., Abe, T., Kuno, S.-Y., & Fukunaga, T. (1995). Training-induced changes in muscle architecture and specific tension. *European journal of applied physiology and occupational physiology, 72*(1), 37-43.

Keller, T. S., Colloca, C. J., Harrison, D. E., Harrison, D. D., & Janik, T. J. (2005). Influence of spine morphology on intervertebral disc loads and stresses in asymptomatic adults: implications for the ideal spine. *Spine J, 5*(3), 297-309.

Khosla, S., Atkinson, E. J., Riggs, B. L., & Melton, L. J. (1996). Relationship between body composition and bone mass in women. *J Bone Miner Res, 11*(6), 857-863. doi: 10.1002/jbmr.5650110618

Khurelbaatar, T., Kim, K., & Kim, Y. H. (2015). A cervico-thoraco-lumbar multibody dynamic model for the estimation of joint loads and muscle forces. *J Biomech Eng-T ASME, 137*(11), 111001.

Kiefer, A., Shirazi-Adl, A., & Parnianpour, M. (1998). Synergy of the human spine in neutral postures. *Eur Spine J, 7*(6), 471-479.

Kim, K.-C., Shin, D.-H., Lee, S.-Y., Im, J.-A., & Lee, D.-C. (2010). Relation between obesity and bone mineral density and vertebral fractures in Korean postmenopausal women. *Yonsei Med J, 51*(6), 857-863. doi: 10.3349/ymj.2010.51.6.857

Koyanagi, A., Stickley, A., Garin, N., Miret, M., Ayuso-Mateos, J. L., Leonardi, M., . . . Haro, J. M. (2015). The association between obesity and back pain in nine countries: a cross-sectional study. *BMC public health, 15*(1), 1.

Kumar, S. (1996). Isolated planar trunk strengths measurement in normals: Part iii—results and database. *International Journal of Industrial Ergonomics, 17*(2), 103-111.

Larivière, C., Bilodeau, M., Forget, R., Vadeboncoeur, R., & Mecheri, H. (2010). Poor back muscle endurance is related to pain catastrophizing in patients with chronic low back pain. *Spine, 35*(22), E1178-E1186.

Larivière, C., Gagnon, D., & Genest, K. (2009). Offering proper feedback to control for out-of-plane lumbar moments influences the activity of trunk muscles during unidirectional isometric trunk exertions. *Journal of biomechanics, 42*(10), 1498-1505.

Larivière, C., Gagnon, D., Gravel, D., Arsenault, A. B., Dumas, J.-P., Goyette, M., & Loisel, P. (2001). A triaxial dynamometer to monitor lateral bending and axial rotation moments during static trunk extension efforts. *Clinical Biomechanics, 16*(1), 80-83.

Larivière, C., Gravel, D., Gagnon, D., Arsenault, A. B., Loisel, P., & Lepage, Y. (2003). Back strength cannot be predicted accurately from anthropometric measures in subjects with and without chronic low back pain. *Clinical Biomechanics, 18*(6), 473-479.

Laslett, L., nee Foley, S. J., Quinn, S., Winzenberg, T., & Jones, G. (2012). Excess body fat is associated with higher risk of vertebral deformities in older women but not in men: a cross-sectional study. *Osteoporosis Int, 23*(1), 67-74. doi: 10.1007/s00198-011-1741-8

Lean, M., Han, T., & Seidell, J. (1998a). Impairment of health and quality of life in people with large waist circumference. *Lancet, 351*(9106), 853-856.

Lean, M., Han, T., & Seidell, J. (1998b). Impairment of health and quality of life in people with large waist circumference. *The Lancet, 351*(9106), 853-856. doi: 10.1016/S0140-6736(97)10004-6

Leboeuf–Yde, C., Kyvik, K. O., & Bruun, N. H. (1999). Low back pain and lifestyle. Part II-Obesity: Information from a population-based sample of 29,424 twin subjects. *Spine, 24*(8), 779-784.

Leclerc, A., Tubach, F., Landre, M. F., & Ozguler, A. (2003). Personal and occupational predictors of sciatica in the GAZEL cohort. *Occup Med, 53*(6), 384-391.

Lee, Y.-H., & Kuo, C.-L. (2000). Factor structure of trunk performance data for healthy subjects. *Clinical Biomechanics, 15*(4), 221-227.

Lidar, Z., Behrbalk, E., Regev, G. J., Salame, K., Keynan, O., Schweiger, C., . . . Keidar, A. (2012). Intervertebral disc height changes after weight reduction in morbidly obese patients and its effect on quality of life and radicular and low back pain. *Spine, 37*(23), 1947-1952.

Lin, C.-F., Liu, H., Gros, M. T., Weinhold, P., Garrett, W. E., & Yu, B. (2012). Biomechanical risk factors of non-contact ACL injuries: A stochastic biomechanical modeling study. *Journal of Sport and Health Science, 1*(1), 36-42.

Lipson, S. J., & Muir, H. (1981). Proteoglycans in Experimental Intervertebral Disc Degeneration. *Spine, 6*(3), 194-210.

Liu, Z., Tsai, T.-Y., Wang, S., Wu, M., Zhong, W., Li, J.-S., . . . Li, G. (2016). Sagittal plane rotation center of lower lumbar spine during a dynamic weight-lifting activity. *Journal of biomechanics, 49*(3), 371-375.

Liuke, M., Solovieva, S., Lamminen, A., Luoma, K., Leino-Arjas, P., Luukkonen, R., & Riihimäki, H. (2005). Disc degeneration of the lumbar spine in relation to overweight. *Int J Obes, 29*(8), 903-908. doi: 10.1038/sj.ijo.0802974

Lund, M. E., Andersen, M. S., de Zee, M., & Rasmussen, J. (2015). Scaling of musculoskeletal models from static and dynamic trials. *International Biomechanics, 2*(1), 1-11.

Macintosh, J. E., Bogduk, N., & Gracovetsky, S. (1987). The biomechanics of the thoracolumbar fascia. *Clinical Biomechanics, 2*(2), 78-83.

Maden-Wilkinson, T., Degens, H., Jones, D., & McPhee, J. (2013). Comparison of MRI and DXA to measure muscle size and age-related atrophy in thigh muscles. *Journal of Musculoskeletal and Neuronal Interactions, 13*.

Malakoutian, M., Street, J., Wilke, H.-J., Stavness, I., Fels, S., & Oxland, T. (2016). A musculoskeletal model of the lumbar spine using ArtiSynth–development and validation. *Computer Methods in Biomechanics and Biomedical Engineering: Imaging & Visualization*, 1-8.

Malchaire, J. B., & Masset, D. F. (1995). Isometric and dynamic performances of the trunk and associated factors. *Spine, 20*(15), 1649-1656.

Marchand, F., & Ahmed, A. M. (1990). Investigation of the laminate structure of lumbar disc anulus fibrosus. *Spine, 15*(5), 402-410.

Marras, W. S., Davis, K. G., & Jorgensen, M. (2003). Gender influences on spine loads during complex lifting. *Spine J, 3*(2), 93-99.

Marras, W. S., Lavender, S. A., Leurgans, S. E., Fathallah, F. A., Ferguson, S. A., Gary Allread, W., & Rajulu, S. L. (1995). Biomechanical risk factors for occupationally related low back disorders. *Ergonomics, 38*(2), 377-410.

Martelli, S., Kersh, M. E., & Pandy, M. G. (2015). Sensitivity of femoral strain calculations to anatomical scaling errors in musculoskeletal models of movement. *J Biomech*.

Matrangola, S. L., Madigan, M. L., Nussbaum, M. A., Ross, R., & Davy, K. P. (2008). Changes in body segment inertial parameters of obese individuals with weight loss. *J Biomech, 41*(15), 3278-3281.

McGill, S., & Sharratt, M. (1990). Relationship between intra-abdominal pressure and trunk EMG. *Clinical Biomechanics, 5*(2), 59-67.

McGill, S. M. (1991). Kinetic potential of the lumbar trunk musculature about three orthogonal orthopaedic axes in extreme postures. *Spine, 16*(7), 809-815.

McGill, S. M. (1992). A myoelectrically based dynamic three-dimensional model to predict loads on lumbar spine tissues during lateral bending. *Journal of biomechanics, 25*(4), 395-414.

McGill, S. M. (1996). A revised anatomical model of the abdominal musculature for torso flexion efforts. *J Biomech, 29*(7), 973-977.

McGill, S. M., & Norman, R. W. (1985). Dynamically and statically determined low back moments during lifting. *Journal of biomechanics, 18*(12), 877-885.

McGill, S. M., Norman, R. W., & Cholewicki, J. (1996). A simple polynomial that predicts low-back compression during complex 3-D tasks. *Ergonomics, 39*(9), 1107-1118.

Mcneill, T., Warwick, D., Andersson, G., & Schultz, A. (1980). Trunk strengths in attempted flexion, extension, and lateral bending in healthy subjects and patients with low-back disorders. *Spine, 5*(6), 529-538.

Meakin, J. R., Gregory, J. S., Smith, F. W., Gilbert, F. J., & Aspden, R. M. (2008a). Characterizing the shape of the lumbar spine using an active shape model: reliability and precision of the method. *Spine, 33*(7), 807-813.

Meakin, J. R., Shrive, N. G., Frank, C. B., & Hart, D. A. (2003). Finite element analysis of the meniscus: the influence of geometry and material properties on its behaviour. *Knee, 10*(1), 33-41.

Meakin, J. R., Smith, F. W., Gilbert, F. J., & Aspden, R. M. (2008b). The effect of axial load on the sagittal plane curvature of the upright human spine in vivo. *J Biomech, 41*(13), 2850-2854.

Meijer, G. J., Homminga, J., Veldhuizen, A. G., & Verkerke, G. J. (2011). Influence of interpersonal geometrical variation on spinal motion segment stiffness: implications for patient-specific modeling. *Spine, 36*(14), E929-E935.

Melton, L. J., Riggs, B. L., Keaveny, T. M., Achenbach, S. J., Hoffmann, P. F., Camp, J. J., . . . Atkinson, E. J. (2007). Structural determinants of vertebral fracture risk. *J Bone Miner Res, 22*(12), 1885-1892. doi: 10.1359/jbmr.070728

Meng, X., Bruno, A. G., Cheng, B., Wang, W., Bouxsein, M. L., & Anderson, D. E. (2015). Incorporating six degree-of-freedom intervertebral joint stiffness in a lumbar spine musculoskeletal model-method and performance in flexed postures. *J Biomech Eng-T ASME, 137*(10), 101008.

Merryweather, A. S., Loertscher, M. C., & Bloswick, D. S. (2008). A revised back compressive force estimation model for ergonomic evaluation of lifting tasks. *Work (Reading, Mass.), 34*(3), 263-272.

Mirka, G. A., & Marras, W. S. (1993). A stochastic model of trunk muscle coactivation during trunk bending. *Spine, 18*(11), 1396-1409.

Mohammadi, Y., Arjmand, N., & Shirazi-Adl, A. (2015). Comparison of trunk muscle forces, spinal loads and stability estimated by one stability-and three EMG-assisted optimization approaches. *Med Eng Phys, 37*(8), 792-800.

Montazeri, A., & Mousavi, S. (2010). Quality of life and low back pain. *Handbook of disease burdens and quality of life measures*, 3979-3994.

Mörl, F., & Blickhan, R. (2006). Three-dimensional relation of skin markers to lumbar vertebrae of healthy subjects in different postures measured by open MRI. *European Spine Journal, 15*(6), 742-751.

Murrie, V., Dixon, A., Hollingworth, W., Wilson, H., & Doyle, T. (2003). Lumbar lordosis: study of patients with and without low back pain. *Clin Anat, 16*(2), 144-147.

Nachemson, A. (1960). Lumbar intradiscal pressure: experimental studies on post-mortem material. *Acta Orthop, 31*(S43), 1-104.

Narimani, M., & Arjmand, N. (2018). Three-dimensional primary and coupled range of motions and movement coordination of the pelvis, lumbar and thoracic spine in standing posture using inertial tracking device. *Journal of biomechanics, 69*, 169-174.

Naserkhaki, S., Jaremko, J. L., Adeeb, S., & El-Rich, M. (2016). On the load-sharing along the ligamentous lumbosacral spine in flexed and extended postures: Finite element study. *Journal of biomechanics, 49*(6), 974-982.

Natarajan, R. N., & Andersson, G. B. (1999). The influence of lumbar disc height and cross-sectional area on the mechanical response of the disc to physiologic loading. *Spine, 24*(18), 1873.

National Center for Health Statistics. (1999-2014). *National health and nutrition examination survey data*. Retrieved from: http://www.cdc.gov/nchs/nhanes/

Ng, J. K. F., Parnianpour, M., Richardson, C. A., & Kippers, V. (2001). Functional roles of abdominal and back muscles during isometric axial rotation of the trunk. *J Orthopaed Res, 19*(3), 463-471.

Ng, J. K. F., Richardson, C. A., Parnianpour, M., & Kippers, V. (2002). EMG activity of trunk muscles and torque output during isometric axial rotation exertion: a comparison between back pain patients and matched controls. *J Orthopaed Res, 20*(1), 112-121.

Niemeyer, F., Wilke, H.-J., & Schmidt, H. (2012). Geometry strongly influences the response of numerical models of the lumbar spine—a probabilistic finite element analysis. *Journal of biomechanics, 45*(8), 1414-1423.

Nikooyan, A. A., Veeger, H., Chadwick, E., Praagman, M., & van der Helm, F. C. (2011). Development of a comprehensive musculoskeletal model of the shoulder and elbow. *Medical & biological engineering & computing, 49*(12), 1425-1435.

Noon, M. L., & Hoch, A. Z. (2012). Challenges of the pregnant athlete and low back pain. *Cur Sports Med Rep, 11*(1), 43-48.

O'sullivan, P. B., Dankaerts, W., Burnett, A. F., Farrell, G. T., Jefford, E., Naylor, C. S., & O'sullivan, K. J. (2006). Effect of different upright sitting postures on spinal-pelvic curvature and trunk muscle activation in a pain-free population. *Spine, 31*(19), E707-E712.

Oddsson, L. I., & De Luca, C. J. (2003). Activation imbalances in lumbar spine muscles in the presence of chronic low back pain. *Journal of Applied Physiology, 94*(4), 1410-1420.

Otten, E. (2003). Inverse and forward dynamics: models of multi–body systems. *Philosophical Transactions of the Royal Society of London. Series B: Biological Sciences, 358*(1437), 1493-1500.

Oxland, T. R., Lin, R. M., & Panjabi, M. M. (1992). Three-dimensional mechanical properties of the thoracolumbar junction. *J Orthopaed Res, 10*(4), 573-580.

Paik, J. M., Rosen, H. N., Katz, J. N., Rosner, B. A., Rimm, E. B., Gordon, C. M., & Curhan, G. C. (2019). BMI, Waist Circumference, and Risk of Incident Vertebral Fracture in Women. *Obesity, 27*(9), 1513-1519.

Panjabi, M. M., Goel, V. K., & Takata, K. (1982). Physiologic strains in the lumbar spinal ligaments. An in vitro biomechanical study 1981 Volvo Award in Biomechanics. *Spine, 7*(3), 192-203.

Panjabi, M. M., Oxland, T., Yamamoto, I., & Crisco, J. (1994). Mechanical behavior of the human lumbar and lumbosacral spine as shown by three-dimensional load-displacement curves. *The Journal of Bone & Joint Surgery, 76*(3), 413-424.

Park, M. S., Moon, S.-H., Lee, H.-M., Kim, S. W., Kim, T.-H., Lee, S. Y., & Riew, K. D. (2013). The effect of age on cervical sagittal alignment: normative data on 100 asymptomatic subjects. *Spine, 38*(8), E458-E463.

Park, W., Ramachandran, J., Weisman, P., & Jung, E. S. (2010). Obesity effect on male active joint range of motion. *Ergonomics, 53*(1), 102-108.

Parnianpour, M., Li, F., Nordin, M., & Frankel, V. (1988). Reproducibility of trunk isoinertial performances in the sagittal, coronal, and transverse planes. *Bulletin of the Hospital for Joint Diseases Orthopaedic Institute, 49*(2), 148-154.

Parnianpour, M., Nordin, M., Kahanovitz, N., & Frankel, V. (1988). The triaxial coupling of torque generation of trunk muscles during isometric exertions and the effect of fatiguing isoinertial movements on the motor output and movement patterns. *Spine, 13*(9), 982-992.

Pascual, S. A., & Naqvi, S. (2008). An investigation of ergonomics analysis tools used in industry in the identification of work-related musculoskeletal disorders. *International Journal of Occupational Safety and Ergonomics, 14*(2), 237-245.

Paterson, J. K., & Burn, L. (2012). *Back pain: an international review*: Springer Science & Business Media.

Pavlova, A. V., Muthuri, S., Saunders, F. R., Adams, J., Kuh, D., Aspden, R. M., . . . Barr, R. (2016). Variations in spine shape with body size, BMD and sex in individuals entering early old age. *Osteoarth Cartilage, 24*, S246-S247. doi: 10.1016/j.joca.2016.01.475

Pearcy, M. J., & Bogduk, N. (1988). Instantaneous axes of rotation of the lumbar intervertebral joints. *Spine, 13*(9), 1033-1041.

Pearsall, D. J. (1994). *Segmental inertial properties of the human trunk as determined from computed tomography and magnetic resonance imagery.* (PhD), Queen's University.

Pearsall, D. J., Reid, J. G., & Livingston, L. A. (1996). Segmental inertial parameters of the human trunk as determined from computed tomography. *Ann Biomed Eng, 24*(2), 198-210.

Perry, W., Broers, A., El-Baz, F., Harris, W., Healy, B., & Hillis, W. D. (2008). Grand challenges for engineering. *National Academy of Engineering, Washington, DC*.

Phillips, S., Mercer, S., & Bogduk, N. (2008). Anatomy and biomechanics of quadratus lumborum. *P I Mech Eng H, 222*(2), 151-159.

Pintar, F. A., Cusick, J. F., Yoganandan, N., Reinartz, J., & Mahesh, M. (1992). The biomechanics of lumbar facetectomy under compression-flexion. *Spine, 17*(7), 804-810.

Pirro, M., Fabbriciani, G., Leli, C., Callarelli, L., Manfredelli, M. R., Fioroni, C., . . . Mannarino, E. (2010). High weight or body mass index increase the risk of vertebral fractures in postmenopausal osteoporotic women. *J Bone Miner Res, 28*(1), 88-93. doi: 10.1007/s00774-009-0108-0

Plamondon, A., Denis, D., Larivière, C., Delisle, A., Gagnon, D., St-Vinvent, M., & Nastasia, I. (2014). Biomechanics and ergonomics in women materials handlers. Montreal: IRSST.

Porter, R., Adams, M., & Hutton, W. (1989). Physical activity and the strength of the lumbar spine. *Spine, 14*(2), 201-203.

Potvin, J. (1997). Use of NIOSH equation inputs to calculate lumbosacral compression forces. *Ergonomics, 40*(7), 691-707.

Potvin, J. R. (2012). Predicting maximum acceptable efforts for repetitive tasks: an equation based on duty cycle. *Human factors, 54*(2), 175-188.

Pries, E., Dreischarf, M., Bashkuev, M., Putzier, M., & Schmidt, H. (2015). The effects of age and gender on the lumbopelvic rhythm in the sagittal plane in 309 subjects. *J Biomech, 48*(12), 3080-3087. doi: http://dx.doi.org/10.1016/j.jbiomech.2015.07.030

Pruim, G., De Jongh, H., & Ten Bosch, J. (1980). Forces acting on the mandible during bilateral static bite at different bite force levels. *Journal of biomechanics, 13*(9), 755-763.

Pryce, R., & Kriellaars, D. (2014). Body segment inertial parameters and low back load in individuals with central adiposity. *J Biomech, 47*(12), 3080-3086.

Raikova, R. (1999). About weight factors in the non-linear objective functions used for solving indeterminate problems in biomechanics. *Journal of biomechanics, 32*(7), 689-694.

Rajaee, M. A., Arjmand, N., Shirazi-Adl, A., Plamondon, A., & Schmidt, H. (2015). Comparative evaluation of six quantitative lifting tools to estimate spine loads during static activities. *Appl Ergon, 48*, 22-32.

Ranger, T. A., Newell, N., Grant, C. A., Barker, P. J., & Pearcy, M. J. (2017). Role of the Middle Lumbar Fascia on Spinal Mechanics: A Human Biomechanical Assessment. *Spine, 42*(8), E459-E465.

Rannou, F., Lee, T.-S., Zhou, R.-H., Chin, J., Lotz, J. C., Mayoux-Benhamou, M.-A., . . . Shyy, J. Y.-J. (2004). Intervertebral disc degeneration: the role of the mitochondrial pathway in annulus fibrosus cell apoptosis induced by overload. *Am J Pathol, 164*(3), 915-924.

Rapoport, J., Jacobs, P., Bell, N. R., & Klarenbach, S. (2004). Refining the measurement of the economic burden of chronic diseases in Canada. *Chronic Dis Inj Can, 25*(1), 13.

Rasmussen, J., Zee, M. d., Damsgaard, M., Christensen, S. T., Marek, C., & Siebertz, K. (2005). *A general method for scaling musculo-skeletal models.* Paper presented at the International symposium on computer simulation in biomechanics.

Reeves, N. P., & Cholewicki, J. (2003). Modeling the human lumbar spine for assessing spinal loads, stability, and risk of injury. *Crit Rev Biomed Eng, 31*(1&2), 73-139.

Rohlmann, A., Dreischarf, M., Zander, T., Graichen, F., Strube, P., Schmidt, H., & Bergmann, G. (2013a). Monitoring the load on a telemeterised vertebral body replacement for a period of up to 65 months. *European Spine Journal, 22*(11), 2575-2581.

Rohlmann, A., Dreischarf, M., Zander, T., Graichen, F., Strube, P., Schmidt, H., & Bergmann, G. (2013b). Monitoring the load on a telemeterised vertebral body replacement for a period of up to 65 months. *Eur Spine J, 22*(11), 2575-2581.

Rohlmann, A., Gabel, U., Graichen, F., Bender, A., & Bergmann, G. (2007). An instrumented implant for vertebral body replacement that measures loads in the anterior spinal column. *Medical Engineering & Physics, 29*(5), 580-585.

Ross, R., Dagnone, D., Jones, P. J., Smith, H., Paddags, A., Hudson, R., & Janssen, I. (2000). Reduction in obesity and related comorbid conditions after diet-induced weight loss or exercise-induced weight loss in men: a randomized, controlled trial. *Ann Intern Med, 133*(2), 92-103. doi: 10.7326/0003-4819-133-2-200007180-00022

Roy, S. H., De Luca, C. J., & Casavabt, D. A. (1989). Lumbar muscle fatigue and chronic lower back pain. *Spine, 14*(9), 992-1001.

Rozumalski, A., Schwartz, M. H., Wervey, R., Swanson, A., Dykes, D. C., & Novacheck, T. (2008). The in vivo three-dimensional motion of the human lumbar spine during gait. *Gait posture, 28*(3), 378-384.

Samartzis, D., Karppinen, J., Cheung, J. P. Y., & Lotz, J. (2013). Disk degeneration and low back pain: are they fat-related conditions? *Glob Spine J, 3*(03), 133-144.

Sato, K., Kikuchi, S., & Yonezawa, T. (1999). In vivo intradiscal pressure measurement in healthy individuals and in patients with ongoing back problems. *Spine, 24*(23), 2468.

Scheys, L., Spaepen, A., Suetens, P., & Jonkers, I. (2008). Calculated moment-arm and muscle-tendon lengths during gait differ substantially using MR based versus rescaled generic lower-limb musculoskeletal models. *Gait posture, 28*(4), 640-648.

Schieve, L. A., Cogswell, M. E., Scanlon, K. S., Perry, G., Ferre, C., Blackmore-Prince, C., . . . Group, N. C. W. (2000). Prepregnancy body mass index and pregnancy weight gain: associations with preterm delivery. *Obstet Gynecol, 96*(2), 194-200.

Schmidt, H., Galbusera, F., Rohlmann, A., & Shirazi-Adl, A. (2013). What have we learned from finite element model studies of lumbar intervertebral discs in the past four decades? *Journal of biomechanics, 46*(14), 2342-2355.

Schmidt, H., & Shirazi-Adl, A. (2018). Temporal and spatial variations of pressure within intervertebral disc nuclei. *Journal of the mechanical behavior of biomedical materials, 79*, 309-313.

Schmidt, H., Shirazi-Adl, A., Galbusera, F., & Wilke, H.-J. (2010). Response analysis of the lumbar spine during regular daily activities—a finite element analysis. *Journal of biomechanics, 43*(10), 1849-1856.

Schneider, S., Randoll, D., & Buchner, M. (2006). Why do women have back pain more than men?: A representative prevalence study in the Federal Republic of Germany. *Clin J Pain, 22*(8), 738-747.

Schroeder, Y., Wilson, W., Huyghe, J. M., & Baaijens, F. P. (2006). Osmoviscoelastic finite element model of the intervertebral disc. *European Spine Journal, 15*(3), 361-371.

Schultz, A., Andersson, G., Örtengren, R., Björk, R., & Nordin, M. (1982). Analysis and quantitative myoelectric measurements of loads on the lumbar spine when holding weights in standing postures. *Spine, 7*(4), 390-397.

Schultz, A., Andersson, G., Ortengren, R., Haderspeck, K., & Nachemson, A. (1982). Loads on the lumbar spine. Validation of a biomechanical analysis by measurements of intradiscal pressures and myoelectric signals. *J Bone Joint Surg, 64*(5), 713-720.

Schultz, S. E., & Kopec, J. A. (2003). Impact of chronic conditions. *Health Rep, 14*(4), 41-53.

Senteler, M., Weisse, B., Rothenfluh, D. A., & Snedeker, J. G. (2015). Intervertebral reaction force prediction using an enhanced assembly of OpenSim models. *Comput Method Biomec*, 1-11.

Seo, A., Lee, J.-H., & Kusaka, Y. (2003). Estimation of trunk muscle parameters for a biomechanical model by age, height and weight. *J Occup Health, 45*(4), 197-201.

Seo, H., Cordier, F., & Magnenat-Thalmann, N. (2003, July 26 - 27). *Synthesizing animatable body models with parameterized shape modifications.* Paper presented at the Proceedings of the 2003 ACM SIGGRAPH/Eurographics Symposium on Computer Animation, Switzerland.

Shahvarpour, A., Shirazi-Adl, A., & Larivière, C. (2016). Active–passive biodynamics of the human trunk when seated on a wobble chair. *J Biomech, 49*(6), 939-945.

Shahvarpour, A., Shirazi-Adl, A., Larivière, C., & Bazrgari, B. (2015a). Computation of trunk stability in forward perturbations-Effects of preload, perturbation load, initial flexion and abdominal preactivation. *J Biomech, 48*(4), 716-720.

Shahvarpour, A., Shirazi-Adl, A., Larivière, C., & Bazrgari, B. (2015b). Trunk active response and spinal forces in sudden forward loading–analysis of the role of perturbation load and pre-perturbation conditions by a kinematics-driven model. *J Biomech, 48*(1), 44-52.

Sharma, M., Langrana, N. A., & Rodriguez, J. (1995). Role of ligaments and facets in lumbar spinal stability. *Spine, 20*(8), 887-900.

Sheldon, W. H., Stevens, S. S., & Tucker, W. B. (1940). *The varieties of human physique*. New York: Harper & Row Publishers.

Shi, X., Cao, L., Reed, M. P., Rupp, J. D., Hoff, C. N., & Hu, J. (2014). A statistical human rib cage geometry model accounting for variations by age, sex, stature and body mass index. *J Biomech, 47*(10), 2277-2285.

Shirazi-Adl, A. (1994a). Biomechanics of the lumbar spine in sagittal/lateral moments. *Spine, 19*(21), 2407-2414.

Shirazi-Adl, A. (1994b). Nonlinear stress analysis of the whole lumbar spine in torsion—mechanics of facet articulation. *J Biomech, 27*(3), 289-299.

Shirazi-Adl, A. (2006). Analysis of large compression loads on lumbar spine in flexion and in torsion using a novel wrapping element. *J Biomech, 39*(2), 267-275.

Shirazi-Adl, A., Ahmed, A., & Shrivastava, S. (1986). A finite element study of a lumbar motion segment subjected to pure sagittal plane moments. *J Biomech, 19*(4), 331-350.

Shirazi-Adl, A., & Drouin, G. (1988). Nonlinear gross response analysis of a lumbar motion segment in combined sagittal loadings. *J Biomech Eng-T ASME, 110*(3), 216-222.

Shirazi-Adl, A., El-Rich, M., Pop, D., & Parnianpour, M. (2005). Spinal muscle forces, internal loads and stability in standing under various postures and loads—application of kinematics-based algorithm. *Eur Spine J, 14*(4), 381-392.

Shirazi-Adl, A., & Pamianpour, M. (1993). Nonlinear response analysis of the human ligamentous lumbar spine in compression: On mechanisms affecting the postural stability. *Spine, 18*(1), 147-158.

Shirazi-Adl, A., Sadouk, S., Parnianpour, M., Pop, D., & El-Rich, M. (2002). Muscle force evaluation and the role of posture in human lumbar spine under compression. *Eur Spine J, 11*(6), 519-526.

Shiri, R., Karppinen, J., Leino-Arjas, P., Solovieva, S., & Viikari-Juntura, E. (2009). The association between obesity and low back pain: a meta-analysis. *Am J Epidemiol*, kwp356.

Shiri, R., Lallukka, T., Karppinen, J., & Viikari-Juntura, E. (2014). Obesity as a risk factor for sciatica: a meta-analysis. *Am J Epidemiol*, kwu007.

Shiri, R., Solovieva, S., Husgafvel-Pursiainen, K., Telama, R., Yang, X., Viikari, J., . . . Viikari-Juntura, E. (2013). The role of obesity and physical activity in non-specific and radiating low back pain: the Young Finns study. *Semin Arthritis Rheu, 42*(6), 640-650.

Shojaei, I., Vazirian, M., Croft, E., Nussbaum, M. A., & Bazrgari, B. (2016). Age related differences in mechanical demands imposed on the lower back by manual material handling tasks. *J Biomech, 49*(6), 896-903.

Singh, D., Park, W., Hwang, D., & Levy, M. (2015). Severe obesity effect on low back biomechanical stress of manual load lifting. *Work, 51*(2), 337-348.

Sis, H. L., Mannen, E. M., Wong, B. M., Cadel, E. S., Bouxsein, M. L., Anderson, D. E., & Friis, E. A. (2016). Effect of follower load on motion and stiffness of the human thoracic spine with intact rib cage. *Journal of biomechanics, 49*(14), 3252-3259.

Smuck, M., Kao, M.-C. J., Brar, N., Martinez-Ith, A., Choi, J., & Tomkins-Lane, C. C. (2014). Does physical activity influence the relationship between low back pain and obesity? *Spine J, 14*(2), 209-216.

Snook, S. H., & Ciriello, V. M. (1991). The design of manual handling tasks: revised tables of maximum acceptable weights and forces. *Ergonomics, 34*(9), 1197-1213.

Soderberg, G. L., & Knutson, L. M. (2000). A guide for use and interpretation of kinesiologic electromyographic data. *Phys Ther, 80*(5), 485-498.

Song, J., & Qu, X. (2014). Effects of age and its interaction with task parameters on lifting biomechanics. *Ergonomics, 57*(5), 653-668.

Song, Y. W., & Chung, M. K. (2004). Quantitative assessment of trunk muscle coactivation in sub-maximal isometric exertion tasks. *International Journal of Industrial Ergonomics, 34*(1), 13-20.

Sousa, A. S., & Tavares, J. M. R. (2012). Surface electromyographic amplitude normalization methods: a review. *Electromyography: new developments, procedures and applications*.

Statistics Canada. (2019). Obesity in Canadian Adults.

Staub, B. N., Holman, P. J., Reitman, C. A., & Hipp, J. (2015). Sagittal plane lumbar intervertebral motion during seated flexion-extension radiographs of 658 asymptomatic nondegenerated levels. *Journal of Neurosurgery: Spine, 23*(6), 731-738.

Stokes, E. K. (2011). *Rehabilitation outcome measures*: Churchill Livingstone Edinburgh, Scotland.

Stokes, I. A., & Gardner-Morse, M. (1999). Quantitative anatomy of the lumbar musculature. *J Biomech, 32*(3), 311-316.

Stokes, I. A., & Gardner-Morse, M. (2001). Lumbar spinal muscle activation synergies predicted by multi-criteria cost function. *Journal of biomechanics, 34*(6), 733-740.

Stokes, I. A., & Gardner-Morse, M. (2016). A database of lumbar spinal mechanical behavior for validation of spinal analytical models. *Journal of biomechanics, 49*(5), 780-785.

Stokes, I. A., Gardner-Morse, M., Churchill, D., & Laible, J. P. (2002). Measurement of a spinal motion segment stiffness matrix. *Journal of biomechanics, 35*(4), 517-521.

Stokes, I. A., Gardner-Morse, M. G., & Henry, S. M. (2010). Intra-abdominal pressure and abdominal wall muscular function: Spinal unloading mechanism. *Clin Biomech, 25*(9), 859-866.

Stokes, I. A., Henry, S. M., & Single, R. M. (2003). Surface EMG electrodes do not accurately record from lumbar multifidus muscles. *Clinical Biomechanics, 18*(1), 9-13.

Stokes, I. A., & Iatridis, J. C. (2004). Mechanical conditions that accelerate intervertebral disc degeneration: overload versus immobilization. *Spine, 29*(23), 2724-2732.

Streuber, S., Quiros-Ramirez, M. A., Hill, M. Q., Hahn, C. A., Zuffi, S., O'Toole, A., & Black, M. J. (2016). Body talk: crowdshaping realistic 3D avatars with words. *ACM Trans Graphics, 35*(4), 54. doi: 10.1145/2897824.2925981

Swink Hicks, G., Duddleston, D. N., Russell, L. D., Holman, H. E., Shepherd, J. M., & Andrew Brown, C. (2002). Low Back Pain. *The American Journal of the Medical Sciences, 324*(4), 207-211. doi: 10.1097/00000441-200210000-00007

Taanila, H. P., Suni, J. H., Pihlajamäki, H. K., Mattila, V. M., Ohrankämmen, O., Vuorinen, P., & Parkkari, J. P. (2012). Predictors of low back pain in physically active conscripts with special emphasis on muscular fitness. *Spine J, 12*(9), 737-748.

Tafazzol, A., Arjmand, N., Shirazi-Adl, A., & Parnianpour, M. (2014). Lumbopelvic rhythm during forward and backward sagittal trunk rotations: combined in vivo measurement with inertial tracking device and biomechanical modeling. *Clin Biomech, 29*(1), 7-13.

Takahashi, I., Kikuchi, S.-i., Sato, K., & Sato, N. (2006). Mechanical load of the lumbar spine during forward bending motion of the trunk–a biomechanical study. *Spine, 31*(1), 18-23.

Takatalo, J., Karppinen, J., Taimela, S., Niinimäki, J., Laitinen, J., Sequeiros, R. B., . . . Remes, J. (2013). Association of abdominal obesity with lumbar disc degeneration–a magnetic resonance imaging study. *PloS one, 8*(2), e56244. doi: 10.1371/journal.pone.0056244

Tang, R., Gungor, C., Sesek, R. F., Gallagher, S., Davis, G. A., & Foreman, K. B. (2019). Prediction models for the cross-sectional areas of lower lumbar intervertebral discs and vertebral endplates. *International Journal of Industrial Ergonomics, 72*, 12-34.

Tayashiki, K., Takai, Y., Maeo, S., & Kanehisa, H. (2016). Intra-abdominal pressure and trunk muscular activities during abdominal bracing and hollowing. *International journal of sports medicine, 37*(02), 134-143.

Tencer, A., Ahmed, A., & Burke, D. (1982). Some static mechanical properties of the lumbar intervertebral joint, intact and injured. *Journal of biomechanical engineering, 104*(3), 193-201.

Tomlinson, D., Erskine, R., Morse, C., Winwood, K., & Onambélé-Pearson, G. (2015). The impact of obesity on skeletal muscle strength and structure through adolescence to old age. *Biogerontology*, 1-17. doi: 10.1007/s10522-015-9626-4

Toumanidou, T., & Noailly, J. (2015). Musculoskeletal Modeling of the Lumbar Spine to Explore Functional Interactions between Back Muscle Loads and Intervertebral Disk Multiphysics. *Frontiers in bioengineering and biotechnology, 3*.

Tsao, H., Galea, M., & Hodges, P. (2008). Reorganization of the motor cortex is associated with postural control deficits in recurrent low back pain. *Brain, 131*(8), 2161-2171.

Tsirakos, D., Baltzopoulos, V., & Bartlett, R. (1997). Inverse optimization: functional and physiological considerations related to the force-sharing problem. *Critical Reviews™ in Biomedical Engineering, 25*(4-5).

Türker, K. S. (1993). Electromyography: some methodological problems and issues. *Phys Ther, 73*(10), 698-710.

Tüzün, C., Yorulmaz, I., Cindaş, A., & Vatan, S. (1999). Low back pain and posture. *Clin Rheumatol, 18*(4), 308-312.

Ulrich, J. A., Liebenberg, E. C., Thuillier, D. U., & Lotz, J. C. (2007). ISSLS prize winner: Repeated disc injury causes persistent inflammation. *Spine, 32*(25), 2812-2819.

Urban, J. P., Smith, S., & Fairbank, J. C. (2004). Nutrition of the intervertebral disc. *Spine, 29*(23), 2700-2709.

Urquhart, D. M., Kurniadi, I., Triangto, K., Wang, Y., Wluka, A. E., O'Sullivan, R., . . . Cicuttini, F. M. (2014). Obesity is associated with reduced disc height in the lumbar spine but not at the lumbosacral junction. *Spine, 39*(16), E962-E966.

Valente, G., Pitto, L., Stagni, R., & Taddei, F. (2015). Effect of lower-limb joint models on subject-specific musculoskeletal models and simulations of daily motor activities. *J Biomech*.

van Dieën, J., Weinans, H., & Toussaint, H. (1999). Fractures of the lumbar vertebral endplate in the etiology of low back pain: a hypothesis on the causative role of spinal compression in aspecific low back pain. *Med Hypotheses, 53*(3), 246-252. doi: 10.1054/mehy.1998.0754

van Dieën, J. H., Cholewicki, J., & Radebold, A. (2003). Trunk muscle recruitment patterns in patients with low back pain enhance the stability of the lumbar spine. *Spine, 28*(8), 834-841.

van Tulder, M., & Koes, B. (2002). Low back pain and sciatica: chronic. *Clinical Evidence*(7), 1032.

Velardo, C., & Dugelay, J.-L. (2010). Weight estimation from visual body appearance. *4th IEEE Int Conf BTAS*, 1-6.

Vergroesen, P.-P., Kingma, I., Emanuel, K. S., Hoogendoorn, R. J., Welting, T. J., van Royen, B. J., . . . Smit, T. H. (2015a). Mechanics and biology in intervertebral disc degeneration: a vicious circle. *Osteoarthritis and Cartilage, 23*(7), 1057-1070.

Vergroesen, P.-P., Kingma, I., Emanuel, K. S., Hoogendoorn, R. J., Welting, T. J., van Royen, B. J., . . . Smit, T. H. (2015b). Mechanics and biology in intervertebral disc degeneration: a vicious circle. *Osteoarthritis Cartilage, 23*(7), 1057-1070. doi: 10.1016/j.joca.2015.03.028

Videman, T., Battié, M. C., Gibbons, L. E., & Gill, K. (2014). Aging changes in lumbar discs and vertebrae and their interaction: a 15-year follow-up study. *Spine J, 14*(3), 469-478.

Videman, T., Gibbons, L. E., Kaprio, J., & Battié, M. C. (2010). Challenging the cumulative injury model: positive effects of greater body mass on disc degeneration. *The Spine Journal, 10*(1), 26-31.

Vigouroux, L., Quaine, F., Labarre-Vila, A., & Moutet, F. (2006). Estimation of finger muscle tendon tensions and pulley forces during specific sport-climbing grip techniques. *Journal of biomechanics, 39*(14), 2583-2592.

Vismara, L., Menegoni, F., Zaina, F., Galli, M., Negrini, S., & Capodaglio, P. (2010). Effect of obesity and low back pain on spinal mobility: a cross sectional study in women. *J Neuroeng Rehabil, 7*(1), 1.

Walsh, K., Cruddas, M., & Coggon, D. (1991). Interaction of height and mechanical loading of the spine in the development of low-back pain. *Scand J Work Env Hea*, 420-424.

Walter, J. P., Kinney, A. L., Banks, S. A., D'Lima, D. D., Besier, T. F., Lloyd, D. G., & Fregly, B. J. (2014). Muscle synergies may improve optimization prediction of knee contact forces during walking. *Journal of biomechanical engineering, 136*(2), 021031.

Wang, J.-L., Parnianpour, M., Shirazi-Adl, A., & Engin, A. E. (2000). Viscoelastic finite-element analysis of a lumbar motion segment in combined compression and sagittal flexion: Effect of loading rate. *Spine, 25*(3), 310-318.

Wang, J., Parnianpour, M., Shirazi-Adl, A., Engin, A., Li, S., & Patwardhan, A. (1997). Development and validation of a viscoelastic finite element model of an L2/L3 motion segment. *Theoretical and Applied Fracture Mechanics, 28*(1), 81-93.

Wang, X., Sanyal, A., Cawthon, P. M., Palermo, L., Jekir, M., Christensen, J., . . . Black, D. M. (2012a). Prediction of new clinical vertebral fractures in elderly men using finite element analysis of CT scans. *J Bone Miner Res, 27*(4), 808-816. doi: 10.1002/jbmr.1539

Wang, Y., & Battié, M. C. (2014). Epidemiology of lumbar disc degeneration *The intervertebral disc* (pp. 139-156): Springer.

Wang, Y., Videman, T., & Battié, M. C. (2012b). ISSLS prize winner: Lumbar vertebral endplate lesions: associations with disc degeneration and back pain history. *Spine, 37*(17), 1490-1496.

Wang, Y. C., McPherson, K., Marsh, T., Gortmaker, S. L., & Brown, M. (2011). Health and economic burden of the projected obesity trends in the USA and the UK. *Lancet, 378*(9793), 815-825.

Waters, T. R., Putz-Anderson, V., Garg, A., & Fine, L. J. (1993). Revised NIOSH equation for the design and evaluation of manual lifting tasks. *Ergonomics, 36*(7), 749-776.

Watkins, R., Watkins, R., Williams, L., Ahlbrand, S., Garcia, R., Karamanian, A., . . . Hedman, T. (2005). Stability provided by the sternum and rib cage in the thoracic spine. *Spine, 30*(11), 1283-1286.

Webb, R., Brammah, T., Lunt, M., Urwin, M., Allison, T., & Symmons, D. (2003). Prevalence and predictors of intense, chronic, and disabling neck and back pain in the UK general population. *Spine, 28*(11), 1195-1202.

WHO. (2016a). Controlling the global obesity epidemic. from http://www.who.int/nutrition/topics/obesity/en/

WHO. (2016b). Global Health Observatory (GHO) data. from http://www.who.int/gho/ncd/risk_factors/overweight/en/

Wilke, H.-J., Neef, P., Hinz, B., Seidel, H., & Claes, L. (2001). Intradiscal pressure together with anthropometric data–a data set for the validation of models. *Clin Biomech, 16*, S111-S126.

Wilke, H. J., Neef, P., Caimi, M., Hoogland, T., & Claes, L. E. (1999). New in vivo measurements of pressures in the intervertebral disc in daily life. *Spine, 24*(8), 755-762.

Winter, D. A. (2009). *Biomechanics and motor control of human movement*. Toronto: John Wiley & Sons.

Wood, S., Pearsall, D., Ross, R., & Reid, J. (1996). Trunk muscle parameters determined from MRI for lean to obese males. *Clin Biomech, 11*(3), 139-144.

Yaktine, A. L., & Rasmussen, K. M. (2009). *Weight Gain During Pregnancy: Reexamining the Guidelines*: National Academies Press.

Yar, T. (2008). Spinal shrinkage as a measure of spinal loading in male Saudi university students and its relationship with body mass index. *Saudi Med J, 29*(10), 1453-1457.

Yip, Y., Ho, S., & Chan, S. (2001). Tall stature, overweight and the prevalence of low back pain in Chinese middle-aged women. *Int J Obes Rel Metabol Dis, 25*(6), 887-893.

Yoshioka, T., Tsuji, H., Hirano, N., & Sainoh, S. (1990). Motion characteristic of the normal lumbar spine in young adults: instantaneous axis of rotation and vertebral center motion analyses. *Journal of spinal disorders, 3*(2), 103-113.

Zander, T., Dreischarf, M., & Schmidt, H. (2016). Sensitivity analysis of the position of the intervertebral centres of reaction in upright standing–a musculoskeletal model investigation of the lumbar spine. *Medical Engineering & Physics, 38*, 297-301.

Zander, T., Dreischarf, M., Timm, A.-K., Baumann, W. W., & Schmidt, H. (2017). Impact of material and morphological parameters on the mechanical response of the lumbar spine–a finite element sensitivity study. *Journal of biomechanics, 53*, 185-190.

APPENDIX A MUSCLE ARCHITECTURE

Table 10.1 Muscle architecture of the reference model (sex=male, age=41.8 year, BH=173.0 cm, and BW=75.1 kg (Ghezelbash et al., 2016b) (Chapter 3))

Muscle Name	PCSA (mm^2)	Upper Attachment				Lower Attachment			
		x (mm)	y (mm)	z (mm)	Level	x (mm)	y (mm)	z (mm)	Level
EO	670.6	-66.0	143.6	209.0	T11	-111.0	107.1	80.0	S1
EO	234.4	-36.5	150.1	179.5	T11	-90.0	124.6	-15.0	S1
EO	273	-3.9	134.1	160.2	T11	-29.8	135.6	44.3	S1
EO	670.6	-66.0	-143.6	209.0	T11	-111.0	-107.1	80.0	S1
EO	234.4	-36.5	-150.1	179.5	T11	-90.0	-124.6	-15.0	S1
EO	273	-3.9	-134.1	160.2	T11	-29.8	-135.6	44.3	S1
EO	397.4	14.7	102.5	147.3	T12	-4.0	125.6	57.5	S1
EO	397.4	14.7	-102.5	147.3	T12	-4.0	-125.6	57.5	S1
ICPL	108	35.7	33.9	159.3	L1	63.0	57.6	-7.0	S1
ICPL	108	35.7	-33.9	159.3	L1	63.0	-57.6	-7.0	S1
ICPL	154	29.8	36.1	126.9	L2	49.0	57.6	12.0	S1
ICPL	154	29.8	-36.1	126.9	L2	49.0	-57.6	12.0	S1
ICPL	182	21.9	37.9	95.3	L3	44.0	60.6	18.0	S1
ICPL	182	21.9	-37.9	95.3	L3	44.0	-60.6	18.0	S1
ICPL	189	19.3	40.7	63.9	L4	37.0	63.6	23.0	S1
ICPL	189	19.3	-40.7	63.9	L4	37.0	-63.6	23.0	S1
ICPT	330	95.5	66.6	263.0	T11	39.9	59.6	-10.0	S1
ICPT	330	95.5	-66.6	263.0	T11	39.9	-59.6	-10.0	S1
ICPT	123	85.0	71.6	236.0	T11	34.9	64.6	-5.0	S1
ICPT	123	85.0	-71.6	236.0	T11	34.9	-64.6	-5.0	S1
ICPT	147	73.7	76.6	205.0	T12	29.9	69.6	0.0	S1
ICPT	147	73.7	-76.6	205.0	T12	29.9	-69.6	0.0	S1
IO	409.6	-111.0	98.5	30.0	T11	-86.6	107.5	-16.9	S1
IO	226	-120.9	98.5	211.9	T11	-66.0	124.5	18.5	S1
IO	267.6	-81.5	114.5	164.0	T11	-44.0	132.0	40.0	S1
IO	235	-41.5	134.5	148.5	T11	-15.5	122.0	48.5	S1
IO	409.6	-111.0	-98.5	30.0	T11	-86.6	-107.5	-16.9	S1
IO	226	-120.9	-98.5	211.9	T11	-66.0	-124.5	18.5	S1
IO	267.6	-81.5	-114.5	164.0	T11	-44.0	-132.0	40.0	S1
IO	235	-41.5	-134.5	148.5	T11	-15.5	-122.0	48.5	S1
IO	207.2	-14.0	129.5	140.0	T12	7.5	112.0	66.5	S1

IO	207.2	-14.0	-129.5	140.0	T12	7.5	-112.0	66.5	S1
IP	252	12.0	23.2	174.3	L1	-40.0	92.2	-88.0	S1
IP	252	12.0	-23.2	174.3	L1	-40.0	-92.2	-88.0	S1
IP	295	-3.0	25.4	140.6	L2	-40.0	92.2	-88.0	S1
IP	295	-3.0	-25.4	140.6	L2	-40.0	-92.2	-88.0	S1
IP	334	-9.0	30.1	105.4	L3	-40.0	92.2	-88.0	S1
IP	334	-9.0	-30.1	105.4	L3	-40.0	-92.2	-88.0	S1
IP	311	-12.8	34.3	68.5	L4	-40.0	92.2	-88.0	S1
IP	311	-12.8	-34.3	68.5	L4	-40.0	-92.2	-88.0	S1
IP	182	-17.5	38.6	30.7	L5	-40.0	92.2	-88.0	S1
IP	182	-17.5	-38.6	30.7	L5	-40.0	-92.2	-88.0	S1
LGPL	79	35.0	27.7	159.6	L1	59.0	56.9	-8.4	S1
LGPL	79	35.0	-27.7	159.6	L1	59.0	-56.9	-8.4	S1
LGPL	91	28.4	31.6	128.2	L2	50.0	56.3	0.1	S1
LGPL	91	28.4	-31.6	128.2	L2	50.0	-56.3	0.1	S1
LGPL	103	22.0	34.5	90.2	L3	44.0	55.2	7.3	S1
LGPL	103	22.0	-34.5	90.2	L3	44.0	-55.2	7.3	S1
LGPL	110	19.3	35.6	58.6	L4	39.0	52.7	13.3	S1
LGPL	110	19.3	-35.6	58.6	L4	39.0	-52.7	13.3	S1
LGPL	116	20.7	41.6	20.6	L5	34.0	48.5	0.0	S1
LGPL	116	20.7	-41.6	20.6	L5	34.0	-48.5	0.0	S1
LGPT	795	88.6	43.4	262.9	T11	43.0	22.6	-30.0	S1
LGPT	795	88.6	-43.4	262.9	T11	43.0	-22.6	-30.0	S1
LGPT	167	81.4	44.5	236.0	T11	40.0	25.6	-25.0	S1
LGPT	167	81.4	-44.5	236.0	T11	40.0	-25.6	-25.0	S1
LGPT	138	73.6	45.3	205.0	T12	37.0	28.6	-20.0	S1
LGPT	138	73.6	-45.3	205.0	T12	37.0	-28.6	-20.0	S1
MF	120	66.0	5.3	252.1	T11	52.0	19.9	164.5	L1
MF	80	66.0	5.4	240.0	T11	39.2	19.7	139.3	L2
MF	40	55.4	5.5	202.9	T11	39.2	19.7	139.3	L2
MF	40	63.0	5.4	228.9	T11	24.6	23.8	103.1	L3
MF	40	62.2	5.4	198.7	T11	24.6	23.8	103.1	L3
MF	40	62.2	5.4	198.7	T11	13.4	26.4	76.4	L4
MF	120	66.0	-5.3	252.1	T11	52.0	-19.9	164.5	L1
MF	80	66.0	-5.4	240.0	T11	39.2	-19.7	139.3	L2
MF	40	55.4	-5.5	202.9	T11	39.2	-19.7	139.3	L2
MF	40	63.0	-5.4	228.9	T11	24.6	-23.8	103.1	L3
MF	40	62.2	-5.4	198.7	T11	24.6	-23.8	103.1	L3

MF	40	62.2	-5.4	198.7	T11	13.4	-26.4	76.4	L4
MF	40	54.8	5.5	172.4	T12	24.6	23.8	103.1	L3
MF	40	61.7	5.4	168.2	T12	13.4	26.4	76.4	L4
MF	40	61.7	5.4	168.2	T12	19.7	32.4	43.6	L5
MF	40	54.8	-5.5	172.4	T12	24.6	-23.8	103.1	L3
MF	40	61.7	-5.4	168.2	T12	13.4	-26.4	76.4	L4
MF	40	61.7	-5.4	168.2	T12	19.7	-32.4	43.6	L5
MF	96	54.9	5.6	145.0	L1	54.0	48.3	-7.4	S1
MF	96	54.9	-5.6	145.0	L1	54.0	-48.3	-7.4	S1
MF	40	47.9	6.3	130.8	L1	13.4	26.4	76.4	L4
MF	42	54.5	5.6	129.0	L1	19.7	32.4	43.6	L5
MF	40	47.9	-6.3	130.8	L1	13.4	-26.4	76.4	L4
MF	42	54.5	-5.6	129.0	L1	19.7	-32.4	43.6	L5
MF	19	54.5	5.6	165.0	L1	39.2	19.7	135.0	L2
MF	19	54.5	-5.6	165.0	L1	39.2	-19.7	135.0	L2
MF	138	48.8	5.6	110.0	L2	56.0	51.0	-16.5	S1
MF	138	48.8	-5.6	110.0	L2	56.0	-51.0	-16.5	S1
MF	39	38.0	5.3	106.1	L2	19.7	32.4	43.6	L5
MF	39	38.0	-5.3	106.1	L2	19.7	-32.4	43.6	L5
MF	22	48.8	5.6	125.0	L2	24.6	23.8	98.0	L3
MF	22	48.8	-5.6	125.0	L2	24.6	-23.8	98.0	L3
MF	211	40.6	5.7	68.4	L3	61.0	44.7	-28.3	S1
MF	211	40.6	-5.7	68.4	L3	61.0	-44.7	-28.3	S1
MF	23	40.6	5.6	88.0	L3	13.4	26.4	59.0	L4
MF	23	40.6	-5.6	88.0	L3	13.4	-26.4	59.0	L4
MF	186	40.6	4.6	43.4	L4	65.0	33.5	-29.5	S1
MF	186	40.6	-4.6	43.4	L4	65.0	-33.5	-29.5	S1
MF	17	40.6	5.6	49.0	L4	19.7	32.4	21.0	L5
MF	17	40.6	-5.6	49.0	L4	19.7	-32.4	21.0	L5
MF	134	43.9	5.4	15.2	L5	67.0	10.7	-30.4	S1
MF	134	43.9	-5.4	15.2	L5	67.0	-10.7	-30.4	S1
QL	101.6	30.5	49.9	182.0	T12	26.0	89.9	32.0	S1
QL	101.6	30.5	-49.9	182.0	T12	26.0	-89.9	32.0	S1
QL	20	30.5	49.9	182.0	T12	28.6	43.4	126.9	L2
QL	50.7	30.0	61.9	169.4	T12	21.0	45.2	95.3	L3
QL	11.8	21.9	80.5	149.2	T12	17.1	48.0	63.9	L4
QL	20	30.5	-49.9	182.0	T12	28.6	-43.4	126.9	L2
QL	50.7	30.0	-61.9	169.4	T12	21.0	-45.2	95.3	L3

QL	11.8	21.9	-80.5	149.2	T12	17.1	-48.0	63.9	L4
QL	70.3	34.8	41.2	159.3	L1	26.0	89.9	32.0	S1
QL	70.3	34.8	-41.2	159.3	L1	26.0	-89.9	32.0	S1
QL	63.9	28.6	43.4	126.9	L2	27.0	79.9	30.0	S1
QL	63.9	28.6	-43.4	126.9	L2	27.0	-79.9	30.0	S1
QL	59.9	21.0	45.2	95.3	L3	28.0	68.9	26.0	S1
QL	59.9	21.0	-45.2	95.3	L3	28.0	-68.9	26.0	S1
QL	55.9	17.1	48.0	63.9	L4	28.0	59.9	21.0	S1
QL	55.9	17.1	-48.0	63.9	L4	28.0	-59.9	21.0	S1
RA	567	-155.0	52.0	265.0	T11	-80.7	40.1	-80.0	S1
RA	567	-155.0	-52.0	265.0	T11	-80.7	-40.1	-80.0	S1
SP	24	61.0	-7.9	245.1	T11	50.0	-8.1	176.0	T12
SP	32	61.0	-7.9	245.1	T11	54.9	-8.1	145.0	L1
SP	40	61.0	-7.9	245.1	T11	48.8	-8.1	110.0	L2
SP	48	61.0	-7.9	245.1	T11	40.6	-8.3	68.4	L3
SP	24	61.0	7.9	245.1	T11	50.0	8.1	176.0	T12
SP	32	61.0	7.9	245.1	T11	54.9	8.1	145.0	L1
SP	40	61.0	7.9	245.1	T11	48.8	8.1	110.0	L2
SP	48	61.0	7.9	245.1	T11	40.6	8.3	68.4	L3

APPENDIX B MODEL FLOWCHART

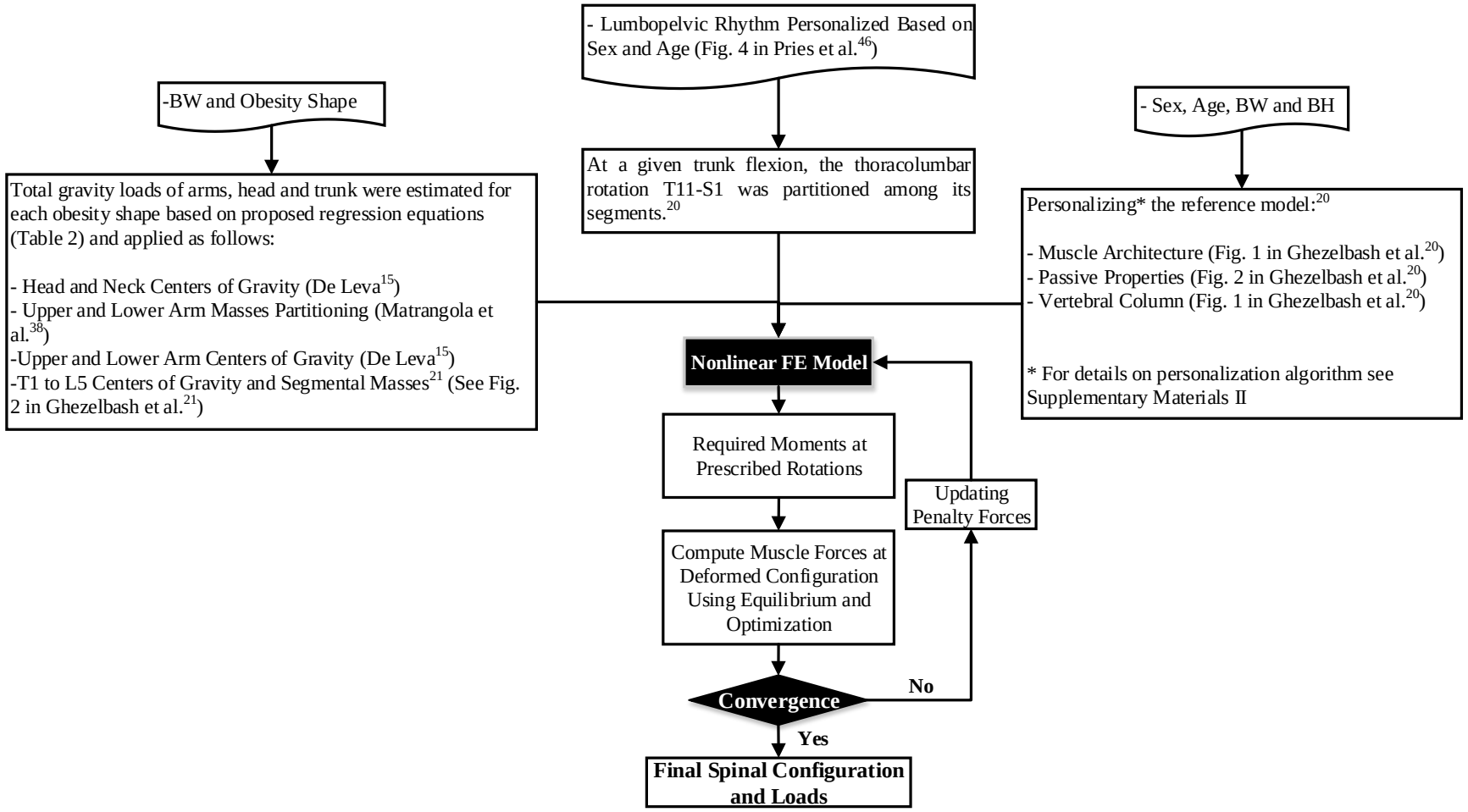

Figure B.1 The flowchart of the subject-specific musculoskeletal model

APPENDIX C FLOWCHART OF THE SCALING ALGORITHM

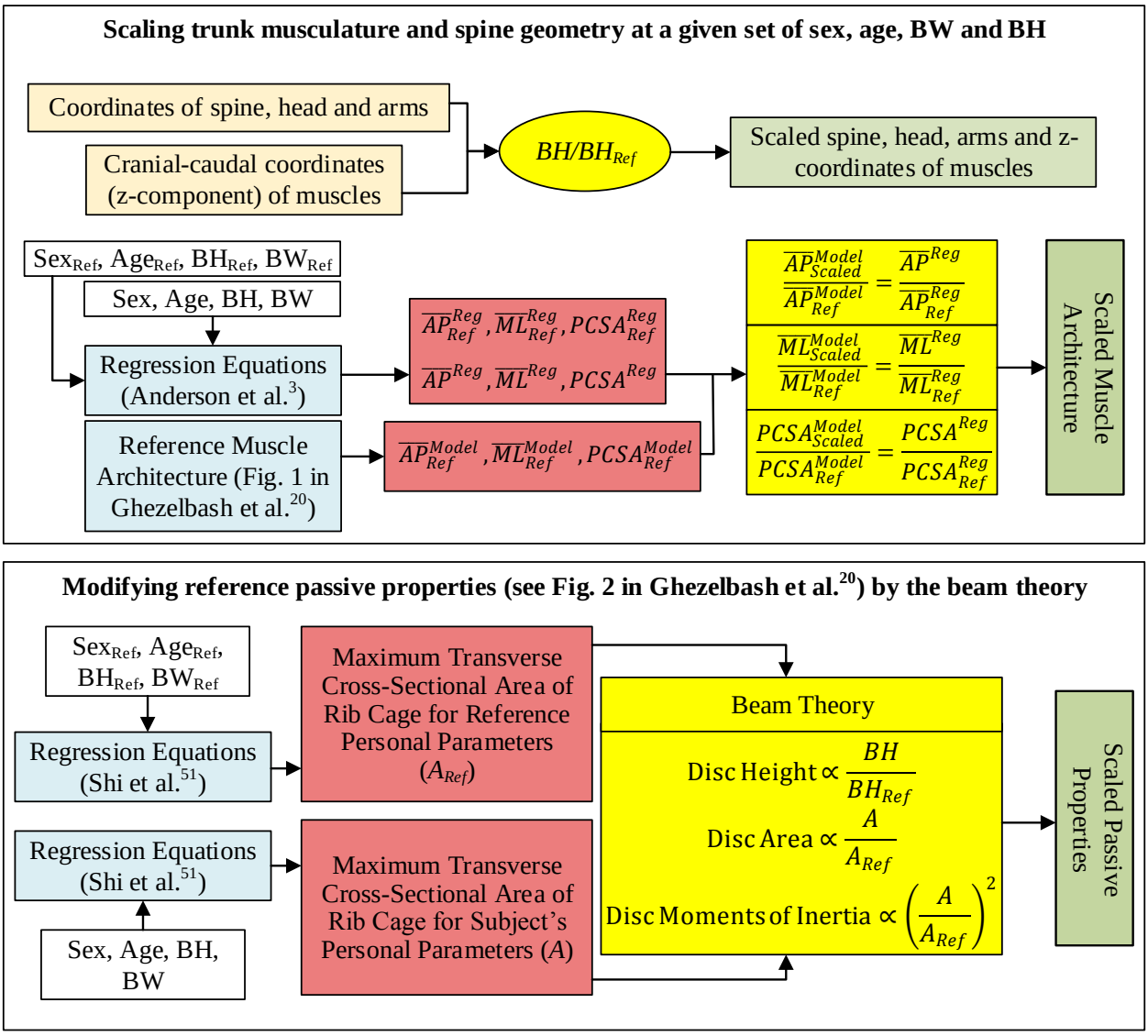

Figure C.1 The flowchart of the scaling algorithm. BH: body height; BW: body weight; PCSA: physiological cross-sectional area; $\overline{AP}$: average anterior-posterior distance of a muscle centroid (when cut by a transverse plane at the corresponding vertebral height) from vertebrae; $\overline{ML}$: average medio-lateral distance of a muscle centroid (when cut by a transverse plane at the corresponding vertebral height) from vertebrae; A: maximum transverse cross-sectional area of the rib cage; subscript "Ref": values from the reference configuration; subscript "Scaled": values from the

patient-specific model; superscript “Reg”: values calculated from regression equations. Reference personal parameters are sex_{ref}=male, age_{ref}=41.8 year, BH_{ref}=173.0 cm, and BW_{ref}=75.1 kg (Ghezelbash et al., 2016b) (Chapter 3).

APPENDIX D DEFINITION OF FLEXION ANGLE

The fixed global XYZ coordinate system is defined with three orthonormal base vectors ($\boldsymbol{e}_X, \boldsymbol{e}_Y, \boldsymbol{e}_Z$), Figure D.1. To calculate the asymmetry angle (A) at each task, the projections of three points at T11 (P^{T11}), T1 (P^{T1}), and mass center of the hand-load (P^M) to the XYplane (floor) were calculated:

$$Q^i = \boldsymbol{T}\, P^i, \qquad \text{(Eq. D.1)}$$

and

$$\boldsymbol{T} = \begin{bmatrix} 1 & 0 & 0 \\ 0 & 1 & 0 \\ 0 & 0 & 0 \end{bmatrix} \qquad \text{(Eq. D.2)}$$

where Q denotes coordinates of these three projected points; $i = T11, T1$ or M. By fitting a line to Q^i with a unit direction vector ($\boldsymbol{v}$) in the XY plane, the asymmetry angle is evaluated as follows:

$$\mathrm{A} = \cos^{-1}(v.\boldsymbol{e}_X). \qquad \text{(Eq. D.3)}$$

At each task, the rigid body rotation matrix of T11 from the upright standing to a flexed position (R^{T11}) is considered. It is assumed that a convective coordinate system ($x'y'z'$ was initially parallel to the global XYZ coordinate system at the upright standing) was rigidly attached to T11. Flexion angle (F) was evaluated as follows:

$$\mathrm{F} = \cos^{-1}(\boldsymbol{e}_{z'}.\boldsymbol{e}_Z), \qquad \text{(Eq. D.4)}$$

in which $\boldsymbol{e}_{z'} = R^{T12}\boldsymbol{e}_Z$.

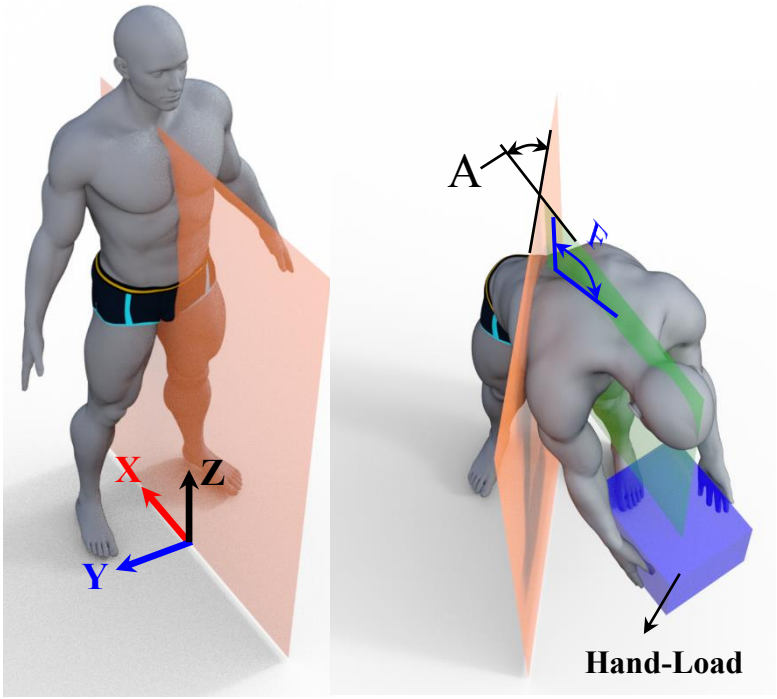

Figure D.1: Schematic illustration of the global coordinate XYZ as well as asymmetry angle (A) and flexion angle (F) during an asymmetric lifting task

APPENDIX E ALTERNATIVE REGRESSION EQUATIONS WITH LOAD LOCATIONS AS INPUTS

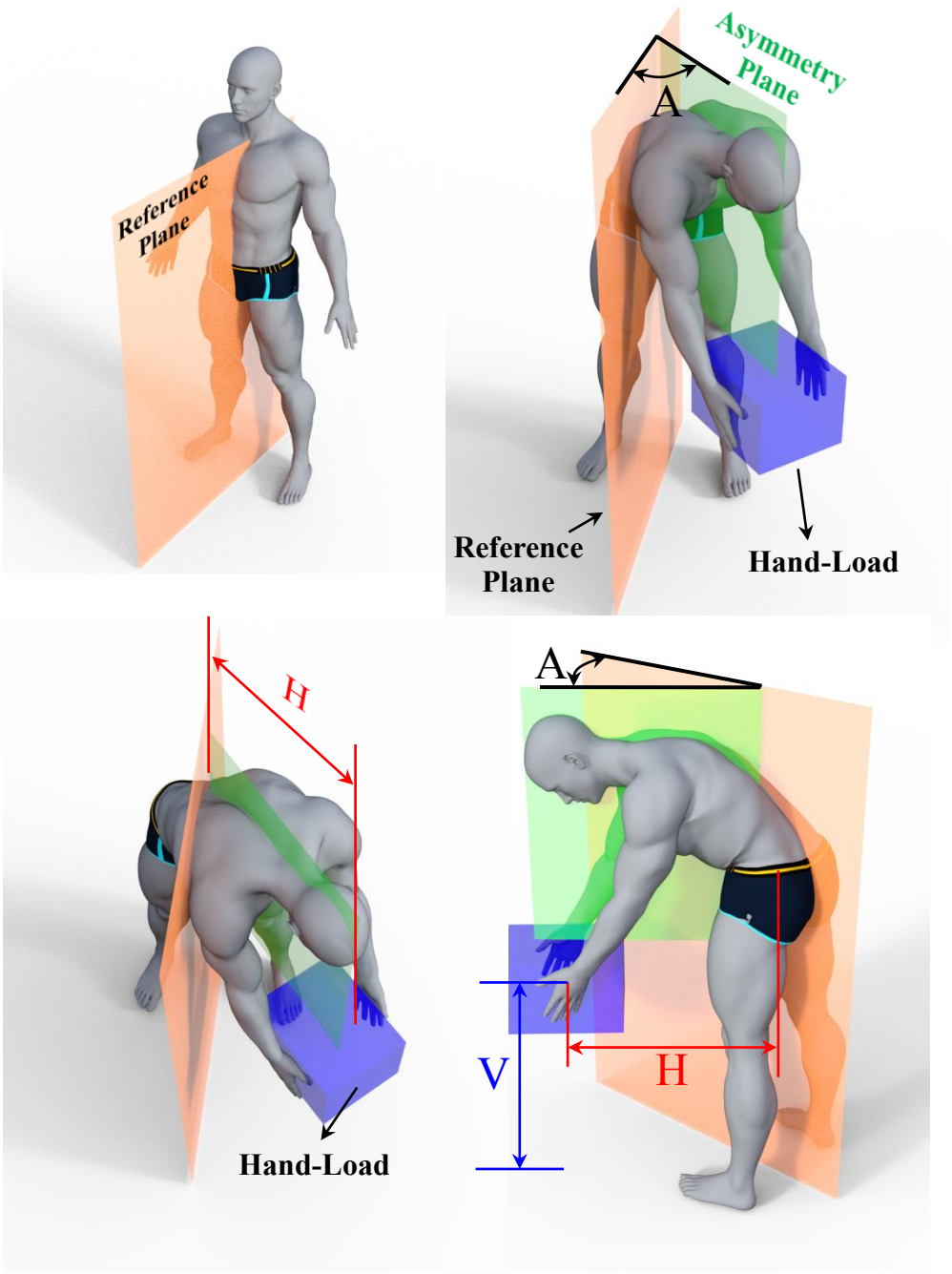

Figure E.1: Schematic representation of the global coordinate system and an asymmetric lifting task (A: asymmetry angel; H: horizontal distance between hands (load) and L5-S1 joint; V: vertical

distance of hands (load) from the floor). The asymmetry plane (perpendicular to the transverse plane - highlighted in green) is defined to pass through thorax and hand-load in the deformed posture. Detailed definitions of asymmetric angle (A) and flexion angle (F) were presented in Appendix D.

Table E.1: Computed regression coefficients, R^2, root mean squared error (RMSE) and p-values at upright standing

Parameter	*L4-L5*				*L5-S1*			
	Compression		Shear		Compression		Shear	
	Coef.*	p-value	Coef.*	p-value	Coef.*	p-value	Coef.*	p-value
Constant	-461.546	0.0024	-39.9894	0.141076	-509.148	0.007021	-83.8469	0.354969
Sex†	-155.357	0.0190	-1.11898	0.71999	-291.905	0.000545	-133.371	0.001009
BH	1.906233	0.0621	-0.09754	0.554196	2.067349	0.101561	0.094889	0.875668
BW	3.572582	<0.0001	0.164711	0.39227	2.770836	0.002309	0.987103	0.023769
M	87.09542	<0.0001	11.89614	<0.0001	89.13993	<0.0001	34.12302	<0.0001
A	33.18844	<0.0001	5.934122	<0.0001	39.65694	<0.0001	15.30935	<0.0001
D	16.89952	<0.0001	1.010205	0.000139	15.65991	<0.0001	5.687704	0.000402
Sex×BH	0.737213	0.04916	-	-	1.214098	0.008792	0.495549	0.026007
Sex×BW	-	-	-	-	-	-	-	-
Sex×M	3.412234	<0.0001	0.481894	0.045133	5.786153	<0.0001	2.501665	<0.0001
Sex×A	-2.76422	<0.0001	-0.4208	<0.0001	-3.37342	<0.0001	-1.185	<0.0001
Sex×D	-	-	-	-	1.255303	0.00371	0.487341	0.018998
BH×BW	-	-	-	-	-	-	-	-
BH×M	-0.38762	<0.0001	-0.05438	<0.0001	-0.41083	<0.0001	-0.14608	<0.0001
BH×A	-0.09901	<0.0001	-0.02233	<0.0001	-0.12044	<0.0001	-0.04779	<0.0001
BH×D	-0.08037	<0.0001	-	-	-0.08301	0.000241	-0.02492	0.021579
BW×M	-0.07069	0.021018	-0.02988	0.001541	-0.08358	0.027232	-0.05272	0.003781
BW×A	0.10834	<0.0001	0.031366	<0.0001	0.132096	<0.0001	0.060342	<0.0001
BW×D	0.099063	<0.0001	0.007046	0.030983	0.121227	<0.0001	0.042414	<0.0001
M×A	-0.33706	<0.0001	-0.01026	0.02411	-0.38509	<0.0001	-0.13745	<0.0001
M×D	1.796233	<0.0001	0.245545	<0.0001	2.005772	<0.0001	0.741474	<0.0001
A×D	-	-	-	-	-	-	-	-
R^2	0.991		0.970		0.989		0.984	
RMSE (N)	80.66		24.95		99.67		47.90	
Mean (N)	2086.15 ± 822.37		256.35 ± 143.01		2192.24 ± 929.80		858.38 ± 372.67	

* Coef.: Coefficient; † Female =1; Male = 0

Table E.2: Computed regression coefficients, R^2, root mean squared error (RMSE) and p-values at flexed postures

Parameter	*L4-L5*				*L5-S1*			
	Compression		Shear		Compression		Shear	
	Coef.*	p-value	Coef.*	p-value	Coef.*	p-value	Coef.*	p-value
Constant	-345.253	0.3809	-535.554	<0.0001	-334.403	0.390153	-782.455	<0.0001
Sex†	-348.96	0.00062	77.03659	<0.0001	1.433657	0.974633	48.67486	0.000887
BH	5.001094	0.0567	3.203364	<0.0001	1.979706	0.440966	5.980029	<0.0001
BW	17.36228	<0.0001	4.625171	<0.0001	13.63702	<0.0001	4.586557	0.000451
M	64.75562	<0.0001	16.17949	<0.0001	58.70708	<0.0001	25.96138	<0.0001
A	25.96295	<0.0001	2.893589	<0.0001	27.86343	<0.0001	8.277086	<0.0001
F	-9.97231	<0.0001	0.170675	0.667378	-3.07439	0.224231	3.171757	0.001012
D	14.62676	<0.0001	4.347489	<0.0001	15.50324	<0.0001	8.686701	<0.0001
Sex×BH	1.555161	0.02887	-	-	-	-	-	-
Sex×BW	2.280377	<0.0001	-	-	1.904289	<0.0001	-	-
Sex×M	8.739079	<0.0001	-	-	7.407236	<0.0001	1.550727	0.00014
Sex×A	-3.17654	<0.0001	-0.55001	<0.0001	-4.08337	<0.0001	-1.23906	<0.0001
Sex×F	-2.26871	<0.0001	-0.64821	<0.0001	-2.4506	<0.0001	-0.69122	<0.0001
Sex×D	2.749036	<0.0001	0.222647	0.000605	3.837132	<0.0001	1.08512	<0.0001
BH×BW	0.062234	0.00128	0	0	0.104864	<0.0001	0.028969	<0.0001
BH×M	-0.58969	<0.0001	-0.09728	<0.0001	-0.55384	<0.0001	-0.28513	<0.0001
BH×A	-0.12402	<0.0001	-0.01212	<0.0001	-0.09094	<0.0001	-0.04795	<0.0001
BH×F	0.046639	0.0058	-0.00659	0.012749	0.029563	0.080303	-0.03465	<0.0001
BH×D	-0.14148	<0.0001	-0.02417	<0.0001	-0.14774	<0.0001	-0.07861	<0.0001
BW×M	0.192336	<0.0001	-	-	0.200355	<0.0001	0.03333	0.03558
BW×A	0.019269	0.0247	-	-	-	-	0.014956	<0.0001
BW×F	-0.21091	<0.0001	-0.02999	<0.0001	-0.22776	<0.0001	-0.05414	<0.0001
BW×D	0.159377	<0.0001	0.013422	<0.0001	0.153789	<0.0001	0.044933	<0.0001
M×A	-0.1277	<0.0001	-0.04516	<0.0001	-0.23874	<0.0001	-0.07428	<0.0001
M×F	0.140254	<0.0001	0.024043	<0.0001	0.170315	<0.0001	0.204731	<0.0001
M×D	2.53994	<0.0001	0.306466	<0.0001	2.655784	<0.0001	0.997618	<0.0001
A×F	0.132136	<0.0001	0.024349	<0.0001	0.111082	<0.0001	0.076977	<0.0001
A×D	-0.03297	<0.0001	-0.01593	<0.0001	-0.08144	<0.0001	-0.0233	<0.0001
F×D	-	-	-0.00335	0.000771	0.014528	0.021942	0.041844	<0.0001
R^2	0.974		0.969		0.974		0.963	
RMSE (N)	196.81		30.84		197.03		75.05	
Mean (N)	2925.21 ± 1211.28		388.59 ± 175.63		3032.31 ± 1205.98		1056.23 ± 392.21	

* Coef.: Coefficient; † Female =1; Male = 0

APPENDIX F SIMPLIFIED REGRESSION EQUATIONS

Simplified regression equations: To simplify regression equations, we did not consider sex and body height (as independent variables) due to their minor roles in spinal loads, and took into account only of significant terms ($p<0.05$).

Table F.1: Computed regression coefficients, R^2, root mean squared error (RMSE) and p-values at upright standing for simplified regression equations

Parameter	*L4-L5*				*L5-S1*			
	Compression		Shear		Compression		Shear	
	Coef.*	p-value	Coef.*	p-value	Coef.*	p-value	Coef.*	p-value
Constant	-204.351	0.0318	-37.9325	<0.0001	-248.898	0.0225	-101.123	0.0387
BW	4.679044	<0.0001	-	-	4.205276	0.0019	1.28281	0.0347
M	36.82329	<0.0001	4.231926	<0.0001	37.62007	<0.0001	17.28064	<0.0001
A	14.87763	<0.0001	1.762924	<0.0001	16.81412	<0.0001	6.518624	<0.0001
D	6.084262	0.0003	1.361311	<0.0001	5.036162	0.0084	2.737565	0.0014
BW×M	-0.26962	<0.0001	-0.03851	<0.0001	-0.29877	<0.0001	-0.1301	<0.0001
BW×A	0.084762	<0.0001	0.027077	<0.0001	0.101963	<0.0001	0.048093	<0.0001
BW×D	0.047192	0.0184	-	-	0.063031	0.0060	0.021919	0.0331
M×A	-	-	0.036045	<0.0001	-	-	-	-
M×D	1.492331	<0.0001	0.183784	<0.0001	1.652713	<0.0001	0.586288	<0.0001
A×D	0.045116	0.0003	0.010277	0.0003	0.063599	<0.0001	0.024133	0.0002
R^2	0.96		0.94		0.96		0.95	
RMSE (N)	159.57		35.51		182.79		82.00	
Mean (N)	2086.15±822.37		256.35±143.01		2192.24±929.80		858.38±372.67	

* Coef.: Coefficient

Table F.2: Computed regression coefficients, R^2, root mean squared error (RMSE) and p-values at flexed postures for simplified regression equations

Parameters	*L4-L5*				*L5-S1*			
	Compression		Shear		Compression		Shear	
	Coef.*	p-value	Coef.*	p- value	Coef.*	p- value	Coef.*	p- value
Constant	92.21616	0.0431	-70.1973	<0.0001	71.3142	0.00948	-49.8027	<0.0001
BW	8.722677	<0.0001	1.314008	<0.0001	9.654267	<0.0001	4.434174	<0.0001
M	-	-	3.130555	<0.0001	-	-	3.66045	<0.0001
A	17.46986	<0.0001	2.842044	<0.0001	20.6088	<0.0001	8.363289	<0.0001
F	-3.24825	<0.0001	0.49279	<0.0001	-5.42554	<0.0001	-	-
D	-4.71189	0.0050	1.049813	<0.0001	-	-	-	-
BW×M	-	-	-0.02008	0.0026	0.069926	0.00168	-	-
BW×A	-	-	-	-	-	-	-	-
BW×F	0.231067	<0.0001	0.034287	<0.0001	0.240893	<0.0001	0.068312	<0.0001
BW×D	0.048462	0.0118	-	-	0.029001	0.00404	-	-
M×A	-0.06832	0.0029	-0.03431	<0.0001	-0.17423	<0.0001	-0.04069	<0.0001
M×F	0.905165	<0.0001	0.108536	<0.0001	0.913375	<0.0001	0.22104	<0.0001
M×D	2.441194	<0.0001	0.302128	<0.0001	2.538994	<0.0001	1.068737	<0.0001
A×F	-0.09638	<0.0001	-0.02123	<0.0001	-0.09936	<0.0001	-0.06633	<0.0001
A×D	-0.02195	0.0403	-0.01147	<0.0001	-0.06479	<0.0001	-0.00166	0.6534
F×D	0.052136	<0.0001	-0.00393	0.0014	0.022737	0.00760	-0.00484	0.0844
R^2	0.94		0.95		0.94		0.92	
RMSE (N)	287.38		40.78		292.38		110.45	
Mean (N)	2925.21±1211.28		388.59±175.63		3032.31±1205.98		1056.23±392.21	

* Coef.: Coefficient

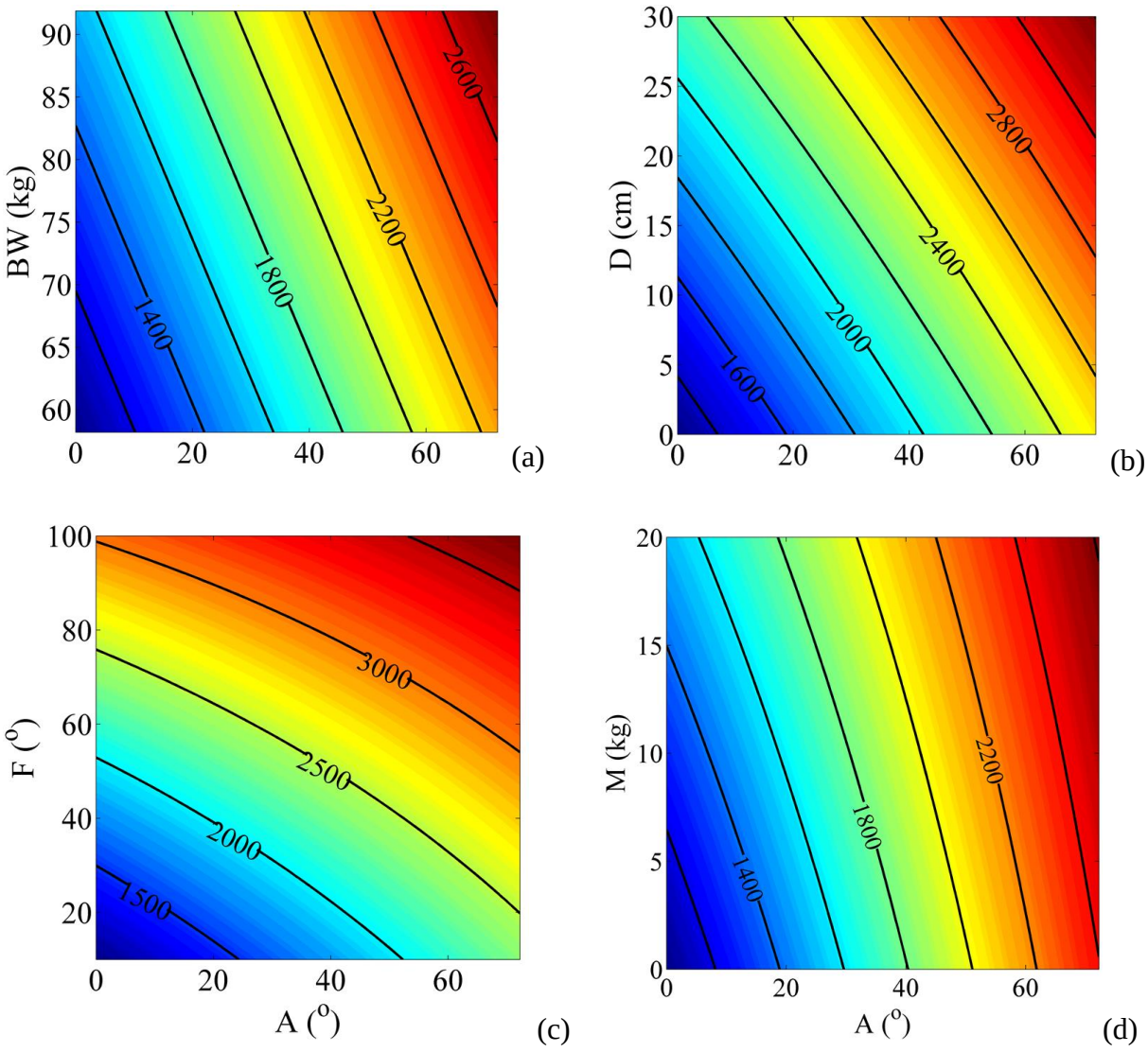

Figure F.1: L5-S1 compression forces (N) computed from simplified regression equations during asymmetric flexion with variations in (a) body weight (BW), (b) horizontal distance of the external load from the shoulder joint (D), (c) flexion angle (F) and (d) external load magnitude (M) versus asymmetry angle (A). If not acting as an independent variable, regression parameters in this figure were set at D=0 cm, M=10 kg, BW=75 kg and F=20°.

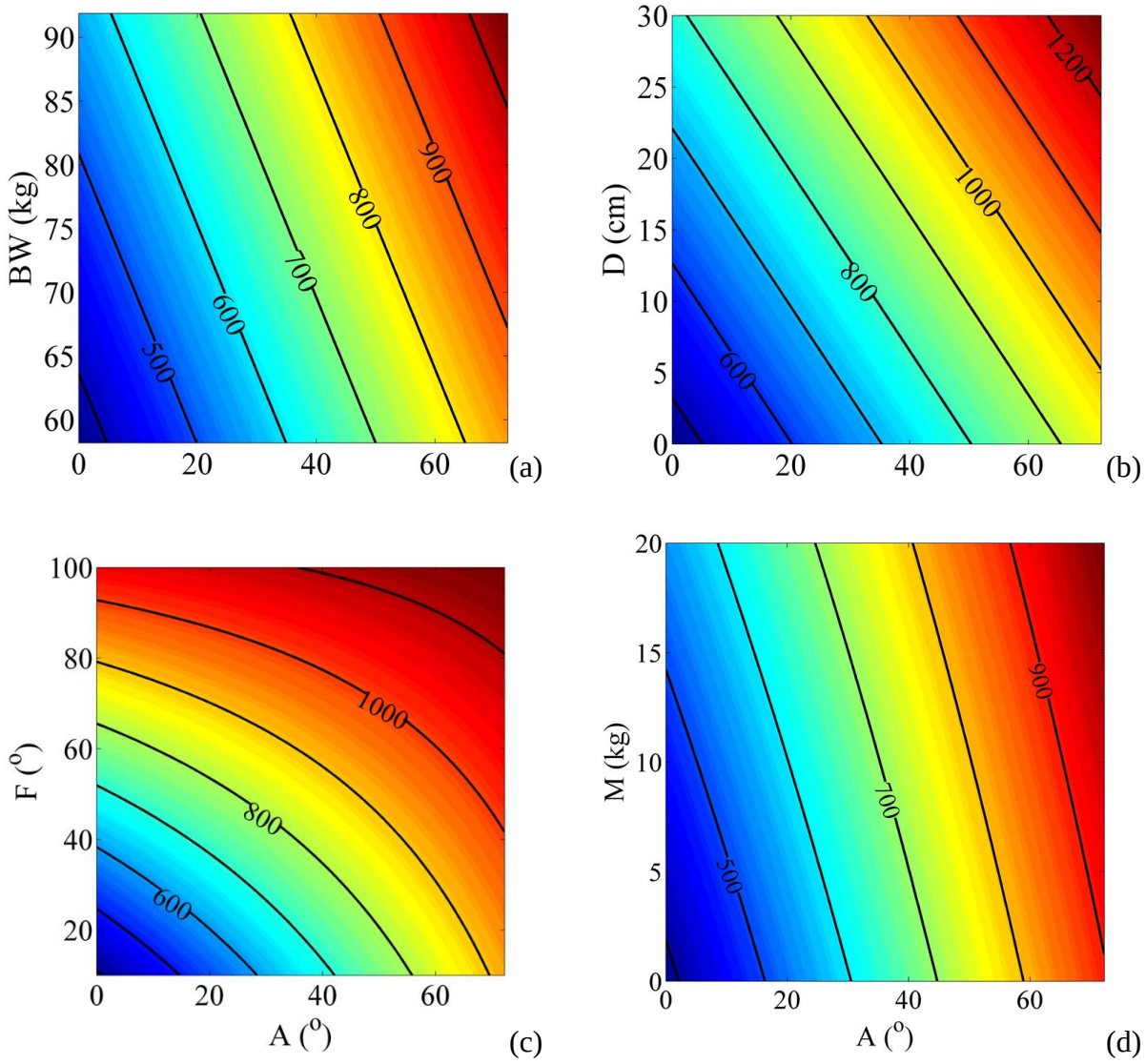

Figure F.2: L5-S1 shear forces (N) computed from simplified regression equations during asymmetric flexion with variations in (a) body weight (BW), (b) horizontal distance of the external load from the shoulder joint (D), (c) flexion angle (F) and (d) external load magnitude (M) versus asymmetry angle (A). If not acting as an independent variable, regression parameters in this figure were set at D=0 cm, M=10 kg, BW=75 kg and F=20°.

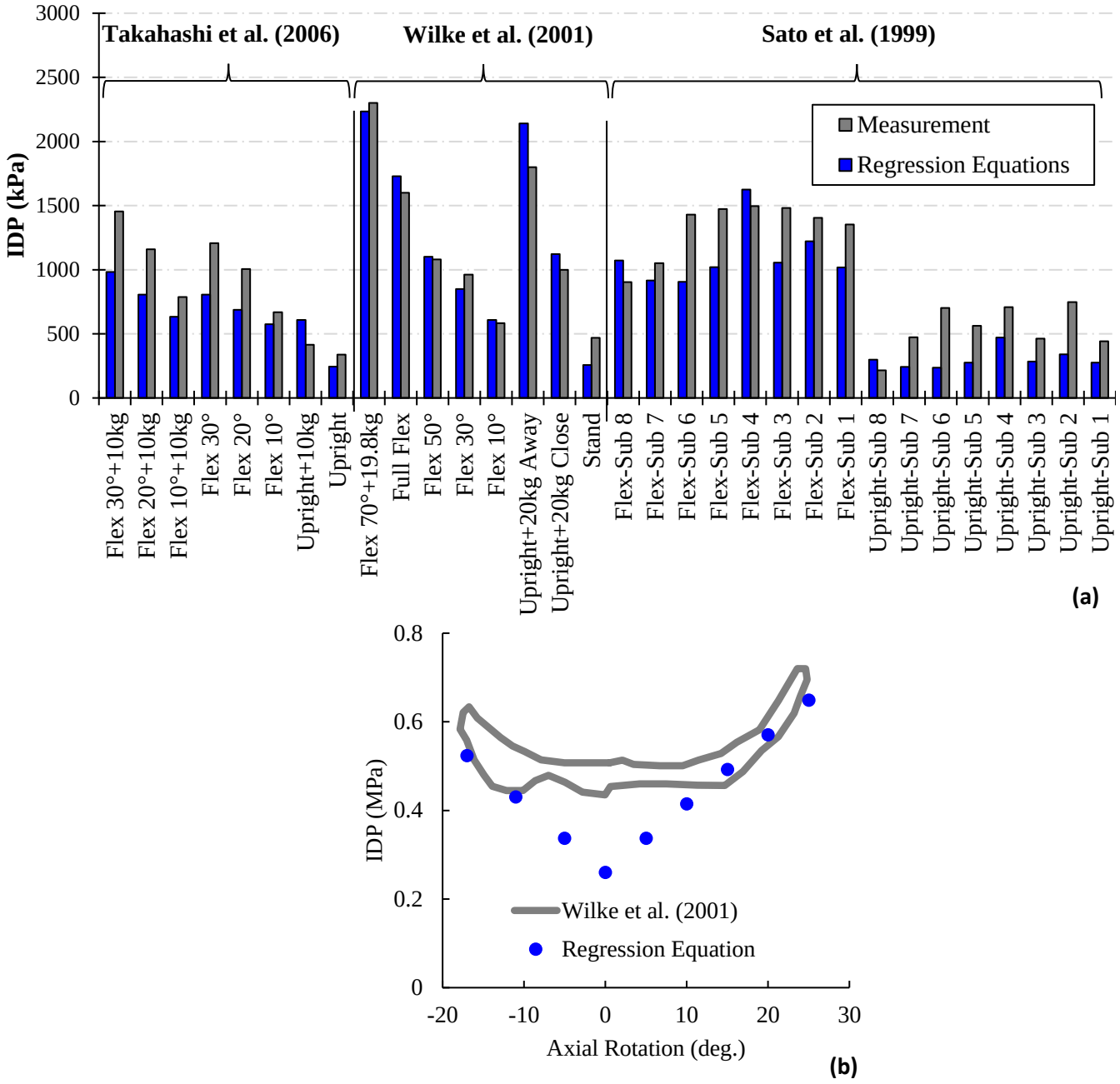

Figure F.3: Estimated IDPs from simplified regression equations versus measurements during (a) sagittally symmetric tasks (Flex: Flexion; Sub: Subject – Sato et al. (1999) measured IDP of 8 subjects) and (b) axial rotation